YAP-Regulation of dynamic cell behaviour underlying organogenesis

Porazinski, Sean

Award date:
2014

Awarding institution:
University of Bath

YAP-regulation of dynamic cell behaviour underlying organogenesis

Sean Porazinski

A thesis submitted for the degree of Doctor of Philosophy

University of Bath
Department of Biology and Biochemistry
October 2013

Index

List of abbreviations

AJ - adherens junction
ANKRD1 - ankyrin repeat domain 1
aPKC - atypical protein kinase C
AREG - amphiregulin
bd - binding domain
BMP - bone morphogenetic protein
BSS - balanced salt solution
CAF - cancer-associated fibroblast
CDs - Cuvierian ducts
Crb - Crumbs
CTGF - connective tissue growth factor
CYR61 - cysteine-rich angiogenic inducer 61
DC - deep cell
DDC - duplication-degeneration-complementation
Dvl - dishevelled
ECM - extracellular matrix
ECSCR - endothelial cell-specific chemotaxis regulator
EGFP/GFP - enhanced green fluorescent protein/green fluorescent protein
ELC - essential light chain
EMT - epithelial-mesenchymal transition
ENU - N-ethyl-N-nitrosourea
EVL - enveloping layer
FGF - fibroblast growth factor
FN - fibronectin
FRET - Förster resonance energy transfer
fli1 - Friend leukemia integration
GPCR - G-protein-coupled receptor
hir - hirame
hpf - hours post-fertilisation
ICM - intermediate cell mass
ID - inner diameter
IHC - immunohistochemistry
IRS1 - insulin receptor substrate 1
ISH - *in situ* hybridisation
KD - knockdown
LATS - large tumour suppressor
LPA - lysophosphatidic acid
LPM - lateral plate mesoderm
LWR - length/width ratio

Mer - merlin
MET - mesenchymal-epithelial transition
METRO - message transport organiser region
MMP - matrix metalloproteinases
MNFP - EGFP-CAAX + H2B-RFP
MRLC - myosin regulatory light chain
MST - mammalian sterile 20-like
MTOC - microtubule-organising centre
MYH - myosin heavy chain
NA - numerical aperture
NC - neural crest
NE - neuroepithelial
NF - normal fibroblast
NMII - non-muscle myosin II
NT - neural tube
OD - outer diameter
PCP - planar cell polarity
PIV - particle image velocimetry
PRB - lens placode-retina boundary
PS - primary stream
RA - retinoic acid
RFP - red fluorescent protein
RGD - Arginylglycylaspartic acid
ROCK - Rho-associated, coiled coil-containing kinase
S1P - sphingosine-1-phosphate
SBMO - splicing blocking morpholino
SDF1 - stromal cell-derived factor 1
Sav1 - salvador
SH3 - Src homology 3
Shh - sonic hedgehog
SS - secondary stream
SWH - Salvador/Warts/Hippo
TA - transcription activation
TAZ - transcriptional coactivator with PDZ-binding motif
tb - TEAD-binding
TBMO - translation blocking morpholino
TEAD - TEA domain
TEF - transcription enhancer factor
TGFβ - transforming growth factor β
TJ - tight junction
VEGF - vascular endothelial growth factor

WT - wild type

YAP - Yes-associated protein

Yki - Yorkie

YSL - yolk syncytial layer

ZO - zona occludens

List of figures

List of tables

Publications

Porazinski, S.R., Wang, H., Furutani-Seiki, M. 2011. Essential techniques for introducing medaka to a zebrafish laboratory--towards the combined use of medaka and zebrafish for further genetic dissection of the function of the vertebrate genome. *Methods in Molecular Biology*, pp. 211-41.

Miyamoto, T., **Porazinski, S.**, Wang, H., Borovina, A., Ciruna, B., Shimizu, A., Kajii, T., Kikuchi, A., Furutani-Seiki, M., Matsuura, S. 2011. Insufficiency of BUBR1, a mitotic spindle checkpoint regulator, causes impaired ciliogenesis in vertebrates. *Human Molecular Genetics*, 20 (10), pp. 2058-70.

Porazinski, S.R., Wang, H., Furutani-Seiki, M. 2010. Dechorionation of medaka embryos and cell transplantation for the generation of chimeras. *Journal of Visualised Experiments*, 46, 2055.

Porazinski, S.R., Wang, H., Furutani-Seiki, M. 2010. Microinjection of medaka embryos for use as a model genetic organism. *Journal of Visualised Experiments*, 46, 1937.

Acknowledgements

I would like to thank the following people for their help in completing this PhD and for making the last four years very enjoyable: My supervisor Makoto Furutani-Seiki for his guidance, expertise, enthusiasm and very useful and interesting discussions; Robert Kelsh for the provision of the fish facility without which there would be no data; Huijia Wang for her technical assistance, great conversations and greater Chinese cooking; My many undergraduate and MRes students, with particular thanks going to Lizzy Potter and Joseph Robinson for their help with cell behavioural analysis; Marc Shedden for his maintenance of the fish and everyone else in laboratory 0.39. Yoichi Asaoka, Jun Hirayama, Tatsuo Miyamoto and Shoji Hata are thanked for their help with the biochemical data. I would also like to thank the University of Bath and the BBSRC for funding.

I must also take this opportunity to sincerely thank Professor Hideaki Nagase and Dr James Doughty for their kind and generous support, which proved invaluable in the final year. My gratitude is also extended to Professor Carl-Philip Heisenberg and Dr Tetsu Kudoh for allowing me to visit their labs and perform vital experiments and learn invaluable new techniques. In particular I would like to thank Hitoshi Morita, Michael Smutny and Martin Behrndt for assistance and useful discussions whilst in Austria. I would like to thank Gregory Paull and Okhyun Lee for their kind and generous help whilst visiting Exeter.

The Kennedy family gets a huge thanks for the kindest and greatest hospitality anyone could wish for whilst studying. I must also thank my family and friends for support during this highly exciting time in my life. Lastly, but by no means the least, I would like to deeply thank LKK for her unwavering patience, tolerance, support, companionship and understanding during the last four years. Without which, none of this would have been remotely possible.

Abstract

In the vertebrate body each tissue/organ acquires three-dimensional (3D) structure during embryonic development and becomes aligned relative to other tissues/organs to generate the global body shape. The existence of a gene essential for orchestrating the complex process of building 3D body shape has not previously been suspected. Understanding the mechanisms by which 3D organs are built and organised is essential for the advancement of regenerative medicine, which aims to facilitate 3D tissue/organ formation and integrate these transplanted tissues/organs in the proper 3D alignment within the host to allow their full functionality. A large-scale ENU mutagenesis screen in medaka (*Oryzias latipes*) identified the *hirame* (*hir*) mutant where the morphogenesis of epithelial tissues is affected causing a flattened body in which individual organs/tissues collapse and are misaligned. The *hir* mutant also exhibits cell migration defects of the primary blood vessels and the heart. *hir* is a recessive lethal mutation with full penetrance and a robust phenotype. Positional cloning showed the unique *hir* phenotype is caused by a point mutation in the region of the Yes-associated protein (YAP) gene that encodes the WW1 protein domain of YAP. This mutant can therefore serve as a useful tool for the study of how 3D tissues and organs are generated and how they align to give rise to the global body shape.

This work details how the combined use of medaka and zebrafish (*Danio rerio*) allowed the identification of YAP as essential for shaping the vertebrate body and its biophysical properties. In this thesis, it is reported for the first time that YAP is essential for the fundamental process of organogenesis at the whole-body scale. Analysis of YAP function in intact mutant animals by a variety of means including time-lapse confocal microscopy and intricate cell-transplantation experiments reveals a previously unrecognised but pivotal role for YAP. YAP governs various cell behaviours including oriented division and cell stacking to generate 3D tissues with proper tissue tension. In turn this tissue tension mediates extracellular matrix assembly and integrin signalling, which allows the correct alignment of adjacent tissues to produce functional organs that undergo coordinated morphogenesis to produce the overall 3D body shape. Furthermore, it is shown that these two major functions of YAP are mediated by actomyosin-dependent tension as demonstrated by *in vivo* force measurements.

Reference table summarising the common stages of medaka development cited in this work and the corresponding hours of development

Developmental stage	Hours post-fertilisation (hpf)
2 (1-cell)	0.5-1
5 (8-cell)	2.33
6 (16-cell)	3
12	10.33
13	13
15 (50% epiboly)	17.5
16 (75% epiboly)	21
17	25
18	26
19 (100% epiboly)	27.5
20	31.5
21	34
22	38
23 (formation of tubular heart)	41
24 (heart beating commences)	44
25 (onset of blood circulation)	50
26	54
27	58

Zebrafish developmental stages are not included in the table since these are stated as hours post-fertilisation (hpf) within the text.

Chapter 1: General introduction

1.1 Motivations behind this work

The 3D shape of an organ is built up by coordinated alignment of multiple tissues. The proper 3D shape of each organ, and the correct relative alignment of the various organs in the body, is important for physiological function. For instance, the eye is constructed from a nascent lens and retina epithelia that are formed in close apposition and undergo coordinated invagination in order to correctly position the lens in the eye cup (Chauhan *et al*., 2009) to provide fully functional vision.

It has long been recognised that producing the 3D structure of tissues/organs involves mechanical forces. Biomechanical approaches using *in vitro* cell and tissue culture have suggested that 3D tissue morphogenesis depends on interplay between force-generating machineries, e.g. actomyosin networks and adhesive clusters that transmit tensile forces at the cell cortex and stabilise cell-cell and cell-extracellular matrix (ECM) interfaces (Mammoto and Ingber, 2010). However, the mechanism by which 3D tissues are coordinately aligned to build an organ and generate the appropriate spatial organisation between different organs remains to be elucidated. Moreover, the presence of a key regulator that orchestrates the complex processes for building 3D body shape has not previously been suspected.

A genome-wide phenotype-driven screen in medaka fish identified the *hirame* (*hir*) mutant (Furutani-Seiki *et al*., 2004), which presented with a unique flattened phenotype where epithelial tissues and organs collapsed. Positional cloning identified the cause of the *hir* phenotype to be a null mutation in the *YAP1* gene. This work has the overall aim of investigating the role of yes-associated protein (YAP) in regulating cell behaviour for the morphogenesis involved in the generation of 3D tissues and their alignment to form organs that give rise to the global 3D body shape in vertebrates. This will be done by analysing the mechanisms underlying the unique *hir* phenotype.

1.2 The role of the extracellular matrix in the formation of 3D organs

The ECM, a complex assembly of many proteins and polysaccharides forming the basement membrane and the interstitial matrix sites, serves as a scaffold for the generation of 3D tissues (Daley *et al*., 2008; Yamada and Cukierman, 2007). Integrin-mediated assembly of the ECM glycoprotein fibronectin (FN), into fibrils tethered to the cell surface is the most upstream event for assembling other ECM proteins (Figure 1.1) (Daley *et al*., 2008). Mechanical cues such as tissue tension are required for FN assembly (Singh *et al*., 2010), and the elaborate and dynamic 3D meshwork of ECM is constantly remodeled during development and varies between anatomical regions. It is thus essential to analyse intact animals and identify mutants affecting these processes in order to understand precisely how the ECM is assembled according to *in vivo* tissue tension, and the relationship between ECM formation and organ development.

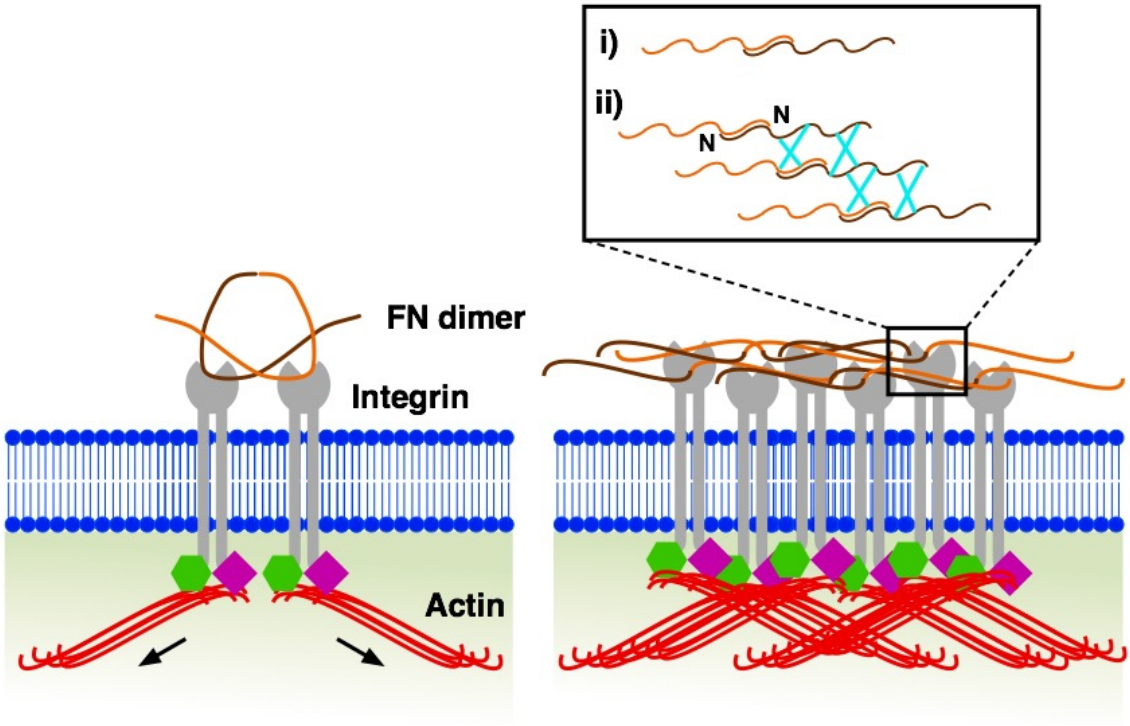

Figure 1.1. Schematic representing the process of fibronectin fibrillogenesis. Fibronectin (FN) fibrillogenesis can be seen as a stepwise process. Compact FN dimers (brown and orange) bind to integrins (grey). Intracellular proteins such as talin and vinculin (green hexagons and purple diamonds) are recruited to the cytoplasmic domains of integrins connecting them to the actin cytoskeleton (red). These connections increase contractility of the cell (black arrows) causing conformational changes in the extracellular bound FN. Clustering of integrins and the exposure of cryptic FN binding sites results in further FN-FN interactions which subsequently cause further FN conformational changes. These steps lead to the production of an insoluble and stable fibrillar matrix. The inset box highlights interactions between single subunits of FN dimers where N is the N-terminus. **(i)** End-to-end interactions between FN dimers which are mediated by the N-terminal assembly domain lead to the formation of fibrils. **(ii)** Fibrillisation is also mediated by the lateral association of fibrils (blue crosses). Adapted from Singh *et al*. (2010).

1.3 The role of forces in the formation and development of 3D organs

Analysis of forces *in vivo* is becoming possible due to advances in imaging, bioprobes and model animals, such as *Drosophila* and zebrafish (Heisenberg and Bellaïche, 2013). The mechanisms by which collective effects from the cumulative and combinatorial activities of local tissue deformations influence global tissue-scale deformations are beginning to be unraveled. Both exogenous global force application from adjacent tissues and mechanosensation within tissues appear to play decisive roles, although the precise molecular and cellular mechanisms underlying force

integration and mechanosensation within tissues are still not entirely clear. The analysis of actin-myosin dynamics in individual cells provides insights into how mechanical forces are locally generated and transmitted via cell-cell junctions to neighbouring cells. However, only the integration of these local forces into a global tissue force pattern determines the resulting changes in cell and tissue shape. How the overall function of actomyosin is regulated is still not well known. The mechanical information of individual cells is dynamic and can be influenced by many factors including architecture of the tissue and alignment of the tissue with other tissues. However, due to the lack of mutants in vertebrates, the presence of a key gene that integrates these complex processes for building 3D body shape has not previously been identified.

1.4 The discovery of the oncoprotein Yes-associated protein

Yes-associated protein (YAP) was first identified from chicken embryonic fibroblasts as a WW-domain protein that binds to the Src family kinase c-Yes via its SH3 binding motif (Sudol, 1994). YAP homologues have since been identified in mice and humans (Sudol *et al*., 1995b) and an orthologue (Yorkie, Yki) in *Drosophila* (Huang *et al*., 2005), as well as a mammalian paralogue called TAZ (transcriptional coactivator with PDZ-binding motif) (Wang *et al*., 2009). TAZ is also sometimes referred to as WWTR1. Thus, like the signalling pathway to which it belongs (Section 1.5.1), YAP is evolutionarily conserved. It has been generally shown that YAP has a role more in epithelium whereas TAZ is more mesenchymally expressed (Hong and Yaffe, 2006).

1.4.1 Yes-associated protein is a multifunctional adaptor protein with many functions

The human *YAP1* gene located on the 11q22 amplicon (Lamar *et al*., 2012), encodes the 504 amino acid YAP (Zhang *et al*., 2012), which is an adaptor protein with 6 protein-binding domains and a transcriptional activation (TA) domain (Figure 1.2). In medaka, *YAP1* is located on chromosome 13 and encodes a protein of 452 amino acids in length (www.ensembl.org). The protein binding domains within YAP include a TEAD binding domain (the main transcription factor partner for YAP), a 14-3-3 binding domain (involved in cytoplasmic sequestering of YAP, see Section 1.5.1), two WW domains which are central mediators of protein binding events in the Hippo pathway via interactions with proline-rich motifs (Cherrett *et al*., 2012), a SH3 domain and a PDZ domain (Sudol *et al*., 2012). The PDZ domain is important for YAP crosstalk with proteins involved in organ size regulation, including members of TGFβ signalling (PALS1, AMOT and PATJ) and the Wnt pathway (Dishevelled, Dvl) (Cherrett *et al*., 2012).

YAP is a 65kDa proline-rich phosphoprotein (Sudol *et al*., 1995a) that acts as a transcriptional co-activator. YAP positively regulates cell survival, growth and proliferation to orchestrate organ growth (Saucedo and Edgar, 2007). YAP is highly expressed in stem cells thus it may play a role in regulating the stem cell compartment especially as YAP activation can expand the population of multipotent undifferentiated progenitor cells in the small intestine (Camargo *et al*., 2007). Indeed, YAP has been shown to regulate the neural progenitor pool in multiple reports. In *Xenopus*, YAP overexpression expanded the *Pax3*$^{+}$ neural progenitor pool in conjunction with TEAD binding (Gee *et al*., 2011). Similar results were obtained in the neural tube of the chick where YAP overexpression induced *cyclin D1* causing accelerated proliferation and an increase in the number of Sox2^{+} progenitor cells (Cao *et al*., 2008).

YAP activity and location is regulated by its phosphorylation at various sites. Human YAP has five conserved HXRXXS motifs (H is histidine, R is arginine, S is serine) that are phosphorylated by LATS (Section 1.5.1) and studies have shown that these HXRXXS sites may differentially regulate YAP activity. For example, phosphorylation at Serine 127 (S127) inhibits YAP nuclear translocation by causing binding to 14-3-3 in the cytoplasm (Zhao *et al*., 2007). S381 phosphorylation has been shown to result in the ubiquitinaton and degradation of YAP (Zhao *et al*., 2010b). The functions of phosphorylation at the three other sites (S61, S109 and S164) by LATS (large tumour suppressor) remain unknown (Zhao *et al*., 2010b). However, mutation of all five phosphorylation sites from serine to alanine, completely preventing LATS phosphorylation and thus promoting nuclear localisation (called YAP5SA), produces a form of YAP that is more active in promoting cell proliferation than mutation of serine to alanine at just one site (YAPS127A), suggesting these other serine residues may have important roles for YAP activity (Zhao *et al*., 2009).

1.5 The Hippo signalling pathway is a key pathway regulating epithelial growth

The Hippo signalling pathway is regarded to be a major regulator of epithelial tissue and organ growth (Dong *et al*., 2007; Camargo *et al*., 2007), as well as tissue homeostasis during adult life, tissue regeneration and self-renewal of stem cells (Cherrett *et al*., 2012). The Hippo pathway is so-called due to the overgrowth phenotype caused by its deregulation (Section 1.5.1.2) and was initially known as the Salvador/Warts/Hippo (SWH) pathway due to the founding members. This pathway contains several tumour suppressor genes (Zhao *et al*., 2007) and these core components were uncovered in *Drosophila melanogaster* during loss-of-function genetic screens for regulators of tissue growth (Udan *et al*., 2003). The pathway does however, exhibit high levels of conservation within mammals (Saucedo and Edgar, 2007). In 2007, YAP was found to be a downstream component of the Hippo pathway acting as a nuclear executor of the upstream inputs (Zhao *et al*., 2007).

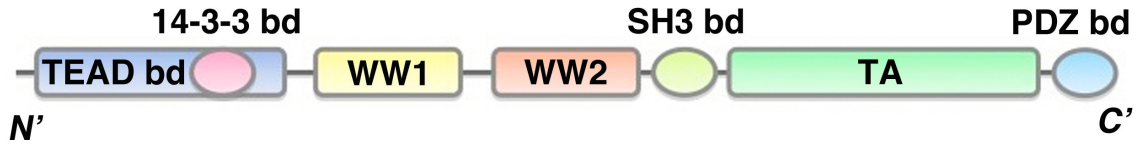

Figure 1.2. Schematic representation of the different domains of the YAP protein. TEAD bd: TEAD binding domain, TEAD1-4 are the main transcription factor partners for YAP; 14-3-3 bd: 14-3-3 binding domain, important for sequestering YAP in the cytoplasm when phosphorylated; WW1 and WW2: tryptophan-tryptophan residues that bind to PPxY motifs that are found in the Smads, Dvl, p73 and LATS1/2 (Cherrett *et al*., 2012); SH3: SRC Homology 3 domain; TA: transcription activation domain; PDZ bd: PDZ binding domain, important for YAP crosstalk with proteins involved in organ size regulation (Cherrett *et al*., 2012).

1.5.1 Components of the mammalian Hippo signalling pathway

The core Hippo pathway consists of several serine-threonine kinases (Figure 1.3), which act to negatively regulate the nuclear executors of the pathway, YAP or TAZ. This kinase cascade is proposed to extend from the cell membrane through the cytoplasm and into the nucleus. Many of the components of Hippo signalling have WW domains that bind to PPxY domains in other proteins (Cherrett *et al*., 2012). Core components of the Hippo mammalian pathway (Figure 1.3) include the MST (mammalian sterile 20-like) 1/2 kinases, each autophosphorylating its activation loop, and then consequently phosphorylating and forming an active complex with Sav1. Once complexed with Sav1, MST1/2 can phosphorylate the LATS (large tumour suppressor) 1/2 kinases and their co-activator MOB1 (Cherrett *et al*., 2012). LATS1 or LATS2 subsequently phosphorylates YAP at S127. This step is crucial in the regulation of YAP since phosphorylation enables 14-3-3 proteins to bind and sequester YAP in the cytoplasm (Figure 1.3). The Hippo pathway has been shown to be more complex in vertebrates than in *Drosophila*. The core components in *Drosophila*, with vertebrate homologues also shown in parentheses, include Hippo (MST1/2), Sav (Sav1), Warts (LATS1/2), MATS (MOB1) and Yorkie (YAP/TAZ) (Cherrett *et al*., 2012).

When not phosphorylated (i.e. when the Hippo pathway is not active), YAP translocates into the nucleus where it indirectly binds DNA mainly through the TEAD family of transcription factors. Since YAP/TAZ do not contain DNA-binding domains they must initiate transcription of target genes by partnering with DNA-binding proteins (Figure 1.3) (Cherrett *et al*., 2012). YAP has been shown to bind and regulate several transcriptional regulators such as p53-binding protein-2 (Espanel and Sudol, 2001), p73 (Strano *et al*., 2005), as well as the TEA domain-containing (TEAD1-4) transcription factors (Vassilev *et al*., 2001) and the SMADs (Section 1.6). YAP

regulation of organ growth is mediated by binding to the TEAD family of transcription factors as this activates transcription of genes involved in proliferation, survival and differentiation as well as morphogenesis (Saucedo and Edgar, 2007). Each TEAD transcription factor (1-4) exhibits a marginally different expression pattern with regards to location and timing during development (Cherrett *et al*., 2012), suggesting this may enable YAP to function slightly differently within different tissues and at different developmental times. Target genes that are transcribed when YAP translocates to the nucleus include *Ctgf* (connective tissue growth factor), *Areg* (amphiregulin), *Ankrd1* (ankyrin repeat domain 1) and *CYR61* (cysteine-rich angiogenic inducer 61) amongst others. The expression levels of these genes are often used as a readout for the transcriptional activity of YAP (Aragona *et al*., 2013).

Although YAP was initially described to only have a role in the nucleus there are now an increasing number of reports showing YAP also functions within the cytoplasm. For example, when phosphorylated, YAP can be sequestered at adherens junctions by α-catenin and this has been termed the non-canonical Hippo pathway (Schlegelmilch *et al*., 2011). However, this regulation of YAP appears to be specific to the skin in mice as well as cell-density dependent. YAP is also regulated by tight junctions where it can bind Angiomotin of the Crumbs complex (Varelas and Wrana, 2012, Section 1.5.1.1).

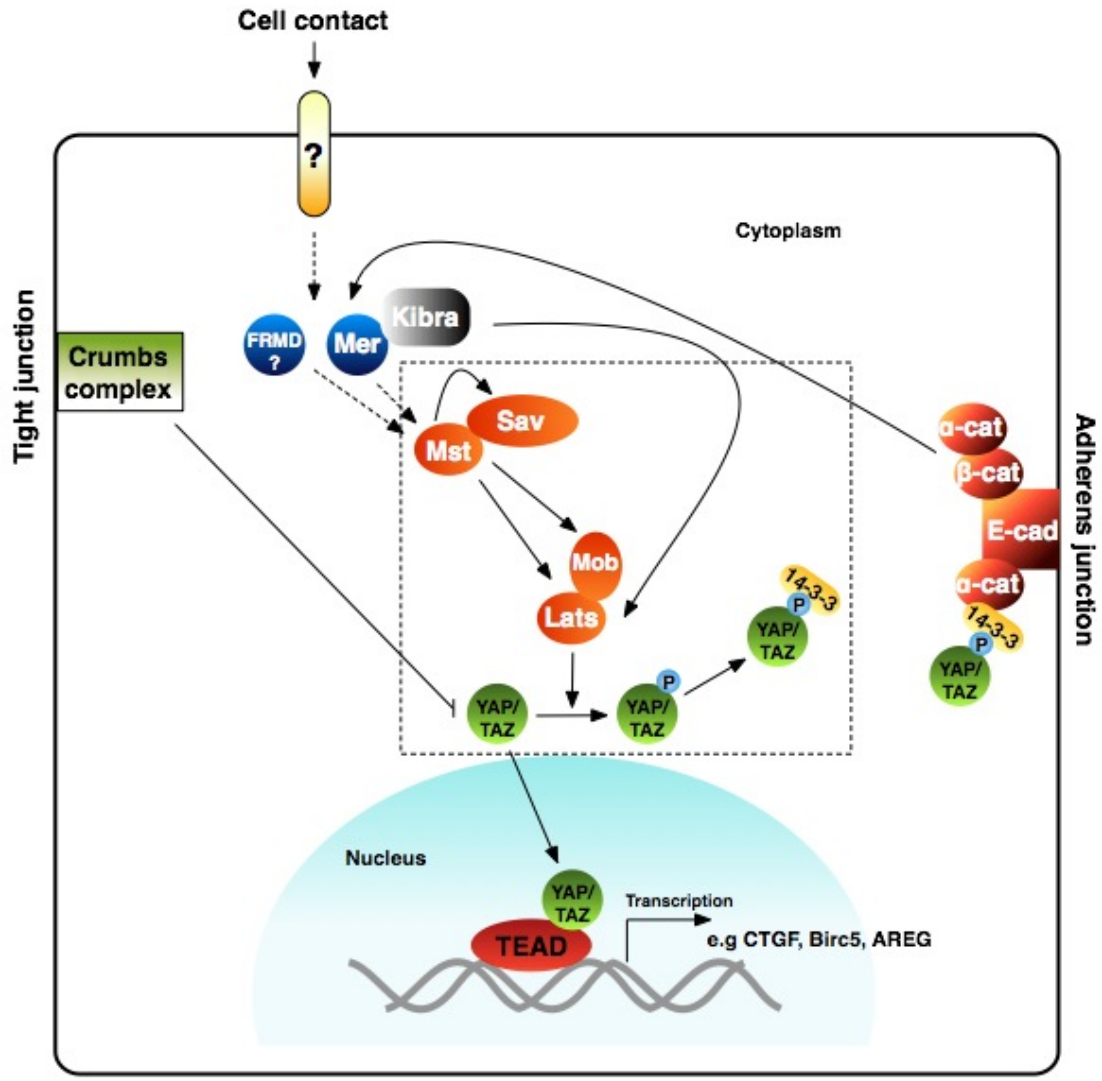

Figure 1.3. The mammalian Hippo pathway. The Hippo pathway is a serine/threonine kinase cascade and the core components of the pathway are contained within the dashed box. YAP/ TAZ is the nuclear executor of the pathway and exerts its function by shuttling into the nucleus where it indirectly binds DNA via various transcription factors to activate transcription of various target genes. The upstream components of the pathway serve to negatively regulate YAP/TAZ by phosphorylation which results in the cytoplasmic sequestering of YAP/TAZ. Recent reports have shed light on other factors that can regulate YAP/TAZ, such as interactions with the Crumbs complex at tight junctions and α-catenin at adherens junctions. This simplified diagram represents the complex and seemingly multi-layered regulation of YAP that is important to ensure epithelial growth is tightly maintained. Dashed arrows represent unknown mechanisms, and question marks indicate unconfirmed members of the pathway.

1.5.1.1 Additional members of the Hippo pathway

There has been significant interest in the upstream regulators/inputs that activate Hippo signalling. Recently, many additional components of the Hippo pathway have been uncovered giving clues as to how cells may sense when to stop growing via extracellular/inter-cellular cues and activate the Hippo pathway to suppress growth. For example, in *Drosophila*, the tight junction-associated Crumbs (Crb) complex regulates Expanded (Ex, Parsons *et al*., 2010), which itself is an upstream regulator of the Hippo pathway. Furthermore, the Crb complex can also directly regulate the nuclear translocation of YAP, inhibiting this movement when there is high cell density (Figure 1.3). The transmembrane protein E-cadherin that is an essential component of adherens junctions can also regulate Hippo signalling. This regulation occurs during contact inhibition, which prevents cellular proliferation when confluence is reached. E-cadherin recruits β-catenin to the membrane and in turn β-catenin activates the Hippo pathway by interacting with Merlin/neurofibromin (Mer/NF2, Figure 1.3) (Kim *et al*., 2011). Furthermore, when phosphorylated, YAP can be sequestered at adherens junctions by α-catenin and this has been termed the non-canonical Hippo pathway (Schlegelmilch *et al*., 2011). These extra members of the pathway are not necessarily considered core members and may only function under certain conditions or in specific tissues. Further work is needed to fully characterise all of the upstream regulators and inputs of the Hippo pathway as this knowledge will be of paramount importance for the modulation of this important signalling pathway.

1.5.1.2 The Hippo pathway in organ size regulation

The Hippo pathway regulates organ growth by balancing the processes of cell proliferation, survival, differentiation and polarity (Cherrett *et al*., 2012). Deregulation of the Hippo pathway has been shown to cause organ overgrowth in many scenarios. Overexpression of YAP using the hyperactive S127A form specifically in the liver using the ApoE promoter and Tet-on (Doxycycline-inducible) system caused a 4-fold increase in liver size in just 4 weeks (Figure 1.4) (Dong *et al*., 2007). Interestingly, the 4-fold increase in size after 4 weeks was reversible with removal of Doxycycline from the drinking water, taking around 2 weeks to return to normal size. When the core Hippo pathway proteins MST1/2 and Sav1 were knocked out in mouse livers, essentially creating the same effect as upregulating YAP since these negative regulators are no longer present, the organs were also observed to be significantly larger than those of wild-type mice (Zhou *et al*., 2009; Lu *et al*., 2010; Song *et al*., 2010; Lee *et al*., 2010). Furthermore, an enlarged heart phenotype has also been reported in Sav1-knockout mice, which was caused by an increase in cardiomyocyte proliferation (Heallen *et al*., 2011). Such organ enlargement has also been observed in *Drosophila* heads and imaginal discs (Kango-Singh *et al*., 2009). Importantly in all cases of overgrowth, the architecture of the organ in question appeared normal.

There is also evidence that aberrant signalling via the Hippo pathway can result in mammalian carcinogenesis. Constitutive overexpression of YAP using S127A specifically in the liver using the ApoE promoter and Tet-on system caused tumorous nodules within 8 weeks, followed by severe hepatocellular carcinoma after 12 weeks of overexpression (Figure 1.4, Dong *et al*., 2007). Moreover, the liver-specific deletion of MST1/2 or Sav1 has been shown to provoke multi-focal tumourigenesis (Lu *et al*., 2010; Song *et al*., 2010; Lee *et al*., 2010). In immortalised mammary and pancreatic epithelial cells, YAP/TAZ overexpression has been shown to cause epithelial-mesenchymal transition (EMT, Varelas *et al*., 2010b), which is an essential process in development but is also deregulated in cancer when metastasis occurs. Finally, mutations in components of the Hippo pathway, including NF2, LATS1/2, MST1/2, WW45, MOB, and KIBRA, have been reported in multiple human cancers including: breast cancer; soft tissue sarcoma; melanoma; colorectal cancer; ovarian carcinoma; retinoblastoma; astrocytoma; and neurofibromatosis type 2 (Pan, 2010; Zhao *et al*., 2010a; Bao *et al*., 2011; Hill *et al*., 2011).

1.6 Crosstalk between Hippo signalling and other pathways

The structure of YAP suggests it may coordinate/engage multiple signalling networks. Indeed, YAP and Hippo signalling have now been shown to interact with many signalling pathways including members of the canonical Wnt pathway (β-catenin and Dishevelled, Dvl), BMP/TGFβ signalling, JAK/STAT signalling, Notch signalling, PI3K/Akt signalling, Shh signalling (all reviewed in Cherrett *et al*., 2012) as well as G-protein-coupled receptor (GPCR) signalling (Yu and Guan, 2013). Many of these pathways are essential during development and the crosstalk occurs in both the cytoplasm and nucleus. Since several of these pathways are implicated in organ formation, their interactions with Hippo signalling will now be briefly discussed. The Hippo pathway can inhibit Wnt/β-catenin signalling through the binding of phosphorylated YAP/TAZ with Dvl in the cytoplasm (Varelas *et al*., 2010a). This in turn means Dvl is not phosphorylated and cannot inhibit formation of the β-catenin destruction complex. Consequently β-catenin is phosphorylated and targeted for ubiquitination and proteosomal degradation instead of translocating into the nucleus to activate transcription of Wnt target genes. This interaction between Hippo and Wnt signalling may be important for controlling tubulogenesis in epithelial organs such as the kidney, gut, lung and mammary gland (Bernascone and Martin-Belmonte, 2013). YAP can also interact with β-catenin in the nucleus to induce the expression of Wnt and Hippo target genes (Bernascone and Martin-Belmonte, 2013). This YAP-β-catenin complex has been shown to upregulate *Sox2* and *Snai* genes causing an increase in heart size (Heallen *et al*., 2011).

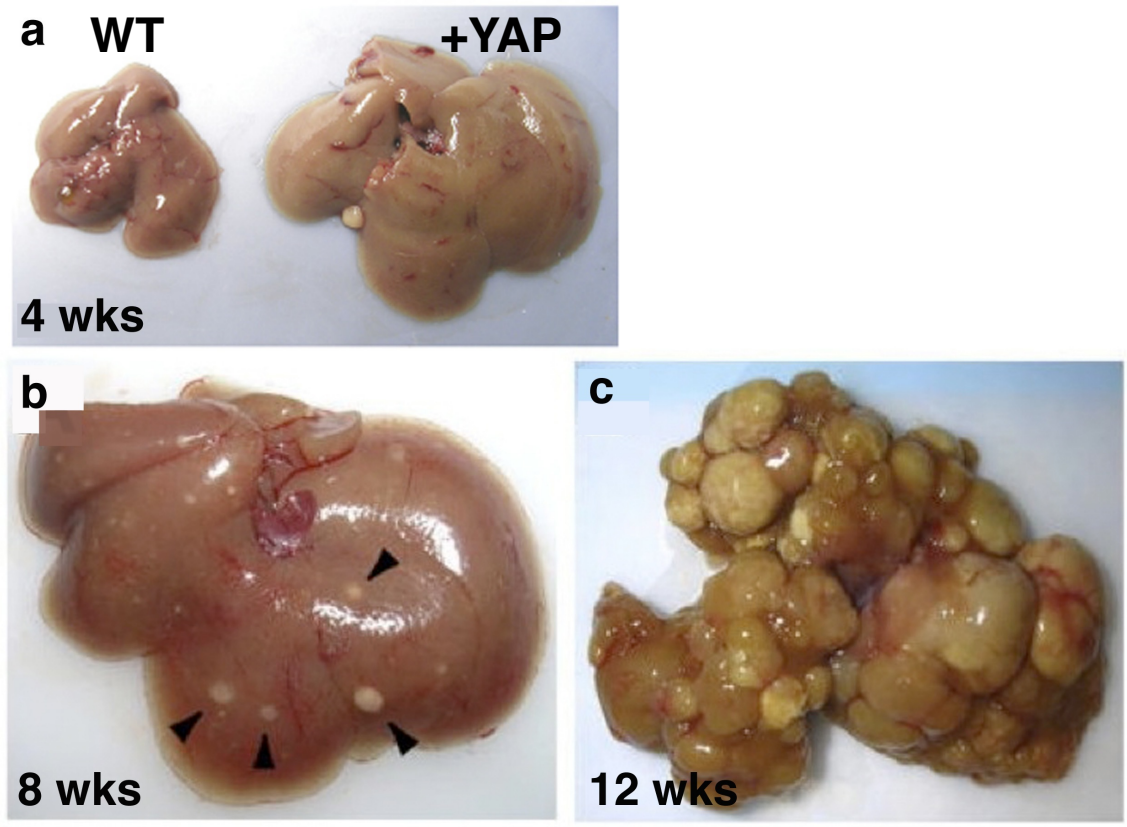

Figure 1.4. YAP overexpression can drastically and rapidly enlarge the liver in mouse, eventually causing cancer. (a) After 4 weeks of YAP overexpression the liver has increased in size approximately 4-fold when compared to the control on the left. **(b)** Following 8 weeks of overexpression, tumorous nodules begin to appear (arrowheads). **(c)** By 12 weeks of overexpression there is widespread and severe hepatocellular carcinoma. Adapted from Dong *et al*. (2007).

Hippo signalling can also inhibit TGFβ (transforming growth factor β) and BMP (bone morphogenetic protein) signalling (Varelas *et al*., 2010b). TGFβ/BMP signalling is involved in a wide range of tissues and organs regulating processes such as bone and cartilage induction as well as development of the kidney, skin and muscle along with vascular homeostasis (Miyazono *et al*., 2009). When TGFβ or BMP interact with their respective membrane-bound receptors, Smad proteins in the cytoplasm are activated by phosphorylation and translocate to the nucleus forming transcription factor complexes. Nuclear Smad2/3 (activated by TGFβ receptors) can complex with YAP/ TAZ to upregulate genes that promote EMT (Varelas *et al*., 2010b). By complexing, Smad2/3 proteins are prevented from translocating back to the cytoplasm. Furthermore, if the Hippo pathway is activated, Smad2/3 proteins that are YAP/TAZ-

bound will then be cytoplasmically sequestered so that transcription of TGFβ/BMP target genes does not occur. Similar regulation occurs with the Smad1/5/8 proteins, which are activated by BMP receptors. Finally, Notch signalling is normally activated by the ligand Delta. Nuclear Yki (*Drosophila* orthologue of YAP) inhibits Delta leading to an inhibition of Notch activation (Reddy *et al*., 2010).

The JAK/STAT, Shh and PI3K/Akt pathways all inhibit Hippo signalling resulting in the increased nuclear localisation of YAP (Karpowicz *et al*., 2010; Fernandez *et al*., 2009; Yuan *et al*., 2010). In *Drosophila*, nuclear Yki causes transcription of cytokines that promote JAK/STAT signalling following injury. Expression of *YAP1* mRNA is upregulated by Shh signalling, which also stabilises IRS1 (insulin receptor substrate 1). IRS1 acts as a nuclear retention factor for YAP. Shh signalling also results in decreased levels of phosphorylated LATS. Akt phosphorylates MST1 at a highly conserved Threonine 120 residue. This prevents the kinase activity of MST1, which is normally regulated by phosphorylation of Threonine 183. Therefore subsequent activation of more downstream components of the Hippo pathway does not occur meaning YAP is not phosphorylated.

Finally, GPCR signalling may allow the regulation of YAP/TAZ by diffusible signals such as growth factors. To date, none of the very well known growth factors such as EGF (epidermal growth factor) or insulin have been shown to affect YAP/TAZ nuclear localisation (Yu and Guan, 2013). Instead, other diffusible factors such as LPA (lysophosphatidic acid) and S1P (sphingosine-1-phosphate) can activate YAP/TAZ by binding their corresponding GPCRs to signal through Rho GTPase (Yu and Guan, 2013). Furthermore, epinephrine, glucagon, and a dopamine receptor can inhibit YAP/TAZ activity as can dobutamine, showing GPCR signalling can positively or negatively affect YAP/TAZ (Yu and Guan, 2013). Since GPCRs are the largest family of plasma membrane receptors, this suggests that GPCRs may play an important role in finely adjusting YAP/TAZ activity depending on both the cell type and the extracellular environment of the cell (Yu and Guan, 2013). This in turn may allow distinct control of facets such as cell survival, proliferation, and tissue growth depending on the situation.

1.7 Medaka and zebrafish as model organisms

The choice of appropriate strain/genetic background is crucial to reveal the phenotype of mutant animals, mainly due to the divergence of functional overlap between the vertebrate strains. Zebrafish (*Danio rerio*) and medaka (*Oryzias latipes*), the embryos of which develop in a similar manner, can be used as one animal model with divergent genetic backgrounds that allow identification of new phenotypes/gene functions (Furutani-Seiki and Wittbrodt, 2004). Almost twenty years ago the results of the systematic mutant screen in zebrafish were published (Haffter *et al*., 1996). A

phenotype-driven mutagenesis screen was also carried out in medaka some years later for mutations affecting a diverse array of developmental processes (Furutani-Seiki *et al*. 2004). Systematic comparison of mutant phenotypes of medaka and zebrafish (Haffter *et al*. 1996; Furutani-Seiki *et al*., 2004) identified many new phenotypes by virtue of rapid independent evolution of duplicated genes in their ancestor. During eye development, for example, the *rx* genes (*rx1-3*) are expressed in an overlapped manner in zebrafish but in a non-overlapped manner in medaka, allowing further dissection of the components of relevant signalling pathways in medaka (Furutani-Seiki and Wittbrodt, 2004).

1.7.1 Medaka as a model organism

Medaka are a freshwater teleost fish native to SE Asia and as such tolerate a varying range of temperatures and salinity (Wittbrodt *et al*., 2002). The medaka fish has been an emerging model vertebrate system over the last twenty years or so and in many ways is complementary to the zebrafish (Wittbrodt *et al*., 2002; Furutani-Seiki and Wittbrodt, 2004). It is particularly useful for sex-determination studies (Matsuda *et al*., 2002), toxicology testing (Metcalfe *et al*., 2001) and developmental genetics studies (Furutani-Seiki and Wittbrodt, 2004). This is in part due to its transparency during embryonic stages and a relatively small genome (≈800Mb). The development of strains that maintain this transparency into adulthood (e.g. Wakamatsu, 2001) has meant non-invasive studies charting molecular and morphological events can be continued for the duration of the teleost's life. In such a context, the medaka serves as a very powerful model organism for *in vivo* imaging. This is coupled with its established physiology (Figure 1.5), relative ease of handling and developing genetic toolkit (Wittbrodt *et al*., 2002). With a draft genome sequence published (Kasahara *et al*., 2007) alongside the many mutant phenotypes already identified (Furutani-Seiki *et al*., 2004), this vertebrate is becoming ever more useful as a model organism for areas such as carcinogenesis research (Law, 2001) as well as regeneration studies (e.g. Katogi *et al*., 2004). Furthermore, it can faithfully model human disorders, for example polycystic kidney disease (Mochizuki *et al*., 2005).

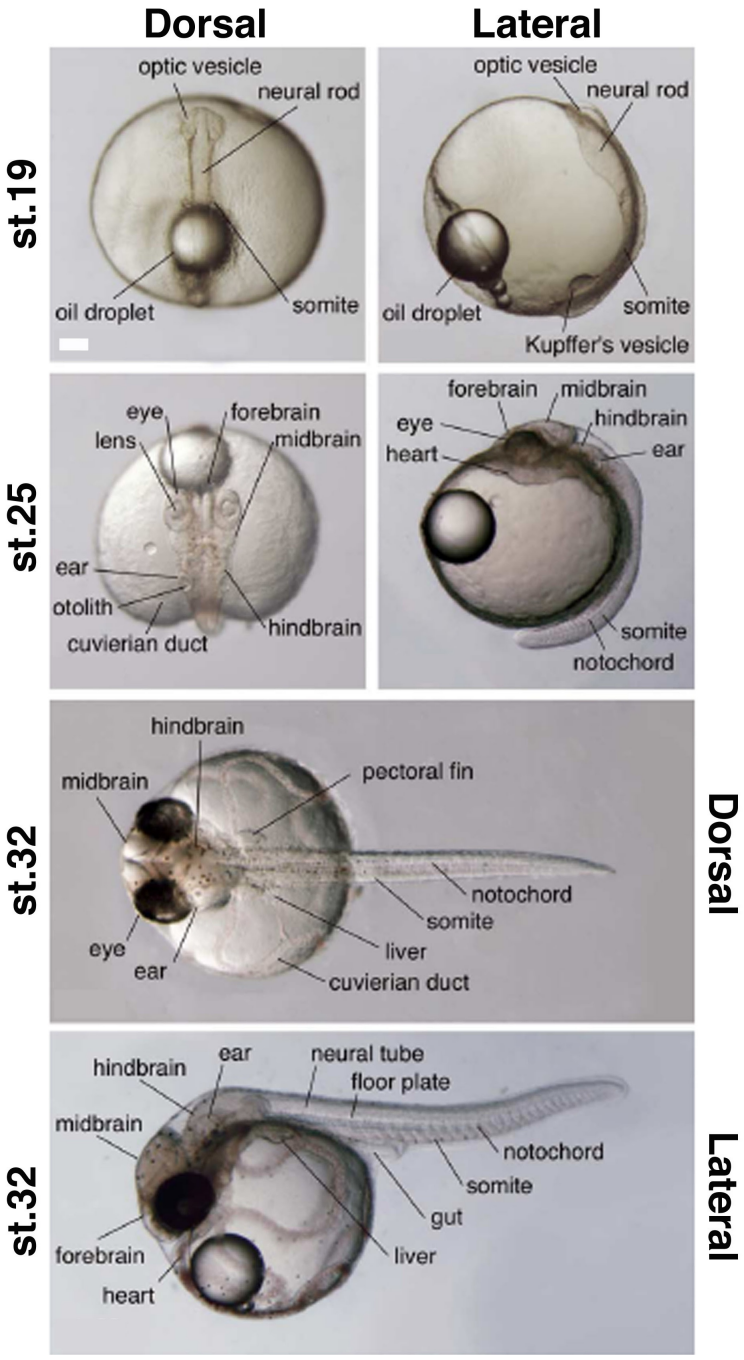

Figure 1.5. Medaka as a vertebrate model organism. This teleost is a powerful organism for imaging. Scale bar: 200µm. Adapted from Furutani-Seiki *et al*. (2004). Shown are key physiological features. st.19 = 27.5 hpf, st.25 = 50 hpf, st.32 = 101 hpf.

1.7.1.1 The medaka mutant screen and the identification of *hirame*

Genetically defined alterations in gene loci, or mutants, especially those with phenotypic outcomes, are one of the most important tools for obtaining insights into the function of genes at the whole-organism level (Porazinski *et al*., 2011). Systematic phenotype-driven mutant screens involve the generation of mutants by random

mutagenesis of the genome followed by screening for the phenotype affecting the process of interest. The advantage of using mutagenesis is that it identifies the relatively small fraction of genes with unique and at least partially non-redundant functions (Haffter *et al*., 1996). Thus, the phenotype-driven screen is an unbiased approach to elucidate gene function (Porazinski *et al*., 2011). Conversely, a gene-driven approach to remove the function of particular genes (i.e. knockout mutants) provides a complementary method. In systematic unbiased mutant screens, mutants are classified according to phenotypes, and the genes required for each class of mutants are defined by genetic complementation analysis. The value of phenotype-oriented mutant screens are that they systematically dissect the biological processes into genetically defined steps, i.e. phenotypic classes, and the genes required for each step can be identified (Porazinski *et al*., 2011). In vertebrates, systematic mutant screens have been carried out in two teleost fish species, zebrafish (Haffter *et al*., 1996) and medaka (Furutani-Seiki *et al*., 2004), as well as in the mouse (Hrabe de Angelis *et al*., 2000; Nolan *et al*., 2000a; Nolan *et al*., 2000b).

In the medaka mutant screen, mutations were introduced into the germ line by treating male founder adult fish with ENU (N-ethyl-N-nitrosourea). ENU introduces point mutations very efficiently and randomly in spermatogonia (Russell and Montgomery, 1982) making it an ideal chemical for such screens. This was followed by a three-generation in-crossing scheme to generate F3 embryos homozygous for mutations induced in founder males (Figure 1.6) (Furutani-Seiki *et al*., 2004). Amongst the 2031 embryonic lethal mutations identified, 312 that caused defects in organogenesis were further analysed. From these, 126 mutations were characterised genetically and assigned to 105 genes (Furutani-Seiki *et al*., 2004). Mutants included those affecting the forebrain, somites, eyes, thymus, liver, gonad, lateral line and primordial germ cells. Interestingly, many of the mutations in medaka caused unique phenotypes previously unrecorded in zebrafish (Haffter *et al*., 1996; Furutani-Seiki *et al*., 2004). Furthermore, even when mutations in the two fish species caused a similar phenotype (e.g. one-eyed-pinhead or parachute), more genes were found in medaka that produced the same phenotype when mutated (Furutani-Seiki *et al*., 2004). An extremely important mutant to come out of this screen was *hirame* (*hir*) and this mutant was classed as one where tissue organisation was affected (Furutani-Seiki *et al*., 2004). Positional cloning identified a non-sense point mutation in the sequence encoding the WW1 domain of the YAP protein in *hir* mutants (at Leucine 164, TTG to TTA - stop codon), producing a truncated product that is assumed to be non-functional and targeted for degradation (Makoto Furutani-Seiki, *personal communication*). The *hir* mutants displayed a markedly flattened body where tissues and organs were misaligned (Figures 1.6 and 3.2). Up to mid-neurulation at stage 21 (st.21), 34 hours post fertilisation (hpf), patterning of *hir* mutant embryos along the antero-posterior (A-P) and dorso-ventral (D-

V) axes was normal. From st.21 (34 hpf), the body of the *hir* mutant embryos gradually collapsed (Figure 3.2). However, they survived until just before hatching at 6 days post fertilization (dpf) allowing detailed analysis of organogenesis.

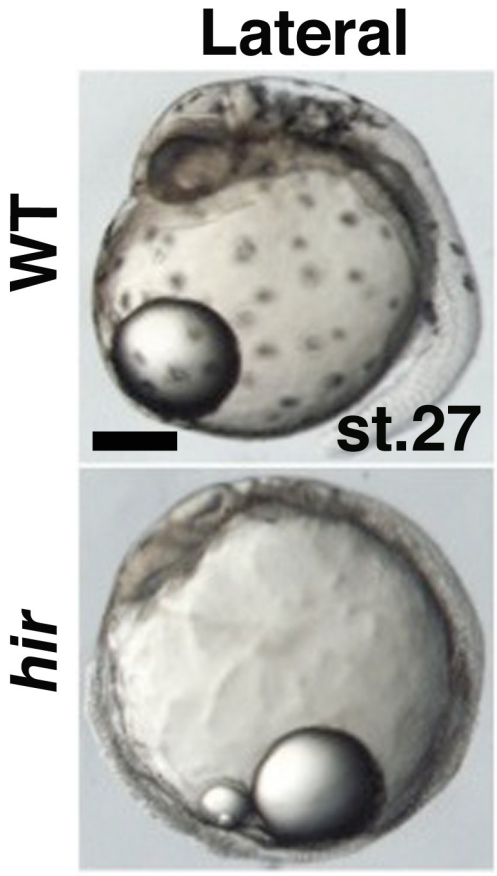

Figure 1.6. The flattened *hirame* phenotype. The *hir* mutants display a markedly flattened body where tissues and organs are misaligned. Anterior is to the left. Scale bar: 150μm.

In vertebrates however, the use of a single species to perform gene loss-of-function analysis will not be sufficient to uncover all gene functions for several reasons, including: (1) functional overlap exists amongst related genes; (2) the manner of development for the analysis of phenotypes, e.g. accessibility of an embryo that allows identification of dynamic phenotypes; (3) repeated use of the same gene during development – early lethality due to the early requirement of a gene means later phenotypes may not be detected; (4) species-specific differences in gene function due to changes in the nature of interacting partners, such as is seen in signalling cascades (Loosli *et al*., 2003).

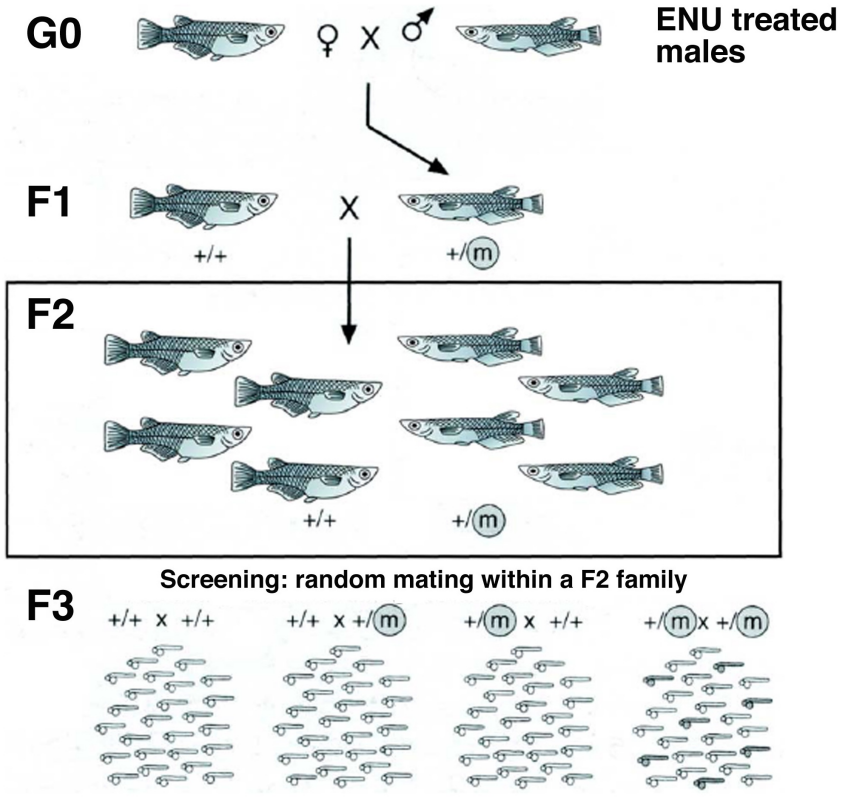

Figure 1.7. Screening approach used in the genome-wide screens in medaka and zebrafish. After treatment with ENU, males were mated with wild-type females to produce F1 progeny. These are heterozygous carriers of mutations derived from the mutagenised paternal genome. By mating many F1 fish, F2 families are generated and a mutation, m, in a F1 parent is transmitted to one-half of the F2 families. Random sibling mating within the F2 family then produces homozygotes for the mutation at a 25% frequency assuming Mendelian inheritance. Adapted from Furutani-Seiki *et al*. (2004) and Haffter *et al*. (1996).

1.7.2 Zebrafish as a model organism

Zebrafish share many of the advantageous characteristics that make medaka a powerful model organism. These include a transparent body and external development of eggs; high fecundity; fast development; transgenic strains; a fully sequenced genome and easy experimental manipulation amongst others (Furutani-Seiki and Wittbrodt, 2004).

1.7.2.1 The zebrafish mutant screen

The systematic mutant screen in zebrafish using ENU identified over 4,200 mutants of which 1163 were characterised. Mutants displayed defects in early development (e.g. epiboly), notochord, brain, spinal cord, somites, muscles, heart, circulation, blood, skin,

fins, eyes, otic vesicle, jaw and branchial arches, pigment patterning, pigment formation, gut, and liver amongst others (Haffter *et al*., 1996).

1.7.3 Medaka and zebrafish are complementary model organisms for gaining insights into the function of the vertebrate genome

Following the genome-wide large-scale mutagenesis screens in medaka and zebrafish, there is accumulating evidence that the use of two fish species facilitates the discovery of novel phenotypes (Loosli *et al*., 2003; Furutani-Seiki *et al*., 2004). A duplication of the genome occurred in the ancestor of teleosts around 350 million years ago (mya). Medaka and zebrafish were separated from their last common ancestor 110-160 mya (Wittbrodt *et al*., 2002). The generation of two functionally equivalent genes (paralogues) by this genome duplication facilitated rapid evolution resulting in three fates based on the duplication-degeneration-complementation (DDC) model (Force *et al*., 1999): (1) one of the paralogues lost its function (dis-functionalisation); (2) one paralogue acquired a new function (neo-functionalisation); or (3) the paralogues divided the function of the ancestral gene (sub-functionalisation) (Ohno, 1970).

Thus, the analysis of medaka and zebrafish allows functions unidentifiable in one species to be uncovered in the other for the following reasons: (1) phenotypes masked by the redundancy between genes can be visible in another species in the case of dis-functionalisation; (2) phenotypes of later functions normally masked by early lethality of the embryo due to early gene function can be seen if the early and late functions have been divided between the paralogues by sub-functionalisation. This sub-functionalisation is likely to be different in different teleost species; (3) new phenotypes can be detected for the gene generated by neo-functionalisation (Porazinski *et al*., 2011). Analysis of mutant phenotypes in medaka and zebrafish as well as functional and evolutionary interpretation is relatively straightforward, since medaka and zebrafish embryos develop in a similar manner. Divergent phenotypes between the two species may also be due to differences in the way the phenotype manifests. This may be due to factors such as visibility of the target organ and physiology. For example, in live embryos, the liver is more prominent in medaka than in zebrafish, whereas the opposite is true of the notochord (Porazinski *et al*., 2011). Furthermore, medaka and zebrafish have several species-specific features that are amenable to genetic studies. Two particularly good examples of such features are sex determination (Schartl, 2004) and adult pigment patterning (Odenthal *et al*., 1996), which are best studied in medaka and zebrafish, respectively (Furutani-Seiki and Wittbrodt, 2004).

Among the vertebrate model organisms, medaka and zebrafish complement the mouse in genetically dissecting vertebrate development and organogenesis for several reasons, including: (1) observation of development at multiple points facilitates isolation

of mutants, since phenotypic manifestation can be dynamic. The transparent bodies and external development of fish embryos allows observation of dynamic cellular behaviours underlying development throughout the life-cycle; (2) unlike mouse embryos, fish embryos with compromised circulation or aberrant development can survive for longer allowing isolation of mutants that might otherwise be missed. This is exemplified by the large number of zebrafish heart mutants (Stainier *et al*., 1996); (3) embryos with weaker phenotypes than null-mutants survive for longer and often allow discovery of later phenotypes. Such weaker phenotypes can be generated by chemical mutagens that induce point mutations or anti-sense morpholino oligonucleotides (Porazinski *et al*., 2011); (4) the presence of maternal RNA in fish embryos also prevents early lethality of mutants during gastrulation. Zygotic mutant embryos survive longer in the presence of normal maternal RNA provided by the mother, even if zygotic transcription that starts after the 1,000-cell blastula stage is compromised (Porazinski *et al*., 2011).

Overall development in zebrafish proceeds much faster than in medaka. Therefore the timing of hatching is different between the two species; medaka embryos hatch from their chorion in 7 days and immediately start to swim and eat, whereas zebrafish embryos hatch in 2 days but do not start to swim and eat until 5–6 days (Porazinski *et al*., 2011). Consequently, the developmental timing of appearance of organs/tissues is slightly different in medaka when compared with zebrafish, i.e. in medaka somitogenesis occurs after the onset of brain development whereas in zebrafish somitogenesis precedes brain development (Furutani-Seiki and Wittbrodt, 2004). An overview of some of the common similarities and differences between medaka and zebrafish is shown in Table 1.1.

1.8 General aims of this work

In order to play a key regulatory role for organ size, YAP would need to orchestrate many different cell behaviours, especially since organ expansion via YAP overexpression occurs whilst appearing to maintain the complex architecture of the organ in question. These processes might include cell migration, cell-cell interactions and cell-ECM interactions for example, since these processes are essential to transform a 2D tissue into a 3D organ with distinct form and function. It is not currently known how YAP may regulate these activities. Therefore, the major aim of this work is to elucidate how YAP might be regulating organ size *in vivo* by orchestrating single-cell behaviour. Loss-of-function analysis in the *hir* mutant will be used to achieve this goal. Within each chapter, the specific aims to address the major objectives of that chapter will be described.

Characteristic/Feature	Zebrafish	Medaka
Generation time	10 weeks	8 weeks
Temperature range for development	25-33°C	4-35°C
Overall development	Fast	Slower
Hatching	2 days	7 days
Swimming	5 days	7 days
Embryo	Hardy	Softer
Sex determination	Unknown	XY chromosomes
Inbred strains	No	15 strains
Genome size	1,700 Mb	800 Mb
Genetic polymorphisms	Low (<1/1,000 bp)	High (1/100 bp)
Transgenesis	Yes	Yes
Morpholino knockdown	Yes	Yes
Manipulation of embryos	Simpler	More involved

Table 1.1 A comparison of features to be considered when working with medaka and zebrafish in a single laboratory. In order to successfully utilise these two vertebrate fish species as complementary models it is important to consider their similarities and differences. Table adapted from Porazinski *et al*. (2011).

Chapter 2: Materials and methods

2.1 Fish husbandry

Medaka and zebrafish strains were grown and stored in the fish facility at the University of Bath according to Home Office regulations. Fish were exposed to a 14-hour light and 10-hour dark cycle at 24°C.

2.1.1 Medaka strains used

Embryos of the Kyoto-Cab inbred medaka (*Oryzias latipes*) strain (Furutani-Seiki and Wittbrodt, 2004) were used for all experiments. To visualize the heart, the *cmcl2*::*EGFP* transgenic medaka line was used which expresses enhanced green fluorescent protein (EGFP) in cardiac cells including their progenitors. To observe Cuvierian duct (CD) formation the transgenic *fli::EGFP* strain was utilised which expresses EGFP in endothelial cells including progenitors. The YAP mutant strains *hirame*$^{54\text{-}20C}$, *hirame*$^{54\text{-}20C}$ *cmlc2*::*EGFP* and *hirame*$^{54\text{-}20C}$ *fli*::*EGFP* were employed for the loss of function analyses. The *fli::EGFP* strain was used to precisely evaluate the rescued mutant phenotype following transplantation experiments (Section 2.7).

2.1.2 Zebrafish strains used

Embryos of the Ab strain were used for all zebrafish (*Danio rerio*) experiments. To visualise the enveloping layer (EVL) of zebrafish embryos undergoing gastrulation, transgenic lines of *utrophin::mcherry* and *utrophin::EGFP* were utilised, which label actin with cherry and EGFP respectively. To enable observation of the actomyosin ring for laser ablation experiments and assessment of cortical tension, transgenic embryos of the *actb1::myl12.1::eGFP* line were used which labels actomyosin with EGFP. Finally, to allow visualisation of both actin and myosin simultaneously for EVL time-lapse and epiboly analysis, embryos of the *myl::EGFP-utrophin::mcherry* transgenic line were used. All of the transgenic zebrafish lines listed here were kindly supplied by the fish facility at IST Austria.

2.1.3 Incubation and staging of embryos

After collection and cleaning, fertilised eggs were incubated in 5cm petri dishes (Sterilin Ltd., UK) containing embryo medium for medaka embryos (NaCl 251.4mM, KCl 8.5mM, $CaCl_2 \cdot 2H_2O$ 16.5mM, $MgSO_4 \cdot 7H_2O$ 16.5mM) at 27°C to enable development to the required stage. For zebrafish, embryos were raised in E3 medium (5mM NaCl, 0.17mM KCl, 0.33mM $CaCl_2$, 0.33mM $MgSO_4$, adjusted to pH 7.2 with NaOH and autoclaved) and were kept at 25-31°C due to their tropical nature. Embryos were staged using either medaka developmental staging tables (Iwamatsu, 2004) or zebrafish staging tables (Kimmel *et al*., 1995).

2.2 cDNA cloning and construction

Total RNAs were converted to cDNA using an RNA-PCR kit ver.3 (Takara Bio, Japan) followed by PCR using KOD plus polymerase (Toyobo, Japan). Partial cDNAs of *Sox3* and *delta-crystallin* were cloned into pBluescript SK- for Digoxigenin (DIG) labelled riboprobe synthesis.

2.3 Microinjection of embryos

mRNA, DNA or morpholino oligonucleotides were injected at 1-cell (0.5 hpf) or later stages (e.g. 8-cell, approximately 2 hpf) to deliver them to all cells or in a mosaic manner respectively. Unless noted otherwise, injection was done at the 1-cell stage. Injection needles were made from borosilicate glass capillaries (GC100F-10, 1mm OD and 0.58mm ID, Harvard Apparatus Ltd., UK). The injection needles were pulled on a model PP-830 micropipette puller (Narishige scientific instrument lab, Japan). All injections were performed using a Leica MZ FL III dissecting microscope and Microinjector 5242 apparatus (Eppendorf, Germany). The volume of one-shot of injection material was adjusted to be 0.5pl.

2.4 Morpholino oligonucleotide knockdown analysis

Mopholinos were synthesised by Gene Tools (USA) and were as follows:

MF YAP TB	TGCGAACTCTTTGCGGCCCGAAAAC
MF YAP SB	AGTGCTAGCCTGAGTTACAAAGAAG
MF TAZ TB	CGCGTCCATGTCGCCAGAAGTCAGA
MF TAZ SB	AACCCAGAGGAAGACCTTACTTCAG
ZF YAP 5'UTR	CTCTTCTTTCTATCCAACAGAAACC
ZF YAP TB	GATCCATGACTCCAGATAAAAGTAA
ZF YAP SB	AGCAACATTAACAACTCACTTTAGG
ZF TAZ TB	GAGGATTACCGCTCATGGTCAAAAC
ZF TAZ SB	GTCTGTATGTGTTTCACACTCACCC
Control	CCTCTTACCTCAGTTACAATTTATA

In medaka (MF above), specificity of knockdown by morpholino (MO) was confirmed by two types of oligonucleotide, translation blocking (TB) and splicing blocking (SB) MOs, and by rescue of the phenotype by co-injecting corresponding mRNAs with the appropriate morpholino. Specificity of knockdown by MO was confirmed in a slightly different manner in zebrafish (ZF above). Since rescue of the phenotype by mRNA injection did not work effectively in zebrafish, three different types of morpholinos, TB, SB and 5'UTR were used and it was confirmed that all of them induced a similar phenotype. To determine efficiency of knockdown, semi-quantitative reverse transcriptase-PCR was carried out using primers that distinguish splicing defective transcripts from normal forms of mRNA (Figure 2.1). For PCR templates, total RNAs

were extracted from five morpholino-injected embryos using TRIzol (Invitrogen, USA) and were converted to cDNA by RNA-PCR kit ver.3 (Takara Bio, Japan).

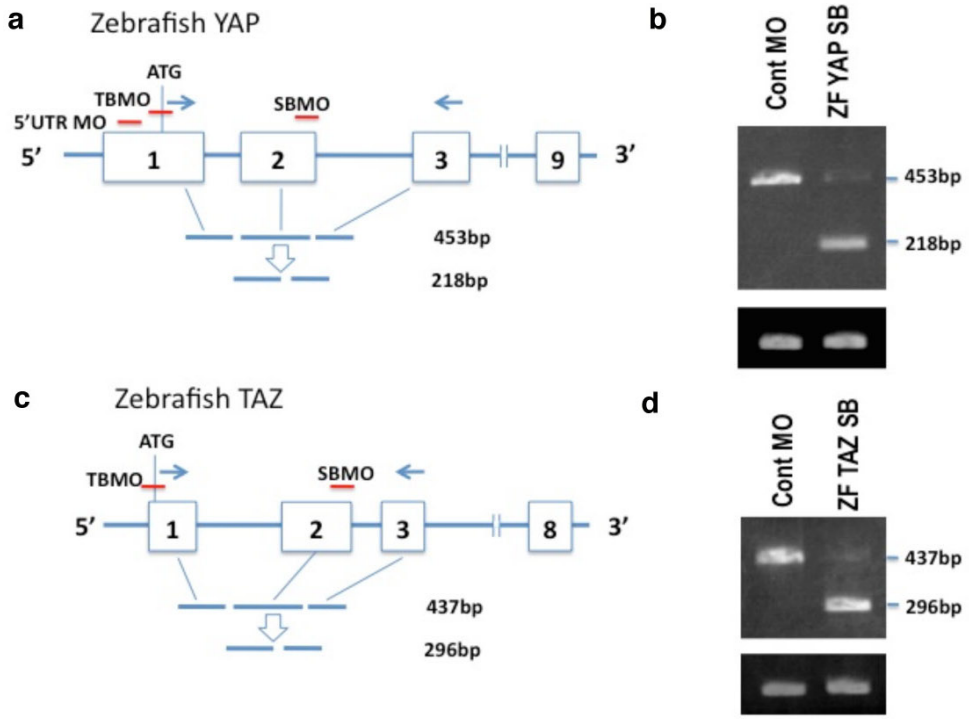

Figure 2.1. Efficiency of morpholino knockdown in zebrafish. Zebrafish (ZF) wild type embryos were injected with three distinct ZF YAP MOs (TB, 5'UTR and SB) and two TAZ MOs. Efficiencies of ZF YAP and TAZ SB MO KD (1.5ng each) were assessed by RT-PCR (b and d) using the primers depicted in a and c.

2.5 Dechorionation of embryos

Both medaka and zebrafish are surrounded by an acellular envelope known as the chorion (Bonsignorio *et al*., 1996). In medaka the chorion consists of a hard inner layer and a softer outer layer (Porazinski *et al*., 2011), meaning manual dechorionation is extremely difficult. Therefore removal requires a two-step protease treatment using a general protease and a hatching enzyme. In zebrafish the chorion consists of three layers and is approximately 3.5μm thick (Bonsignorio *et al*., 1996). In contrast to the medaka chorion the zebrafish envelope is much softer.

Prior to dechorionation, all tools were sterilised with 70% ethanol. Medaka embryos were gently rolled on specialised sandpaper (P2000 fine grit size) to remove the hairs on the surface of the chorion and gently score its surface. Rolled embryos were

incubated at 27°C in Pronase (Calbiochem, USA) for 60 minutes. Following removal of Pronase and after being washed five times with embryo medium, embryos were incubated in hatching enzyme (made as described in Porazinski *et al*., 2011) at 27°C for approximately 20 minutes. Embryos were then transferred to sterile 1X BSS (130g NaCl, 8g KCl, 4g $MgSO_4.7H_2O$, 4g $CaCl_2.2H_2O$, and 10mg Phenol Red in 1L Milli Q water; diluted 1:20 in Milli Q water and pH adjusted to 7.4 by addition of 5% $NaHCO_3$ in Milli Q water) using a glass Pasteur pipette when it could be seen that the chorion had partially disintegrated. Chorions were removed manually for zebrafish embryos in glass dishes containing Danieau's buffer (58 mM NaCl, 0.7mM KCl, 0.4 mM $MgSO_4$, 0.6mM $Ca(NO_3)_2$, 5.0mM HEPES, pH 7.6). Watchmaker forceps (55 INOX A.DUMONT&FILS) were used to remove the soft chorion.

2.6 Mounting of medaka embryos for time-lapse observation of eyes and Cuvierian ducts

Embryos were dechorionated at stage 18 (st.18, 26 hpf) and kept in sterile 1X BSS. Embryos were placed into 3% ultra-low gelling temperature agarose solution (Type IX-A: Sigma, USA) and transferred to 3.5cm culture chambers with glass bases (Iwaki, Japan). Embryos were oriented using a sterilised hair-loop while the agarose solution was still molten. The chamber was then placed on ice for 10 minutes to allow agarose solidification.

2.6.1 Time-lapse imaging of medaka embryos

For an overview of Cuvierian duct (CD) formation and eye development, a Leica MZ16 FA fluorescence-dissecting microscope with attached Leica DFC 350 FX camera was used to record images every 10 minutes. Z-stacks were taken at 10μm intervals over ranges of 100-500μm (depending on the tissue being imaged) to allow for thickening of the embryo as it developed. Exposure and gain were adjusted accordingly for each embryo as the time-lapse proceeded. Environmental temperature was maintained at 27°C to enable normal development. Time-lapse movies were edited where appropriate using LAS AF (version 1.9.0, Leica Microsystems, Germany).

For single-cell analysis of the CDs and eye development, confocal time-lapse microscopy was carried out. Embryos were embedded as outlined above and a Leica SP5 confocal microscope was used to record z-stacks every 2.5 minutes from st. 19/20-25 (31.5-50 hpf). Z-stacks varied by embryo and ranged from 105-135μm for the CD with 2μm intervals and 75-115μm for the eyes with 1μm intervals. A 40X water immersion objective (0.8 NA) was used for observing the CDs and a 63X oil objective for viewing the eyes (1.3 NA). Time-lapse images/movies were analyzed using ImageJ 1.43u software (NIH), Imaris 7.3 (Bitplane, ANDOR technology UK) and Amira 5.1 (Visage imaging, USA).

2.6.2 Endothelial cell tracking in medaka embryos

Confocal time-lapse movies of CD formation were analysed with ImageJ. The manual tracking plug-in was used for analysis of single cell migration in the primary and secondary streams. Analysis was carried out over approximately 3 hours starting from st.20 (31.5 hpf). To determine the migration speeds, displacement and straightness of endothelial cells in the secondary stream, cell tracking in Imaris was utilised.

2.6.3 Protrusion analysis of cells in the Cuvierian ducts of medaka embryos

Protrusions of endothelial progenitor cells in the secondary stream were analysed from confocal time-lapse movies of *fli*::*EGFP* wild type and *hir* embryos. To determine protrusion angle relative to migration direction, the direction of migration was set at 0° and a plane was drawn through the midline of the cell along this migration path. A second plane was then drawn through the midline of the extension being analysed (Figure 3.7b). Filopodia extension angle was then measured as the angle between the 0° plane and extension plane using the angle function in Amira for embryos at st.22 (38 hpf). The angle of each new/separate protrusion was measured for each cell over a 45-minute period. Protrusion angles were plotted as rose diagrams in Rose Graph v1.0 (available from: http://ystop.com/java/rosegraph/). For quantification of the number of protrusions extended in the forwards and backwards directions relative to migration direction, cells were equally divided into forward and backward halves based on migration direction, with a plane dividing the cell perpendicular to the direction of migration (Figure 3.8a). Relative to this perpendicular plane, the protrusions in the forwards and backwards directions of migration were counted. When a cell made a major change in direction the plane was adjusted appropriately. Protrusions of the secondary stream endothelial progenitor cells were counted, as these cells were more spread out compared to primary stream cells, therefore protrusions were more easily and accurately observed. Furthermore it was assumed that observing less densely packed cells may limit the effect of contact inhibition on protrusion formation. Protrusions were counted across the same number of frames from the time-lapse movies for wild type and *hir* embryos for consistency (st.21-25, 34-50 hpf).

2.7 Cell transplantation in medaka embryos

Donor embryos for transplantation were injected with 3% rhodamine-dextran (D-3308: Molecular Probes, USA) at the 1-blastomere stage and monitored again 10 minutes after injection for successful and even labelling. Host and donor embryos were dechorionated and developed to st.12/13 (10.33-13 hpf). Glass cavity microscope slides were sterilised overnight in 70% ethanol prior to transplantation. Slides were placed in 9cm petri dishes (Sterilin Ltd., UK) and to the centre of each slide depression a small amount of 3% methylcellulose (M-0387: Sigma, USA) was spread thinly and allowed to dry for one minute. 350µl of sterile 1X BSS was added to each cavity, along

with one donor and four recipient embryos. Embryos were oriented with their blastoderms upwards using a hair loop. 3-15 cells were taken from the blastoderm of donor embryos and transplanted into each of the recipient embryo blastoderms. Two recipient embryo blastoderm sites were used during transplantation based on previously published fate maps; one for CD transplantation and another for eye transplantation (Figure 6.3).

To target donor cells to the recipient CD, 10-15 cells were transplanted to a more ventral and lateral region from which cells go on to form the blood and endothelial ectoderm (Figure 6.3, Warga and Nüsslein-Volhard, 1999). For the eye transplantation approximately 3-5 cells were transplanted to a region approximately near the animal pole in the dorsal half of the blastoderm as cells here form lineages such as the brain and eyes (Figure 6.3, Hirose *et al*., 2004). All transplantations were performed using a fluorescence−dissecting microscope (as previously described), and a rig consisting of a needle and Hamilton syringe coupled to a micrometer drive oil−flow apparatus to allow extraction and insertion of donor cells. Oil was purged between dishes to ensure all cells from the previous donor were expelled. Recipient embryos hosting transplanted donor cells were developed at 27°C in the dark to prevent fading of the rhodamine-dextran. Phenotypic rescue was observed using a Leica MZ16FA microscope with a DFC350FX digital camera at the relevant stage for the development of the tissue of interest (st.20-24 for the eye, 31.5-44 hpf, and st.20-26 for the CD, 31.5-54 hpf). Recipient embryos with successfully integrated donor cells were analysed further using confocal microscopy as described above. For transplantation and phenotypic rescue experiments, embryos were genotyped by PCR where necessary.

2.7.1 Genotyping transplantation embryos

As transplantation was carried out before the stage at which wild type and mutant embryos could be differentiated phenotypically, it was necessary to genotype the donors to confirm they were *hir* mutant embryos. Where appropriate, donor embryos were recovered after transplantation and transferred to PCR tubes containing 25µl of 17mg/ml Proteinase K (P8044: Sigma, USA; diluted 1:10 in Tris-EDTA) for 4 hours at 55˚C and 10 minutes at 94°C. Donor embryo DNA underwent PCR with primers for wild type (5’-3’ sequence: GCAAAGCCCTGCTCCAGTT) and *hir* (5’-3’ sequence: GCAAAGCCCTGCTCCAGTA) YAP sequences (initialization: 95°C for 2 minutes; denaturation: 95°C for 30 seconds; annealing: 60°C for 30 seconds; extension: 72°C for 30 seconds; repeated for 35 cycles; final elongation: 72°C for 5 minutes; using Taq polymerase, Fermentas). Post−PCR samples were run on a 0.9% agarose gel along with wild type and *hir* DNA controls to genotype them.

2.8 Enveloping layer cell shape analysis during gastrulation

Zebrafish and medaka embryos at 60-90% epiboly stages were fixed in pre-warmed paraformaldehyde (PFA) to prevent contraction of the blastoderm (deep cells and enveloping layer, EVL). Fixed embryos were then Phalloidin (A22283, Invitrogen USA) antibody stained to demarcate the filamentous actin (F-actin) located at the cortex of EVL cells. Imaging was performed using the confocal setup previously described. Length-width (LWR) analysis for EVL cells was performed by measuring the ratio of the longest to shortest axis for cells at and up to 8 cells back from the EVL-yolk syncytial layer (YSL) margin as previously described (Köppen *et al*., 1996). For cells at the leading edge of the EVL margin, length was measured as the distance between the midpoint of the leading edge of the cell and the animal-most region of the cell (Figure 5.6b). Cell width was measured as the distance between the midpoints of the lateral cell boundaries of a cell, perpendicular to the length axis (Figure 5.6b). For cells back from the leading edge of the EVL, length was defined as the longest axis of the cell along the animal to vegetal axis. Width measurements were made in the same way as for cells at the leading edge (Figure 5.6b). Measurements were performed using Amira.

2.8.1 Laser ablation of the actomyosin ring in zebrafish embryos

The actomyosin ring in the YSL of developing zebrafish embryos was laser ablated using a Zeiss Axio Observer Z1 inverted spinning disk confocal microscope paired with a custom made UV laser cutter (IST Austria: laser cutter setup is described in Behrndt *et al*. (2012) supplementary methods). A 63X (1.2 NA) water objective was used to visualise the actomyosin ring at the germ ring stage (5.7 hpf) to the shield (6 hpf) stage of development (50-60% epiboly) in control and YAP/TAZ KD embryos, as well as at 70-80% epiboly in controls prior to cutting. A dissection plane of 20μm in length was set perpendicular to the EVL-YSL boundary (Figure 5.12). The plane was positioned to start cutting 20μm from the EVL-YSL boundary with 25 ultraviolet pulses of 1000Hz applied at 40 equidistant points along the plane. Image stacks of the embryos were captured using an iXon DU-897-BV camera (Andor Technology) using an exposure time of 380ms and a 0.5s frame rate using LabVIEW (v10.0.1), before and directly after cutting of the actomyosin ring to assess the quality of laser cut.

In particular, embryos were observed for 140 seconds post-cutting to ensure no wound response ensued and that the actomyosin network of the ring recovered suitably. This ensured only the circumferential tension of the ring was tested and that cytoplasm leakage through damaged YSL membranes did not factor. Temperature of the embryos during imaging was kept constant at 28.5 ± 1°C using a stage incubation chamber (Life Imaging services) coupled with a homemade objective heater and prior to cutting embryos were kept at 28.5°C. The confocal stacks were converted to maximal projection stacks using Fiji (v1.47u) and analysed using custom scripts in Matlab

(v7.12, courtesy of Martin Behrndt and Guillame Salbreaux). These scripts calculated cortical recoil velocity for the cortical laser ablation using particle image velocimetry (PIV). PIV analysis measured how quickly the two opposing edges either side of the cut opened by calculating the speed of movement of the actomyosin particles either side of the cut, as well as the directionality of these actomyosin particles (Figure 5.13).

2.8.2 Assessment of epiboly progression in zebrafish and medaka embryos

Due to the speed of progression of zebrafish epiboly, continual time-lapse imaging was used. Zebrafish embryos were mounted in 0.5% low melting temperature agarose (Type IX-A: Sigma, USA) and oriented using a hair loop in 3.5cm culture chambers with glass bases (Iwaki, Japan). Pre-warmed Danieau's solution (28.5°C) was added to the dish to cover the embryos and embryos were imaged by confocal time-lapse microscopy using a Leica SP5 setup as described above. A 20X dry objective was used (0.7 NA) to allow a global view of the progression of epiboly. Z-stacks were captured over ranges of 200-250μm at 2μm intervals depending on the embryo. The temperature of the embryos during imaging was kept constant at 28.5 ± 1°C using a stage incubation chamber (Life Imaging services). Imaging was commenced at the germ ring to shield stage (5.7-6 hpf) and was continued until epiboly had finished (bud stage, 10 hpf). The extent of deep cell (DC) or EVL epiboly was calculated as the percentage coverage of the yolk by either of these layers. Time-lapse series were used to measure the EVL-to-DC distance as epiboly progressed or at specific developmental stages. The distance between the margin of the EVL and the margin of the DC was measured in Imaris using the measurement points feature (Figure 5.10).

For medaka epiboly, which is slower than zebrafish, embryos were periodically imaged at each developmental stage from st.15-21 (17.5-34 hpf) using the fluorescence-dissecting microscope setup described above. By placing embryos in custom-made moulds, epiboly was calculated as a percentage by measuring the coverage of the margin of the DC over the underlying yolk. Embryos were maintained at 27°C throughout this process.

2.8.3 Analysis of actin intensity and localisation in the enveloping layer of zebrafish embryos

Maximum projection stills from the time-lapse movies detailed above were subjected to analysis in Imaris. Using only the red channel for *utrophin::mcherry*, three measurement lines were drawn across the EVL to trisect it at 60% epiboly (Figure 5.11). The actin signal intensity was measured along these three lines to ascertain whether it varied. An intensified signal would suggest actin accumulation whereas a reduced intensity might indicate a reduction of actin. The maximum intensity was plotted as a peak that would vary along the line as intensity varied.

2.9 Whole-mount immunohistochemistry (IHC) of medaka embryos

Embryos were fixed at the appropriate stage in either 4% PFA, dent fixative (80% MeOH/20% DMSO) or 1% trichloroacetic acid (TCA) depending on the antibody to be used. Embryos were washed briefly three times in 1X phosphate-buffered saline (PBS: 800ml of distilled H_2O, 8g of NaCl, 0.2g of KCl, 1.44g of Na_2HPO_4 and 0.24g of KH_2PO_4, topped up to 1L with additional distilled H_2O. pH adjusted to 7.4 and sterilised by autoclaving) at room temperature (RT). This was followed by three washes with 1X phosphate-buffered saline with 0.1% tween-20 (PBST: 800ml of distilled H_2O, 8g of NaCl, 0.2g of KCl, 1.44g of Na_2HPO_4 and 0.24g of KH_2PO_4, topped up to 1L with additional distilled H_2O. pH adjusted to 7.4 and sterilised by autoclaving. 1ml of Tween-20 added to give a concentration of 0.1%). Embryos were then permeabilised in 0.5% Triton X-100/PBS overnight at 4°C with gentle shaking. Three washes with 1X PBST were performed at RT to remove all traces of Triton. Embryos were incubated in blocking solution (PBDT: 49ml PBST, 1ml 2% sheep serum, 0.1g BSA, 0.02% Sodium Azide) for 2 hours at RT. Blocking solution was removed and primary antibody was added for incubation at 4°C overnight. Embryos were then washed three times in 1X PBST, 10 minutes for each wash at RT. Secondary antibody was added for incubation overnight at 4°C. Embryos were then washed three times in 1X PBST, 10 minutes for each wash at RT. Embryos were then imaged following refixation with 4% PFA/PBS at RT for 2 hours and mounting.

Antibodies used were: anti-Fibronectin antibody (Ab), Sigma F3648, 1:100 dilution; β-integrin monoclonal Ab, 8c8 (Developmental Studies Hybridoma Bank, USA) at 1:10 dilution; and anti-phosphohistoneH3 (#06-570, rabbit polyclonal antibody, Upstate, USA) at 1:750 dilution. Embryos were counterstained with Alexa Fluor 488 or 546 Phalloidin (A12379 and A22283, Invitrogen USA) at 1:250 and Topro3 (T3605, Invitrogen, USA) at 1:1000. Embryos were then embedded as outlined above and imaged with a Leica SP5 confocal microscope and 20X dry objective (0.7 NA).

2.9.1 Sectioning of embryos to assess ventricle angle following gravity embedding

Embryos were fixed as appropriate and washed three times in 1X PBS for 10 minutes each wash. Embryos were then transferred to 10% sucrose with 0.02% azide until they equilibrated, after which they were moved to 20% sucrose with 0.02% azide with continuous gentle mixing. Sucrose incubation helps to ensure all water is removed from tissues prior to cryosectioning at low temperatures. After were equilibrated in the 20% sucrose, they were transferred to 15% cold water fish gelatin (Sigma) with 15% sucrose until they equilibrated. This was followed by immersion in 25% gelatin with 15% sucrose, again until equilibration. Gelatin treatment pads out tissues to offer support during sectioning. The gelatin and embryos were cooled on ice and transferred

to moulds where they were oriented using a hair loop and then frozen on dry ice. The frozen gelatin (containing the sample) was removed from the mould and trimmed with a razorblade before gluing it to a specimen disc using OCT embedding medium (Tissue-Tek). Specimen discs were transferred to a Leica CM1850 Cryostat set to -28°C for 30 minutes to equilibrate and prevent melting. 15µm sections were cut and collected on superfrosted glass slides made in-house.

Sections on the slide were drawn around with a pap pen and allowed to dry for several minutes at room temperature (RT). Sectioned tissue was permeabilised by placing slides into a staining jar with acetone for 30 seconds followed by a 30 second wash with 1X PBS. Slides were placed in a moist slide chamber and immersed in blocking solution (PBDT) for 1 hour at RT. Blocking reagent was removed and primary antibody was added. Slides were incubated at RT for 1–2 hours. Slides were then washed with 1X PBS three times at RT for 10 minutes each wash. The secondary antibody diluted in blocking solution was then added and incubated for 1–2 hours at RT in the dark. Slides were washed with 1X PBS three times at RT for 10 minutes each wash in the dark. Mounting medium (Vectashield, Vector laboratories, UK) and a coverslip was then added to each slide in the dark at RT.

2.9.2 Immunohistochemistry for cell death/proliferation in medaka

Unless otherwise stipulated, washes were carried out at RT with gentle agitation. Embryos were dechorionated and fixed at the appropriate stage (st.20-28, 31.5-64 hpf) in 4% PFA/PBS for 3 days at 4°C. Embryos were then washed three times in 1X PBST for 15 minutes each wash. Embryos for storage were gradually dehydrated through a methanol (MeOH) series using the following graduations: 25%, 33%, 50%, 66%, 75%, 90% MeOH/PBST and 100% MeOH. The 100% MeOH was removed and replaced with fresh 100% MeOH and the embryos were stored at -20°C. Embryos were rehydrated using a series opposite to that above and washed in 1X PBST three times for 15 minutes each wash. Embryos were then washed three times in 1X PBS for 10 minutes each wash at RT on a shaker. Embryos were transferred to 1.5ml Eppendorf tubes (Catalogue No. 0030120086, Eppendorf, UK) and the PBS was removed.

For the cell death assay, TdT-mediated dUTP-biotin nick end labelling (TUNEL) was performed. TUNEL staining is based on the ability of the enzyme terminal deoxynucleotidyl transferase (TdT) to incorporate labelled dUTP into free 3'-hydroxyl termini that are generated when genomic DNA fragments into low molecular weight double-stranded DNA and high molecular weight single-stranded DNA (Gavrieli *et al*., 1992). Whilst TUNEL staining has been well adopted as the method of choice for apoptosis detection *in situ*, it should be noted that TUNEL staining is not limited to the detection of apoptotic cells as it can also be used to detect DNA damage associated

with non-apoptotic events such as necrotic cell death (Gavrieli *et al*., 1992). The Roche *In Situ* Cell Death Detection Kit (TMR red, Catalogue No. 12156792910) was used according to manufacturers guidelines. An appropriate volume of reaction mix was added to each tube (5-7µl per embryo). Tubes were placed on a shaker for O/N incubation in the dark at RT. Control embryos were subjected to the label mixture only (no TdT enzyme added to tube, just labelled dUTP). The TUNEL mix was removed and embryos were washed five times in PBST in the dark for 5 minutes each wash. TUNEL staining was assessed using fluorescence microscopy before carrying out staining for cell proliferation.

To analyse cell proliferation, embryos were re-fixed in 4% PFA/PBS O/N at 4°C following TUNEL staining. PFA was removed and embryos were washed three times in 1X PBST. PBST was removed and 0.5% Triton/PBST was added to each tube O/N at 4°C with agitation, to permeabilise embryos. Embryos were washed six times in 1X PBST for 10 minutes each wash. Blocking solution (PBDT) was added for 2 hours at RT on a shaker. A primary antibody against phosphohistone-3 (PH3) was diluted 1:750 in PBDT and incubated O/N at 4°C on a shaker. Embryos were washed three times with 1X PBST, 10 minutes for each wash. A secondary antibody (anti-rabbit GFP), diluted 1:250 in PBDT was then added after removing the PBST. Tubes were covered with foil and incubated O/N at 4°C. Embryos were then washed three times with 1X PBST, 10 minutes for each wash. Embryos were re-fixed in 4% PFA/PBS at RT for 2 hours and analysed for staining using a Leica MZ16FA microscope with a DFC350FX digital camera.

2.10 Whole-mount *in situ* hybridisation in medaka

In situ hybridisation (ISH) was carried out as described in detail in Porazinski *et al*. (2011). RNA antisense probes used were synthesised in-house: *delta-crystallin* (1:10 dilution) and *Sox3* (1:10 dilution). For whole-mount imaging, embryos were re-fixed for one hour in 4% PFA/PBST at RT and transferred through a glycerol series (20, 50, 80 and 100%) and imaged using a Leica DFC 300FX digital camera attached to an Zeiss Axioplan2 compound microscope using Leica Application Suite software.

2.11 Cell division plane analysis in medaka

Cell division planes in the retina and lens were measured using snapshots from Imaris, which were analysed in ImageJ using the angle tool. Division angles were considered only in 2D using a dorsal view and measurements were plotted in GraphPad Prism 5 software or SPSS 20 (IBM). Cell division in the retina was analysed from st.21-23 (34-41 hpf) using the apical lumen as the 0° plane. Thus cell divisions occurring along or parallel to this plane were classified as having a 0° division angle and divisions perpendicular to the apical plane were recorded as having a 90° division angle.

Division angles between 0° and 90° were therefore measured accordingly. In the lens placode, divisions were measured at early st.21 (34 hpf). Here the placode-retina boundary (PRB) was used as the reference plane (0°) against which division angle was measured. Neural tube (NT) cell divisions in the Z-axis from st.22-26 (38-54 hpf) were quantified using Amira and the ObliqueSlice and 3D Angle features. The ventricular zone running from dorsal to ventral was used as the 0° plane. The telophase cell closest to the ventricle determined how the division axis was drawn and thus whether division was classed as < or > 90°. For both the eyes and NT the plane of the dividing cell was fixed by drawing a plane through the dividing cell through both spindle poles (Figures 4.8, 4.9 and 4.17). Angles for divisions were plotted as rose diagrams in Rose Graph v1.0 (available from: http://ystop.com/java/rosegraph/).

2.12 Nuclear shape measurement in medaka

Nuclear shape measurements in the retina, lens and ear were carried out at st.20-22 (31.5-38 hpf) in Amira using Isosurface (to 3D-render the nuclei) and the 3D Length feature to measure the longest (major) and shortest (minor) axes (Figure 4.10). The ratios of the major to the minor axes of nuclei were calculated using these lengths and plotted over time as line graphs in SPSS 20. Nuclear shape measurements in the NT were performed at st.22-23 (38-41 hpf) and st.26-27 (54-58 hpf) using Amira to 3D-render individual nuclei and measure the major and minor axes using the 3D Length feature in a similar manner.

2.13 Quantification of neural tube shape and neuroepithelial cell behaviour in medaka

NT size measurements were conducted from time-lapse movies from st.22-27 (38-58 hpf) using Amira. NT height was measured along the midline dorso-ventrally using the 3D length tool at anterior, mid and posterior regions along the antero-posterior axis of the NT. The width of the NT was measured along the longest axis perpendicular to the midline, again at anterior, mid and posterior positions along the antero-posterior axis of the embryo. For both the height and width the three values along the antero-posterior axis were averaged and plotted over time in SPSS 20 as line graphs.

Post-mitotic cell behaviour was analysed using Amira and Imaris (Ortho slicer tool) by tracking single cells from st.22-24 (38-44 hpf) in the NT of embryos with cell membranes labelled green (EGFP-CAAX) and nuclei labelled red (H2B-RFP), termed MNFP. Cell behaviour was categorised in several ways: ventral cell slippage – where one daughter cell slipped in the ventral direction to sit alongside the other daughter cell; dorsal cell slippage – where one daughter cell slipped dorsally to sit alongside the other daughter cell; orthogonal division – the neuroepithelial cell divided perpendicular relative to the midline/ventricular zone; cell stacking – the neuroepithelial cell divided

roughly parallel to the midline/ventricular zone resulting in stacking of the daughter cells.

2.13.1 Analysis of crossing divisions in medaka

1-cell embryos were injected with 1ng of Kaede mRNA and photoconverted (from green to red, Figure 4.18) at st.15.5 (≈19 hpf) to label half of the blastoderm red. Crossing divisions (C-divisions) were analysed using the confocal microscope setup detailed above. Images of half-converted embryos were taken at st.15.5 (≈19 hpf), st16.5 (≈23 hpf), st.20.5 (≈32.5 hpf) and st.23 (41 hpf) to assess how red and green cells had mixed and thus indicate the level of C-divisions occurring.

2.14 Statistical analyses

Statistical significance between groups was tested using a Student's *t*-test or a one-way ANOVA with a Dunnett's T3 post-hoc test in SPSS 21. To test for differences in mitotic orientation between wild type and *hir* the Kolmogorov-Smirnov (KS) test was performed. Available at: http://www.physics.csbsju.edu/stats/KStest.n.plot_form.html. Error bars on graphs show ± standard error of the mean (S.E.M). P values of <0.05 were taken as statistically significant. All graphs were drawn in SPSS 21 or GraphPad Prism 5.

2.15 Western blotting

Dechorionated embryos were transferred to 1.5ml Eppendorf tubes and washed with PBS which was removed prior to homogenising the embryos with a pestle. 1ml of PBS was added and tubes were spun down at 3,000rpm for 2 minutes at 4°C followed by removal of supernatant. PBS washing and spinning was then repeated as was supernatant removal. These steps remove the yolk so that lysis steps are not affected.

To perform lysis, 1X RIPA+ buffer (1ml RIPA- buffer (50mM Tris-HCl at pH 8, 150mM NaCl, 5mM EDTA, 15mM $MgCl_2$, 1% NP-40), 50µl 10% DOC, 1µl of 1M DTT, 1µl of 1.7mg/ml Aprotinin, 5µl of 200mM PMSF, 1µl of 100mM Na_3VO_4) containing 2mM Iodoacetic acid was added (0.5-1µl per embryo). Tubes were incubated on ice for 10 minutes followed by spinning down at 12,500rpm for 15 minutes at 4°C. Supernatant was transferred to a new tube and 4X sample (16ml of 0.5M Tris-HCl at pH 6.8, 16ml glycerol, 3.2g SDS, 8ml β-mercaptoethanol, 32mg of bromophenol blue, made to 40ml volume with H_2O) buffer was added. Tubes were boiled at 100°C for 10 minutes and placed on ice. Samples were then run on SDS-PAGE gels at 60V for 30 minutes followed by 1.5-2 hours at 130V to allow separation. Gels were then wet transferred to PVDF membranes over 3 hours at 350mA. Membranes were washed with deionised water and incubated with 2% skim milk/TBS followed by multiple washes with deionised water. Primary antibodies in 5% BSA/TBS/0.03% NaN_3 were then added

overnight at 4°C. This was followed by fives washes of the membrane with deionised water and secondary antibody incubation (in 2% skim milk/TBS) for 1-2 hours at RT. Membranes were washed with 0.2% TBST fives times for 3 minutes each wash and twice with deionised water. Detection was performed using the Western Chemilumi HRP kit (Femto).

Western blotting antibodies used were anti-p-MRLC (Serine 19, Cell Signalling #3671) at a dilution of 1:1000; anti-fibronectin (Sigma #F3648) with a dilution of 1:500 (2% skim-milk), anti-YAP antibody (Cell Signalling #4912) diluted 1:500 and anti-GAPDH (Millipore MAB374) diluted 1:2000.

Chapter 3: YAP is required for the formation of the Cuvierian ducts

3.1 Aims

The *hirame* (*hir*) mutant, null for the protein YAP, was identified in a genome-wide screen looking for mutations affecting organogenesis in medaka (Furutani-Seiki *et al*., 2004). The *hir* displays three major traits as part of its phenotype. Firstly, epithelial tissues and organs are collapsed/flattened. Secondly, tissues are mislocated such that coordinated growth and morphogenesis does not occur properly. And thirdly, there are prominent cell migration defects. The first organ to form in the vertebrate embryo is the circulatory system (Marcelo *et al*., 2013), thus understanding how this key network forms may have important clinical implications. The Cuvierian ducts (CDs) in medaka are superficial parietal epithelial tissues that are easily visualised to allow cell behavioural analysis at the single-cell level in a living embryo. It is assumed that cell migration plays an important role for the development of these blood-carrying vessels in fish (Iwamatsu, 2004; Fujita *et al*., 2006), *Xenopus* (Levine *et al*., 2003), rat (Endo *et al*., 1996) and humans (Chen *et al*., 2004). The role of YAP *in vivo* for cell migration is not yet clear. As the *hir* mutant exhibits prominent cell migration defects, this chapter analyses CD formation in *hir* using time-lapse imaging coupled with more detailed cell behavioural analysis to address whether YAP has a role for the formation of this relatively simple but important epithelium.

3.2 Introduction

To be a key regulator of organ size as previously proposed (Dong *et al*., 2007), YAP must be regulating many factors during development, such as the extracellular matrix (ECM), as well as various different cell behaviours such as cell migration, as these processes are fundamental for morphogenesis, organ development and growth. Since relatively little is known regarding the initiation and development of the vascular epithelial organ, the CDs in medaka, and it is has not been previously reported what contribution endothelial progenitor cell migration makes to the formation of this organ, it was investigated whether YAP orchestrates this process as the *hir* mutant displays clear cell migration defects.

3.2.1 Formation of the vertebrate vasculature

The first organ to form in the vertebrate embryo is the circulatory system that plays a pivotal role in the delivery of oxygen and nutrients to developing tissues, as well as the removal of waste metabolites (Marcelo *et al*., 2013). Vasculogenesis is the process by which new blood vessels form when there are no pre-existing vessels. The development of the vascular system in different vertebrate species occurs in a characteristic and predictable manner, with most vertebrates sharing common early developmental features (Fujita *et al*., 2006). This typically involves the formation of a vascular plexus from blood islands on the yolk sac, which connects, to the vascular system of the embryonic body via transverse vessels (Fujita *et al*., 2006). This circuit or connection is the primary circulation and consists of the ventral aorta, aortic arches,

dorsal aorta, transverse vessels, vitelline capillary plexus, and the marginal vein, which are all generated by vasculogenesis (Fujita *et al*., 2006). In teleosts, the CDs act as the vitelline veins, with the posterior cardinal vein acting as the afferent vein into the CDs at the earliest stages (Fujita *et al*., 2006). Vasculogenesis requires the determination and differentiation of endothelial progenitor cells from the lateral and extra-embryonic mesoderm (Era *et al*., 2008), followed by their consequent migration and organisation into vessels (Jones and Li, 2007). Once vascularisation is complete, angiogenesis, which is the sprouting of new vessels from those already present along with remodelling of the primitive vasculature occurs, to generate a mature circulatory system (summarised in Figure 3.1). This is followed by recruitment of vascular smooth muscle cells to the vessels and stabilisation of the vessels by deposition of matrix proteins (Karnik *et al*., 2003).

Key signalling molecules during vasculogenesis include fibroblast growth factor-2 (FGF-2), vascular endothelial growth factor (VEGF) as well as VEGF receptor-2 (VEGFR-2). FGF-2, as well as bone-morphogenetic protein 4 (BMP4, Marcelo *et al*., 2013) induces pluripotent cells from the mesoderm to undergo angioblast (endothelial progenitor cell) specification, and VEGF/VEGFR-2 signals from the surrounding tissue are important for inducing endothelial cell differentiation, migration, and tube formation (Poole *et al*., 2001). VEGF signalling is required for the assembly of new blood vessels but not for the maintenance of blood vessels, as inhibiting VEGF activity only disrupts blood vessel formation during vasculogenesis and not when pre-existing blood vessels are present (Argraves *et al*., 2002). The transformation of epithelial cells to mesenchymal cells (EMT) is a key process during embryonic development, and is seen when angioblasts segregate from the mesoderm prior to their assembly into the blood vessels (Poole *et al*., 2001). Vasculogenesis also occurs in adult life where it is important for vascular repair and involves the differentiation of endothelial progenitor cells (reviewed in Asahara *et al*., 2011).

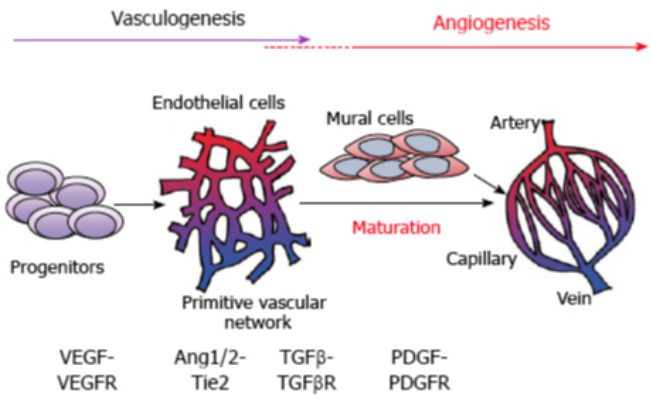

Figure 3.1. Summary of the key signalling involved in vasculogenesis and angiogenesis. Adapted from Takuwa et al., 2010.

3.2.1.1 Properties of endothelial cells

Once vasculogenesis has occurred, endothelial progenitor cells become circulatory expressing a variety of cell surface markers, though a specific marker has not yet been defined (Yoder, 2012). Classical markers used have been CD34 and KDR (also VEGFR-2) to identify endothelial cells, with positivity for the additional CD133 marker identifying endothelial progenitors (reviewed by Yoder, 2012). In order to try and better characterise endothelial cells a list of criteria has been proposed as follows: “a circulating cell that gives rise to progeny displaying clonal proliferative potential and differentiation restricted to the endothelial lineage, ability to form lumenised capillary-like tubes *in vitro* (cells must display cytoplasmic vacuolation capacity), and ability to form stable blood vessels (cells must secrete a basement membrane) when implanted into tissues (with or without a scaffold) that become an integrated part of the host circulatory system and display potential to undergo remodelling to form the intima of arterial, venous, and capillary structures.” (Yoder, 2012).

Endothelial cells are involved in blood vessel formation, repair and remodelling though these processes are regulated by different mechanisms (reviewed by Yoder, 2012). Endothelial cells also act as a source for molecules influencing the structural and functional integrity of the circulation as they synthesise and secrete a wide variety of soluble factors. In recent years several endothelial-specific genes that mediate endothelial cell migration have been discovered including Robo4 (roundabout 4), CLEC14A (C-type lectin 14A) and ECSCR (endothelial cell-specific chemotaxis regulator, Zhuang, 2011). Defects in endothelial cell development, as well as vessel formation and function are embryonic lethal and are important in the pathogenesis of various vascular diseases.

3.2.1.2 Emergence of the endothelial cell lineage in medaka

In medaka, the vascular endothelial progenitor cells arise from the hemangioblasts in the lateral plate mesoderm (LPM) on either side of the embryo (Kinoshita *et al*., 2009, p.210). As development proceeds, the number of progenitor cells on either side of the embryo increases, before these progenitors migrate to the midline to form the intermediate cell mass (ICM) between the seventh and fifteenth somite. Cell-tracing experiments in zebrafish have suggested that the arterial-venous cell fate decision of angioblasts may be made prior to this migration (Zhong *et al*., 2001). The ICM can be clearly observed below the notochord by stage 23 (st.23, 41 hpf) and also gives rise to the embryonic hematopoietic cells, which is similar for most teleosts (Kinoshita *et al*., 2009, p.212). The vascular endothelial cells form the vessels of the medaka and the hematopoietic cells give rise to the blood cells. The vasculature in medaka is well studied and characterised later in development from when the heart begins beating at st.24 (44 hpf) onwards (Fujita *et al*., 2006). However, less seems known regarding early development of the primary vascular system, in particular how the Cuvierian

ducts (CDs) arise. In all vertebrate species, the early circulatory system has an important role in yolk absorption (Fujita *et al*., 2006) and in accordance with this, the CDs in medaka sit superficially on the yolk surface.

3.2.1.3 The Cuvierian ducts are conserved from vertebrates to humans

The CDs are the first components of a parietal vessel system and are conserved from vertebrates to human embryos and young children where they persist from development as the coronary sinus (Chen *et al*., 2004, p.58). The CDs in early humans are short transverse veins that open into the sinus venosus, and act as embryonic blood vessels where they connect the embryo and the placenta (Chen *et al*., 2004, p. 60). This conservation means studying the formation of the CDs in medaka may provide useful insights into the formation of these vessels in humans.

3.2.1.4 Development of the Cuvierian ducts in medaka

In medaka the mechanism of development of the CDs has not been well studied in detail to this author's knowledge. Iwamatsu (2004) provides gross morphological observations of the CDs formation but detailed analysis appears lacking in the literature. Endothelial progenitor cells of the CDs can first be seen on the surface of the yolk at around st.18 (26 hpf) of development using markers such as *fli-1* or *lmo2* (Kinoshita *et al*., 2009, pp.210-211). It is hypothesised that the migration of these endothelial progenitor cells plays a key role in the development of the CDs, but this has not been previously conclusively shown. In medaka, the CDs are a pair of common cardinal veins comprising the anterior cardinal vein returning blood from the head and the posterior cardinal vein from the trunk (Iwamatsu, 2004). The CDs in medaka become easily distinguishable on the surface of the yolk from st.23 (41 hpf) but are still incomplete along with the vitello-caudal vein by the time the heart starts beating at st. 24 (44 hpf, Iwamatsu, 2004). By st.25 (50 hpf) of development when the blood circulation begins in medaka, the CDs and carotid artery are connected by the optic plexus (Iwamatsu, 2004). Medaka fish use these common cardinal veins for yolk absorption to provide nutrients during development (Fujita *et al*., 2006). The CDs in medaka are superficial epithelial tissues that are easily visualised to allow cell behavioural analysis at the single-cell level in a living embryo and thus are expected to be a very useful model for studying the importance and contribution of cell migration to early embryonic vasculature development, as well as how this cell migration is regulated (see Figure 3.10).

3.2.2 Why do cells need to migrate?

In order to build an embryo properly, cells need to undergo complex rearrangements in their organisation in order to pattern tissues, shape tissues and build 3D tissues and organs from 2D sheets (Wolpert and Tickle, 2011, pp.289-290). Cell migration is key for these early developmental activities and is particularly prominent during vertebrate

gastrulation, which is the process by which the three germ layers, ectoderm, mesoderm and endoderm are specified (Wolpert and Tickle, 2011, p.302). Cell migration is crucial for these gastrulation processes such as epiboly, involution/ ingression and convergent extension. Cell migration is also essential later in development for the emergence of more complex tissues such as the vasculature, bone, muscle, cartilage and the nervous system (Wolpert and Tickle, 2011, p.318). Cell migration has also been shown to play an important role for the formation of various organs such as the heart (Stainier, 2001), as cell migration and rearrangements can help to create various structures such as clefts/grooves, capsules, tubes, pits and columns, which serve as the foundations for functioning organs (Joshi and Davidson, 2012). Furthermore, the immune response, wound response and regeneration within the body require cell migration as immune cells move towards foreign bodies to prevent infection and cells move towards the sites of wounds to aid repair and regeneration. It is therefore crucial to understand the factors regulating cell migration and how these are affected in various disease states such that effective therapies can be devised.

3.2.2.1 Examples highlighting the importance of cell migration in development

There are many examples of cell migration during development as outlined above. Two well-studied systems of cell migration include zebrafish heart formation (Stainier, 2001) and the formation and dissemination of the neural crest (Kuriyama and Mayor, 2008). Lessons from these systems may give insights into how the CDs form as there may be common mechanisms conserved during the development of these highly migratory tissues. The vertebrate heart tube forms from two bilateral cell populations in the lateral plate mesoderm (LPM, McFadden and Olson, 2002), similar to the CDs. These populations move medially and fuse to form the heart tube, which is composed of myocardial, and endocardial layers (Trinh and Stainier, 2004). Myocardial specification as well as interaction between the myocardial progenitors and endoderm (Yelon *et al*., 2000) are both essential for heart tube formation as mutants lacking these processes display cardia bifida (Stainier *et al*., 1996).

In chick embryos it has been reported that fibronectin (FN) deposited between the mesoderm and endoderm is important for myocardial migration (Linask and Lash, 1986). Furthermore, FN also seems necessary for myocardial migration in mice as FN-null embryos are embryonic lethal with defects in heart formation (George *et al*., 1993). Myocardial differentiation is unaffected in these mice but myocardial precursors do not migrate correctly (George *et al*., 1997). More recently in zebrafish it was shown that myocardial precursors form polarised epithelia that mature whilst migrating medially to the midline of the embryo in a coherent manner (Trinh and Stainier, 2004). Interestingly, these authors showed that FN deposition at the midline is dispensable for the actual migration of myocardial cells and is instead important for their temporal

regulation and their epithelial organisation whilst migrating. This raises an interesting question of whether FN located more laterally is important for precursor migration and formation of the heart tube.

The neural crest (NC) is one of the most pluripotent and migratory embryonic tissues (Kuriyama and Mayor, 2008). Cells deriving from the NC migrate over extreme distances and inhabit nearly all tissues of the embryo including cartilage, muscle, neurons and glia as well as organs such as glands, the heart, neck, face and skin (Kuriyama and Mayor, 2008). The NC arises at the neural plate border (Mayor *et al*., 1995) and NC cells undergo epithelial-to-mesenchymal transition (EMT) prior to their migration. This process requires loss of epithelial polarity in which tight and adherens junctions are gradually replaced by gap junctions, accompanied by changes in cell adhesion, often indicated by a change in cadherin expression (Kuriyama and Mayor, 2008). However, this cadherin expression change is not essential for EMT unlike remodelling of the extracellular matrix (ECM) by matrix metalloproteases (MMPs, Fingleton, 2006). Once EMT is complete, NC cells then migrate following specific pathways and can migrate as groups or singly. For example, the cephalic NC cells migrate as three major streams that are spatially restricted and it has recently been shown that the ephrins and semaphorins are important molecular regulators of this process (Merrill *et al*., 2006; Eickholt *et al*., 1999). In migration of the trunk NC a third group of molecules has also been implicated. Slit/Robo signalling has been suggested to act in both a repulsive and attractive manner to regulate the motility of trunk NC cells (De Bellard *et al*., 2003).

Whilst the NC cells migrate with persistent directionality and in both streams and individually, no definitive chemotaxis mechanism has yet been elucidated. Instead it has been proposed that planar cell polarity (PCP) signalling, that is more commonly associated with epithelial tissue polarity, may be important for the migration of mesenchymal NC cells. Analysis of zebrafish PCP mutants has shown a failure of NC migration (Jessen *et al*., 2002). In this model, PCP is suggested to be regulating the mildly cohesive NC migratory cells to produce directional migration by regulating the small GTPases and consequently the actin cytoskeleton and cellular adhesion (Kuriyama and Mayor, 2008). Interestingly, parallels have recently been made between how neural and vascular networks pattern in terms of guidance and cues (Jones and Li, 2007). Proteins such as the ephrins and semaphorins that regulate the process of axon guidance have likewise been shown to play a crucial role in blood vessel migration (Jones and Li, 2007). There are also anatomical similarities between endothelial tip cells and neuronal growth cones. The study of NC migration has proved important as it shares many cellular and molecular characteristics with metastatic cancer cells (Kuriyama and Mayor, 2008).

3.2.2.2 Collective cell migration

There are many instances *in vivo* where cells migrate singly, such as in the NC migration detailed above, in immune function (Friedl and Weigelin, 2008), as well as in development and metastasis (Ridley *et al*., 2003). However, cells can also move collectively. This collective migration involves the movement of cells that are more epithelial-like due to being in close contact with each other (Friedl and Gilmour, 2009). The process of collective cell migration is seen in several instances of morphogenesis, such as lateral line development in the zebrafish (Lecaudey *et al*., 2008), border cell migration in the egg chambers of *Drosophila* (Rørth, 2009) and branching morphogenesis in the *Drosophila* trachea, as well as in regeneration and cancer invasion (Friedl and Gilmour, 2009). Each of these model systems for studying collective migration provides a slightly different perspective on the complex process (reviewed in Friedl and Gilmour, 2009). Despite these processes being very different, the underlying cellular and molecular mechanisms of collective migration all require the following criteria: cell–cell cohesion; collective cell polarisation and coordination of cytoskeletal activity; guidance by chemical and physical signals; and a collective position change relative to the substrate (Friedl and Gilmour, 2009).

In zebrafish lateral line formation, the mechanisms governing this coordinated migration process are now coming to light and involve several of the cells of the migrating cohort (over 100 cells collectively) recognising a Sdf1 (stromal cell-derived factor 1) chemokine cue via an active Cxcr4 (C-X-C chemokine receptor type 4) receptor. This causes polarisation such that this part of the group becomes the leading edge, and consequently transmits this polarisation and directionality to other cells in the pack such that collective migration towards the cue occurs (Haas and Gilmour, 2006). The directional migration of the *Drosophila* border cell cluster occurs in two progressive phases. In the first phase, which involves posterior migration, epidermal growth factor (EGF), platelet-derived growth factor- and vascular endothelial growth factor (VEGF)-related factor 1 (PVF1) and PVF2 act as guidance ligands (Bianco *et al*., 2007). The second phase, which is dorsal migration, requires EGF alone. In the forming trachea of *Drosophila*, FGF acts as the cue and this process is repeated in subsequent branching events (Bianco *et al*., 2007). In terms of regeneration, collective cell migration is seen when keratinocytes move over the wound bed during epidermal wound closure (Poujade *et al*., 2007). Collective cell migration is most recognisable during carcinogenesis when epithelial cancers invade the surrounding tissues and some of the aforementioned morphogenetic ligands such as SDF1 and FGF may be important for this cancer progression (Friedl and Gilmour, 2009).

Interestingly, all of these morphogenetic scenarios use a common system whereby only a select few cells can respond to the chemokine in question such that they become leaders of the cohort. These leader cells achieve this sensitivity by expressing different

receptors to the following cells or by actively secreting compounds to dampen the response of the trailing cells to the attractant cue (reviewed in Friedl and Gilmour, 2009).

3.2.3 Mechanisms of cell migration

For cell migration to occur, a cell must be polarised, meaning that the molecular machinery at the front and the back of a migratory cell must be asymmetric. The organisation and composition of these molecular processes at the front or leading edge, and at the rear or trailing edge of the cell are well characterised, particularly concerning the actin cytoskeleton and various adhesions (Ridley *et al*., 2003). The signals leading to the specification of this trailing and leading edge are also spatially segregated within the cell (Ridley *et al*., 2003). In the trailing edge, large bundles of actin filaments support adhesion disassembly and retraction of these large more stable adhesions (Vicente-Manzanares, 2009). Assembly of actin at the leading edge of the cell drives the formation of filopodia in the direction of migration (Le Clainche and Carlier, 2008). Actomyosin contractility helps to provide the locomotory motion required to move the cell (Ridley *et al*., 2003). The Rho GTPases are involved in differentially regulating the polarity of migrating cells at the front and back. For example, Cdc42 and Rac1 signalling mediated by small and dynamic adhesions at the front of the cell, contributes to the forward protrusions of a migrating cell (Ridley *et al*., 2003). At the trailing edge of the cell, RhoA controls cellular contraction by activating myosin II leading to actomyosin contractility which disassembles cell adhesions (Ladwein and Rottner, 2008). Rac1 activity is greatest just back from the front edge of a migrating cell, whereas Cdc42 activity is strongest at the tip of the leading edge (Itoh *et al.*, 2002). Both the activity of Rac1 and Cdc42 decreases rapidly when a cell changes direction (Itoh *et al*., 2002).

Filopodia are relatively long (up to 5μm) and thin (typically around 0.1-0.3μm) protrusions of the plasma membrane that function as a means for cells to probe the environment around them (Yang and Svitkina, 2011). Filopodia are composed of parallel bundles of filamentous actin (F-actin), and the dynamic process of extension (at speeds up to 0.16μm/s, Argiro *et al*., 1985) and retraction of filopodia is heavily dependent on the coordinated polymerisation of actin filaments (Ladwein and Rottner, 2008). Filopodia, along with other cellular protrusions such as lamellipodia and pseudopodia are important for cell migration. Integrins and cadherins are often found at the tips of filopodia, helping to promote adhesion to the extracellular matrix (ECM), which facilitates migration and also stabilises the filopodia themselves (Ridley *et al*., 2003).

Cdc42 is a key regulator of cell polarity, as it regulates the actin dynamics of filopodia. Cdc42 does this via signalling that stimulates the Arp2/3 complex, which occurs via the

activation of WASP and N-WASP (Ridley *et al*., 2003). Cdc42 regulates cell polarity by localising filopodia formation, and furthermore by localising the microtubule-organising centre (MTOC) through a pathway involving PAR6 (Ridley *et al*., 2003). PAR6 exists in a complex with atypical protein kinase C (aPKC) and PAR3. By targeting PAR6, Cdc42 can activate this complex. Furthermore, PAR6 and aPKC play significant roles in sustaining cell polarity during migration (Etienne-Manneville and Hall, 2003). Additionally, myosin II-based contractility is also required for polarity during cell migration by positioning the nucleus (Gomes *et al*., 2005) and for persistence by suppressing lateral protrusions of the membrane (Van Haastert and Devreotes, 2004).

3.2.4 The importance of the extracellular matrix, in particular fibronectin, for cell migration

The ECM serves many purposes including the compartmentalisation of tissues, acting as a scaffold for cell adhesion and assisting cell movement by acting as a substrate upon which cells can migrate. It also directs different cell behaviours including proliferation and differentiation (Teti, 1992). The ECM is composed of two main classes of macromolecules being polysaccharide glycosaminoglycans (or proteoglycans) and fibrous proteins (Teti, 1992). The fibrous proteins consist of those having a structural role (such as elastin and collagen) and those having an adhesive function (including laminin, vitronectin and fibronectin) (Teti, 1992). Fibronectin (FN) in particular is an essential component of the ECM that has been established as being important for cell migration (Mao and Schwarzbauer, 2005).

3.2.4.1 Fibronectin structure and organisation in the extracellular matrix

The fibronectins are large glycoproteins conserved throughout the animal kingdom (Ruoslahti, 1988). There are at least 20 distinct FN proteins in humans, which are generated by the alternative splicing of the RNA transcript of a single gene (Paul *et al*., 1986). FN is encoded by an ~8kb mRNA which yields FN subunits ranging in size from 230–270kDa depending on the alternative splicing (Norton and Hynes, 1990). FN is a modular protein that is composed of repeating units (types I, II, and III). These modules are arranged in such a way that FN has high-affinity binding sites for other components of the ECM such as heparan sulfate, collagen and fibrin and a binding site for specific cell surface receptors (Buck and Horwitz, 1987). This cell surface receptor binding site contains a tripeptide sequence, composed of Arg-Gly-Asp (Arginylglycylaspartic acid, RGD), which is recognised by the cell surface receptor (Ruoslahti and Pierschbacher, 1987). FN dimers exist as two similar peptides linked by two disulfide bonds to form a molecule of around 500kDa and this covalent linkage is essential for converting the dimers to a multimeric fibril (Singh *et al*., 2010). Importantly from a physiological perspective, FN in solution does not form fibrils even when present at very high concentrations (Singh *et al*., 2010).

FN matrix assembly is cell-mediated through integrin binding to the RGD cell binding domain and the primary receptor for FN matrix assembly is α5β1 integrin (Ruoslahti and Obrink, 1996). FN fibrillogenesis, which is the assembly of dimers of FN into fine FN fibrils is a step-wise integrin-dependent process. During fibrillogenesis, compact soluble FN dimers bind to integrin α5β1 via its RGD binding domain (Leiss *et al*, 2008). This in turn induces integrin clustering to bring bound FN dimers closer together, which increases the local FN concentration, and consequently FN-FN interactions, which produces short soluble FN fibrils (summarised in Figure 1.1). FN binding to integrin induces myosin II-mediated reorganisation of the actin cytoskeleton and activates intracellular signalling complexes inside the cell such as Src signalling (Wierzbicka-Patynowski and Schwarzbauer 2002) which can produce lamellapodia (Yu *et al*., 2011). These cytoskeletal rearrangements exert forces on integrin as vinculin and talin tether the cytoskeleton to integrin. Consequently, FN undergoes conformational changes on the outside of the cell, which exposes cryptic FN binding domains, causing FN molecules to align into fibrils through FN intermolecular interactions (see Figure 1.1) (Wierzbicka-Patynowski and Schwarzbauer, 2003). This integrin-mediated assembly of the ECM glycoprotein FN into fibrils tethered to the cell surface is the most upstream event for assembling other ECM proteins (Daley *et al*. 2008). Mechanical cues such as tissue tension are required for this FN assembly (Singh *et al*. 2010), and the elaborate and dynamic 3D meshwork of the ECM is constantly remodelled during development and furthermore varies between anatomical regions. Blocking of integrin-RGD binding using either anti-integrin or anti-FN antibodies inhibits fibril formation (McDonald *et al*., 1987).

3.2.4.2 The role of integrin-fibronectin interactions specifically in blood vessel development

FN fibrillogenesis has been shown to be required for vascular network formation (Astrof and Hynes, 2009). In particular, vasculogenesis has been observed to occur in areas of the ECM rich in FN (Zhou *et al*., 2008). Interestingly, FN-null mice exhibit severe defects in blood vessel development, causing embryonic lethality by E9.5 (George *et al*., 1993). Once the basic vascular network has been established, the level of FN within the vicinity of the developing blood vessels decreases (Peters *et al*., 1996), suggesting FN may be less important for the maintenance of vessel networks and more involved in vasculogenesis.

Contact-dependent interactions between endothelial cells are critical during development of the vascular network. EphB-ephrinB signalling has been shown to mediate cell repulsion and direct endothelial cell migration during blood vessel development (Füller *et al*., 2003). During vasculogenesis, it is thought that cell protrusions are inhibited upon cell contact (Mayor and Carmona-Fontaine, 2010). This inhibition may be mediated by RhoA, which at the point of cell-cell contact is activated

by PCP signalling to antagonise Rac1 and consequently inhibit cell protrusions (Mayor and Carmona-Fontaine, 2010). These cell-cell contacts in turn help to build tubes, which ultimately contribute to the formation of vessels.

3.3 Research questions

The aims of this chapter can be broadly split into the following questions:

1) Is YAP required for the migration of endothelial progenitor cells of the CDs?

2) If YAP is required, how is cell behaviour during the migration process affected in the *hir* mutant?

3) If required, what is the mechanism by which YAP regulates this migration of progenitor endothelial cells?

To track cells of an endothelial lineage *in vivo* in real-time, a transgenic strain with enhanced green fluorescent protein (EGFP) under the control of the *fli* promoter was used. The *fli* promoter is endothelial cell-specific allowing visualisation of endothelial progenitor cells but it should be noted that it also shows some background expression in macrophages (as can be seen in Supplementary movies 1 and 2). This could be for several reasons. Firstly, it may be due to where insertion of the *fli*::*EGFP* transgene occurred in the genome when creating the transgenic line. Alternatively it could be because macrophages have their origin in hematopoietic cells, which express Fli1 (Geissmann *et al*., 2010). This did not however, present any problems for the time-lapse analyses included in this chapter as endothelial progenitor cells have a much slower migratory speed versus macrophages. This coupled with clear morphological differences meant the two cell types were very easily distinguished in the recorded movies and subsequent analysis.

3.4 Results

3.4.1 The *hirame* mutant phenotype displays three major traits including tissue collapse, tissue mislocation/misalignment and cell migration defects

The genome-wide phenotype-driven mutagenesis screen in medaka searching for mutations affecting body shape and organogenesis revealed a mutant with a unique phenotype among medaka and zebrafish mutants. This phenotype was not explicable by the current knowledge of vertebrate body pattern formation and was termed *hirame* (*hir*) for flat fish (Furutani-Seiki *et al*., 2004). The phenotype was also not attributable to cell proliferation defects as cell proliferation was only very slightly reduced, although cell death was significantly increased in *hir* mutants at several stages of development (Figure 3.3a-c). There are however, no cell death mutants in the literature with a phenotype similar to *hir*. In medaka, TAZ (the mammalian paralogue of YAP) knockdown embryos (injection of 0.6ng of translation-blocking morpholino) had strong cell proliferation defects and became early embryonic lethal (Figure 3.3a-c).

Tissues and organs including the brain, eyes, spinal cord, and somites were flattened in the mutant, and were therefore not properly aligned (Figure 3.2a-b'). Particularly, lenses were misaligned outside the retina rather than invaginating into it (Figure 3.2a', arrowheads). Other sensory placodes, such as olfactory and otic placodes, also did not invaginate and were mislocated. The bilateral cardiac progenitors in the mutant were mislocated adjacent to the otic vesicle, a condition called *cardia bifida*, instead of fusing at the midline as in zebrafish (arrowheads in Figure 3.2c'). The Cuvierian ducts, in which blood from the body flows into the heart, were severely truncated (Figure 3.2d', arrowheads). Expressivity of the *hir* phenotype, including tissue collapse and mislocation as well as defective cell migration, was consistent and was inherited in a strictly Mendelian fashion, permitting robust phenotypic rescue experiments (Chapter 5). These results suggest that tissue collapse and misalignment, and defective cell migration underlie the flattened phenotype of the *hir* mutants.

In wild-type medaka embryos, YAP transcripts were ubiquitous throughout development and maternal YAP mRNA was present at st.10 (6.5 hpf) before the onset of zygotic gene expression (Figure 3.2e). In *hir* mutants, YAP mRNA was undetectable after st.21 (34 hpf, Figure 3.2e). It was confirmed that the YAP mutation was responsible for the *hir* phenotype via two independent approaches. Firstly, knockdown of YAP by morpholino anti-sense oligonucleotides led to the same phenotype (Figure 3.2f-h). Secondly, the *hir* phenotype was rescued by ubiquitous YAP mRNA expression (Huijia Wang, *personal communication*). Overexpression of YAP with the *hir* mutation (YAP^{hir}) in wild-type embryos had no effect (Huijia Wang, *personal communication*). All of these data suggest that *hir* is a null mutation of YAP and that YAP plays a pivotal role in the morphogenesis of individual tissue/organs and their alignment in developing vertebrate embryos. The results also suggest that in medaka, YAP and TAZ have more

distinct functions, with YAP playing more of an anti-apoptotic/cell survival role and TAZ being more important for cell proliferation.

3.4.2 The Cuvierian ducts are severely truncated in *hirame*, failing to form complete looping structures and eventually collapse

As described above, the *hir* mutant exhibits cell migration defects pertaining to the heart and blood vessels along with other organs and tissues. One of the organs most clearly disrupted by this defect are the CDs. These common cardinal veins that are also present in humans, develop aberrantly in *hir* mutant embryos. *In vivo* time-lapse analysis was therefore used to address the role of YAP for cell migration and formation of this organ. Imaging revealed very clear differences in the gross morphology and development of the CDs in wild type and *hir*. The CDs were extremely truncated and incomplete in the *hir* mutant (Figure 3.4). In *hir* the CDs failed to form the distinct loop-like structure seen in wild type embryos (compare Figure 3.4f and f'). The *hir* CDs eventually appeared to collapse and start to disintegrate around st.24 (44 hpf, Supplementary movie 2) abolishing what little structure that had assembled.

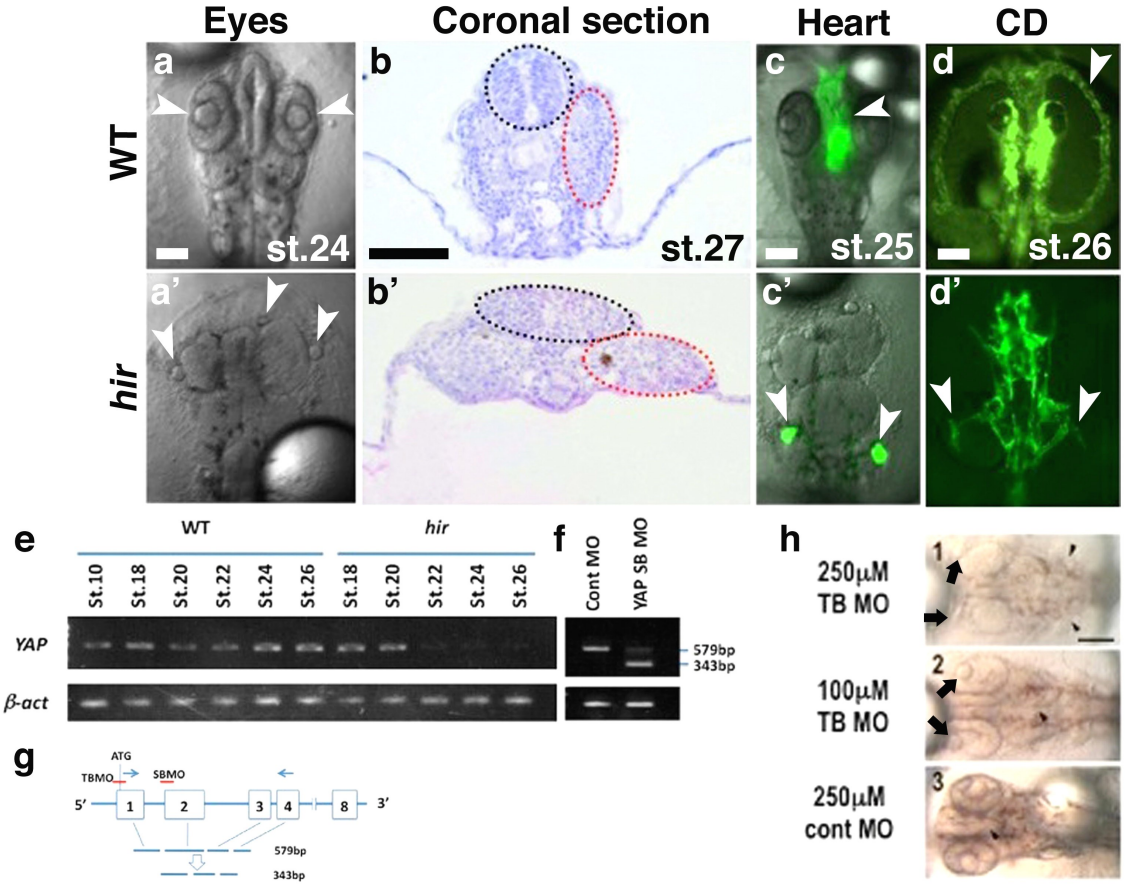

Figure 3.2. The *hirame* phenotype. (a and a') Tissue mislocalisation in the eye (arrowheads demarcate lenses, view is dorsal). **(b and b')** Epithelial tissue and organ collapse (black and red dotted lines demarcate neural tube and somites respectively). Sections in c and c' are taken along the red solid lines in a and a'. Sections are stained with toluidine blue. **(c and c')** Cell migration defects in the heart (arrowheads indicate heart tube in wild type and cardia bifida in *hir*, whereby cardiac progenitors fail to migrate and fuse at the midline, view is dorsal). **(d and d')** Cell migration defects in the CDs (arrowheads indicate complete structure in wild type and truncated ducts in *hir*, view is dorsal). **(e)** RT-PCR analysis of YAP mRNA during development. β-actin as a control. YAP transcripts were not present in *hir* after st.20. (31.5 hpf). **(f and g)** Design of YAP TB and SB MOs relative to translation start (ATG), exons (numbered boxes) and introns. Products of PCR using primers in exon1 and 4 (arrows) are shown for control (579bp) and MO injected (343bp) embryos. Proper splicing of the YAP transcript was nearly fully blocked (<5% of normal level) by the YAP SBMO as assessed by RT-PCR using primers that can distinguish defective splicing shown in (h). To further verify the specificity of YAP MOs, YAP TBMO was co-injected with human YAP mRNA that does not hybridise with the YAP TBMO. **(h)** Phenotype of YAP morpholino embryos mimicked *hir a*nd was dose-dependent (st.25, 50 hpf, arrows show dislocated lenses, arrowheads show cardiac progenitors). Scale bars: (d-d') = 100μm; (a-a') = 60μm; (b-b', c-c', h) = 70μm. Parts e-g in conjunction with Makoto Furutani-Seiki.

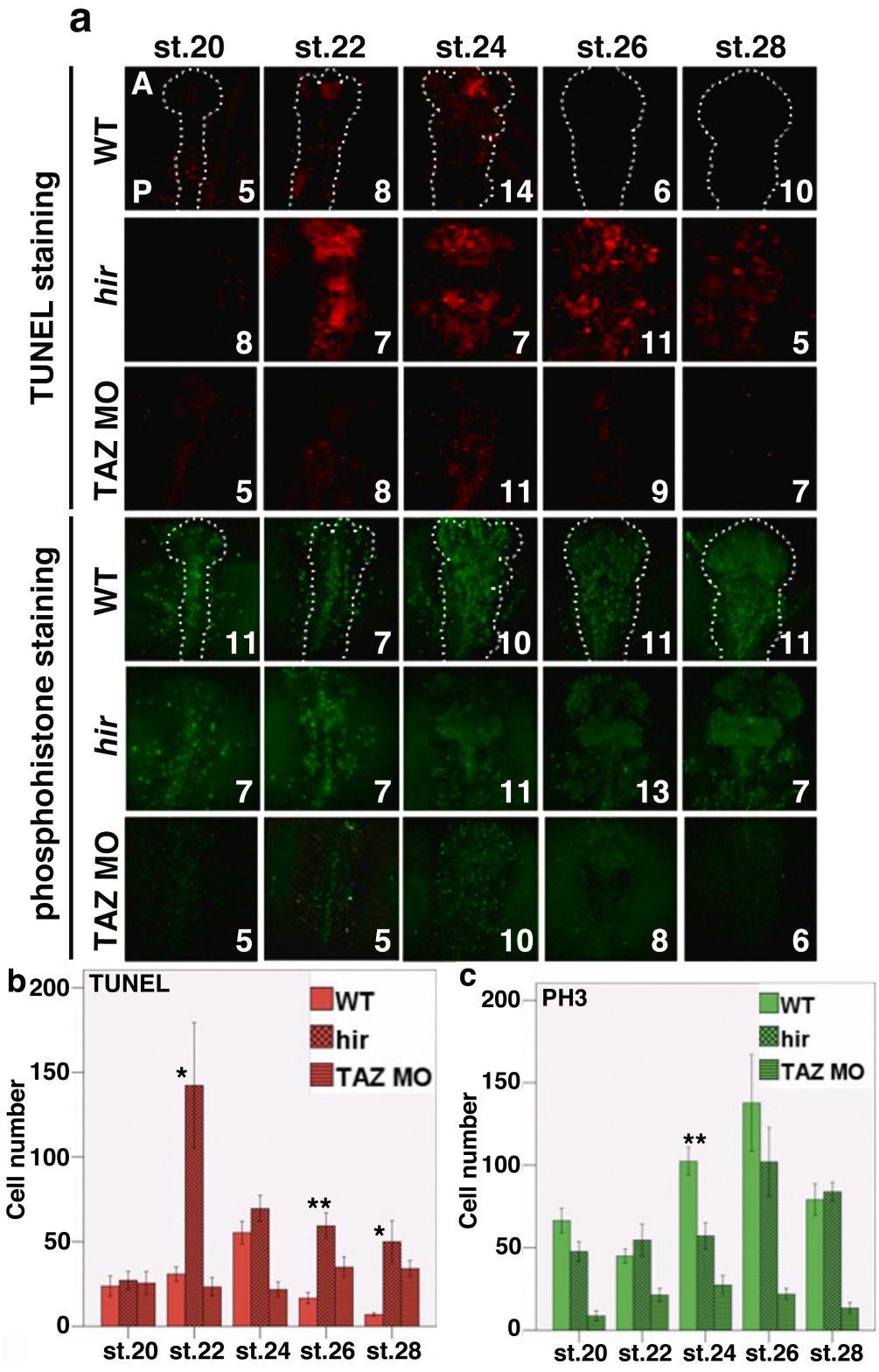

Figure 3.3. Cell proliferation defects do not underlie the *hirame* phenotype. (a) Whole-mount antibody staining for cell death (TUNEL) and cell proliferation (phosphohistone, PH3) at various developmental stages in wild type, *hir* and TAZ morpholino (MO) injected embryos. Staining shows higher cell death in *hir* and reduced cell proliferation in TAZ MO embryos. Embryo numbers are shown in white and also apply to the graphs. Embryos are representatively outlined by white dotted lines and views are dorsal. A: anterior; P: posterior. **(b and c)** Quantification of TUNEL and PH3 staining shown in (a). * = $p < 0.05$, ** = $p < 0.01$. Error bars indicate ± S.E.M.

3.4.3 The Cuvierian ducts derive from two distinct populations of cells to extend anteriorly and connect to the carotid artery of the dorsal aorta

To gain a better understanding of the exact cellular behaviour underlying the CDs defect seen in *hir*, high-resolution analysis of CD formation using confocal time-lapse microscopy was performed. From the imaging described above in Section 3.4.2, the first palpable sign of alteration in *hir* CD formation was observed as early as st.22 (38 hpf) in development. At this time, what appeared to be an endothelial cord could be seen forming in the wild type (Figure 3.4c, arrows). This apparent condensation of endothelial progenitors to form a cord was absent in *hir* (compare Figure 3.4c with c'). Confocal microscopy revealed however, that defects in CD formation started to arise as early as st.20 (31.5 hpf).

Confocal imaging also revealed the existence of two distinct populations of endothelial progenitor cells on either side of the embryo, which could be distinguished from st.20 (31.5 hpf) onwards. The first population was located in a more posterior position near the forming somites, and the other in a more anterior position close to the otic vesicle rudiment (shown at a gross level by the asterisks in Figure 3.4b). In wild type embryos, the CDs were initially observed to be forming by around st.20 (31.5 hpf) by the lateral and to a greater extent anterior migration of a stream of cells away from the embryonic body from this more posterior position near the somites (yellow arrow, Supplementary movie 1). This population of cells was termed the primary stream and strongly contributed to the formation of the rod-like structures arising in the wild type by st.22 (38 hpf, Figure 3.4c and Figure 3.5a-b).

The more anterior group of cells near the otic vesicle was termed the secondary stream, and migrated to a greater extent laterally from st.21 (34 hpf) onwards with some anterior motion to add to the tip of this lengthening primary stream (Figure 3.5c-f). This merging of primary stream and secondary stream cells was fairly complete by st.23 (41 hpf, Figure 3.4c and Figure 3.5g). From st.23 (41 hpf) onwards it could be seen that the secondary stream endothelial cells condensed to ensure the continuous production of a cord in the anterior direction (Figure 3.4d-f and Figure 3.5a-h). What appeared to be collective cell migration then extended the duct cohesively and elegantly in an anterior direction over several hours to form the distinct looping blood vessels that comprise the CDs (white arrow, Supplementary movie 1, also see panels d-f in Figure 3.4 and g-h in Figure 3.5). As well as the CDs moving anteriorly in an orchestrated and coordinated manner, the distance between the forming CDs and the embryonic body increased from st.22 (38 hpf) onwards such that the overall diameter of the CDs was increased (Figure 3.4d-f and Supplementary movie 1).

In *hir*, the two cell populations seemed less distinct even as early as st.21 (34 hpf, Figure 3.5), perhaps indicating that the primary stream in *hir* had migrated out less laterally remaining closer to the body. Additionally the primary cell population/stream seemed to migrate to a lesser extent than cells of the primary stream in the wild type by a similar developmental stage (compare Figure 3.5a-b and a'-b'). Whilst some mutant endothelial cells did migrate away from the embryonic body to a similar extent as in wild type by st.21 (34 hpf), they did not appear to condense and form close contact as observed in the wild type where a focused primary stream formed. Consequently the mutant primary stream did not move significantly anteriorly to be met by the secondary stream (compare Figure 3.5b and b', as well as Figure 3.4c and c'). In *hir*, it was observed that the secondary stream was also affected. Again the cells appeared less migratory and did not migrate as much laterally away from the embryo, with a high proportion of the progenitor cells seeming to stall in migration between the body and the stalling primary stream (compare Figure 3.5e-h with e'-h'). This failure of streams to properly meet and condense meant cohesive anterior migration was not seen in the mutant and the partially formed structures either side of the embryo began to collapse from st.24 onwards (44 hpf, Supplementary movie 2 and Figure 3.4).

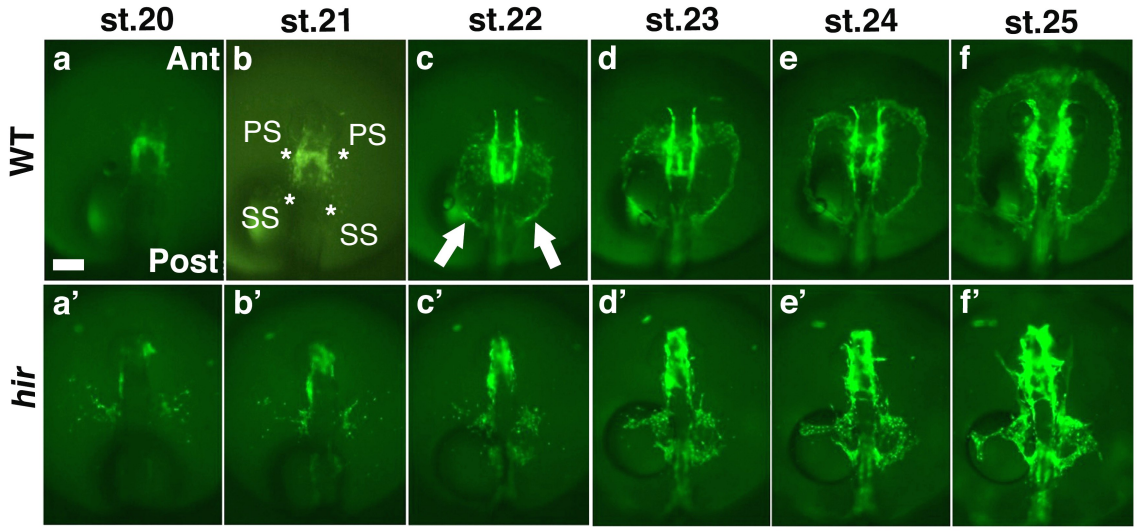

Figure 3.4. The Cuvierian ducts derive from two distinct endothelial progenitor cell populations. (a-f) Time-lapse snapshots of the CDs development in wild type. Asterisks annotate the lateral cell populations that will give rise to the primary stream (PS) and secondary stream (SS) that contribute to CD development. Arrows indicate the formation of a more focussed/condensed PS in wild type that was absent in *hir*. **(a'-f')** Equivalent snapshots in hir showing the failure of the CDs to form in the mutant. Scale bar: 100μm. Ant: anterior; Post: posterior. Views are dorsal. n = 5 embryos for wild type and *hir*.

3.4.4 Cuvierian duct cells in *hirame* lack polarisation

In order to further understand the cellular defect underlying the defective CDs formation in *hir*, single-cell analysis in both contributing populations/streams of endothelial progenitor cells using high magnification confocal time-lapse microscopy was undertaken. Whilst the primary population of cells gave rise to a primary stream to a limited extent in *hir* embryos, it did not form the nascent condensed structures as seen in wild type (Figure 3.4c, arrows). Cells of the *hir* primary stream also had little anterior movement (Figure 3.6a) when compared to wild type at the same developmental stage. Furthermore in *hir*, migration of the cells of the secondary stream seemed severely affected, and they appeared to migrate out slowly and incompletely in a lateral direction to meet the tip of the primary stream (yellow arrow Supplementary movie 2, Figure 3.5d'-h' and Figure 3.6b'). The *hir* secondary stream cells also exhibited almost no anterior migration, as evidenced by the direction of cell tracks in Figure 3.6b'. Those cells of the primary and secondary streams that did migrate in the mutant did so in an irregular manner, moving shorter distances compared to the migratory cells of the wild type streams (compare cell track lengths in Figure 3.6c with c'). Taken together these results suggest YAP is required for coordinated directional endothelial cell migration in the CDs.

Tracking of individual endothelial progenitor cells in *hir* mutant embryos, coupled with the previous time-lapse analysis strongly suggested that failure of the CDs formation was likely to be due to a cell migration defect. Cells of both the primary stream and secondary stream in *hir* failed to migrate correctly. The mean migration speed of secondary stream cells laterally away from the embryo body in *hir* was significantly slower (0.66μm/min ± 0.24, n = 58 cells, p = <0.001) than the speed of migration of cells in wild type (1.14μm/min ± 0.48, n = 39 cells, Figure 3.6d). The secondary stream was chosen for this analysis as the endothelial cells of this population were more spread out thus allowing more accurate observation and tracking. The migration of endothelial cells in *hir* was also observed to be generally inefficient with cells often migrating back and forth such that their mean displacement over 45 minutes was significantly lower (6.98μm ± 3.35, n = 48 cells, p = <0.001) than the mean displacement of endothelial cells in the wild type (30.00μm ± 11.93, n = 28 cells, Figure 3.6e). Furthermore, when the mean straightness of the migration of endothelial cells in *hir* was analysed over 45 minutes, this was also significantly reduced (0.29 ± 0.13, n = 48 cells, p = <0.001, where a value closer to 0 indicates migration with very little straightness and a value closer to 1 means completely straight migration) versus the wild type (0.73 ± 0.18, n = 28 cells, Figure 3.6f). These analyses strongly suggest a lack of directional migration in the endothelial cells of the mutant.

3.4.4.1 Endothelial cells of the *hirame* exhibit higher numbers of protrusions

Since cellular protrusions such as filopodia play an important role for directional cell migration, which appears defective in *hir*, it was decided to examine whether protrusions are affected in *hir* endothelial progenitor cells. High magnification time-lapse confocal imaging of the endothelial progenitor cells in order to visualise the dynamic process of cellular extension and retraction was performed. In wild type embryos the progenitor endothelial cells appeared polarised, extending protrusions (white arrows) predominantly in the direction of migration (yellow arrow, Figure 3.7a left panel). However, in *hir* mutant embryos endothelial cells extended and retracted many protrusions (white arrows) in multiple directions around the circumference of the cell (Figure 3.7a right panel). Quantification of the protrusion extension angle relative to the migration direction of the cell was performed at st.22 (38 hpf) for secondary stream cells over a period of 45 minutes (Figure 3.7b). This showed that wild type endothelial cells extended protrusions within a range of ± 40-60° relative to migration direction (n = 31 cells, Figure 3.7c). In *hir*, this range was vastly extended with what appeared to be filopodia observed at ± 120-190° relative to the migration direction (n = 51 cells, Figure 3.7c). This more randomised orientation of protrusions suggests *hir* progenitor cells are less polarised.

Quantitative analysis of the number of protrusions extended (st.21-25, 34-50 hpf) in the direction of migration (termed forward) versus those extended opposite to the direction of migration (termed backward) in cells of the secondary stream confirmed a lack of polarisation in the mutant (Figure 3.8a-c). The secondary stream was chosen for this analysis as the endothelial cells of this population were more spread out thus allowing more accurate observation of the cellular processes and minimising any effects of contact inhibition. In wild type embryos, the endothelial cells extended significantly ($p = <0.001$, n = 8 cells) more protrusions in the direction of migration (67.67% forward, 32.33% backwards, Figure 3.8b1-1' and c) versus *hir* (n = 8 cells) where the distribution of forward extensions (52.98%) and backward protrusions (47.02%) was not significantly different ($p = 0.083$, Figure 3.8b2-2' and c). Comparing the means of forward processes in wild type and *hir* cells gave a statistically significant difference ($p = <0.05$, Figure 3.8c). Furthermore, endothelial progenitor cells of *hir* embryos extended more cellular protrusions per minute (0.18/min ± 0.06, n = 14 cells) compared to the wild type (0.12/min ± 0.06, n = 5 cells, Figure 3.8d). Consequently, the average number of protrusions extended by endothelial cells of the mutant was significantly higher (mean of 12 protrusions per cell, n = 6 cells, as observed over a period of 60 minutes, $p = <0.05$) compared to the wild type (mean of 8 protrusions per cell, n = 9 cells, Figure 3.8e). These data are somewhat incompatible with that from Figure 3.7b which suggests that the majority of filopodia in *hir* are extended in the direction of migration. This may be due to the developmental times analysed in these respective figures. As mentioned above and shown in Figure 3.5, some cells of the *hir* secondary

stream undergo limited lateral migration towards the primary stream and this is likely captured in Figure 3.7b giving the impression of more filopodia in the direction of migration during this more polarised period. However, when cells of the *hir* secondary stream are analysed over a longer period as in Figure 3.8, the filopodia number in the forwards and backwards direction evens out as cells become more stationary following this initial lateral migration and exhibit a loss of polarisation (see tracks in Figure 3.6b').

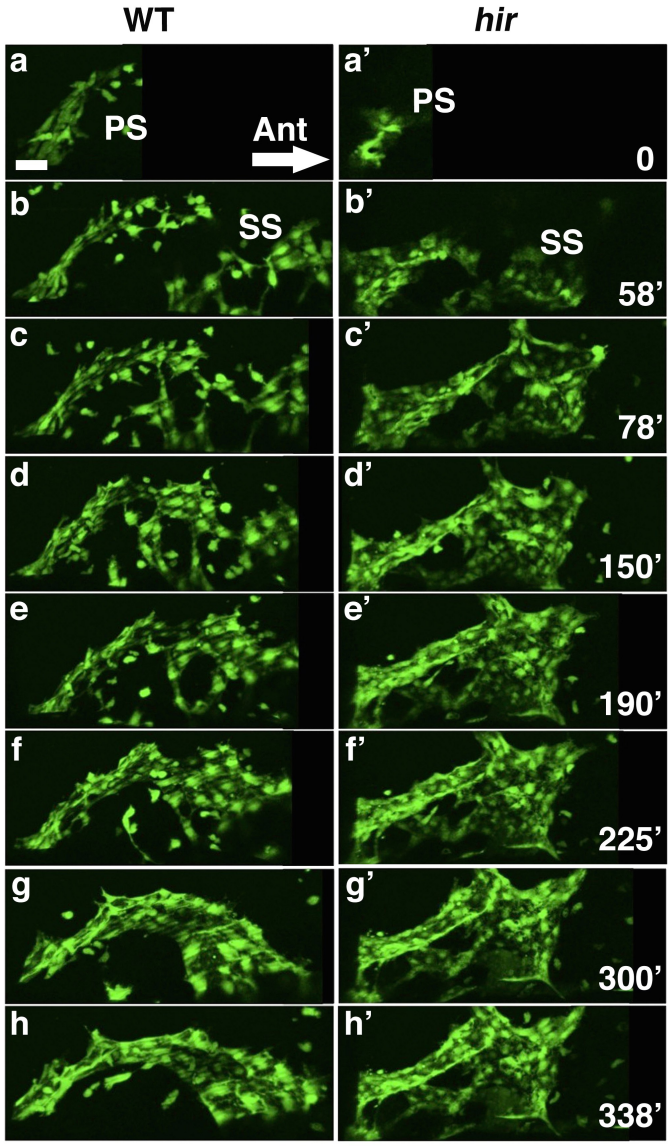

Figure 3.5. The Cuvierian ducts derive from two distinct endothelial progenitor cell populations. (a-h) Confocal time-lapse snapshots of CD development in wild type showing the relationship between the two contributing streams. **(a'-h')** Equivalent snapshots in *hir* showing the duct is less extended anteriorly and the secondary stream does not migrate out completely to merge with the primary stream to form a focussed stream. PS: primary stream; SS: secondary stream. Ant: anterior and arrow indicates the migration direction of the cells/duct. Medial (embryo body) is down and lateral is up. Time elapsed in minutes is indicated and movies started at st.20 (31.5 hpf). Scale bar: 25μm.

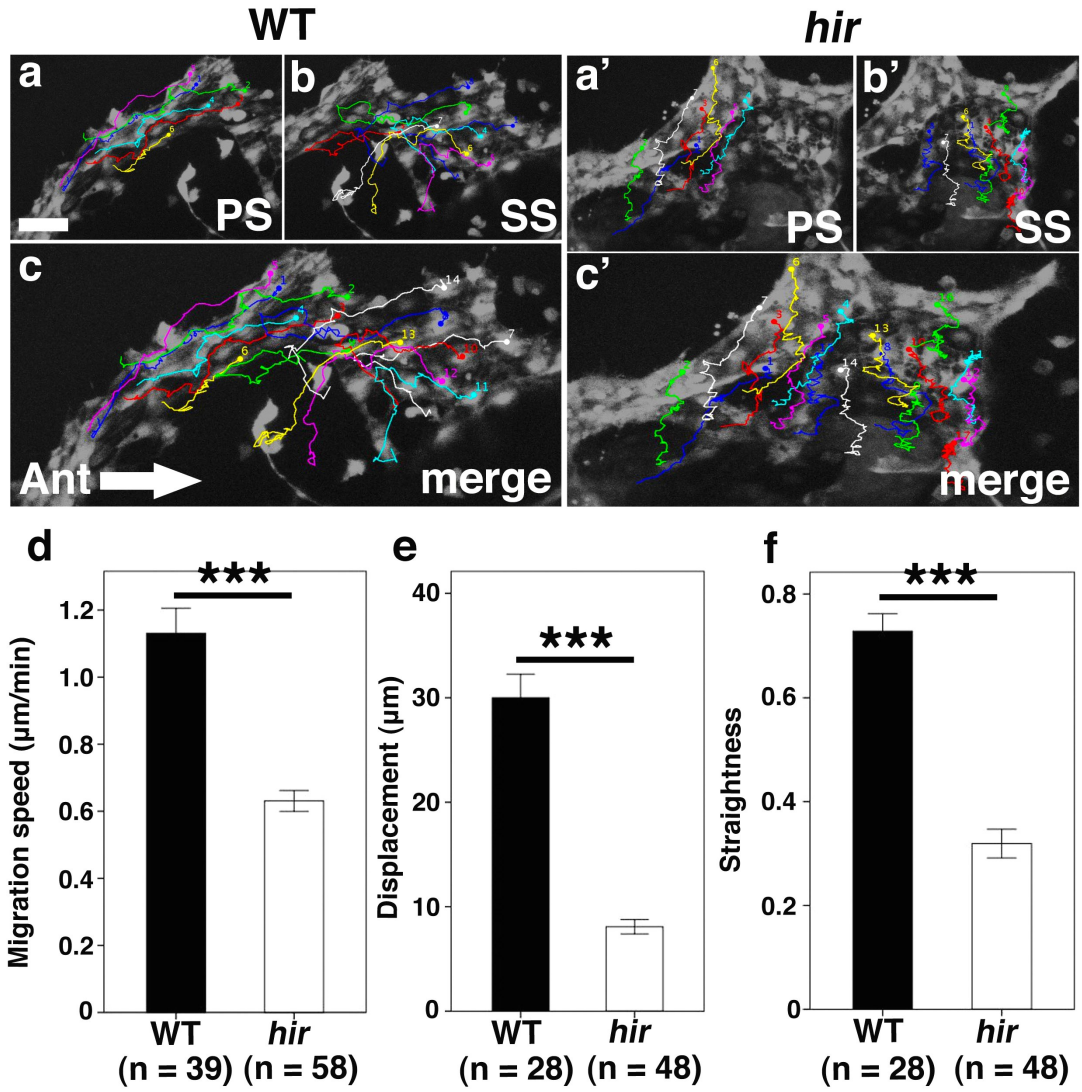

Figure 3.6. Single cell tracking of endothelial progenitor cells reveals a lack of polarisation in *hirame*. (a-c') Individual cell tracking in ImageJ shows how cells of the primary and secondary streams behave in wild type and *hir*. Each different coloured track corresponds to a different single cell and shows that in *hir* there is a distinct lack of anterior migration. PS: primary stream; SS: secondary stream. Ant: anterior and arrow indicates the general migration direction of the cells/duct. Medial is down and lateral is up. Small coloured numbers next to tracks indicate end of the track. Cells were tracked for approximately 3 hours starting at st.20 (31.5 hpf). Scale bar: 30µm. **(d-f)** Quantification of characteristics of single cell behaviour. Mean migration speed, displacement and straightness of migration were all significantly reduced in *hir*. *** = p <0.001. Cell numbers are shown in parentheses below graphs. Error bars indicate ± S.E.M.

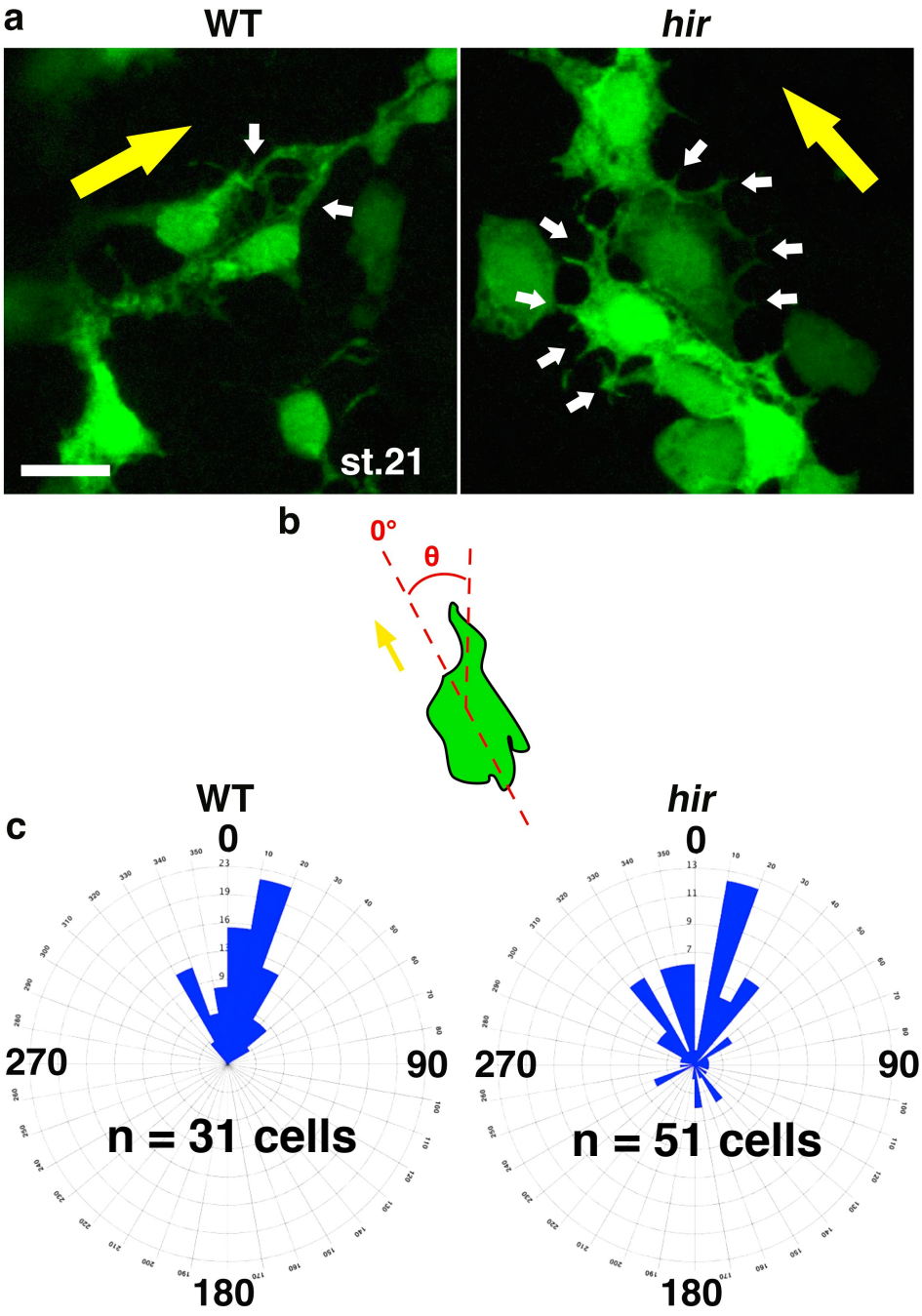

Figure 3.7. Cuvierian duct cells in *hirame* lack polarisation. (a) Snapshots from confocal time-lapse movies showing protrusive activity of migrating endothelial progenitor cells in wild type is lower than that of *hir*. Yellow arrow indicates the general direction of migration of cells, white arrows demarcate protrusions. Anterior is up, posterior down, medial to the right and lateral to the left. Scale bar: 10μm. **(b)** Schematic detailing how protrusion angle (θ) relative to migration direction (yellow arrow, 0°) was calculated. **(c)** Rose diagrams representing quantification of protrusion angle calculated from (b). Wild type cells extend protrusions predominantly in the direction of migration ± 40-60° whereas *hir* protrusions are observed ± 120-190° relative to the migration direction. Blue wedges represent the percentage of cells extending protrusions over the corresponding angle. Each circumferential segment represents 10° and each concentric ring radiating from centre to outer represents 3-4% of cells in wild type and 2% of cells in *hir*.

3.4.5 Overall fibronectin deposition is aberrant in the *hirame* mutant

As filopodia extension has been correlated with fibronectin (FN) rich areas of the ECM (Sanders *et al*., 1994), FN was investigated in *hir* embryos. Whole-mount immunohistochemistry (IHC) was performed to ascertain whether there were any differences between wild type and *hir* in terms of FN protein expression patterns. Since the endothelial cell migration is affected in *hir* from the onset of the CDs formation, it was examined whether FN was also perturbed from an earlier stage of development. Whilst the global coverage of FN appeared to be similar between wild type and *hir* at earlier stages of development (st.17-18, 25-26 hpf, Figure 3.9a and b), higher resolution analysis suggested that wild type embryos had started to form a more dense and possibly finer mesh of FN fibrils on the basal surface of epithelia and mesenchyme by the end of gastrulation/early neurulation (st.17-18, 25-26 hpf). Conversely, *hir* mutants appeared to have sparser and potentially thicker and longer FN fibrils (compare Figure 3.9a' and b'). Quantitative analysis of this is required to confirm this aspect of the phenotype at this stage of development. This FN defect was also maintained later into development where differences between the wild type and *hir* were more apparent, as observed in other tissues such as the eye (Chapter 4).

Interestingly, it was also observed that these aberrant FN fibrils in *hir* mutants appeared converted into shorter or punctate FN by maternal YAP knockdown in the *hir* mutants using 0.6ng of YAP TBMO (termed mYAPKD *hir*, Figure 3.9c', bright dotted appearance). Furthermore, this FN defect was mimicked in wild type embryos by expressing N-terminal 70kDa fragments of FN (McDonald *et al*., 1987). This was achieved by injecting the wild type embryos with mRNA encoding these N-terminal 70kDa fragments of FN (termed FN 70kD from herein) which act in a dominant negative manner to block FN assembly. Consequently only globular FN was observed in wild type FN 70kD embryos (Figure 3.9d-d'). Some of the FN puncta observed in mYAPKD *hir* embryos were larger than those seen in FN 70kD embryos and these larger puncta may have been generated by the rounding up of longer and thicker fibrils in *hir* mutants. Interestingly, injection of FN 70kD into wild type embryos mimicked the CDs defect seen in *hir* (Figure 3.9e) in that FN 70kD embryos also had truncated ducts that failed to complete development. This strongly suggests that defective FN fibrillisation plays a role in the migration defect of endothelial progenitor cells of the CDs in *hir* mutants. Total FN protein levels did not significantly differ between the wild type and mutant as analysed by western blotting at earlier (st.17, 25 hpf) and later (st. 22, 38 hpf) stages of development despite the obvious differences in physical appearance (Figure 3.9f, data kindly provided by Shoji Hata), suggesting FN protein level was not the cause of this deposition defect. Altogether, this pertains to a potential FN structural defect in *hir*, in which FN may not be correctly polymerising to form fibrils.

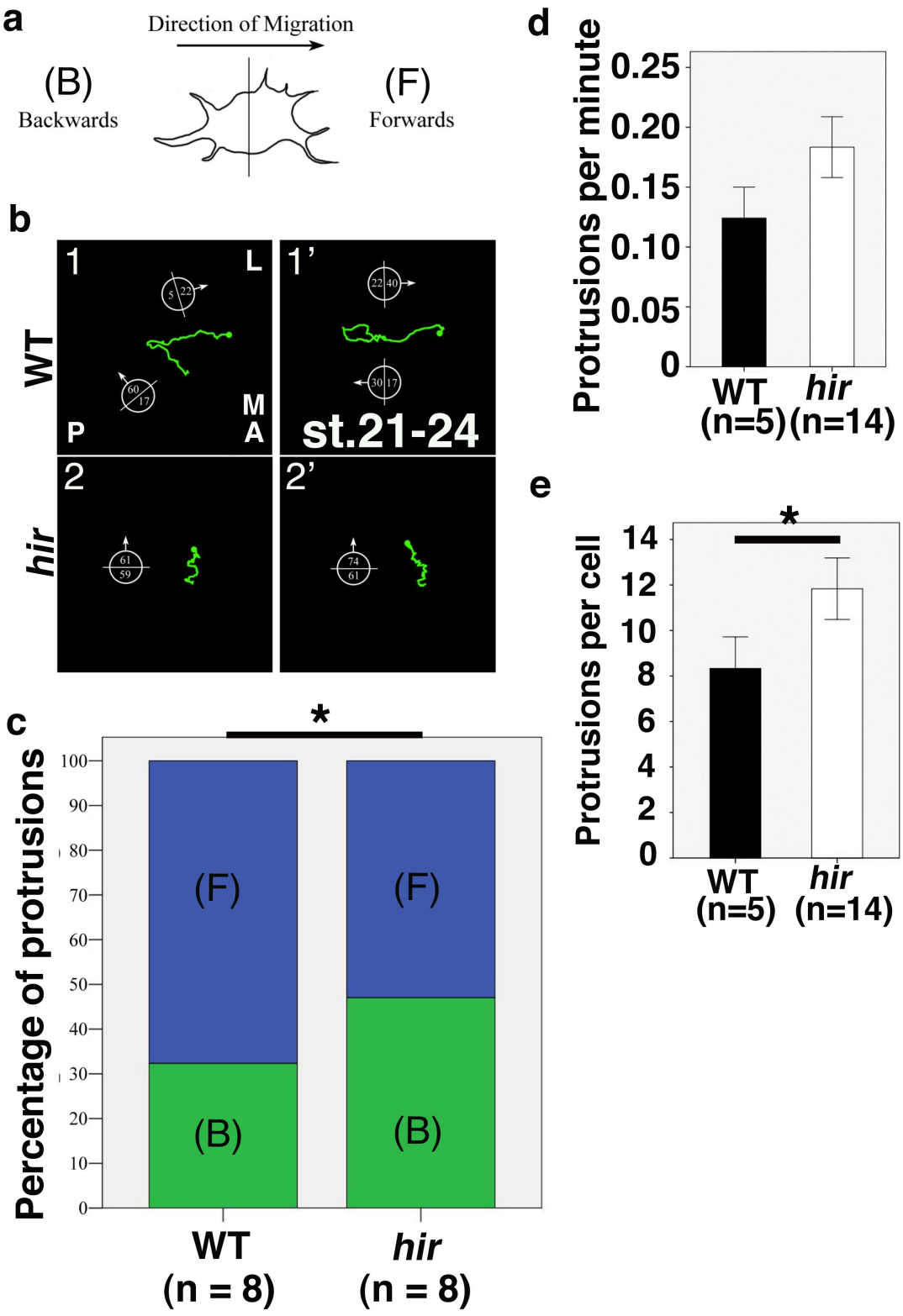

Figure 3.8. Quantification of protrusions in *hirame*. (a-c) Protrusion direction was quantified relative to migration direction of the endothelial progenitor cell (a). Representative cell tracks and the protrusions forwards and backwards are shown in the compass in (b), where the migration direction of the cell is indicated by the arrow. L: lateral; M: medial; A: anterior; P: posterior. The percentage of forward protrusions is significantly higher in wild type (c). **(d)** *hir* exhibits more protrusions per minute. **(e)** Cells in *hir* have a significantly higher average number of protrusions. * = p <0.05. Cell numbers shown in parentheses. Error bars indicate ± S.E.M.

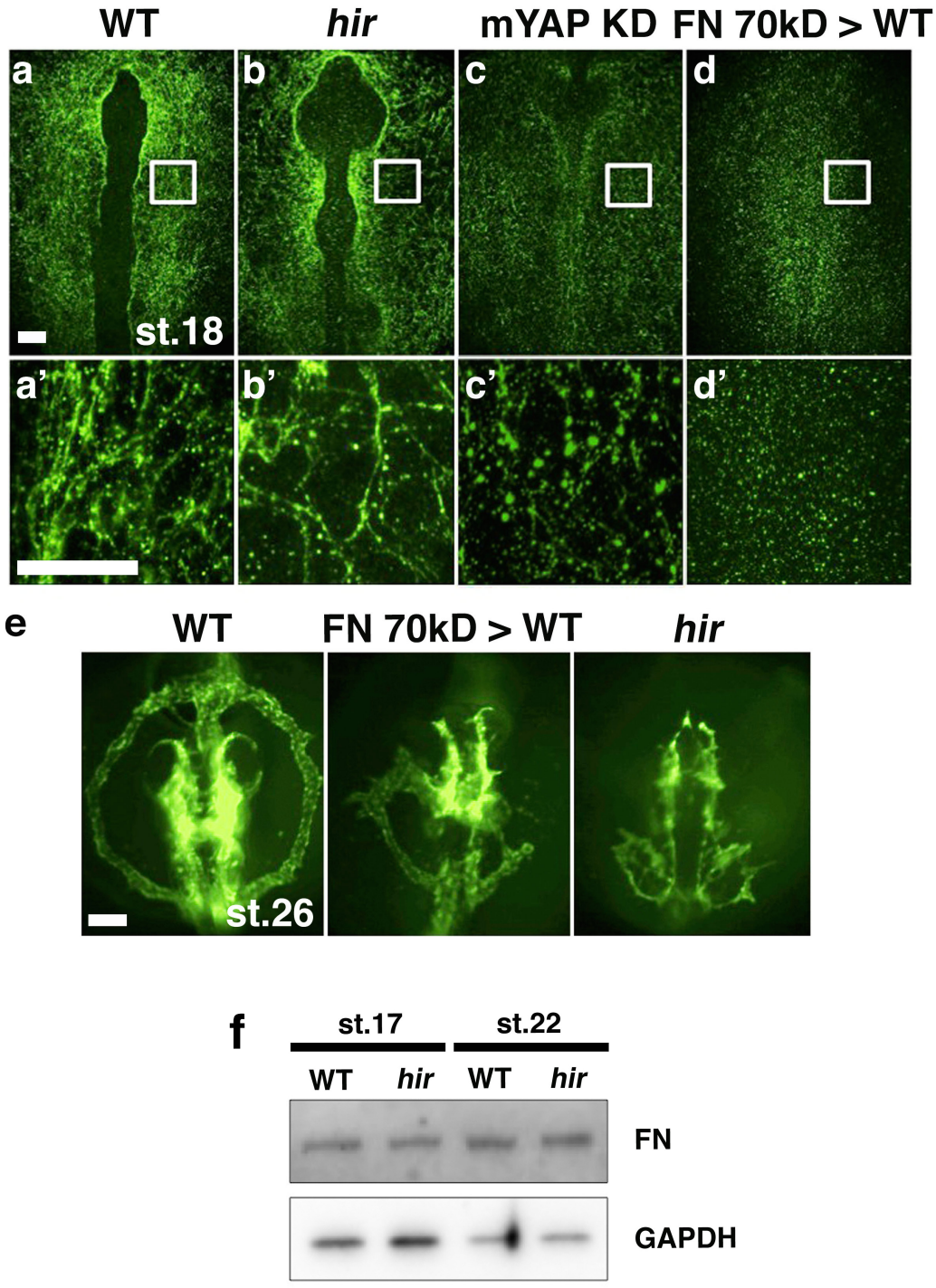

Figure 3.9. Fibronectin architecture appears aberrant in *hirame*. (a-b') Whole-mount FN antibody staining suggests FN fibrils in *hir* may be thicker and longer even by early stages of development. **(c and c')** This fibrillisation defect is exacerbated in mYAP KD *hir* where more globular FN is observed. **(d and d')** FN fibrillisation is completely blocked by injection of dominant negative 70kD FN into wild type embryos such that only FN puncta are observed. **(e)** FN 70kD injection mimics the cell migration defects seen in the CDs of *hir*. **(f)** A reduction in total fibronectin level does not appear to underlie the fibrillisation defect in *hir*. Western blotting for FN shows little difference in total protein level between wild type and *hir*. Scale bars: (a-d') = 40μm; (e) = 100μm. All views are dorsal with anterior up and posterior down. (a'-d') show magnifications of the boxed regions in (a-d).

3.5 Discussion

3.5.1. YAP is a key regulator of 3D body shape in vertebrates and appears to regulate many important developmental processes

For YAP to function as a key regulator of body shape and organ size it needs to regulate many developmental processes. Such YAP-regulated activities might include ECM formation and remodelling, cell migration, differentiation, apoptosis and proliferation amongst others. These processes are fundamental for development, including correct organ growth and organ homeostasis. Indeed YAP has already been shown to be governing many of these processes including cell differentiation, proliferation and death (e.g. Camargo *et al*., 2007). The results presented in this chapter, based on analysis of organogenesis in an intact mutant animal, indicate that YAP is a key regulator of 3D body shape. Positional cloning and biochemical analysis strongly suggest that the *hir* mutant is a YAP-null mutant. In the absence of YAP in *hir*, three main characteristics associated with the mutant phenotype are observed. Firstly, epithelial tissues and organs are collapsed and flattened such as the brain, spinal cord, somites and eyes. In some cases epithelial tissues and organs do not form as is true for the dorsal aorta and the midgut. Secondly, tissues are mislocated in *hir* such that coordinated development of normally adjacent tissues does not occur properly. This is particularly evident in the eyes where the lenses dislocate from the retinas instead of invaginating into them as normally seen. Thirdly, YAP-null mutants display pronounced cell migration defects, particularly evident at earlier stages of development in formation of the primitive blood vessels and the heart, where progenitor cells arrest migration and fail to locate correctly to produce a complete and functioning tissue/organ.

Previous loss of function analysis of YAP or Yorkie (Yki, the *Drosophila* YAP homologue) has been hampered by early lethality of YAP knockout mice (E8.5, Ota & Sasaki 2008) and compromised cell proliferation of Yki-deficient cells (Genevet *et al*. 2009; Hamaratoglu *et al*. 2009; Zhao *et al*. 2008). In contrast, in the medaka *hir* mutants, the presence of maternal YAP mRNA prevents early onset of defects that would otherwise conceal later neural morphogenesis defects. Furthermore, medaka has allowed the decoupling of cell proliferation defects from the other phenotypes of YAP mutants, since cell proliferation occurred nearly normally in *hir* mutants. In the mouse, YAP knockout embryos are early lethal whereas TAZ knockouts are viable (Makita *et al*. 2008). In medaka, TAZ (the mammalian paralogue of YAP) knockdown embryos had strong cell proliferation defects and became early embryonic lethal. These differences may have arisen due to diversification of the functional subdivision between YAP and its paralogue TAZ between mice and medaka. Furthermore, in zebrafish YAP knockdown (KD) embryos, the collapse/flattening phenotype and mislocation phenotype was not reported suggesting a stronger redundancy between YAP and TAZ in zebrafish. Interestingly, zebrafish YAP KD embryos displayed delayed cardiogenesis and hematopoiesis that recovered later in development (Hu *et al*., 2013).

This was not attributed to affected cell migration and the zebrafish YAP KD embryos exhibited normal vasculogenesis unlike *hir*, again suggesting YAP/TAZ redundancy in zebrafish.

3.5.2 YAP is required for correct endothelial progenitor cell migration

Whilst YAP has been shown to induce epithelial-to-mesenchymal transition *in vitro* when overexpressed (Overholtzer *et al*., 2006), less is known about the role for YAP in cell migration *in vivo*. Since the *hir* mutant displayed prominent cell migration defects during phenotypic characterisation, this was investigated in further detail to elucidate the role of YAP for cell migration. To this end the development of the CDs was analysed *in vivo* in real-time. Time-lapse movies of CDs formation show that this process is severely impaired in the *hir* mutant compared to wild type embryos. In wild type, the primary streams of each duct are generated from a population of cells on either side of the embryo near the first few somites. These cells begin to migrate out laterally and anteriorly from the embryo to give rise to a primitive cord-like structure. Endothelial progenitor cells from a secondary population close to the otic vesicle rudiment then migrate out laterally from the body to meet the leading edge of the primary stream. The addition of these secondary stream endothelial progenitor cells continues to extend the primary stream anteriorly to grow the CDs. The seemingly collective migration of the duct eventually gives rise to the distinct looping structure and closed circulatory system prior to the onset of blood circulation at st.25 (50 hpf). These mechanisms are summarised in the model depicted in Figure 3.10. Thus it seems that normal endothelial progenitor cell migration to form the CDs in wild type shares aspects of the migration modes observed in both the formation of the heart (loosely collective migration) and the distribution of the NC cells (streams of migrating cells).

In contrast, both the primary and secondary stream endothelial progenitor cells in *hir* show defective migration. Whilst the primary stream extends by a small amount, the majority of secondary stream cells fail to migrate significantly towards the primary stream tip, and those that do to some extent, do not appear to successfully integrate with the primary stream cells, failing to migrate anteriorly. This results in a failure to extend the primary stream and therefore *hir* embryos are unable to form the CDs demonstrating that YAP is required for CD development in medaka. A more precise role for YAP in CD development may be dissected using transplantation experiments and chimeric analysis similar to that carried out in Chapter 6. The migration of wild type cells targeted to the secondary stream of the *hir* mutant could be observed to give clues about the relative contribution of the aberrantly fibrillised FN substrate to the migration defect seen in the mutant endothelial cells. These experiments may also elucidate whether any proportion of the migration defect is perhaps more cell-autonomous in nature. Furthermore the polarity/protrusions of the wild type cells transplanted into the mutant could also be assessed. Again this would allow

conclusions about the cell autonomy of the polarity defect to be ascertained. Such studies may help to delineate which aspects of the *hir* CD defect are upstream of others. It would also be interesting to examine whether the wild type cells transplanted into *hir* have any effect of the appearance of the FN surrounding the mutant CD both adjacent to the wild type cells and more long-range.

Interestingly, in mice lacking the Src kinase Yes, fibroblasts exhibit impaired migration forming large peripheral adhesions that have a reduced turnover (Klinghoffer *et al*., 1999). It has been previously shown that YAP is required for vasculogenesis in mice, as a homozygous mutation for the *YAP65* gene resulted in disruption of the development of an organised yolk sac vascular plexus which arrested development at E8.5 (Morin-Kensicki *et al.*, 2006). Taken together, these results suggest the requirement of YAP for normal blood vessel formation and development appears to be somewhat conserved amongst vertebrates. Morin-Kensicki *et al*. (2006) however, did not report the mechanism by which YAP contributes to vasculogenesis, which is an important aim of this chapter and will now be discussed.

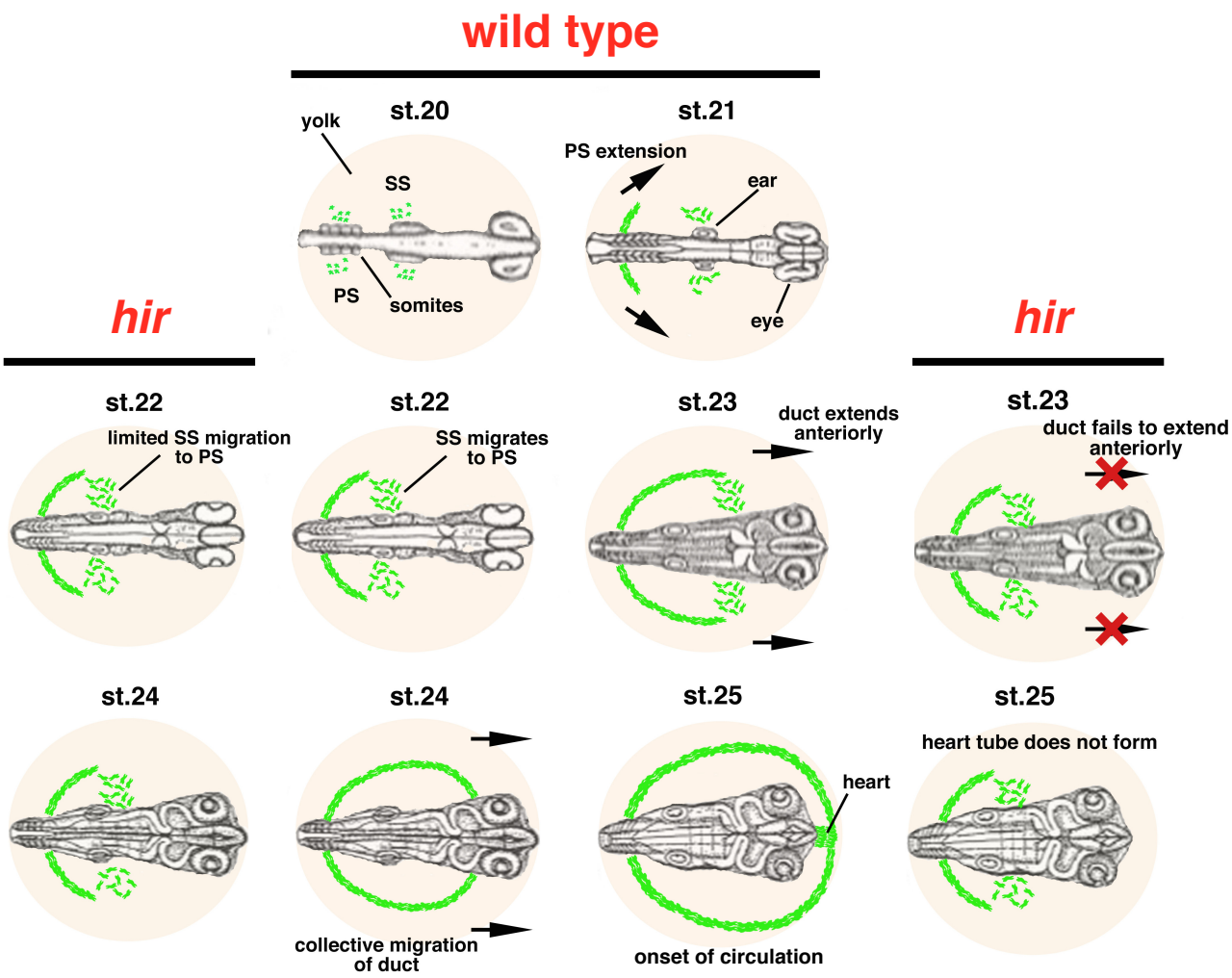

Figure 3.10. Schematic summarising Cuvierian duct formation in wild type and *hirame* medaka embryos. At st.20 (31.5 hpf) the two endothelial cell populations (green) that will give rise to the primary stream (PS) and secondary stream (SS) can be seen either side of the embryo. By st.21 (34 hpf) the PS starts to extend laterally and anteriorly and by st.22 (38 hpf) meets the SS population of cells. The SS cells add to the tip of the PS until late st.23 (41 hpf) and by st.24 (44 hpf, heart beating stage) the CDs have formed a complete circuit. This looping structure continues to increase in size and migrate anteriorly up to st.25 (50 hpf) when the heart is located anteriorly of the head. Differences in *hir* are indicated from st.22 onwards when they become more prominent. Other features of *hir* phenotype not shown for simplicity. Arrows indicate migration direction. Prominent embryonic features/structures are labelled. Drawings of embryos adapted from Iwamatsu (2004). All views are dorsal with anterior to the right and posterior to the left.

3.5.3 YAP regulates fibronectin fibrillisation for correct endothelial progenitor cell migration

The extracellular matrix (ECM) is fundamental in normal development, as it provides support and signals that regulate processes such as cell migration (Bateman *et al*., 2009). Morpholino experiments in *Xenopus* (discussed further below) and zebrafish, and FN mutation in mice (George *et al.*, 1993), have shed light on the importance of FN for cell migration during early development. For example, morpholino knockdown of FN was shown to disrupt cell migration during zebrafish gastrulation (Latimer and Jessen, 2010). Of particular interest is the fact that FN fibrillogenesis has been shown to be important for normal cell migration during blood vessel formation during embryogenesis, as the absence of FN causes defective blood vessel development (George *et al.*, 1993). Interestingly, YAP knockout mice show a phenotype similar to FN knockout mice (Nishioka *et al*., 2009). In *hir*, it appeared FN fibrillisation was aberrant yet the total FN levels between wild type and mutant embryos did not appear significantly different. This suggests the level of FN is less important for cell migration than the conformation or assembly of FN. Therefore it is proposed that YAP is regulating FN fibril formation for endothelial cell migration.

FN–integrin interactions are known to initiate a step-wise process involving conformational activation of FN outside the cell coupled to organisation of the actin cytoskeleton inside the cell (Mao and Schwarzbauer, 2005). In this process, changes in the actin cytoskeleton, which is tethered to integrin receptors via talin, vinculin and α-actinin (Vicente-Manzanares *et al*., 2009) amongst others, causes physical changes in FN dimers bound to integrin. These conformational changes in FN expose cryptic binding sites for FN-FN interactions and further conformational changes in FN, the result being the formation of FN fibrils and eventually the production of an insoluble fibrillar matrix (Singh *et al*., 2010).

In *hir*, the FN fibrils appeared longer and thicker which gave an overall spiked, coarse and rough appearance to the mutant FN deposition compared to the smooth fibrils seen in the wild type. As FN acts as a framework for cell adhesion during the migration of many cell types (Ruoslahti, 1988), if this extracellular scaffold is perturbed, perhaps cells cannot move along the framework correctly and form focal adhesions properly for successful migration. Previous work has shown that single endothelial cells migrate along artificial stiffness gradients towards stiffer regions of the substrate *in vitro* (Gray *et al*., 2003) in a process termed mechanotaxis. Could mechanotaxis be important for endothelial cell migration *in vivo*? In light of this it is tempting to speculate that perhaps the defectively fibrillised FN substrate in the mutant is more or too compliant, hindering migration. From a structural viewpoint this may make sense since a less polymerised FN substrate may not crosslink as well and thus may have less mechanical strength.

Moreover, regulation of matrix stiffness is important for ensuring the correct adhesion level and generation of traction forces by migrating cells (Choquet *et al*., 1997).

Perhaps the FN assembly defects in *hir* mean such stiffness gradients described by Gray *et al*. (2003) cannot be established. Since the migration of the endothelial cells in the CDs occurs from posterior to anterior it would be of interest to examine whether there is any gradient of stiffness in this axis. Moreover, a very recent report suggests filopodia can detect topographies at the nanoscale and even modify the substrate through bending and folding to preferentially align it, which may be important for processes including migration (Albuschies and Vogel, 2013). This raises a couple of possibilities in *hir*. Firstly, since the FN substrate is affected the filopodia in the mutant may not be able to manipulate it to produce a preferential topography. Secondly, perhaps the multiple filopodia being generated can modify the substrate but do so in a circumferential manner around the cell such that all directions seem preferential and polarisation of the cell does not occur resulting in reduced migration, as is seen in *hir*.

Integrin α5β1 (itgα5β1) binds to RGD-containing regions of FN to mediate cell adhesion to FN (Fogerty *et al.*, 1990). In endothelial cells, itgα5β1 receptors mediate FN fibrillogenesis (Zhou *et al*., 2008); therefore it is possible that the defectively fibrillised FN observed around the CDs in *hir* could be due to defects in itgα5β1-FN interactions. As itgα5β1 was not investigated in the endothelial cells of the CDs of *hir*, this remains speculative. However, there is evidence in the literature to support this idea. Inhibiting itgα5β1 with monoclonal antibodies completely blocks FN binding to itgα5β1 (Fogerty *et al.*, 1990). In α5-null mouse embryos, it was observed that there was a marked decrease in the complexity of the vasculature and this was correlated with decreased FN matrix assembly in the basement membranes of α5-null endothelial cells (Francis *et al.*, 2002). Francis *et al*. (2002) showed a similar phenomenon was also observed in embryoid bodies directed towards an endothelial lineage, ruling out the possibility that nutritional deficiencies as a result of vascular defects caused the FN defects seen *in vivo*. itgα5β1-regulated FN fibrillogenesis requires translocation of itgα5β1 to actin filament bundles, generating cytoskeleton tension that initiates early FN fibrillogenesis. If this translocation of itgα5β1 is prohibited, FN fibrillogenesis is inhibited (Pankov *et al.*, 2000). Perhaps itgα5β1 translocation is defective in *hir*, which could cause the aberrant FN fibrillogenesis. Conversely, a structural defect in FN itself could be causing the fibrillogenesis defect. As discussed above, the RGD domain of FN binds itgα5β1 to initiate fibrillogenesis. In mice where this RGD region is replaced with an inactive RGE motif, a similar phenotype to itgα5β1-null mice is seen, including defects in the development of blood vessels causing embryonic lethality at E10 (Takahashi *et al.*, 2007). Therefore some level of structural analysis of both integrin and FN in *hir* may provide further insights.

Endothelial cell–specific chemotaxis receptor (ECSCR) is a cell surface protein expressed by blood endothelial cells and is involved in migration and signal transduction (Armstrong *et al*., 2008). Knockdown of *ecscr* by morpholino causes defective endothelial progenitor cell/angioblast migration in zebrafish (Verma *et al.,* 2010). Interestingly, ECSCR has been shown to localise to actin-rich membrane protrusions in cultured human endothelial cells, and to regulate actin cytoskeleton remodelling (Armstrong *et al*., 2008). So far there are no reports of ECSCR being present in medaka. However, if endothelial cell migration in medaka is at all regulated by chemotaxis (of which there are currently no reports to this author's knowledge), it is possible that due to the enhanced numbers of circumferential filopodia, ECSCR may be present around the circumference of the cell. This means ECSCR would be exposed to any chemoattractant in a less polarised/localised way. If the chemoattractant has a fine-scale gradient perhaps the cell is not sensitised enough to the cue. The mutant endothelial cell polarisation defect would therefore be upstream of this ectopic ECSCR localisation, but since ECSCR is responsible for actin cytoskeleton remodelling in response to external cues, this may exacerbate the polarisation defect in *hir*.

In conclusion, this work has shown that FN fibrillogenesis is defective in the *hir* mutant, but the underlying cause of this FN assembly defect remains to be elucidated and there are several possibilities that warrant further investigation.

3.5.3.1 YAP regulates fibronectin fibrillisation for endothelial progenitor cell polarisation

Morpholino knockdown of FN in *Xenopus* disrupts the polarisation of cellular protrusions, which causes defective cell migration during gastrulation (Davidson *et al.*, 2006). The actin cytoskeleton is important for the formation and retraction of filopodia during cell migration (Etienne-Manneville and Hall, 2002). Without the correct cell-matrix interactions occurring through integrin-FN binding, this cytoskeleton is not reorganised and filopodia are not correctly distributed. This is seen in *hir* where endothelial cells appear to be non-polarised, extending and retracting many filopodia in a more random manner around the circumference of the cell. This lack of polarisation in the mutant endothelial cells is likely contributing to their defective and reduced migration, and may be a secondary defect of the improper FN fibrillogenesis. If itgα5β1 is affected in the CDs of *hir* as discussed above, this could also have implications for the control of cellular protrusions. Integrins are located at the tips of filopodia and their interactions with FN are important for regulating Rho family GTPase activity during cell migration (Cox *et al*., 2001). Important components of the actin cytoskeleton are known to be the GTPases Rho, Rac and Cdc42 (Hall, 2005). Cdc42 inhibition disrupts both the stability and directionality of cellular protrusions, which results in defective cell migration (Srinivasan *et al.*, 2003). In *hir*, perhaps Cdc42 is affected, which may in turn

disrupt downstream signalling through this GTPase. Cdc42 signalling through the PAR6-PAR3-aPKC complex is known to have an important role in regulating cell polarity (Ohno, 2001) and may therefore be a potential cause of the lack of polarisation seen in *hir* endothelial cells. Therefore defects in integrin signalling could have multiple implications for CDs development, affecting filopodia polarisation as well as FN assembly, both of which are important for cell migration.

The Rho GTPases are also essential for FN fibrillogenesis during blood vessel development. For example, cells deficient in Rac1 and Cdc42 display defective FN architecture (Fernandez-Sauze *et al.*, 2009). Furthermore, lumen establishment during blood vessel development is affected by inhibition of Rac1 and Cdc42 (Bayless and Davis, 2002). A recent paper from the Mayor group was the first to perform FRET analysis of the Rho GTPases *in vivo* (Matthews *et al*., 2008). It may be possible to perform similar experiments in *hir* and ascertain the activation status of Cdc42, Rac1 and RhoA in the endothelial cells of the CDs. This would allow determination of whether they play a role in the *hir* CDs phenotype.

In human umbilical vein endothelial cells (HUVECs), Robo4 knockdown by siRNA inhibited endothelial cell migration and tube formation, and overexpression of Robo4 strongly induced filopodia in endothelial cells (Sheldon *et al*., 2009). Both these migration and protrusion phenotypes are seen in *hir*. Furthermore, it has recently been shown that the polarity protein Scrib is essential for directed endothelial cell migration as siRNA against Scrib blocked directed migration of HUVECs and caused an increased number and disruption of orientation of cellular protrusions (Michaelis *et al*., 2013), similar to that seen in *hir*. The ubiquitin ligase Smurf1 regulates the actin cytoskeleton, cellular protrusions and polarity by regulating the ubiquitination degradation of RhoA in filopodia. Interestingly, Smurf1 over-expression resulted in more protrusions at the leading edge, whereas siRNA inhibition of Smurf1 resulted in the loss of protrusions (Wang, *et al.*, 2003). Whilst this increased protrusion phenotype bears some resemblance to the loss of polarity seen in *hir* endothelial cells, Smurf1-induced protrusions were only seen at the leading edge unlike in the *hir* mutant where protrusions were observed circumferentially in endothelial progenitor cells.

In summary, there exist many other candidates outside FN and integrin that can cause loss of polarity and excessive protrusions in migrating cells. In the future it will be essential to narrow down which of these candidates YAP may be regulating in order to establish what is the key molecular link between YAP and directional cell migration in order to fully exploit this function of YAP.

3.5.4 A role for epithelial-to-mesenchymal transition in the formation of the Cuvierian ducts?

Epithelial-mesenchymal transition (EMT) is the transition from an epithelial status to a mesenchymal status and is essential for tissue remodelling during embryonic development (Thiery, 2002). EMT includes changes in morphology, cellular architecture, adhesion and migration (Lee *et al.*, 2006). The opposite transition of mesenchymal-epithelial status (MET) is also seen. A number of characteristic markers of epithelial and mesenchymal cells have been identified which help to define what state a cell is in. For example, epithelial markers include E-cadherin, occludins and claudins, whereas mesenchymal cells express markers such as vimentin and vitronectin (Thiery and Sleeman, 2006). EMT is further characterised by an increase in transcription factors such as Snail1/2, Twist and ZEB1/2 (Lee *et al.*, 2006).

The endothelial progenitor cells of the CDs (also called angioblasts) derive from the lateral plate mesoderm (LPM) and undergo EMT to allow migration to form the primary vasculature. Upon coalescing and undergoing tubulogenesis, angioblasts must then essentially undergo MET (Xu and Cleaver, 2011). It was attempted to assess the epithelial/mesenchymal status of endothelial progenitor cells during the CDs formation to determine EMT/MET patterns in wild type and *hir* embryos. However, this proved technically challenging. During fixation of embryos for whole-mount antibody staining of E-cadherin and vimentin, the yolk often contracted and changed shape. This meant the architecture of the CDs was often not well preserved. Furthermore, at earlier stages of development when the primary and secondary pool of cells are about to migrate, the signal obtained by immunohistochemistry was poor. Consequently it could not be determined whether EMT/MET plays a role in development of the CDs and whether this was altered in *hir*, as this could be another contributing factor to the *hir* cell migration defect phenotype.

3.5.5 The Cuvierian ducts as a model of collective migration?

It is interesting to consider the CDs as a model for collective migration for several reasons. Firstly, there are parallels between the way in which the heart tube forms and how the CDs form in regards to the origin of progenitor cells for both organs, a FN dependency during migration and a highly coordinated and directional movement as what appears to be a cohort. Given the collectively migratory nature of the cardiac progenitors as described by Trinh and Stainier (2004), it is tempting to speculate that collective migration may also be occurring in the CDs. Secondly, the cells at the leading edge of the advancing duct bear a resemblance to the tip cells of the zebrafish lateral line both in terms of appearance and function. In the lateral line system several cells at the front of a migrating cohort of cells act as leader cells to guide the cells behind, which appears similar to what is seen in the anteriorly advancing CDs.

A very recent report by Lucas *et al*. (2013) describes the role of the Hippo pathway in polarising the actin cytoskeleton during collective migration of border cells in *Drosophila*. In this model, the Hippo pathway is proposed to limit actin polymerisation to the outer rim of the cluster of border cells such that polarised and coordinated directional migration occurs. Loss of Hippo signalling, specifically Wts, results in excessive F-actin polymerisation throughout the cluster which leads to slowed migration with a tumbling phenotype. Could this phenotype somehow be analogous to the endothelial cell migration defect in *hir*? Lucas *et al*. (2013) also show that expression of a constitutively active form of Yorkie (Yki, *Drosophila* orthologue of YAP) accelerates border cell migration suggesting Hippo signalling is regulating the actin cytoskeleton independently of Yki. If migration in the CDs is collective then it may prove interesting to analyse the upstream components of the Hippo signalling pathway in *hir*.

3.5.6 Unanswered questions regarding YAP-regulation of the development of the Cuvierian ducts and further work needed

Whilst the work in this chapter sheds light on some of the processes underlying development of the CDs, several questions remain. Whilst the defective FN substrate discussed above is likely to be a major cause of the migration defect given its importance in cell migration, it is possible there are many other factors that are important in CDs formation, which could be affected contributing to the resulting mutant phenotype. Aside from the further experiments that could be performed based on the discussion above, this section will summarise other research that could be a continuation of this work.

First it is interesting to consider whether the failure of ducts to form in the *hir* mutant is attributable only to a cell migration defect (which may be caused by multiple factors), or whether a cell number defect also contributes. Evidence for this comes from Zhou *et al*. (2008) who have shown that in 3D cultures of endothelial cells, endothelial cell number is dependent on the formation of FN fibrils in the surrounding 3D ECM. In this context, it may be possible that a certain number of endothelial progenitor cells are required to extend the primary stream sufficiently in the anterior direction such that the secondary stream can effectively migrate out laterally from the embryo to meet it. This may then allow the whole duct to extend anteriorly to form the complete looping vessels. Perhaps if less progenitor cells are present in *hir* coupled with reduced migratory ability, both possibly due to the FN defect, this leads to the failure of the CDs to form. To test whether cell number is important, endothelial cell number in the wild type could be reduced by laser ablation for example. It is interesting to surmise whether reducing the number of endothelial progenitor cells in wild type to half or a third of the normal numbers would produce a duct that is half truncated or only a third extended respectively, which could easily be assessed by imaging. However, there are classical experiments in salamander (Fankhauser, 1945) and more recent data from *Drosophila*

(Beitel and Krasnow, 2000) that show vessel diameter and length can be regulated independently of cell number.

Related to this cell number quandary is whether cell proliferation plays a significant role in formation of the CDs. Since cell proliferation is nearly normal in *hir* this may not be the case. Since cell proliferation affects cell number directly, addressing whether cell number is important for CDs development may provide insights. However, it remains unknown how the progenitor cell population is generated and maintained. Perhaps the wild type cells divide as they migrate to ensure sufficient numbers of cells for duct formation. This could be analysed using phosphohistone staining of the CDs to ascertain the number of dividing cells in the wild type and mutant.

Further analysis is required to answer the key question regarding whether formation of the CDs is via collective migration. Determining the reliance of migrating cells on one another could help to assess this. This could be achieved by more detailed study of the tracks generated via single cell migration analysis. This may allow elucidation of whether when one of the leading cells moves left at the anterior of the duct, neighbouring cells also move left. Clues about whether collective migration exists could also be gained from examining cell adhesion between the cells, perhaps by examining the cadherins for example. Weber *et al*. (2012) have shown in mesendodermal cells the importance of C-cadherins in sensing local mechanical forces and transmitting these to other cells via the keratin intermediate filament network. If these cadherin-keratin linkages are important for the migration of cells of the CDs, perhaps by pulling the lagging or more rearward cells along, then laser ablation could be used to disrupt these linkages in wild type and observe the consequences. Conversely it could be examined whether these linkages are disrupted in *hir*.

Indeed, Sperry *et al*. (2009) have shown that during EMT and collective migration, actin at adherens junctions (AJs) is reorganised into medial networks that remains connected to other cells through these AJs thus allowing coordination of cell motility throughout the tissue. The existence of such linkages could be investigated in the CDs of wild type and *hir*. A related and interesting question to address is whether migration of endothelial cells of the CDs requires a form of chemotaxis (e.g. VEGF-dependent) and/or haptotaxis (e.g. ECM component-dependent). Both processes are known to influence endothelial cell migration (Li *et al*., 2005), but whether they have a role in CDs formation in medaka remains unknown. However, in the case of haptotaxis, since FN fibrillogenesis is perturbed and is the most upstream event in ECM assembly, it is likely that downstream assembly may also be affected. This should therefore be further investigated in *hir*. If components of the downstream ECM assembly are indeed affected and necessary for haptotaxis of the CDs endothelial cells, then this could further explain the migration defects seen in *hir*.

3.6 Summary

- The *hir* mutant displays three prominent features as part of its phenotype: epithelial organ/tissue collapse, tissue mislocation and cell migration defects
- YAP is required for polarised endothelial progenitor cell migration during development of the Cuvierian ducts
- YAP likely regulates this migration by regulating fibronectin fibrillogenesis, the substrate upon which the endothelial cells migrate

Chapter 4: YAP is required for the coordinated growth and development of the eyes, neural tube and ears

4.1 Aims

As briefly described in Chapter 3, tissues and organs including the brain, eyes, spinal cord, and somites are flattened in the mutant, and are also not properly aligned. In particular, the eyes, neural tube (NT) and ears in *hir* all present with interesting and highly visible phenotypes, particularly regarding coordinated development/growth. As coordinated growth and morphogenesis are important to produce a fully functioning tissue/organ, the role of YAP in these processes was dissected by examining the cause(s) of the phenotypes observed in the eyes, NT and ears.

4.2 Introduction

4.2.1 The role of coordinated growth in development

Coordinated growth during development is essential if a tissue or organ is to function correctly. Classical experiments by Spemann have shown the reliance of various components of an organ upon each other, as have more recent studies in the eye for example, where ablating lens development leads to microophthalmia (Harrington *et al*., 1991). Indeed, the field of regenerative medicine aims to create and transplant 3D tissues/organs into the right place within the recipient's body such that they coordinate with existing tissues and organs in order to function to their maximum potential. Therefore it is important to understand the mechanisms underlying coordinated development from a therapeutic standpoint. Since YAP is proposed to be a key regulator of organ size (Dong *et al*., 2007) and can expand organ size whilst maintaining organ architecture when overexpressed, it may be controlling the coordinated growth of the different tissues comprising various organs.

4.2.2 Oriented cell division is important during vertebrate embryogenesis

Morphogenesis of tissues is controlled by several factors during development, both at the molecular and mechanical level. A key mechanism contributing to the final shape and size of tissues and organs is oriented cell division. Oriented cell division can also control cell fate (Castanon and González-Gaitán, 2011). During vertebrate development, oriented cell divisions can be seen as early as gastrulation during development of the body axis. For example, cells of the epiblast that are located both dorsally and laterally divide parallel to the animal-vegetal axis. And later in development during neurulation stereotypical divisions occur medio-laterally during formation of the neural tube. These medio-lateral divisions result in one of the daughter cells crossing the emerging midline and so are termed crossing divisions (C-divisions). There is evidence to suggest that planar cell polarity (PCP) signalling plays a significant role in regulating these C-divisions (Tawk *et al*., 2007). In fact PCP signalling has been proposed to regulate many different types of oriented cell division (Castanon and González-Gaitán, 2011). Interestingly PCP also regulates oriented cell division in

invertebrates, as well as asymmetric cell division as seen in *Drosophila* and zebrafish, highlighting a conserved mechanism regulating spindle polarity (Ségalen *et al*., 2010).

Other pathways regulating oriented cell division include VEGF, during vessel morphogenesis in zebrafish (Zeng *et al*., 2007), and ERK signalling during development of the lung tubes in mice (Tang *et al*., 2011). The role of extrinsic cues for orienting the mitotic spindle has also been well studied. For example, in epithelial cells it has been found that the spindle is oriented along the longest axis of the cell, and that mechanical deformation of the cell rearranges the spindle accordingly to the new longest axis (O'Connell and Wang, 2000). However, these observations do not necessarily hold true for polarised cells where cortical factors both within and outside the cell are important for orientating the spindle. Extrinsic cortical factors regulating the spindle include cell-ECM (extracellular matrix) interactions and cell-cell adhesions. In the context of cell-ECM adhesion, Fink *et al*. (2011) showed that in dividing HeLa cells, external ECM constraints caused polarisation of subcortical actin and that spindles oriented in association with these actin structures. Work by Toyoshima and Nishida (2007) in non-polarised cells supports this as they showed the spindle orients parallel to the cell-ECM adhesion plane. Cell-cell adhesion components such as E-cadherin have been demonstrated to play important roles in spindle orientation in both mammalian epithelial cells and during zebrafish neurulation (den Elzen *et al*., 2009; Žigman *et al*., 2011).

Aberrantly oriented cell division plays a role in pathologies such as tumourigenesis and diseases such as polycystic kidneys (Quyn *et al*., 2010; Fischer *et al*., 2006). Gaining insights into the regulation of this process may allow clinical treatments of such disease states.

4.2.3 Development of the vertebrate eyes

4.2.3.1 Early development of the eye

The complex organ that is the vertebrate eye is composed of three major tissues, being the retina, lens and cornea. Eye formation is strictly regulated and there are several major steps during its development (Graw, 2010, p.346): during neurulation optic buds appear on either side of the diencephalon; these optic buds enlarge to form the optic vesicles which sit close to the overlying ectoderm. Concurrently, in the overlying surface ectoderm the lens placode is formed as a thickening of this surface ectoderm; this lens placode comes into close contact or apposition with the optic vesicle which consequently folds inwards to form the optic cup; the retina arises from the inner layer of the optic cup and similarly the lens emerges from the lens placode by invagination into the eye cup; the cornea is formed after detachment of the lens placode from the surface epithelium. Therefore the eye is derived from three major sources as follows:

the retina from the neural ectoderm; the lens from the surface ectoderm; and the cornea consists partly of the surface ectoderm and partly of neural crest cells (Graw, 2010, p.346).

In mammals *Shh* and *Six3* are important for the separation of the eye field into the optic buds (Graw, 2010, p.351). In zebrafish, several nodal proteins have been implicated in this process including Ndr2, Squint and Southpaw. Mutations in the genes encoding Ndr2 and Squint cause cyclopia (Rebagliati *et al*., 1998; Pei and Feldman, 2009). The other major cyclopic zebrafish mutant is *one-eye pinhea*d (*oep*) and studies have shown that this gene encodes an EGF-related protein acting as a co-receptor in TGFβ/nodal signalling, thus providing a link between all three zebrafish cyclops mutants (Zhang *et al*., 1998; Pézeron *et al*., 2008). For the transition of the optic vesicles to optic cups, retinoic acid (RA) signalling and the transcription factor Lhx2 (LIM homeobox protein 2) are necessary (Graw, 2010, p.352-353). *Raldh2*$^{-/-}$ mouse embryos that lack RA synthesis in the optic vesicle display defects in optic vesicle invagination (Mic *et al*., 2004) and *Lhx2*$^{-/-}$ mouse embryos exhibit developmental arrest in the optic neuroepithelium just prior to the optic cup formation stage (Yun *et al*., 2009).

Emergence of the lens placode and its subsequent development is dependent upon Pax6, Fgf- and Wnt-signalling cascades, with *Pax6* acting as the master regulatory gene of the lens lineage (Graw, 2010, p.354). Conditional *Pax6* knockout mice showed *Pax6* is essential for development of the lens placode and acts cell-autonomously for this process. It has also been shown that there are two expression phases of Pax6, one pre-placode and one later in development after the placode has formed (reviewed in Lang, 2004). Other prominent transcription factors involved in early lens induction include Six3 and Sox2, and signalling pathways implicated include BMP and FGF signalling (Lang, 2004). In fact it has been suggested that Sox2 and BMP4 may act in a parallel pathway to the traditional Pax6 pathway controlling lens induction, suggesting some level of redundancy in the development of the lens (Lang, 2004).

4.2.3.2 Morphogenesis specific to the lens

Because of the way it develops, the vertebrate lens provides an excellent model in which to study the processes required for epithelial invagination. Tissue invagination via the formation of apically constricted cells is a highly conserved feature of tissue morphogenesis throughout the animal kingdom and actin dynamics leading to coordinated cell shape changes are implicated in this process. Invagination of the lens occurs in a very coordinated manner with invagination of the presumptive retina to ensure their shapes correlate. Inhibiting the Rho family of small GTPases, which are important regulators of actin dynamics (Ridley *et al*., 2003), causes morphological

defects in the lens epithelial cells (Maddala *et al*., 2004). Recent work from Chauhan *et al*. (2009) revealed an interesting feature of interaction between the lens and optic cup, showing that cytoplasmic protrusions emanating from the presumptive lens are in fact filopodia. The formation of these filopodia was found to be Cdc42- and IRSp53-dependent. Furthermore they were found to serve as physical tethers, coordinating invagination of the presumptive lens and retina (Chauhan *et al*., 2009).

4.2.3.3 Eye formation in medaka

In medaka, the optic buds are visible by the late neurula stage (st.18, 26 hpf) and have formed the optic vesicles by st.19 (27.5 hpf). Morphogenesis of the optic vesicles to give the optic cups starts at st.21 (34 hpf) when the lens placodes can be seen in close apposition with the optic vesicles and proceeds through st.22 (38 hpf). By st.23 (41 hpf) the formation of spherical optic lenses is complete. *Sox3* expression is a useful marker of lens placode formation (but is also present in other sensory placodes, Köster *et al*., 2000) and at later stages of eye differentiation, δ-crystallin (delta-crystallin) serves as a useful marker (Shimada *et al*., 2003; Lang, 2004). Eye development in medaka can therefore serve as a useful tool for studying induction and how coordinated growth occurs.

4.2.4 Development of the vertebrate neural tube

Vertebrate neurulation is the process by which the neural tube (NT) forms from the neural plate, which is a thickened epithelial rudiment. It can be described in essence as the rolling up of an epithelial sheet to give an elongated tube (Colas and Schoenwolf, 2001). Neurulation requires the interaction of biophysical properties (such as surface tension) and genes involved in morphogenesis and has four main stages: neural plate formation; neural plate shaping, neural plate bending; and finally neural groove closure (Colas and Schoenwolf, 2001). Neural induction, which is the process by which the ectoderm acquires a neural fate, requires suppression of an epidermal fate as opposed to the induction of a neural fate, as was more classically thought (reviewed in Colas and Schoenwolf, 2001). Neural induction results in a thickening of the pluripotent epiblast layer in the region that will become the neural plate (Clarke, 2009). This neural plate has apico-basal polarity that is determined before induction by the polarised nature of the epiblast (Clarke, 2009). Furthermore, the neural plate is able to form in isolation from the surrounding epidermal ectoderm, demonstrating that once the ectoderm becomes committed to a neural fate, the process of formation of the neural plate is autonomous to the prospective neural plate and does not require the presence of non-neural ectodermal cells (Colas and Schoenwolf, 2001). The morphogenetic movements involved in formation of the NT and the subsequent later stages of brain development are well characterised and require the formation and fusion of neural

folds that give rise to the future forebrain, midbrain and hindbrain regions (Wolpert and Tickle, 2011, pp.316-17).

In the first main stage of neurulation, neural plate shaping is driven by changes in behaviour of the neuroepithelial cells constituting the plate. Apicobasal elongation of cells causes continued apicobasal thickening of the nascent neural plate and cell intercalation occurs as part of convergence and extension movements (Colas and Schoenwolf, 2001). Neural plate shaping can occur independently of more lateral tissues such as the epidermal ectoderm, mesoderm and endoderm (Colas and Schoenwolf, 2001). Bending of the neural plate initiates whilst shaping is still occurring, resulting in the formation of neural folds at the lateral extremes of the neural plate. The location of the bending along the anteroposterior axis varies by species and the process is driven by Shh signalling from the underlying notochord and proceeds in two steps — furrowing and folding (Colas and Schoenwolf, 2001). Furrowing occurs at specific regions known as hinge points followed by folding at these sites. The elevation of these neural folds gives rise to the neural groove which is a trough-like structure. In mice, during this elevation phase, an ectodermal population known as the neural crest derives (Colas and Schoenwolf, 2001). Interestingly, and unlike the second stage of neurulation, neural plate bending requires cell movements in both the plate itself (neuroepithelial cells cause furrowing) as well as cells of the adjacent epidermal ectoderm which cause folding. Finally, the closure of the neural groove by the adhesion and fusion of the neural folds at the dorsal midline gives rise to the neural tube which then separates from the overlying epidermal ectoderm (Colas and Schoenwolf, 2001).

Interestingly, neurulation proceeds in a bidirectional manner occurring anteriorly from an epithelial population of cells (primary neurulation) and posteriorly from a mesenchymal population of cells (secondary neurulation). Primary neurulation gives rise to the brain and most of the spinal cord whereas secondary neurulation leads to formation of the posterior spinal cord only (Wolpert and Tickle, 2011, p.317). As such more detailed knowledge exists on primary neurulation. It is also now known that the neural tube is patterned along its two major axes during earlier stages of its development, anterior-posterior and dorsal-ventral, by Wnt/β-catenin signalling and BMP/Shh signalling respectively (Kiecker and Niehrs, 2001; Le Dréau and Martí, 2012). Here, the Wnts have been found to posteriorise the anterior neuroectoderm in a concentration-dependent manner in both a direct fashion and over longer ranges. In terms of dorsal-ventral signalling, graded Shh controls the identity of ventral NT progenitors (Le Dréau and Martí, 2012). Interestingly it is now emerging that BMP may stimulate the expression of Wnt ligands which in turn antagonise Shh signalling (Le Dréau and Martí, 2012). The early patterning established by Wnt and BMP signalling is then refined at later stages to give rise to the forebrain, midbrain and hindbrain.

Genetic control of neurulation is thought to increase its efficiency and ensure the heritability of NT form and function. Consequently, neurulation has redundant mechanisms acting at both the tissue and cellular level as well as at the molecular level to maintain the organisation of the tissue. For example, experimental manipulations that remove neurulation forces rarely disrupt neurulation. Furthermore, the use of teratogens rarely blocks neurulation (Colas and Schoenwolf, 2001). Defects in NT development, such as failure of the NT to close, cause severe congenital defects such as anencephaly and spina bifida in humans (Colas and Schoenwolf, 2001).

4.2.4.1 Neural tube development in the teleosts

Interestingly, in contrast to the amniotic process of neurulation detailed above, teleosts generate their NT via a different mechanism to other vertebrates. This NT formation has been well studied in zebrafish but also appears well conserved in medaka (Kinoshita *et al*., 2009, p.184). However, it is important to note that only the spinal cord/ anterior trunk region has been well characterised in terms of neurulation in teleosts (Lowery and Sive, 2004). The zebrafish neural plate differs from amniotes in that it lacks apico-basal polarity and thus cannot be considered as a conventional epithelium (Clarke, 2009). Therefore the junctional status of epithelial cells within the neural plate remains unclear (Lowery and Sive, 2004). There are several distinct steps observed in teleost neurulation. The neural plate is established by columnarisation of epithelial cells within the presumptive neural plate region. Neural plate cells then sink to form a solid neural keel in which a clear midline is observed as well as a pseudostratified columnar epithelium on either side of this midline. Unusually, at this stage, daughter cells are able to cross the midline by a phenomenon known as crossing division (C-division) (Clarke, 2009). The neural keel rounds up to form the neural rod primordium. This neural rod then undergoes many cell rearrangements such that a cavity/lumen is formed, opening from ventral to dorsal, to give rise to a hollow tube (Lowery and Sive, 2004).

Whilst there is some debate as to whether teleost neurulation is more similar to secondary or primary neurulation, the cell movements involved in generating the teleost neural tube do resemble the processes seen in primary neurulation in other vertebrates (such as mouse and chick), including cell interdigitation, intercalation and C-divisions (Clarke, 2009). Many zebrafish neurulation mutants have been identified (e.g. *trilobite* and *one-eyed pinhead*) but not all are well characterised. Interestingly, several show mutations in genes that also produce neural tube defects in mice, suggesting the molecular mechanisms of neurulation may be conserved (Lowery and Sive, 2004). Since development of the NT occurs both in the anterior-posterior axis and dorsal-ventral axis, it is a useful tissue for studying how proportional 3D growth is regulated.

4.2.5 Development of the ear in vertebrates

Unlike terrestrial animals, fish do not have an outer ear, as they do not need to direct and magnify sound waves given that water acts as a better conductor of sound than air. However, since the inner parts of the teleost ear that are present develop in a similar manner to the ear in amniotes, specific features of teleost ear development will be detailed.

4.2.5.1 Development of the teleost ear

Studies of ear development in zebrafish have made important contributions to understanding the molecular and cellular mechanisms involved in this process. As for the NT, there are many zebrafish mutants with defective ear formation (several are described in Whitfield *et al*., 2002). More recently the key genes in medaka ear development have come to light (Hochmann *et al*., 2007). Whilst many of the genes and signalling pathways involved in the induction and development of the ears are conserved between zebrafish and medaka, there are some differences in gene expression in terms of timing and spatial distribution (Hochmann *et al*., 2007). For example in medaka, *Pax8* expression appears considerably later during neurulation whereas in zebrafish *Pax8* is the earliest marker of otic lineage and is expressed in preotic cells at 80% epiboly (Hochmann *et al*., 2007). Similar to eye development, the ear forms initially from a sensory placode by ectodermal thickening, which pinches off from the ectoderm and cavitates to give rise to the otic vesicle and eventually all complex structures of the inner ear. The otic placodes arise from a thickening of the overlying ectoderm and are located either side of the hindbrain, emerging during mid-somite stages in zebrafish (14-somite stage, 16 h hpf, Kimmel *et al*., 1995) and earlier in medaka at the onset of somitogenesis (st.19, 27.5 hpf, Iwamatsu, 2004). Unlike Pax6 in the specification of the lens placode, no master regulator of otic placode formation has yet been found (Whitfield *et al*., 2002). In medaka the ear is a single-layered epithelium rendering it useful for studies of how mitotic orientation affects morphogenesis.

In zebrafish, the earliest specific markers of the otic placodes or otic fate are expression of *Pax2*, *Pax5* and *Pax8* (Whitfield *et al*., 2002), and before this expression of *Foxi1* and *Dlx3b* is seen in the presumptive epidermal regions, marking the area that will give rise to the otic placode (Hochmann *et al*., 2007). *Eya1* is expressed at the end of gastrulation around the anterior neural plate and otic tissue (Hochmann *et al*., 2007). Markers of the formed otic placodes in zebrafish include the claudin genes, *cldna* and *cldnb* (Kollmar *et al*., 2001). Signalling pathways implicated in the induction of the otic placodes include FGF, with *Fgf3* and *Fgf8* being particularly important (Whitfield *et al*., 2002). In medaka, *Foxi1* and *Dlx3b* expression is also seen prior to induction of the otic placodes (Hochmann *et al*., 2007) and *Eya1* and *Sox3* can be used as markers of the

otic placodes once formed (Köster *et al*., 2000). Therefore whilst the timing of otic induction between zebrafish and medaka differs, on the whole there is good similarity between the expression patterns of marker genes for otic induction and development. This suggests a highly conserved mechanism of ear development between the two species (Hochmann *et al*., 2007). Whilst there is also good literature regarding the later stages of ear development in the teleosts (Whitfield *et al*., 2002), this will not be discussed here since only the relatively earlier stages of development in medaka were analysed.

4.3 Research questions

This chapter's aims are abridged as follows:

1. What role does YAP play for single-cell behaviour underlying coordinated development and growth of the:
    a. Eyes?
    b. Neural tube?
    c. Ears?

4.4 Results

4.4.1 YAP is required for the coordinated development of the eye

4.4.1.1 The lenses in *hirame* do not invaginate and are dislocated from the retinas which do not basally constrict

Eye development in wild type and *hir* medaka embryos was visualised from st.20-23 (31.5-41 hpf) using time-lapse microscopy. Differences in development of the eyes in wild type and *hir* were evident from st.20 (31.5 hpf) when the shape of the retina in *hir* was rounder versus the antero-posteriorly elongated shape seen in wild type (Figure 4.1a). In wild type embryos injected with EGFP-CAAX + H2B-RFP (herein termed MNFP) to label cell membranes green and nuclei red, the lens placode thickened from st21-21.5 (34-36 hpf, arrowheads in Figure 4.2a-a", Supplementary movie 5) and the retina basally constricted such that it curved to form the characteristic optic cup shape from st.21-23 (34-41 hpf, arrows in Figure 4.1a upper panels). Furthermore, as development proceeded in wild type the lens rounded-up to become spherical concurrently invaginating into the optic cup (Figure 4.1a, Supplementary movie 3).

In *hir* mutant embryos, a lens placode formed adjacent to the retina as in wild type at st.20 (31.5 hpf, Figure 4.1a lower panels). This placode was however, grossly misshapen when compared to the wild type placode at st.21 (34 hpf) by 3D rendering (Figure 4.4). This aberrant placode often appeared fragmented (dotted lines in Figure 4.1a, also see Supplementary movie 4). To confirm these fragments were of lens lineage, *in situ* hybridisation with the sensory placode marker, *Sox3*, was performed (Figure 4.1b). This showed that the fragments observed in *hir* were indeed portions of the lens (arrowheads, Figure 4.1b). During fragmentation the mutant placode did not significantly thicken in the XY (medio-lateral) plane as seen in wild type (compare insets of Figure 4.2a-a'' and b-b'') or in the Z-axis. Following this frequent fragmentation, the mutant lens appeared detached from the retina at st.21 (34 hpf, Figures 4.1a and 4.2b-b'' arrowheads). The detached lens placode fragments gradually rounded up during st.22-23 (38-41 hpf) as development proceeded (Figures 4.1a, 4.2c-c''' arrowheads, and 4.3b-b''' arrowheads). By st.23 (41 hpf), some of the fragments had loosely reattached to the *hir* retina to form ectopic lenses that were never incorporated/invaginated into the retina as seen in the wild type (compare Supplementary movies 3-5, and see Figures 4.1a and 4.2c-c'''). Interestingly, it was also observed that in about 45% of cases (4/9 embryos) several of the mutant dislocated lens fragments coalesced over the course of several hours (Figure 4.3a-a''' arrowheads, Supplementary movie 6) as they rounded-up before loosely reattaching to the retina. In cases where this did not happen (approximately 55% of the time), structures resembling multiple lenses could be observed (Figure 4.1c, asterisk). *Delta-crystallin* staining by *in situ* hybridisation confirmed that these were indeed multiple lenses that had differentiated properly (Figure 4.1c).

This failure of coordinated development of the lens and retina and their separation and rejoining suggests a failure in communication between the two tissues. Therefore it was next asked what the mechanism underlying this lack of communication could be and how YAP might be involved in regulating this mechanism.

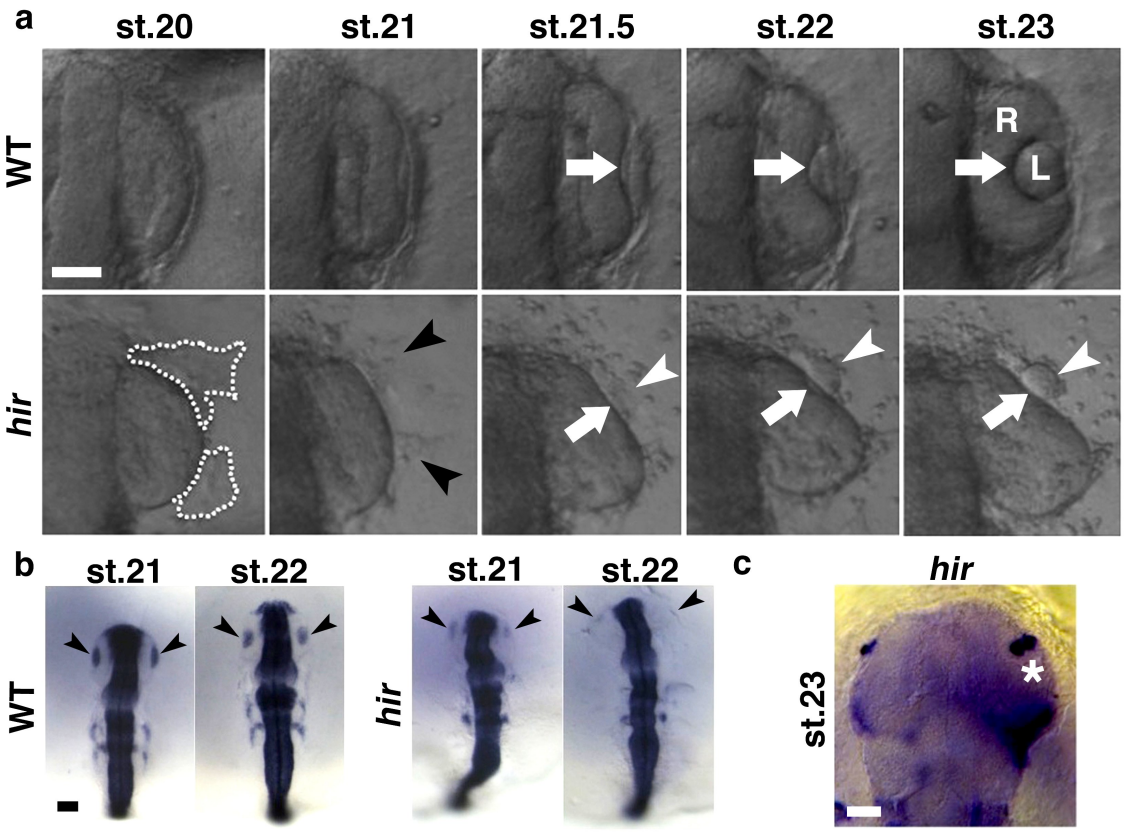

Figure 4.1. Eye development is perturbed in *hirame*. (a) Snapshots from a bright-field time-lapse movie showing normal and mutant eye development. Arrows indicate basal constriction of the retina (R) in wild type and a lack of this in *hir*. Black arrowheads demarcate the fragmented lens placed and white arrowheads mark the ectopic lens (L) in *hir*. Dotted outline indicates the fragmented and misshapen lens placode in *hir*. **(b)** *Sox3 in situ* staining to confirm identity of fragmented/dislocated lenses. Arrowheads demarcate lenses. **(c)** *Delta-crystallin in situ* staining to confirm identity of multiple lenses (asterisk). All views are dorsal and anterior is up. Scale bars: (a and b) = 30μm; (c) = 40μm. Panels in (b) and (c) in conjunction with Huijia Wang.

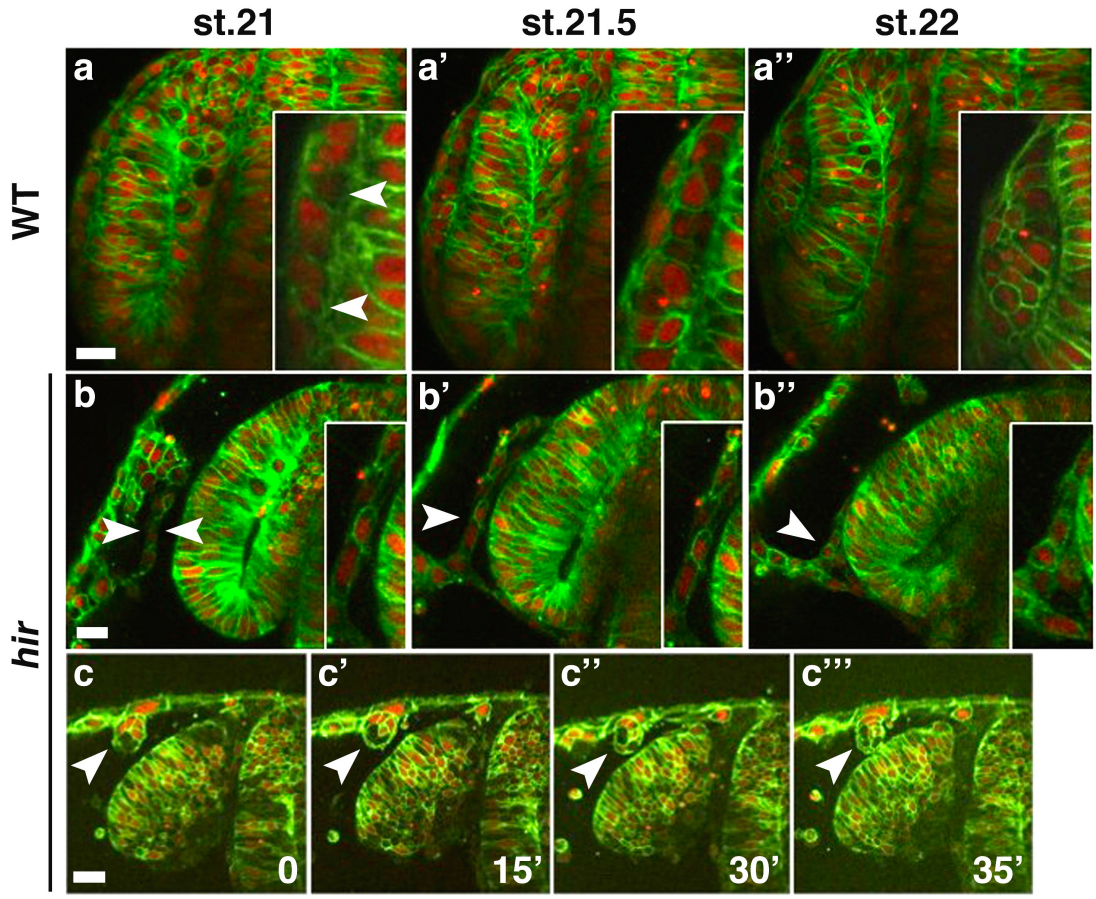

Figure 4.2. The lens placode does not thicken in *hirame* but the lens rounds up later in development and loosely rejoins the retina. (a-b'') The lens placode in wild type thickens medio-laterally but does not in *hir* (arrowheads). **(c-c''')** Detached lenses sometimes loosely reattach in *hir* later in development (arrowheads). Views are all dorsal with anterior up. Time elapsed in minutes is indicated. Scale bars: (a) = 15μm; (b) = 10μm; (c) = 20μm.

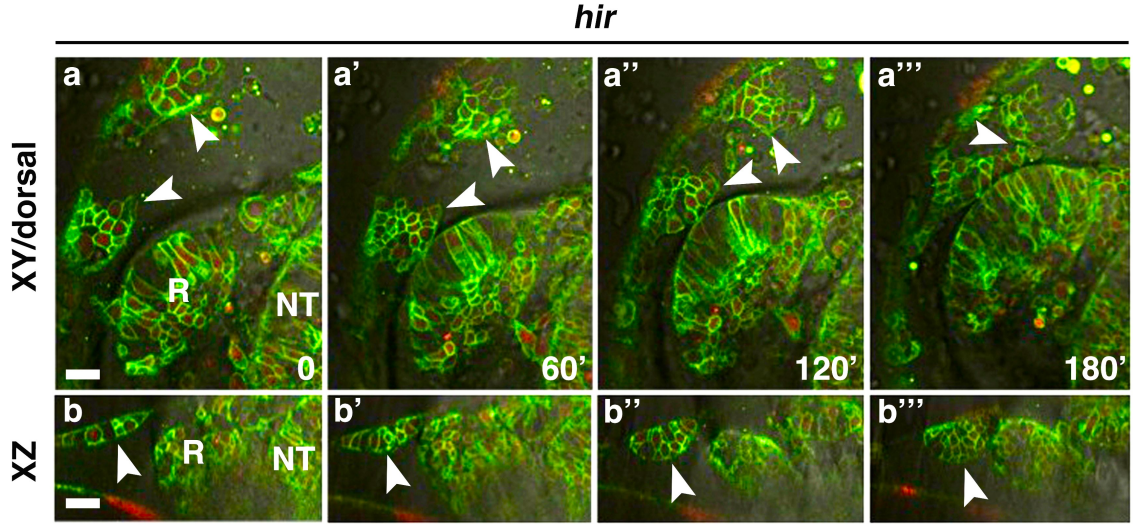

Figure 4.3. Lens fragments in *hirame* rejoin as development proceeds. Fragments demarcated (arrowheads), time elapsed is indicated (mins). **(a-a''')** Dorsal view shows two lens fragments rejoining. **(b-b''')** XZ (frontal optical section) view shows that mutant lenses round up as development proceeds. Scale bars: (a) = 20μm; (b) = 30μm. Anterior up in panels a-a'''.

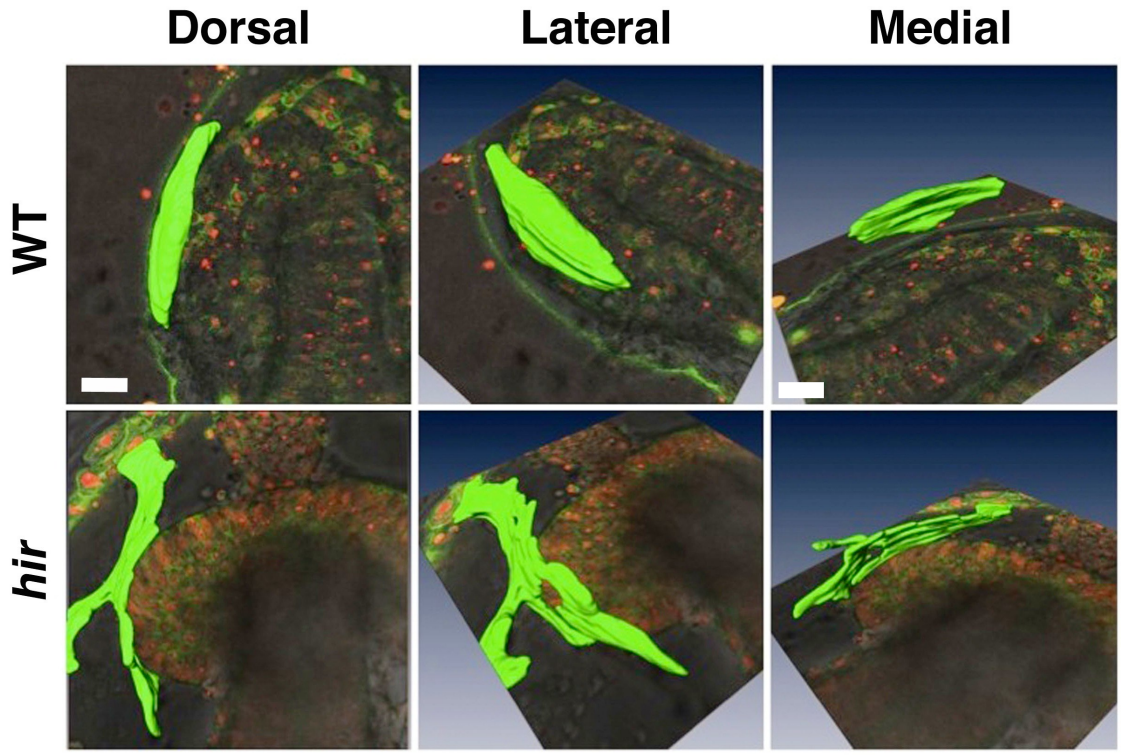

Figure 4.4. The lens placode in *hirame* has aberrant morphology. 3D rendering of the labelled lens placode (green) in MNFP injected embryos. Perspective for each panel is indicated. The *hir* lens placode becomes fragmented and elongated in the anterior-posterior axis earlier in eye development. One plane of a Z-stack of an embryo labelled with MNFP is shown for orientation purposes. Scale bars: 20μm.

4.4.1.2 YAP is required for the lens to tether to the retina via filopodia that form due to fibronectin-integrin signalling

The mechanism underlying the retina-lens tissue dislocation was investigated by further analysing the lens misalignment in *hir* mutants. During normal development, filopodia tether the lens to retina (Chauhan *et al*., 2009). Protrusions were observed in wild type at st.22-23 (38-41 hpf, Figure 4.5) between the lens and retina. However, in *hir*, almost no filopodia were formed between lens and retina at earlier stages (Figure 4.5 bottom left) or even when the aberrant lens had rounded-up and moved to sit in close apposition with the retina (Figure 4.5 bottom right panel). Instead aberrant filopodia were formed from the side of the lens opposite to that facing the retina during the time in development when lens invagination is normally occurring (arrowheads, Figure 4.5 bottom left panel, Supplementary movie 7). These data suggest a polarisation defect within epithelial cells of the *hir* eye, as was seen in the endothelial cells of the CDs in Chapter 3.

Activation of integrin-FN signalling is required for the formation of polarised filopodia (Davidson *et al*., 2006). In the eye, filopodia normally mediate coordinated invagination of the lens and retina (Chauhan *et al*., 2009). As this invagination is affected in *hir* and filopodia appear non-polarised, integrin-β1 was examined in the mutant eye. In wild type embryos integrin-β1 was strongly localised around the region of the invaginated lens and basally constricted retina at st.23-24 (41-44 hpf, Figure 4.6a top panels, arrowheads). In *hir* mutants, localisation of integrin-β1 around the non-invaginating lens was absent (Figure 4.6a, bottom left panel), but subtle localisation was seen around weakly reattached lenses (Figure 4.6a bottom right panel, arrowhead). Taken together, this suggests that failure of integrin activation may contribute to defective filopodia formation between the retina and lens in the mutant, resulting in lens dislocation.

As previously described in Chapter 3, fibronectin (FN) is the main ligand of integrin-α5β1 so the above findings led to the analysis of FN in the eye. At st.23 (41 hpf), the wild-type invaginated lens and constricted retina had a fine meshwork of FN fibrils on their surfaces (Figure 4.6b top right panel, arrowhead). The *hir* retina however, had aberrant FN fibrils all over its surface that were thick, coarse and irregular in appearance. This was also seen on the detached lenses (Figure 4.6b bottom right panel, arrowhead). At st.23 (41 hpf), some of the reattached *hir* lenses appeared to have both aberrant and fine fibrils. Interestingly, this FN fibril defect in the eye mirrors that seen in earlier development when wild-type embryos had a finer mesh of FN fibrils on the basal surface of epithelia and mesenchyme at the end of gastrulation/early neurulation at st.17 (25 hpf), whereas *hir* mutants had coarse and irregular FN fibrils (Figure 4.6 st.18 and st.21 panels, compare insets with st.23 panels on right).

These results suggest that aberrant FN assembly fails to activate integrin signalling and this may affect filopodia formation between lens and retina, resulting in detachment of the lens from the retina. To test this possibility, mRNA encoding N-terminal 70kDa fragments of FN (FN 70kD) was again injected into wild type embryos as for the CDs in Chapter 3. FN antibody staining in wild type showed localisation of FN between the lens and retina in wild type, corroborating its requirement for integrin signalling and filopodia formation in this region (Figure 4.7 panel 2). Blockage of FN assembly in the eye of wild type embryos (compare Figure 4.7 panels 2 and 2') phenocopied the *hir* phenotype, including lens dislocation (Figure 4.7, compare panels 1' and 2' with 1'' and 2'', arrowheads) similar to how defects of the CDs were mimicked in the wild type by FN 70kD injection. Interestingly however, FN 70kD injection into wild type could not mimic the flattened lens and neural tube seen in *hir* (compare Figure 4.7 panels 1-1'', asterisks). This suggests that tissue dislocation and cell migration defects may be due to aberrant FN assembly but that tissue collapse could somehow be upstream of the FN assembly/fibrillogenesis defect.

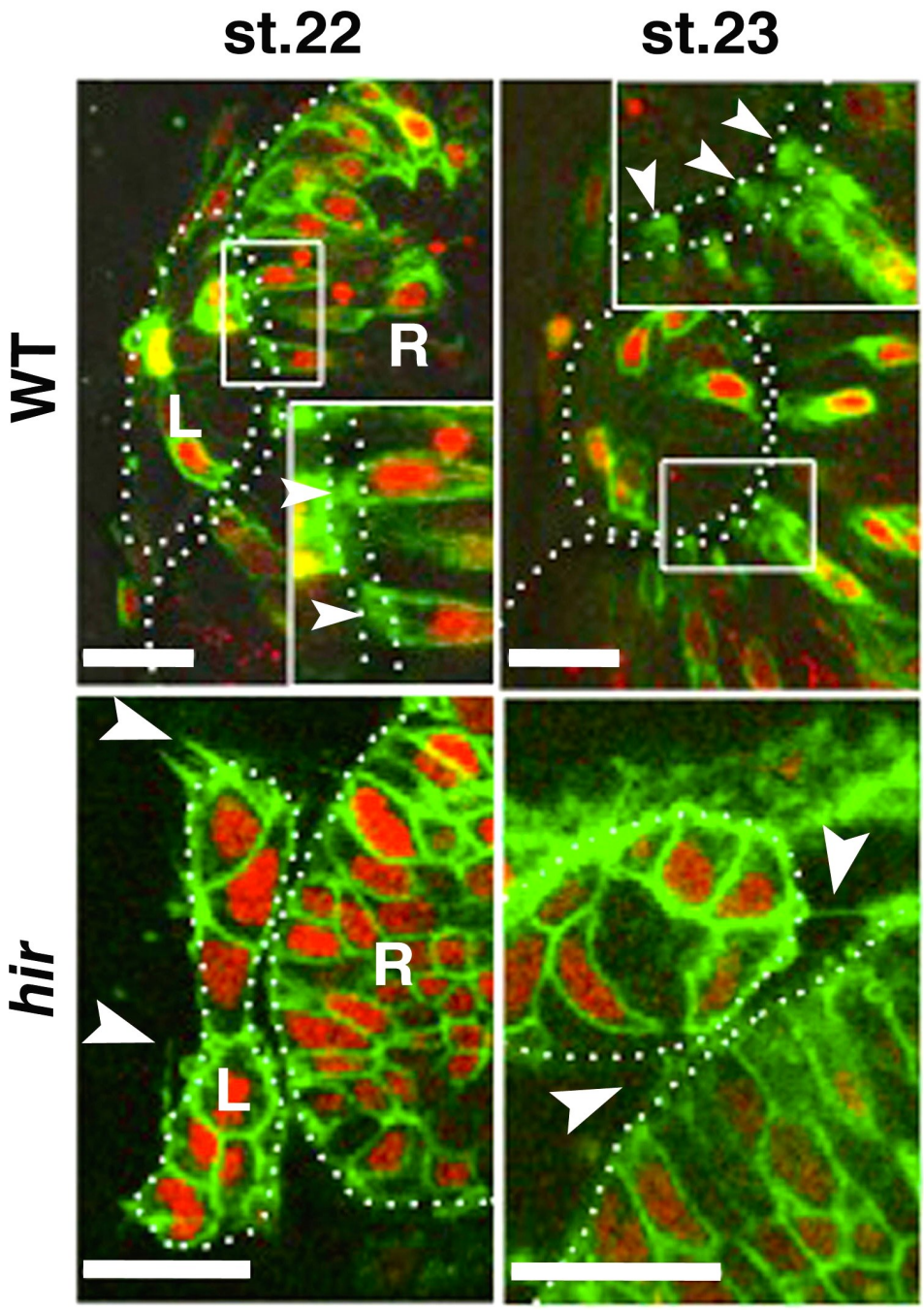

Figure 4.5. Filopodia between the lens and retina fail to form correctly in *hirame*. Stills from confocal time-lapse movies of MNFP injected embryos. Views are dorsal with anterior up, posterior down, lateral left and medial right. Arrowheads demarcate filopodia/protrusions between the lens and retina in wild type, which form ectopically in *hir* and may be reduced in number. Insets show magnifications of boxed regions. Dotted lines demarcate the outlines of the lens and retina. L: lens; R: retina. Scale bars: 20μm.

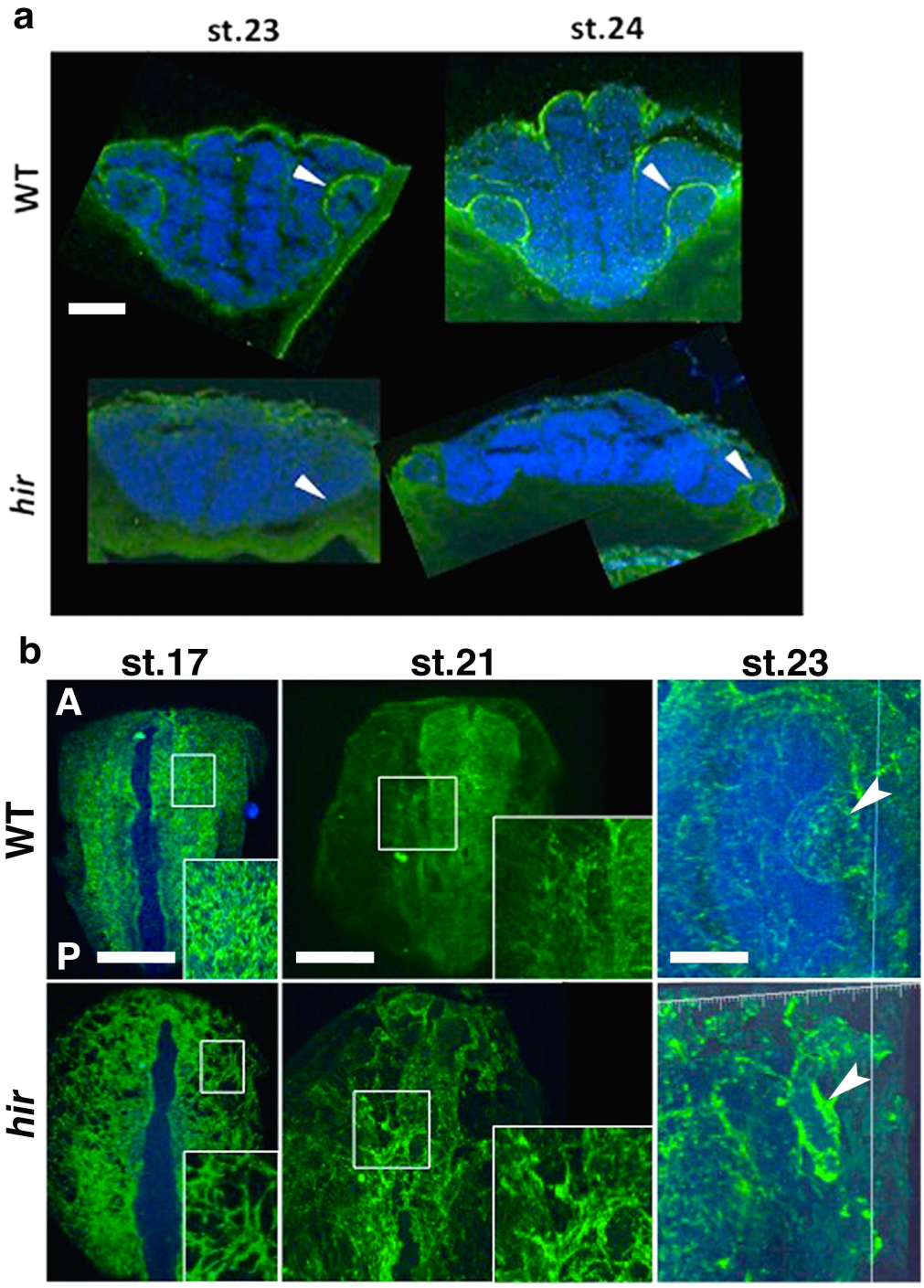

Figure 4.6. Fibronectin-integrin signalling and fibronectin fibrillisation is disrupted in *hirame*. (a) Integrin-β1 antibody staining (green) between the lens and retina (arrowheads) is reduced in *hir*, even when the lens appears loosely reattached. Images show frontal sections, some of which were stitched together due to not fitting in the field of view during imaging. Images in conjunction with Huijia Wang. **(b)** Dorsal views of whole-mount FN1a+b antibody stained (green) embryos at stages indicated. Insets show zooms of boxes in main panels and reveal the coarse and thick nature of FN deposition in *hir*. Arrowheads indicate the lenses in wild type and *hir* in 3D reconstitutions of the right eye surface. Blue staining is nuclear Topro3. Anterior is up. A: anterior; P: posterior. Scale bars: (a) = 30μm; st.17 and st.21 panels = 100μm; st.23 panels = 30μm.

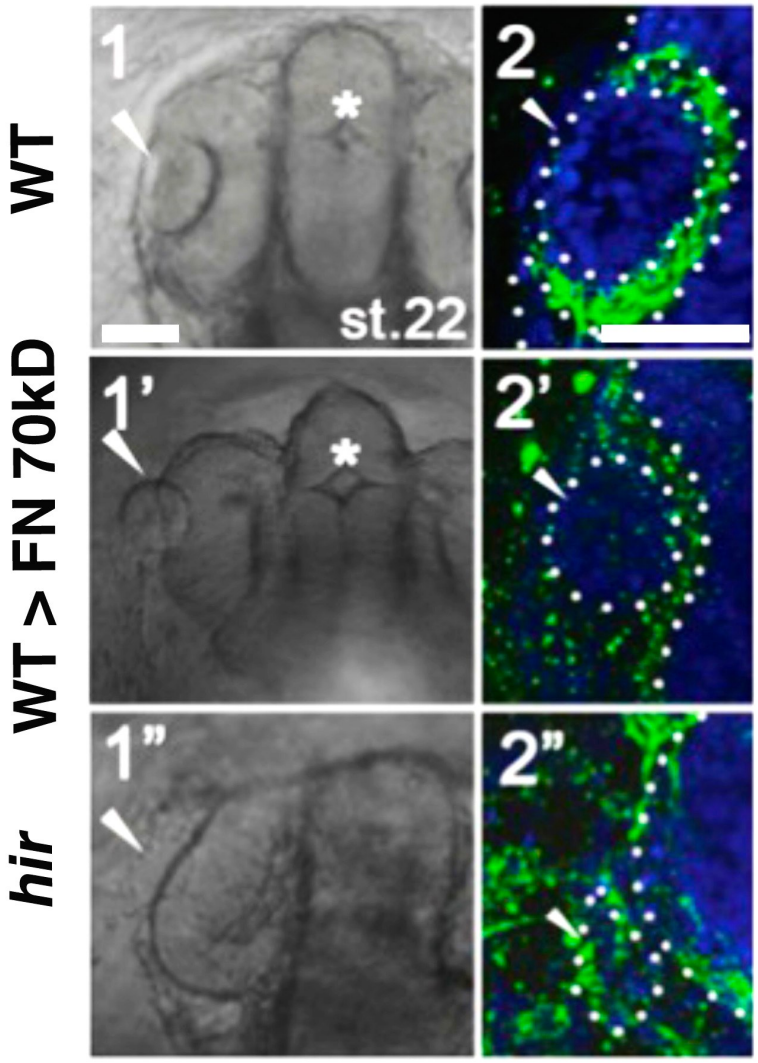

Figure 4.7. Blocking fibronectin fibrillogenesis mimics the lens dislocation phenotype in *hirame* but not tissue collapse. (1-1") Bright-field images at st.22 (38 hpf) where the lens is indicated by an arrowhead and the brain ventricle by an asterisk. FN 70kD injection into wild type mimics lens dislocation as in *hir* but not tissue collapse suggesting this aspect of the mutant phenotype is upstream of FN fibrillogenesis. **(2-2")** FN 1a+b antibody staining (green) of corresponding st.22 (38 hpf) embryos in left panels shows aberrant FN fibrillogenesis in *hir* and a loss of FN fibrils in FN 70kD injected embryos. Again arrowheads indicate the lenses and the retina and lens outlines are demarcated by dotted lines in right panels. All views are dorsal with anterior up. Blue staining is nuclear Topro3. Scale bars: 30μm.

4.4.1.3 The oriented cell division plane is affected in the mutant eye

Since the *hir* lens placode exhibited aberrant lengthening in the antero-posterior axis and a lack of thickening in the medio-lateral plane, the division plane of neuroepithelial cells within the lens was investigated at st.21 (34 hpf). This is the developmental time when the lens starts to undergo rounding up. Because resolution was not sufficient in the Z-axis, the division plane in 2D only (X/Y axes or medio-lateral/antero-posterior axes) was analysed. The lens placode-retina boundary (PRB) was used as a reference plane against which division angle of lens cells was measured (Figure 4.8). Division angle was calculated for cells in telophase, as prior to telophase it has been shown that a dividing cell often rotates as mitosis proceeds (Tibber *et al*., 2004). Thus measuring cells before telophase could give misleading division angles. To allow accurate determination of cells in telophase, MNFP labelling of embryos was used since this allows visualisation of the membrane and nucleus. In the wild type eye, divisions occurring in the lens placode both parallel and perpendicular relative to the PRB were observed (Figure 4.8a, top panels). These occurred at a roughly even frequency (perpendicular = 5 divisions, parallel = 6 divisions, n = 3 embryos, Figure 4.8b) resulting in more proportional growth of the lens in wild type. In *hir*, mitosis of lens placode cells only occurred parallel to the PRB (11 cells/divisions, n = 7 embryos, Figure 4.8a bottom panel and b). Consequently the *hir* lens did not enlarge in the medio-lateral plane remaining narrower in this axis (Figure 4.2b-b''). Instead it became elongated in the antero-posterior axis and aberrantly shaped as seen in Figure 4.4.

As the cell division plane was affected in the lens placode of the mutant, potentially contributing to its malformation, and the retina in *hir* is also misshapen, cell division plane within the retina was next studied at st.22-23 of development (38-41 hpf). These are the developmental stages when morphogenesis of the retina/optic cup occurs prominently. Division angle was measured by calculating the mitotic plane of the dividing neuroepithelial cells relative to the apical lumen of the retina. This was used as a reference plane and classed as 0° as the majority of cells in wild type and *hir* were seen to divide near to this lumen (Figure 4.9a). Mitosis in the wild type happened predominantly (approximately 80%) along or parallel to the apical lumen (0° ± 20°), with a low frequency (≈20%) of wild type cells dividing at ± 30-40° relative to the lumen (Figure 4.9b). This suggests these divisions oriented along the apical lumen may be necessary to assist with the basal constriction and shape change of the retina to form the optic cup. In *hir*, the cell division plane within the retina was much more randomised and evenly spread over a variety of angles such that divisions were seen at up to 70° relative to the apical lumen at a frequency of over 10% with a low frequency (<5%) occurring at up to 90° (Figure 4.9b). These more randomly oriented divisions may be a contributing factor to the overall rounder shape of the mutant retina.

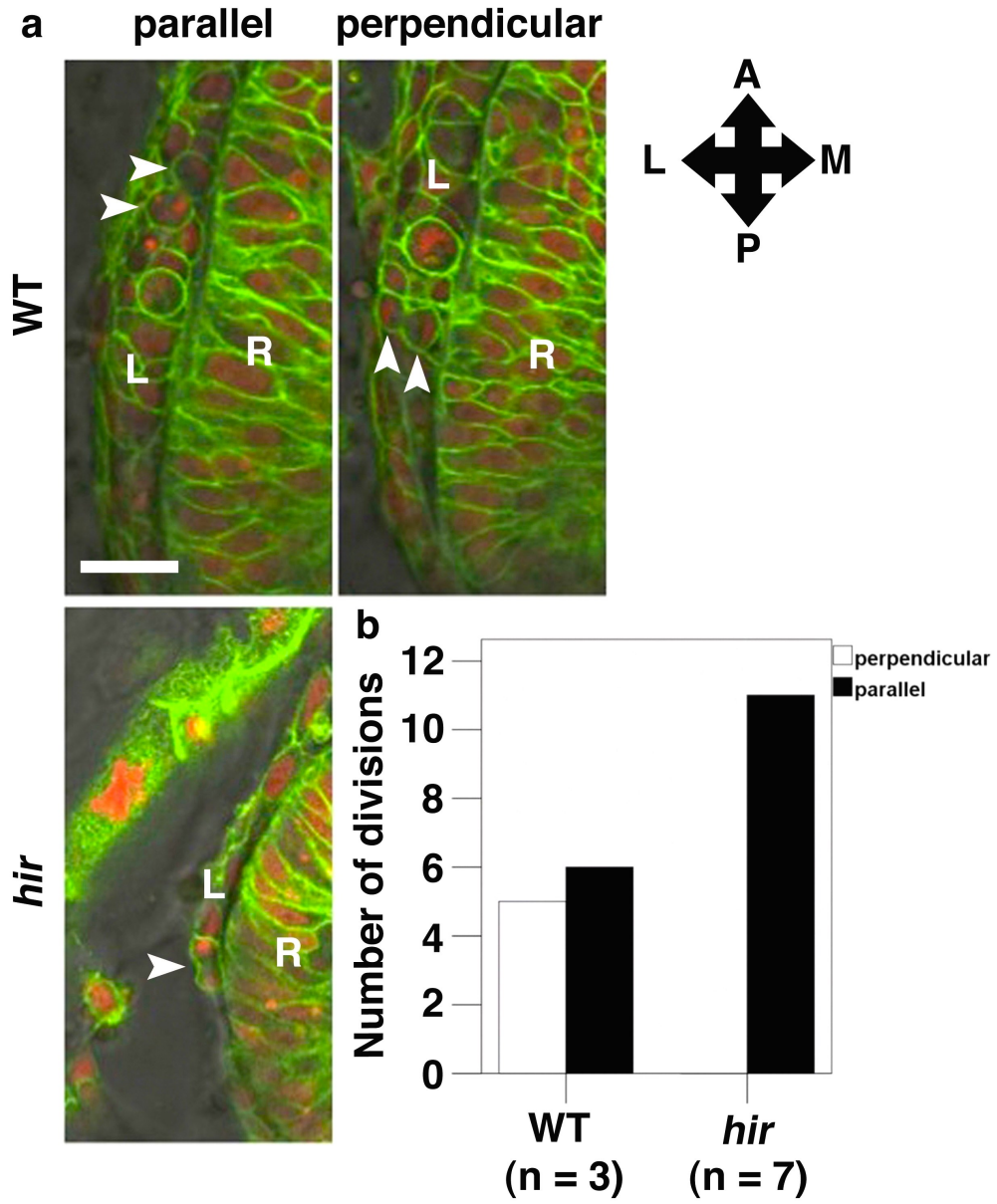

Figure 4.8. Oriented cell division is affected in the *hirame* lens. (a) In the wild type lens placode neuroepithelial (NE) cells divide both parallel and perpendicularly to the retina margin. In *hir* only parallel division is observed. Arrowheads indicate dividing cells in MNFP injected embryos. L: lens; R: retina. **(b)** Quantification of NE cell division in the lens placode of wild type and *hir* at st.21 (34 hpf). Numbers of embryos are shown in parentheses. Views are dorsal of MNFP injected embryos and compass indicates orientation. A: anterior, P: posterior, M: medial; L: lateral. Scale bar: 10μm.

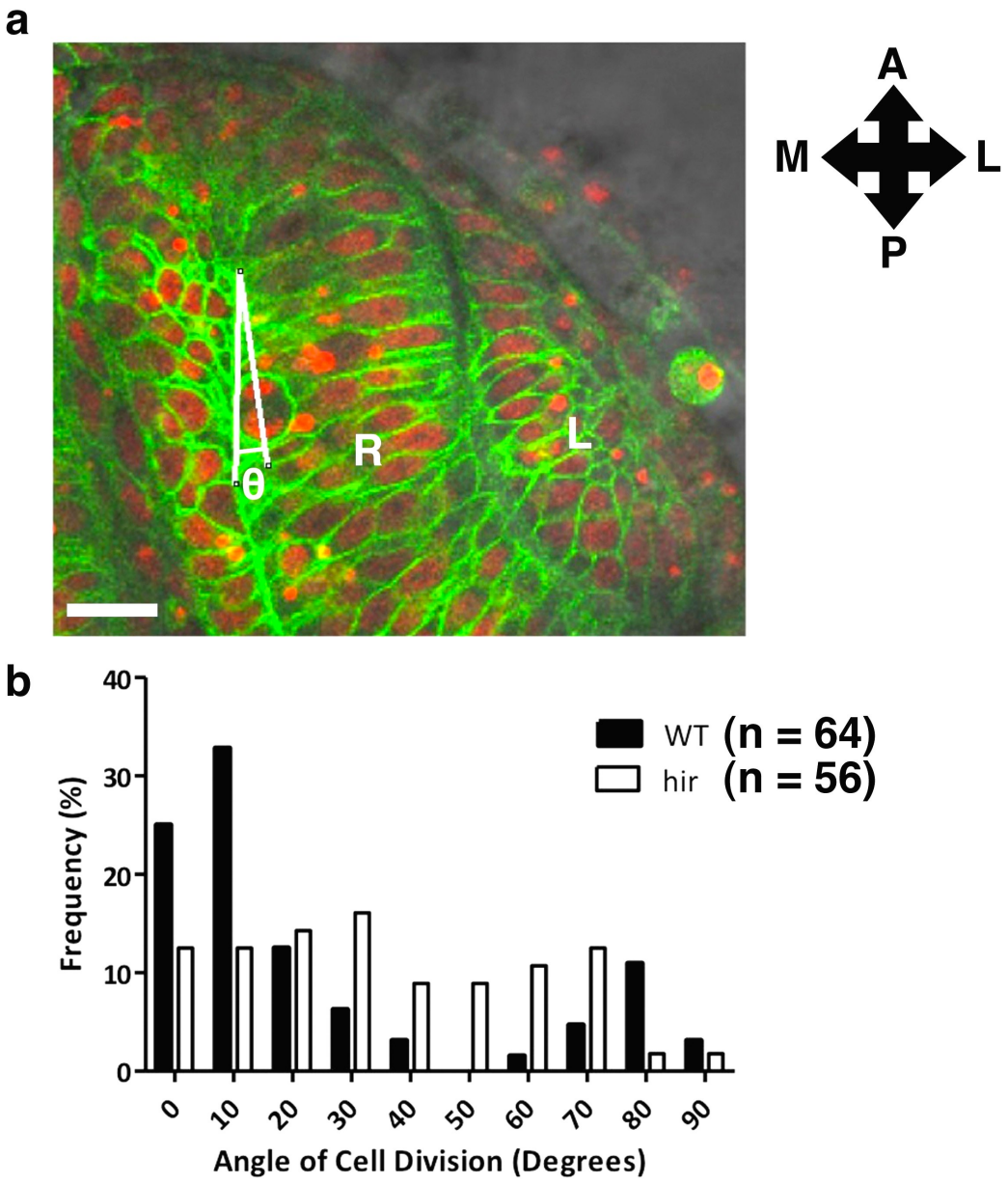

Figure 4.9. Oriented cell division is affected in the *hirame* retina. (a) Representation of how cell division angle was measured relative to the apical lumen of the retina in MNFP-injected embryos. View is dorsal and compass indicates axis orientation as in Figure 4.8. L: lens; R: retina. **(b)** Quantification of the frequency of cells over the ranges of division angles observed. NE cells of the retina in *hir* divide over a wider range of angles compared to wild type. Number of cell divisions is indicated in parentheses on graph. Scale bar: 10μm.

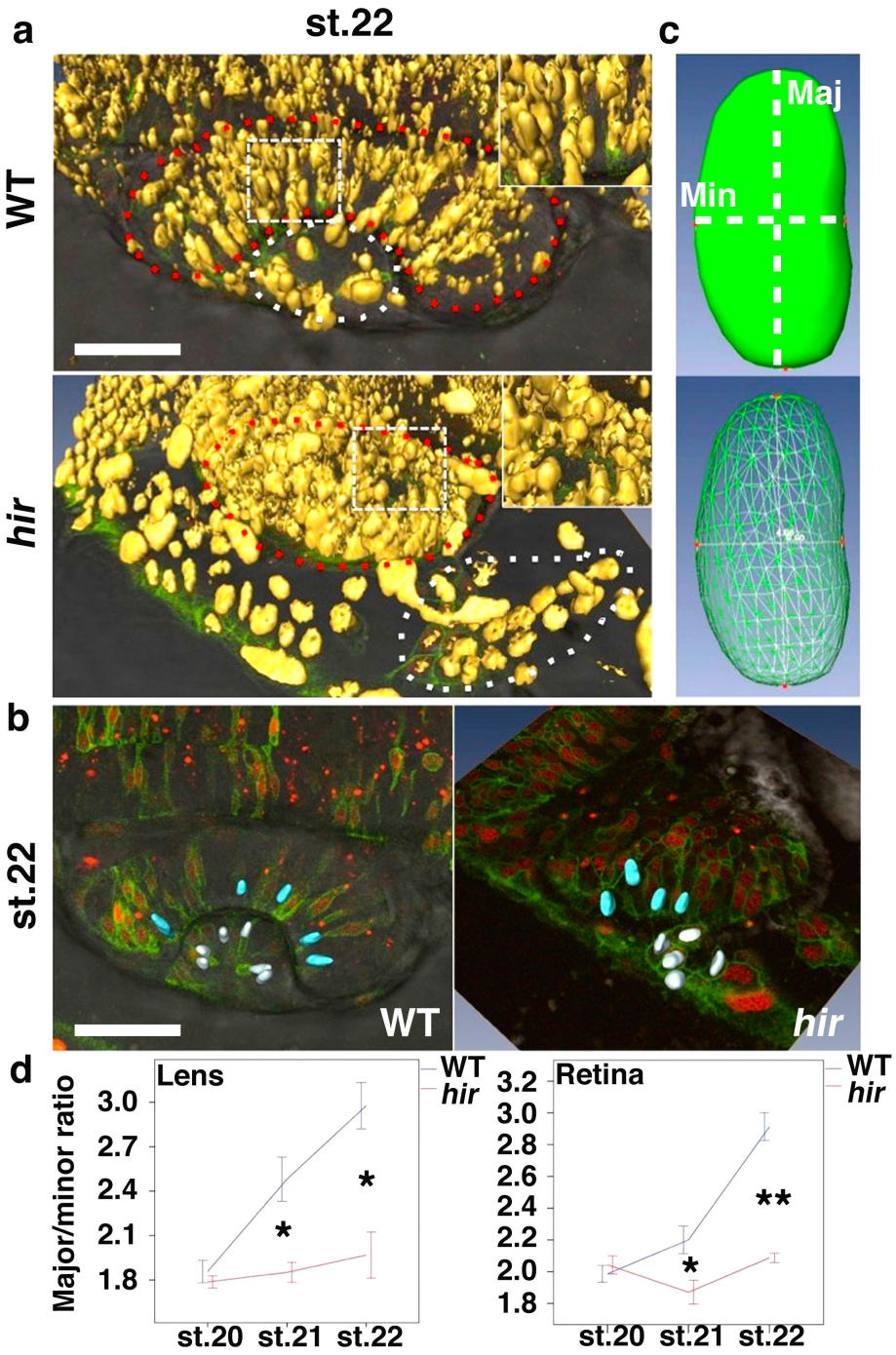

Figure 4.10. Tension appears reduced in the lens and retina of *hirame*. (a) Gross isosurface rendering of nuclei in the lens and retina of wild type and *hir*. Insets show magnifications of the boxes in main panels. Nuclei appear less elongated in *hir*. Red dotted line outlines the retina, white dotted line the lens. View is dorsal with medial upwards. **(b)** 3D rendering of individual nuclei in the retina (blue) and lens (white) to allow measurement. View is dorsal with medial upwards. **(c)** Measurement of nuclei in the lens and retina indicating longest (major, maj) and shortest (minor, min) axes (white dotted lines). **(d)** Quantification of the ratio of longest to shortest axis of nuclei shows wild type lens and retina nuclei elongate with time, suggesting increasing tension and become significantly elongated versus *hir* nuclei. * = p <0.05, ** = p <0.01. Anterior to right in (a) and (b). Scale bars: 20μm. Error bars indicate ± S.E.M.

4.4.1.4 Tissue tension appears reduced in the eyes of *hirame*

The randomised mitotic plane in the eye of *hir* along with the misshapen eye and collapsed tissues led to the hypothesis of a possible tissue tension reduction in the mutant. Thus, nuclear shape within the retina and lens was analysed, as epithelial nuclear shape is correlated with cellular tension (Maniotis *et al*., 1997), which in turn is associated with overall tissue tension. Gross isosurface rendering of nuclei in the retina showed overall nuclear morphology appeared elongated in the wild type and rounder in *hir* (Figure 4.10a, insets). The same trend was observed when 3D rendering individual nuclei of the retina and lens (Figure 4.10b). To confirm these shape differences measurements of the longest and shortest axes of the nuclei were made and their ratios calculated (termed major/minor ratio, Figure 4.10c).

Major/minor ratio calculations showed that interestingly, both wild type and *hir* nuclei of the retina and lens had comparable morphologies at st.20 (31.5 hpf) of development (Figure 4.10d, both graphs), which is the first point at which differences in the wild type and mutant eye can be observed (Figure 4.1a). This major/minor ratio analysis also revealed that nuclei of both the retina and lens in the wild type elongated as development progressed through st.21 (34 hpf) and st.22 (38 hpf), suggesting increasing tissue tension with time (Figure 4.10d, left and right graphs). In *hir*, major/ minor axis evaluation showed that nuclei of the lens elongated fractionally from st. 20-22 (31.5-38 hpf), but nevertheless mutant nuclei remained significantly rounder compared to wild type lens nuclei at st.21 and st.22 (Figure 4.10d, left graph). In the retina of the mutant, the major/minor ratio showed almost no increase during the major morphogenetic developmental stages of the eye (st.20-22, 31.5-38 hpf) such that nuclei of the *hir* retina were significantly rounder at st.21 (34 hpf, $p < 0.05$) and even more so at st.22 (38 hpf) compared to wild type retina nuclei ($p < 0.01$, Figure 4.10d, right graph).

4.4.2 YAP is required to maintain 3D body shape against external forces

4.4.2.1 The neural tube in *hirame* collapses variably

During characterisation of the *hir* mutant phenotype, particularly through taking frontal sections of the collapsed brain, it was observed that the collapse of the neural tube (NT) was somewhat variable in terms of orientation (Figure 4.11a). This collapse was tracked over time by conducting measurements of the height and width of the NT from st.22-27 (38-58 hpf, Figure 4.11b) using time-lapse movies. In wild type (n = 3 embryos) it was observed that both the height (h) and width (w) of the NT increased as development proceeded, indicating roughly proportional growth of the NT in wild type (Figure 4.11c, top graph). In *hir* however (n = 3 embryos), the height (h) of the NT decreased as development progressed from st.23 (41 hpf) onwards as the NT collapsed (Figure 4.11c, bottom graph). Conversely, the mutant NT width (w) increased from st.23 (41 hpf) onwards, widening as the NT collapsed (Figure 4.11c, bottom graph). The ratio of NT width to height (w:h ratio) from st.22-27 (38-58 hpf) was assessed next to give an indication of proportional growth differences. This demonstrated that although there was a small variation in the wild type ratio during st. 23-26 (41-54 hpf), by st.27 (58 hpf) in wild type the NT was approximately as high as it was wide with a ratio of ≈1 (Figure 4.11d, blue line). In *hir*, the w:h ratio steadily increased from st.23-27 (41-58 hpf) by which point the mutant NT was approximately twice as wide as it was high (Figure 4.11d, red line). Taken together these results suggest that the collapse of the NT in *hir* is not due to organ shrinkage, but is instead caused by a change in the dimensions of the organ, suggesting some sort of cell rearrangements may be occurring.

4.4.2.2 The *hirame* mutant neural tube collapses towards gravity

It was reasoned that this variable collapse might be due to reduced tissue tension within the mutant, as alluded to above in the eye, meaning that perhaps the embryo could not withstand external forces acting upon it. With this idea in mind, *hir* embryos were embedded in various orientations and developed to ascertain how the collapse of the NT varied. Wild type embryos were also embedded in matching orientations as controls. Collapse was assessed by gross morphology following sectioning, and by calculating the angle of curvature of the ventricle/lumen to a reference plane (Figure 4.12a, white arrows). When embedded with either the left side or the right side of the embryo facing down, wild type embryos exhibited a very mild curvature of the ventricle towards gravity (Figure 4.12a). They remained unaffected when embedded with the embryo dorsal side upwards/on top of the yolk as well as when the embryo was embedded dorsal downwards/under the yolk (termed dorsal down in Figure 4.12a). In *hir*, the ventricle curved/orientated much more towards gravity when the left or right side of the embryo was embedded facing downwards (Figure 4.12a). Again severe

collapse of tissues/organs was seen in the mutant when the embryo was embedded downwards or under the yolk (dorsal down, Figure 4.12a).

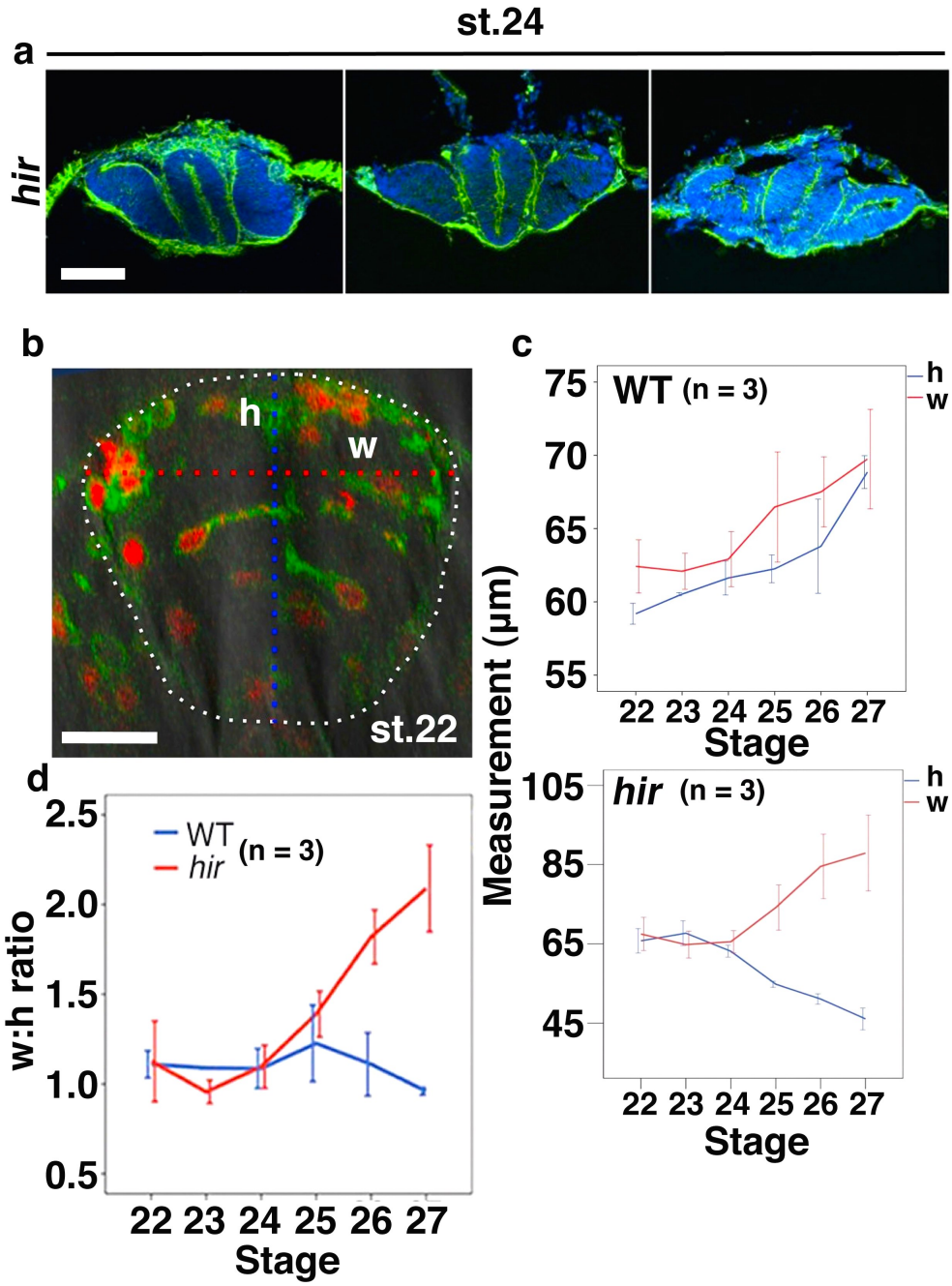

Figure 4.11. The *hirame* neural tube collapses variably. (a) Frontal sections stained with Topro3 (blue) to label nuclei and Phalloidin (green) which labels F-actin. Variable collapse of the NT is observed in *hir*. Images in conjunction with Huijia Wang. **(b)** Height (h, blue dotted line) and width (w, red dotted line) of the NT was measured over time in wild type and *hir* embryos. View shows an optical frontal section of the NT only, anterior up. Dotted white line outlines NT. **(c)** Quantification of h and w shows roughly proportional growth in wild type but flattening and widening of the NT in *hir*. **(d)** Plot of w:h ratio over time. Ratio increases in *hir* indicating widening and flattening. Numbers of embryos are shown in parentheses. Scale bars: (a) = 60µm; (b) = 15µm. Error bars indicate ± S.E.M.

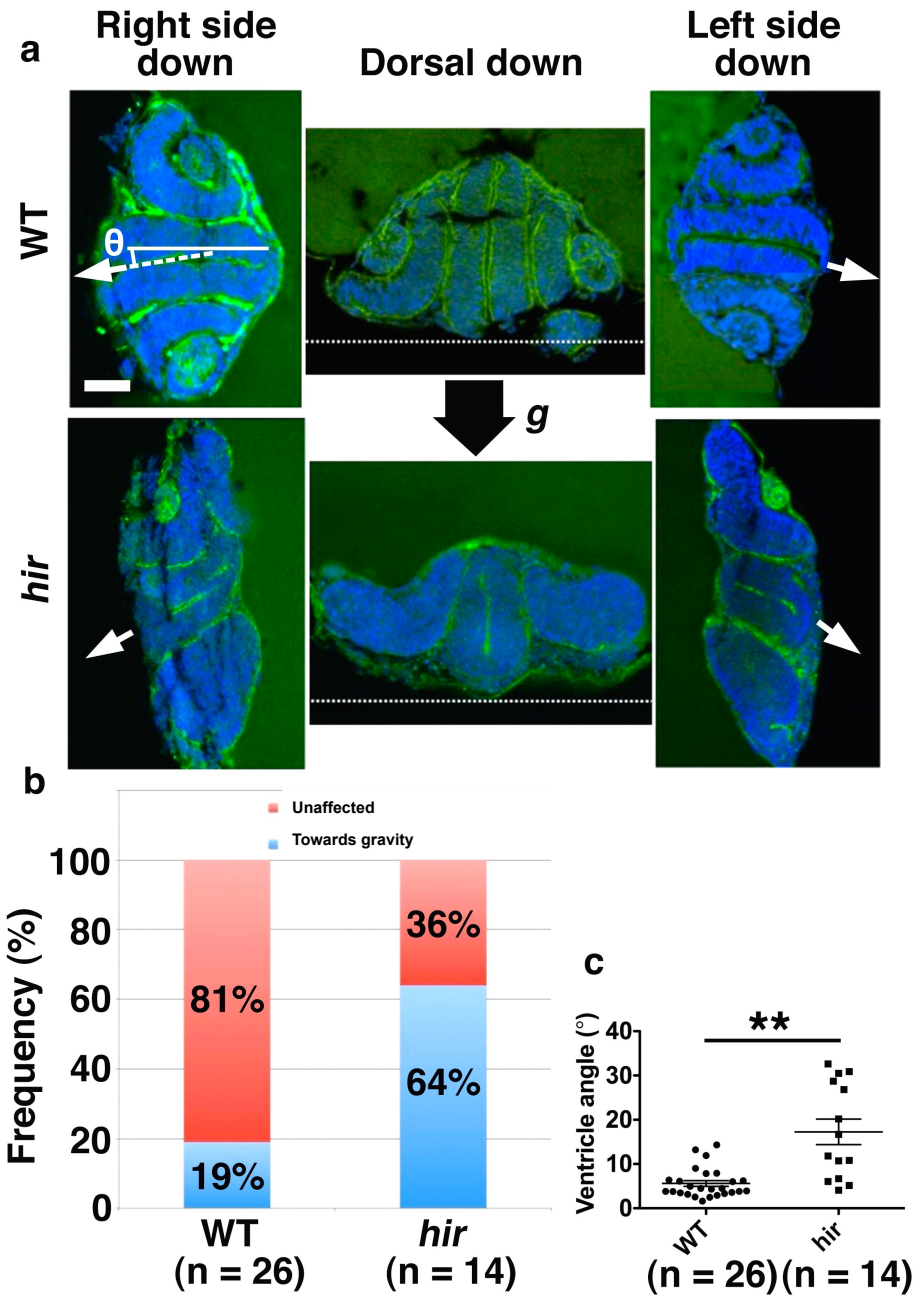

Figure 4.12. The *hirame* neural tube is unable to withstand external forces. (a) Embedding *hir* embryos in various orientations causes variable collapse of the NT as shown by frontal sections stained as in Figure 4.11. Black arrow indicates direction of gravity (*g*). White arrows indicate angle of the brain ventricle and top left panel shows how this angle was measured. White dotted line indicates the dorsal side of the embryo. Images in conjunction with Huijia Wang. **(b)** Quantification of the number of wild type and *hir* embryos affected by gravity/ embedding orientation, showing a higher proportion of *hir* embryos are affected by gravity. **(c)** Quantification of mean ventricle angle from (a). In *hir* the angle of the ventricle is significantly more affected/biased towards gravity. ** = p <0.01. Numbers of embryos are shown in parentheses. Error bars indicate ± S.E.M.

Quantification showed that in wild type, 81% of embryos were unaffected by gravity whereas 19% affected exhibited mild curvature/orientation of the ventricle towards gravity (n = 26 embryos, Figure 4.12b). In *hir* the effects of gravity on embryo growth were much more pronounced with only 36% of embryos unaffected by gravity whereas 64% of mutant embryos were affected showing a severe curvature of the ventricle in the direction of gravity (n = 14 embryos, Figure 4.12b). Indeed, when the angle of the ventricle to a horizontal reference plane was assessed, the average angle in *hir* was θ = 17.3° ± 10.7 (n = 14 embryos, Figure 4.12c), which was significantly greater (p = <0.01) compared to wild-type embryos that had an average ventricle angle of θ = 5.6° ± 3.3 (n = 26 embryos, Figure 4.12c). Interestingly it was also observed that the lumen/ ventricle in *hir* seemed somewhat less pronounced than in wild type. Even by later stages of development it appeared to have opened less significantly (Figure 4.1 and 4.12), suggesting that although the cavitation process occurs in *hir*, the ventricle may not inflate properly or be delayed in opening.

4.4.2.3 Cell rearrangements underlie the NT collapse in *hirame*

Next it was decided to examine the cellular behaviour underlying the NT collapse and shape change in *hir*. This was done by analysing single neuroepithelial cell behaviour in the NT of wild type and mutant embryos using a variety of labelling techniques. Firstly, kaede labelling of neuroepithelial cells was performed. This process allows the specific labelling of regions of the embryo by photoconversion of green fluorescent protein (GFP) to red fluorescent protein (RFP). Secondly, mosaic injection of EGFP-CAAX + H2B-RFP (MNFP) labelled cell membranes green and nuclei red. Both techniques allowed single-cell analysis in the NT when coupled with time-lapse confocal microscopy.

Kaede labelling in wild type (n = 10 embryos) showed that NT growth occurred when cells generated from a single labelled cell, stacked one above another following division to eventually form a thicker tissue (compare brackets in panels 1 and 5 in Figure 4.13). This cell stacking and thickening of the tissue was also evidenced by mosaic MNFP time-lapse imaging, which showed that cells divided and stacked to increase the overall height of the NT in wild type embryos (n = 26 embryos, white shaded area and insets in top panels of Figure 4.14). Conversely in *hir*, cells failed to remain stacked after dividing and instead became aligned side-by-side and formed flatter chain-like arrangements between the medial and lateral regions of the NT (n = 42 embryos, Figure 4.14, bottom panels). These chains of neuroepithelial cells were also observed in sections of the mutant NT where rows of cells were often seen compared to wild type where no more than a few cells appeared to align side-by-side (Figure 4.15, asterisks) along the medial-lateral axis.

In the mutant embryos, failure of cell stacking during st.22-24 (38-44 hpf), which was termed cell slippage, was investigated in more detail to ascertain how the cells slipped post-division during this main period of NT collapse in the mutant. Mosaic MNFP time-lapse revealed two main slipping behaviours within the NT of *hir* (Figure 4.16). Shortly after division at the ventricular zone (approximately 18 minutes in most cases), one of the daughter neuroepithelial cells in the NT of *hir* could be seen to slip either in the ventral direction (ventral slippage) or in the dorsal direction (dorsal slippage, Figure 4.16a, asterisks). In wild type, neuroepithelial cells remained stacked after division (Figure 4.16a). This slippage phenotype in *hir* hints at a possible cell adhesion problem between neuroepithelial cells. These cell slippage events were seen in wild type to some extent (38% of divisions, n = 47 cells) but occurred significantly more frequently in *hir* (70% of divisions, n = 52 cells, p = <0.05) compared to wild type (Figure 4.16b). Cell stacking frequency was significantly increased (p = <0.01) in wild type (40% of divisions, n = 47 cells) versus *hir* (10% of divisions, n = 52 cells, Figure 4.16b). Division that occurred perpendicular (at ≈90°) to the dorsal-ventral axis or ventricular zone (orthogonal division) was also observed in both wild type (22% of divisions, n = 47 cells) and *hir* (20% of divisions, n = 52 cells) but the frequency of occurrence was not significantly different between the two. As such it is unlikely that this orthogonal division significantly contributes to NT widening in *hir*, but instead cell slippage plays a more important role in this aspect of the phenotype.

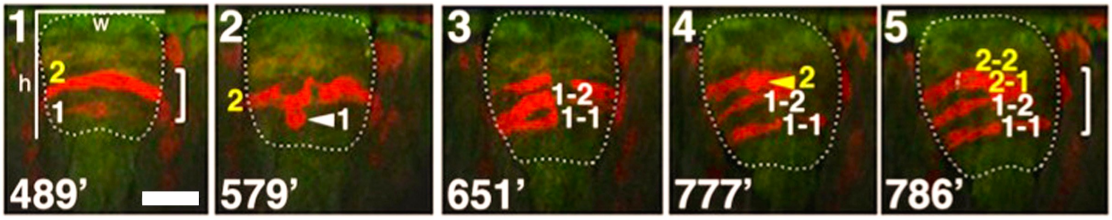

Figure 4.13. The wild type neural tube thickens by cell stacking. Images from confocal time-lapse movies of the NT in wild type. Kaede labelling of cells indicates that daughter cells (indicated by 1-2 and 2-2) stack on top of the mother cells (1-1 and 2-1) to increase NT thickness (compare brackets in 1 and 5). Views are optical frontal sections and the outline of the NT is indicated by the dotted line. Dorsal is up and brackets indicate thickening by cell stacking. Arrowheads indicate rounding-up/dividing cells. Time is indicated as minutes after the start of the movie at st.16.5 (approximately 23 hpf) meaning panel 1 roughly corresponds to st.20 (31.5 hpf). h: height; w: width. Scale bar: 15μm.

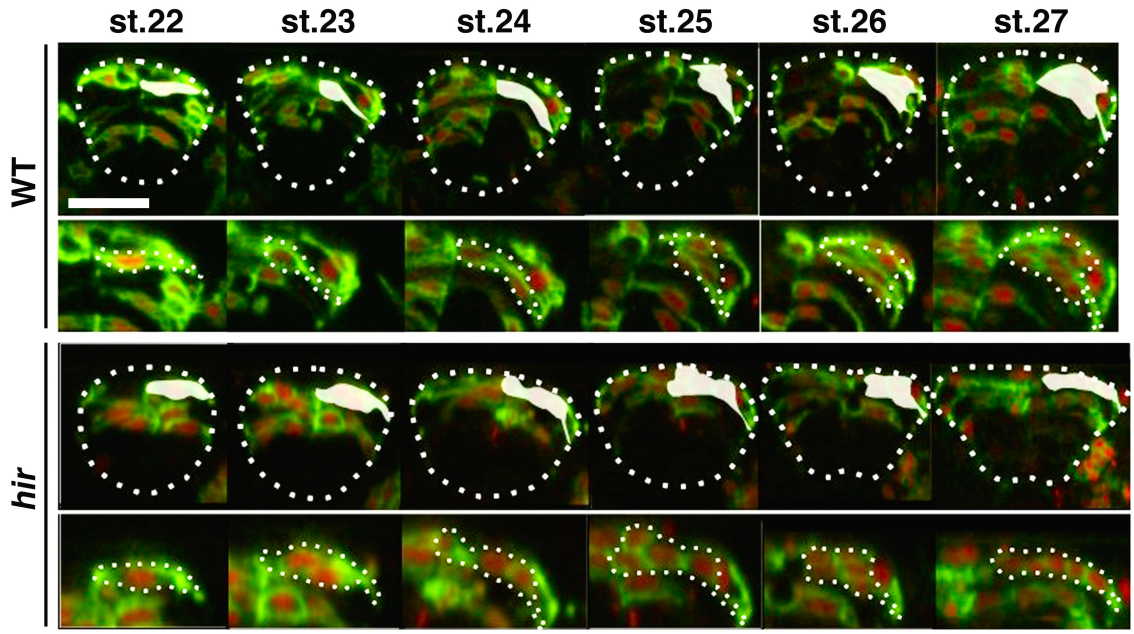

Figure 4.14. Cell stacking in the neural tube does not occur properly in *hirame*. Stills from mosaic MNFP confocal time-lapse movies of the NT in wild type and *hir*. In main panels dotted line outlines NT. Shaded/outlined area shows cell stacking in wild type but chains of cells form in *hir*. Mosaic MNFP labelling and frontal sections are shown, dorsal is up. Scale bar: 40μm.

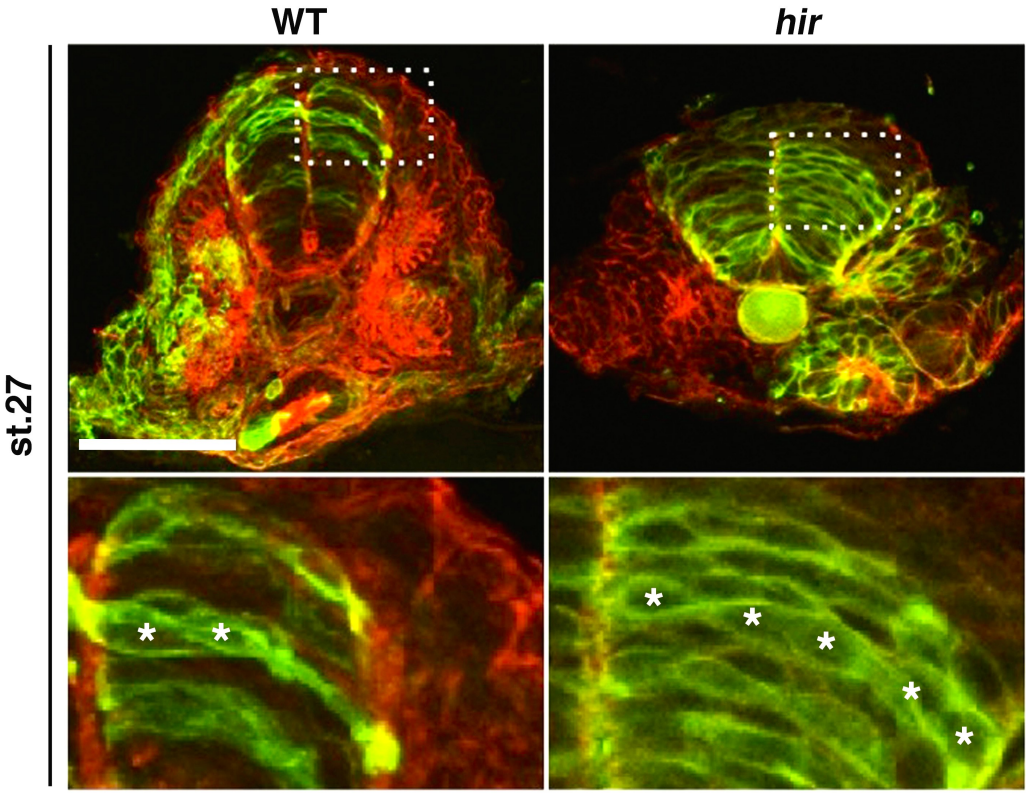

Figure 4.15. Chains of neuroepithelial cells form in the mutant neural tube. Chains of NE cells (asterisks) are also seen in frontal sections of the mutant NT in mosaically injected GFP embryos. Inset shows magnification of dotted box. Dorsal is up. Images in conjunction with Huijia Wang. Cells are stained with GFP antibody (green) and Phalloidin (red). Scale bar: 70μm.

4.4.2.4 Oriented cell division is randomised in the neural tube of *hirame*

To determine whether cell slippage was the main contributor to the emergence of chains of neuroepithelial chains, division orientation of the neuroepithelial cells in *hir* was assessed during collapse of the NT. Mitosis was also analysed since aberrant division was observed in the eye of *hir* and contributed to shape changes of the tissues, which is also seen in the NT. As previously described, mitosis of neuroepithelial cells takes place at the ventricular zone within the NT. Therefore the ventricle was used as a reference plane against which to measure the angle of division. The ventral pole of the ventricle was designated as 0° and the dorsal pole as 180° (Figure 4.17a). Therefore divisions were assessed over 180° relative to the ventricle (Figure 4.17a). Again the mitotic division angle was calculated for cells in the telophase stage.

In wild type at st.22-24 (38-44 hpf), most mitoses (≈77%, n = 38 cells) occurred roughly parallel to the ventricle, within 0-30° or 150-180° relative to the ventricle (Figure 4.17b, top left rose diagram). A small number of cells (≈23%, n = 38 cells) at this stage underwent division between 40-140° relative to the ventricular zone, most likely representing the cells undergoing orthogonal division (Figure 4.17b, top left rose diagram). By st.25-26 (50-54 hpf) in wild type, all division occurred within 0-30° or 150-180° to the ventricle suggesting orthogonal division was no longer taking place and widening of the NT by this method was perhaps nearing completion (Figure 4.17b, top right rose diagram). At earlier stages in *hir* (st.22-24, 38-44 hpf), mitosis was very randomised with division occurring over a full range of angles relative to the ventricle with similar frequency (Figure 4.17b, bottom left rose diagram). At st.25-26 (50-54 hpf) in the mutant, mitosis became less randomised with fewer cells dividing over a wider range of angles. At this stage in *hir*, approximately 80% of neuroepithelial cells divided at 0-30° or 150-180° to the ventricle with only 20% of division occurring at 40-140° relative to the ventricular zone (Figure 4.17b, bottom right rose diagram).

Taken together this suggests *hir* may have lower tissue tension and be unable to build 3D tissues opposite to external forces. This randomised oriented cell division coupled with changes in neuroepithelial cell behaviour post-division, i.e. cell slippage, is likely to contribute to the formation of the chain-like cell arrangements in the mutant NT and its consequent widening and flattening.

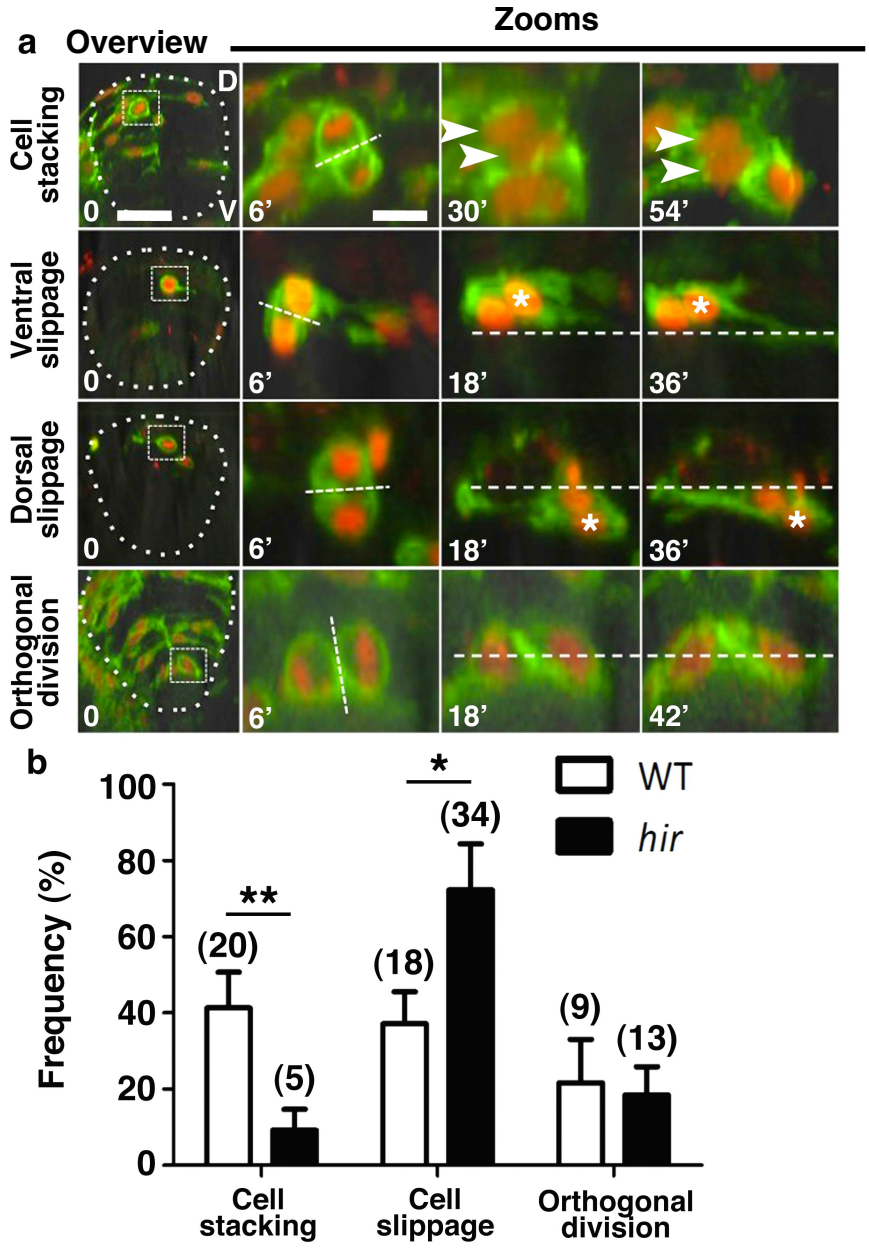

Figure 4.16. Cell slipping behaviour is observed in the neural tube of *hirame*. (a) Images from mosaic MNFP time-lapse movies showing NE cell behaviour in the NT. Cell stacking involves daughter cells remaining on top of each other. In *hir*, daughter cells slip ventrally or dorsally (asterisks) to sit alongside one another. Time after rounding-up is indicated. **(b)** Quantification of the frequency of cell behaviours reveals slippage is significantly more common in *hir* whereas stacking predominates in wild type. * = p <0.05, ** = p <0.01. Scale bar: overview = 20μm; zooms = 10μm. Number of cells shown in parentheses. Error bars indicate ± S.E.M.

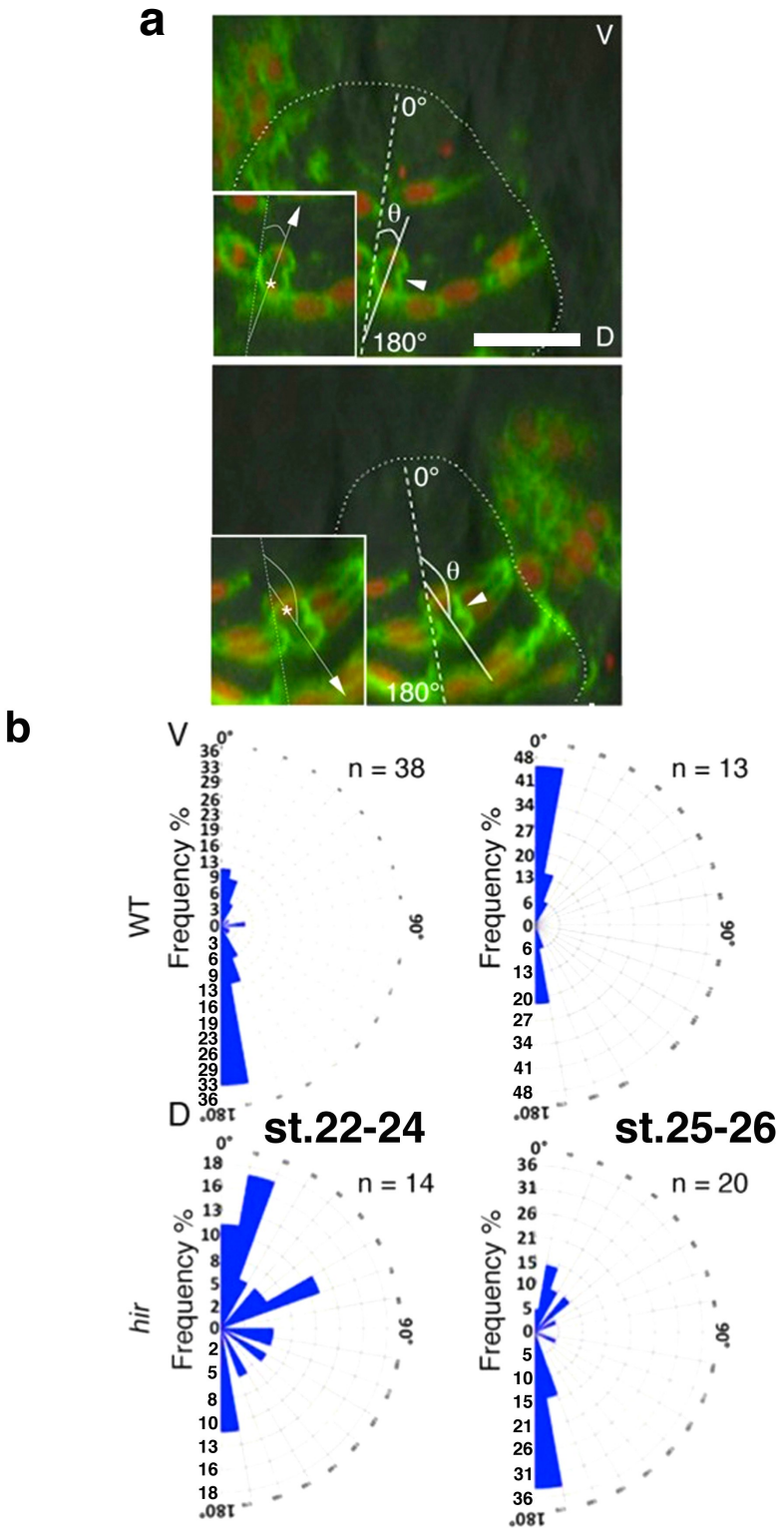

Figure 4.17. Oriented cell division is lost in the neural tube of *hirame*. (a) Schematic representing how division angle (θ) of NE cells in the NT was measured relative to the ventricle. Images show optical frontal sections of mosaically labelled MNFP embryos. Arrowheads indicate telophase cells. Asterisks indicate the cell closest to the ventricle which determined how the division axis was drawn (Section 2.11). D: dorsal; V: ventral. **(b)** Rose diagrams showing quantification of NE cell division angle. Cells divide over a wider range of angles in *hir* whereas in wild type, division occurs mostly along the ventricle. Each circumferential segment represents 10°. Scale bar: 20μm. Number of cells is indicated (*n*).

4.4.2.4.1 Crossing divisions in the *hirame* neural tube appear reduced

Since the lumen in the NT of *hir* appeared somewhat less opened and the oriented division of neuroepithelial cells was aberrant, midline crossing divisions (C-divisions) in the developing NT of *hir* were analysed. During neurulation, C-divisions occur mediolaterally across the forming midline such that daughter cells are distributed on either side of the presumptive midline of the neural rod with mirror-image polarity (Tawk *et al*., 2007). These C-divisions generate two mirrored epithelia as division occurs perpendicular to both the dorso-ventral and antero-posterior axis. C-divisions are important for the generation of the lumen in the NT. C-divisions were assessed using kaede labelling whereby half of the neuroepithelial cells of the NT were photoconverted from green to red at st.17 (25 hpf) at the beginning of neurulation, such that cell mixing in the NT could be clearly observed (Figure 4.18a). In wild type (n = 4 embryos) by st. 20 (31.5 hpf), there appeared to be a high degree of cell mixing evident suggesting many C-divisions had occurred (Figure 4.18b, left panels). In *hir* (n = 6 embryos), the number of cells undergoing C-divisions appeared much more reduced (Figure 4.18b, right panels). Quantification of cell mixing should be performed to confirm this however. These results suggest that C-divisions, another type of oriented cell division, are also affected in the mutant and may contribute to the mildly affected lumen observed in *hir*.

4.4.2.5 Tension appears reduced in the neural tube in *hirame*

Results of the gravity embedding experiments along with cell slippage observations and the randomised oriented cell division in *hir* suggested a tension defect in the mutant NT. Thus the nuclear shape of the neuroepithelial cells in the NT was analysed as previously in the eye. The appearance of the nuclei in the NT of *hir* was much rounder than those in wild type (Figure 4.19a, compare insets). Major/minor nuclear axis measurements were performed over the stages of development where collapse of the mutant NT was most prominent (st.22-27, 38-58 hpf). In the wild type NT at st. 22-23 (38-41 hpf), the major/minor ratio was 2.66 ± 0.56 (n = 33 cells) whereas *hir* was significantly lower at 1.74 ± 0.36 (n = 38, p = <0.001, Figure 4.19b, top graph). Later, by st.26-27 (54-58 hpf), nuclei of the neuroepithelial cells in wild type had further elongated such that the major/minor ratio was now 2.96 ± 0.72 (n = 31 cells). In *hir* the major/minor value had decreased from 1.74 to 1.55 ± 0.33 and was again significantly lower than the ratio in wild type (n = 31 cells, p = <0.001, Figure 4.19b, bottom graph).

These data suggest that even by st.22 (38 hpf) of development, tension in the NT of *hir* was already significantly lower than in wild type and continued to decrease as development and collapse of the NT proceeded. Oppositely, for wild type, cellular tension increased as the NT grew proportionally against external forces.

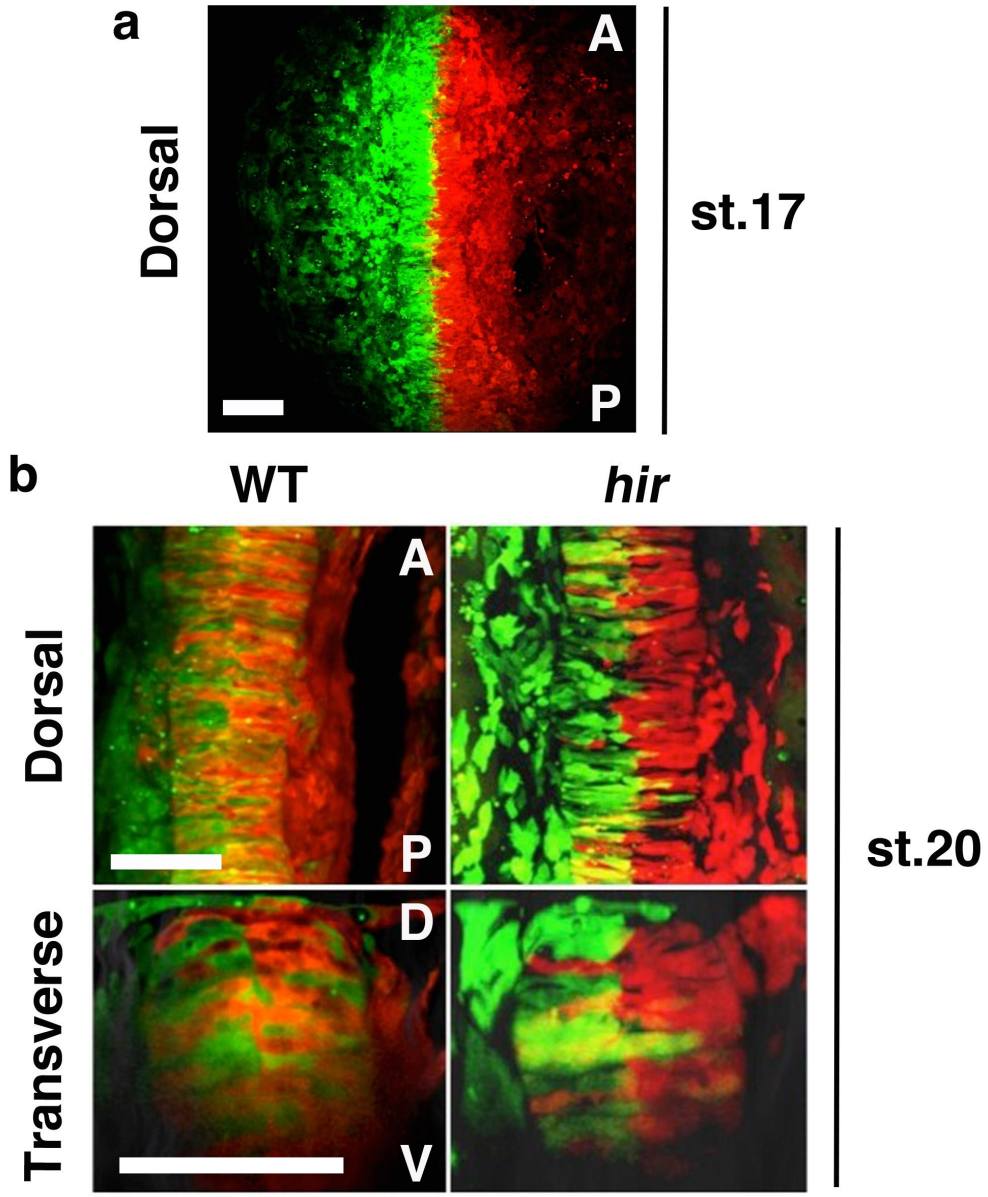

Figure 4.18. Crossing divisions appear reduced in *hirame*. (a) Representative confocal image of kaede labelling in half of the NT at st.17 (25 hpf) to allow determination of cell crossing divisions. A: anterior; P: posterior. **(b)** Dorsal and transverse optical sections of half converted kaede embryos 6.5 hours after conversion showing more C-divisions appear to occur in wild type than *hir*. D: dorsal; V: ventral. Scale bars: (a) = 30μm; (b) = 40μm.

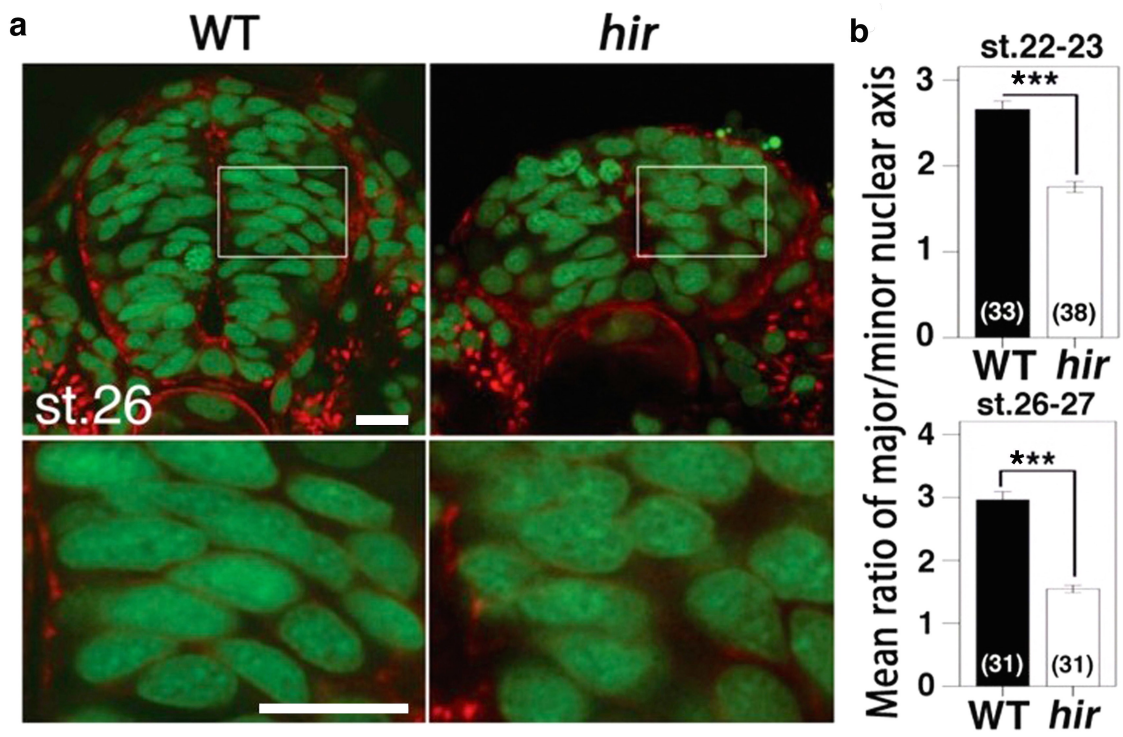

Figure 4.19. Tension appears reduced in the neural tube of *hirame*. (a) Frontal sections stained with Phalloidin (red, F-actin) and Topro3 (green, nuclei) show nuclei are more elongated in the NT of wild type. Dorsal is up. Magnifications are of boxes in main panels. **(b)** Quantification of ratio of the longest to shortest axes of nuclei show wild type nuclei are significantly elongated compared to *hir* at both earlier and later stages of development. *** = p <0.001. Number of nuclei assessed is shown in parentheses. Scale bars: 20μm. Error bars indicate ± S.E.M.

4.4.3 YAP is required for correct development of the ears

4.4.3.1 The ears in *hirame* display a dislocated phenotype similar to that of the eyes

Other sensory placodes were also observed to be misaligned in *hir* similar to the eyes. These placodes also did not invaginate and became mislocated at later stages of development. One such example was the otic placodes from which the ears develop, much like the lens develops from the lens placode. Time-lapse imaging indicated that not only did the otic placodes of *hir* dislocate and fail to invaginate similar to the lens placodes, but also gave rise to what appeared to be multiple ectopic ears/placodes as seen with multiple lenses in the eye (Figure 4.20, arrowheads). This contrasted with the wild type where the otic rudiment lumenised and invaginated to give an incorporated ear by st.25 (50 hpf). Multiple placodes/ears were observed in *hir* embryos at a frequency of around 38% (3/8 embryos) from time-lapse movies but had not developed lumens by st.25 (50 hpf). The identity of these ectopic structures could not be confirmed using *Sox3 in situ* so further characterisation is required. In all cases (8/8 embryos) there was always one 'primary' ear located nearer the hindbrain that did form a lumen (Figure 4.20, structure marked with E) but appeared less closely apposed to the hindbrain.

4.4.3.2 Ear development in *hirame* appears aberrant and delayed

MNFP time-lapse further revealed differences in the development of the ears between wild type and *hir*. At st.20 (31.5 hpf) of development, the wild type and *hir* placode appeared similar. In wild type by st.21 (34 hpf) the lumen/cavity of the ear had formed and begun to open (Figure 4.21a'). This lumen in *hir* was smaller and less open (Figure 4.21b'). In wild type the lumen continued to increase in size and open from st.22-23 (38-41 hpf, Figure 4.21a'' and a'''). At the same time the overall shape of the ear in wild type became elongated in the anterior-posterior axis with single cells spanning from the basal to apical edges around the circumference of the organ (Figure 4.21a'''). In *hir* from st.22-23 (38-41 hpf) the lumen remained smaller and less open (Figure 4.21b'' and b'''). The nuclei of cells in *hir* also appeared rounder in many of the cells from st. 21-23 (34-41 hpf).

The overall morphology of the mutant ear remained rounder and the cellular organisation within the ear also appeared somewhat perturbed in *hir* with multiple cells lying between the apical and basal surfaces of the ear. In wild type, usually only one cell was observed to span the apico-basal axis (compare Figure 4.21a'' and a''' with b'' and b'''). In 25% of cases (2/8 embryos) in *hir* it was noted that the lumen of the 'primary' ear had failed to open, even by st.23 (41 hpf, Figure 4.21c-c'). However, in all cases, these delayed lumens eventually opened by later stages of development (approximately st.25, 50 hpf, Figure 4.23b). Quantification of lumen area or volume

could be performed to empirically determine the differences in lumen formation between wild type and *hir* as development proceeds.

Together these results demonstrate that ear development is also affected in *hir*, particularly regarding later cavity/lumen formation which may also be seen to some extent in the NT of the mutant during ventricle inflation. Furthermore, cellular appearance and organisation in the mutant ear suggests that tension may be again reduced, in line with the findings from the eye and NT already discussed in this chapter.

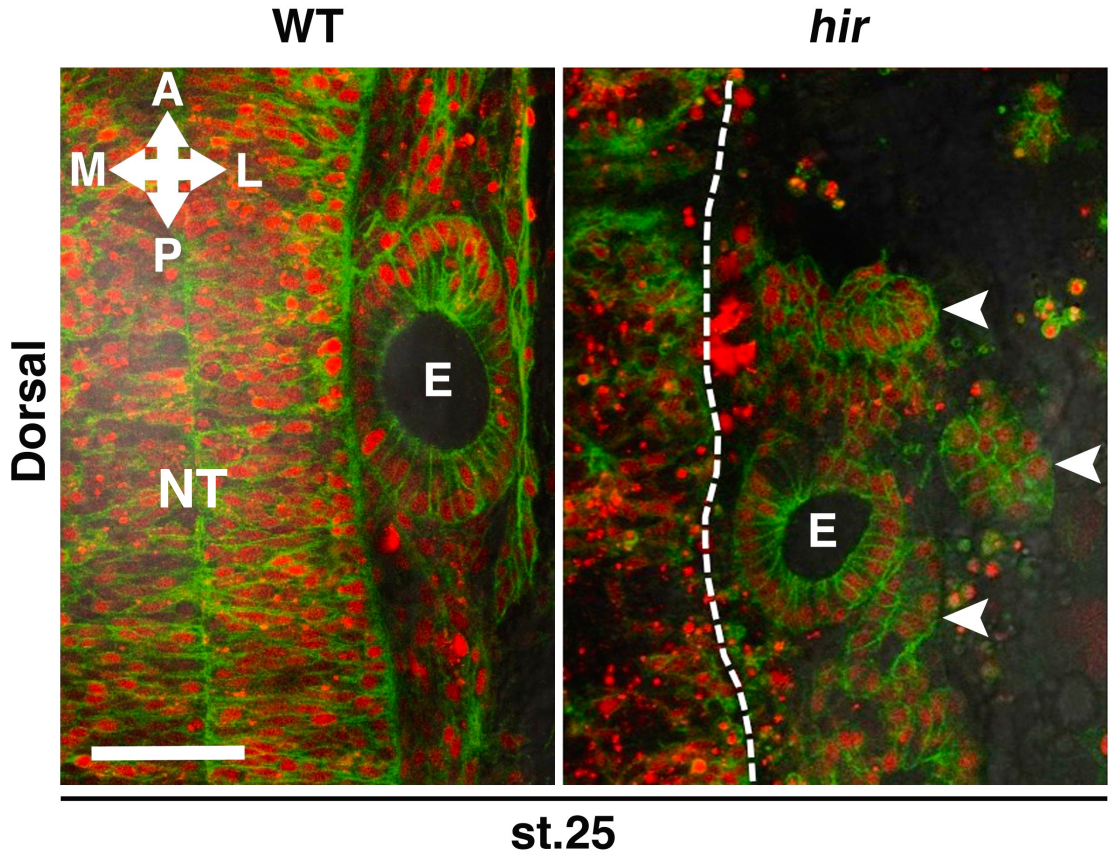

Figure 4.20. Multiple ears/placodes appear to form in *hirame*. Dorsal views from MNFP confocal time-lapse movies. The wild type panel shows a maximum projection. The *hir* panel shows a snapshot at a specific slice of a Z-stack hence the reason why fewer cells appear labelled. E: primary ear. Arrowheads indicate what appear to be multiple placodes or non-lumenised ears in the mutant. Dotted line demarcates the outline of the embryo/NT boundary. A: anterior; P: posterior; M: medial; L: lateral. Scale bar: 30μm.

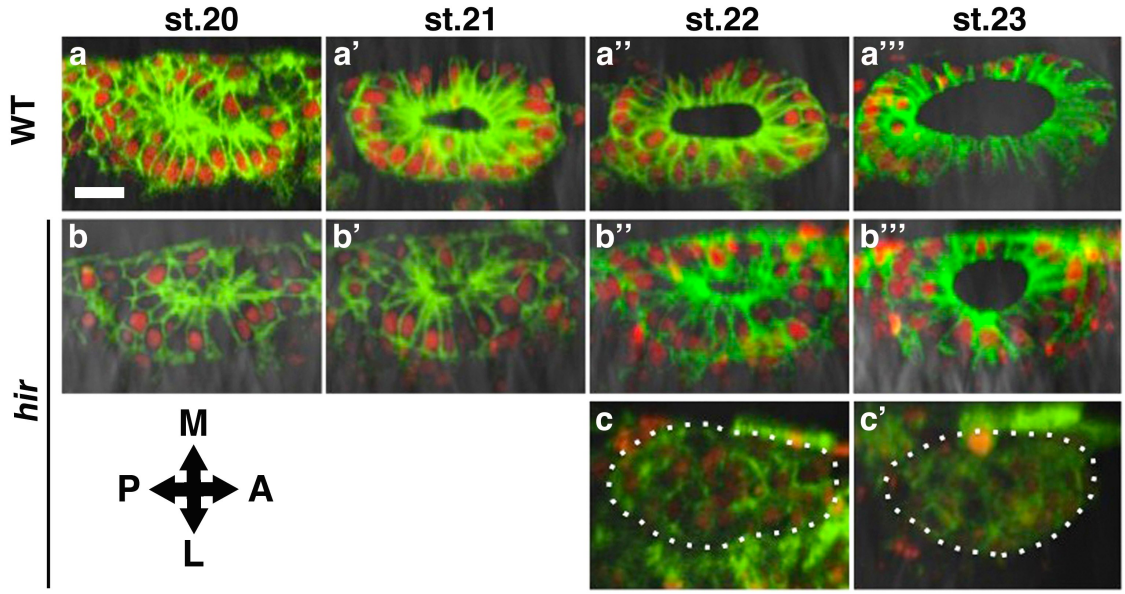

Figure 4.21. Ear development in *hirame* appears delayed. Snapshots from MNFP confocal time-lapse movies showing the development of the primary ears (as depicted in Figure 4.20) in *hir* versus wild type. **(b-b''')** Lumenisation appears delayed in *hir* compared to wild type (a-a'''). **(c and c')** In some cases, the lumen of ears in *hir* had still not opened by st.23 (41 hpf) but in all cases had opened by st.25 (50 hpf). White dotted line marks the outline of the ear. Compass indicates orientation and views are dorsal. Images are sections from confocal Z-stacks and hence not all cells appear labelled. M: medial, L: lateral; P: posterior; A: anterior. Scale bar: 10μm.

4.4.3.3 Nuclear morphology in cells of the *hirame* ear is rounder suggesting reduced tissue tension

Given the initial phenotypic clues that tension may be reduced in the mutant ear, nuclear axis ratios were again established as previously described. In wild type embryos at st.22-23 (38-41 hpf) when the lumen is undergoing expansion, the mean major/minor ratio was 2.03 ± 0.38 (n = 42 cells) versus only 1.37 ± 0.27 in *hir* (n = 43 cells), giving a significant difference (p = <0.001, Figure 4.22a). The same trend was observed later in development at st.26-27 (54-58 hpf) when the wild type major/minor ratio was 2.07 ± 0.31 (n = 28 cells, Figure 4.22b). In *hir*, the nuclear axis ratio had decreased very slightly to 1.29 ± 0.21 (n = 27 cells) at st.26-27 (54-58 hpf, Figure 4.22b) suggesting perhaps a slight decrease in tension and possibly explaining why the ear shape in *hir* remained rounder instead of becoming elongated like in wild type. Again this difference in major/minor ratio at st.26-27 (54-58 hpf) was significantly different between wild type and *hir* (p = <0.001).

4.4.3.4 Mitosis in the *hirame* ear is also randomised

To add further evidence for a tension defect in the mutant, the division plane of cells in the ear of *hir* was assessed. It has previously been shown in the guinea pig cochlea that divisions occur parallel to the luminal surface (Kim and Raphael, 2007). However, the literature suggests that little appears to be known about cell division in the medaka ear, thus wild type was examined first to understand the normal mitotic planes involved in ear development and growth. Two types of cell division were observed: those occurring along the apical lumen edge, which will be described as parallel division, and those taking place at 70-110° relative to the apical lumen edge, termed perpendicular divisions (Figure 4.23a, arrowheads).

Earlier in wild type ear development (st.22-24, 38-44 hpf) when the lumen of the otic vesicle was expanding, 77% of cells divided parallel to the lumen, with 23% dividing perpendicularly (n = 64 cells, Figure 4.23c, left graph). At the equivalent stages in *hir*, the ratio of division types was much more even with 51% dividing parallel to the lumen and 49% dividing perpendicularly (n = 45 cells, Figure 4.23c, left graph). At st.25-26 (44-50 hpf) in wild type, 80% of cells of the ear epithelium divided in a parallel manner and 20% underwent mitosis perpendicular to the lumen edge representing similar frequencies to earlier in ear formation (n = 30 cells, Figure 4.23c, right graph). At the same stages in *hir*, 54% of cells in the ear divided parallel to the lumen whereas 46% divided perpendicularly, again agreeing with the results obtained earlier in development (n = 26 cells, Figure 4.23c, right graph). It may be that the ratio of these parallel and perpendicular cell divisions is important to help sculpt the shape of the forming ear. Furthermore, based on the wild type studies it seems that the higher frequency of perpendicular divisions in *hir* may be aberrant (Figure 4.23b).

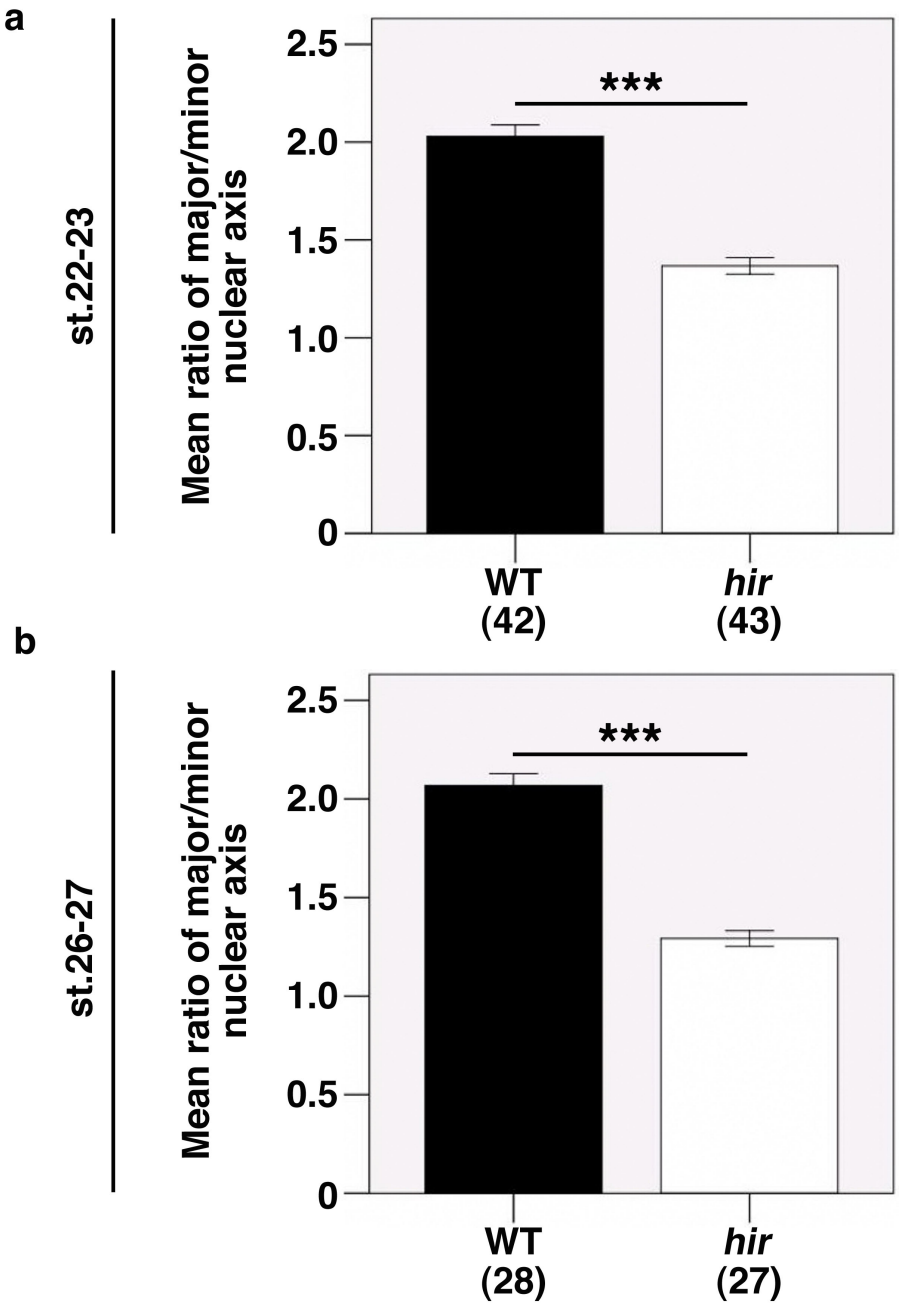

Figure 4.22. Tension appears reduced in the ears of *hirame* at earlier and later stages of development. (a) Quantification of major-to-minor nuclear axis ratio at earlier stages of development (38-41 hpf). **(b)** Ratio quantification at later stages (54-58 hpf) of development. At both early and later stages of development, wild type embryos have significantly elongated nuclei in the ears compared to *hir*. *** = p <0.001. Error bars indicate ± S.E.M.

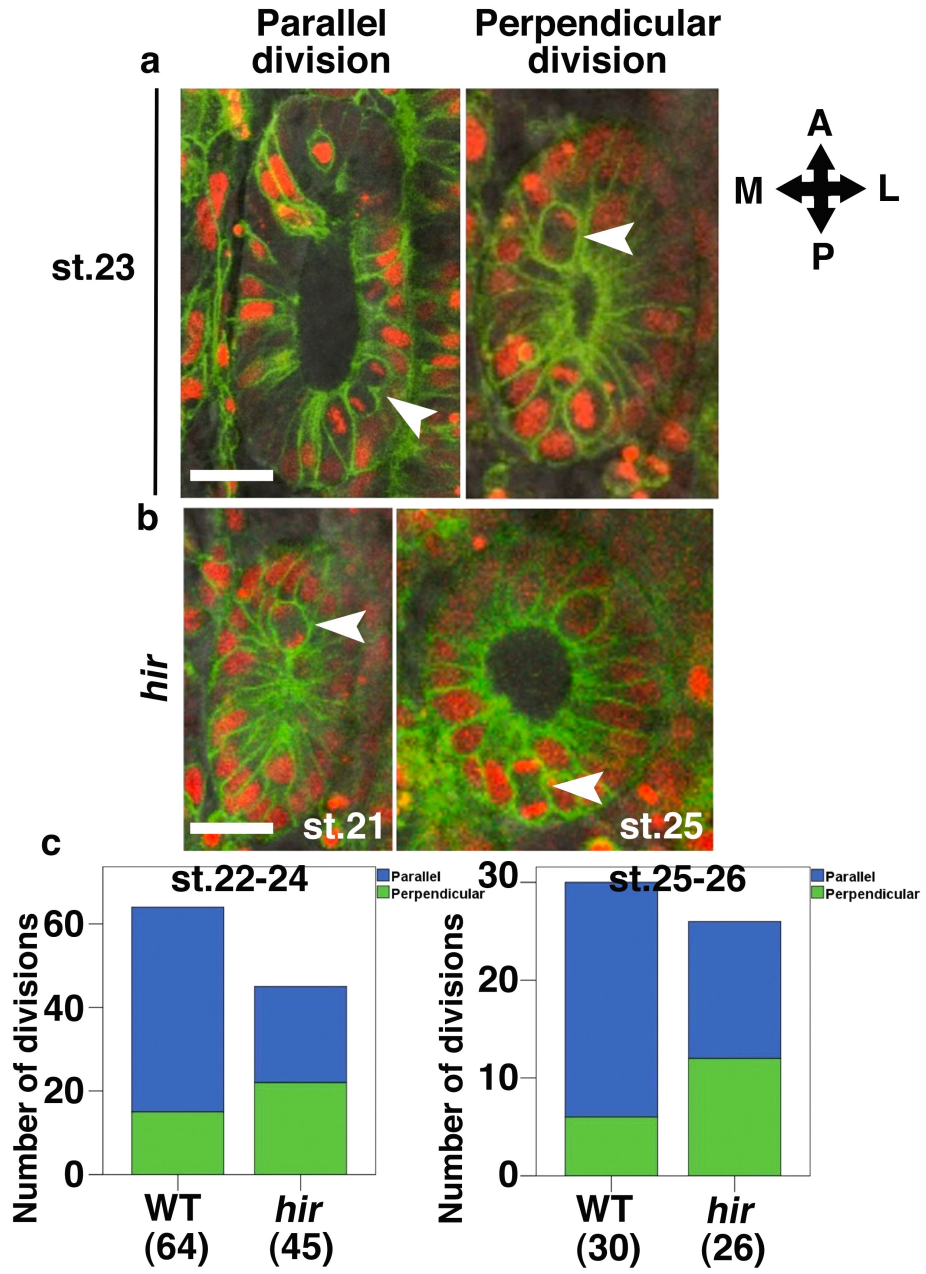

Figure 4.23. Oriented cell division is affected in the ears of *hirame*. (a) Examples of parallel and perpendicular division in the ears. **(b)** Further examples that perpendicular division is predominant in *hir* and persists even later into development. **(c)** Quantification of parallel and perpendicular divisions in wild type and *hir* at earlier and later stages of development. Arrowheads indicate telophase cells. Compass indicates orientation, A: anterior; P: posterior; M: medial; L: lateral. Number of divisions observed is shown in parentheses. Scale bars: 15μm.

4.5 Discussion

4.5.1 The eyes, neural tube and ears of *hirame* exhibit similar phenotypes

Characterisation of the defects underlying the phenotypes observed in the eyes, NT and ears of the mutant revealed several common features. All three organs in *hir* displayed flattening and loss of shape, epithelial cells with rounder nuclei, and a loss of oriented cell division. So what could be a common mechanism that YAP is regulating to cause these effects? Reviewing the literature points to a potential candidate, tissue tension, that if affected could be responsible for these traits. Since the eyes, NT and ears of the mutant all appear to exhibit this common phenotypic defect of reduced tension, YAP may be performing a similar role for the development of each organ.

4.5.1.1 Loss of epithelial tissue/organ shape in *hirame* is associated with cells exhibiting rounder nuclei

Reports have shown that nuclear shape in epithelial cells correlates well with the overall tension of the cell. Specifically, cells under greater tension exhibit an elongated nuclei (Maniotis *et al*., 1997). Rounder nuclear shape was observed and quantified by morphometric measurements in the neuroepithelial cells of the eyes, NT and ears, suggesting all three organs are composed of cells under reduced tension. Concurrently, these rounder nuclei were correlated with drastic changes in shape of all three organs suggesting reduced cellular tension may be an indicator of reduced tissue tension. For example, in the wild type NT, the major/minor nuclear axis ratio increased from st.22-27 (38-58 hpf) concomitant with roughly proportional NT growth. Whereas in *hir,* the ratio decreased over the equivalent developmental time, corresponding with flattening and widening of the mutant NT. Similar trends were observed in the ear and eyes of the mutant where correct morphogenesis also failed and was correlated with a decreasing nuclear axis ratio during key developmental stages for the organ. These severe shape changes suggest that all three organs may have overall reduced tissue tension, and that this reduced tension plays a key role in their collapse/mishaping.

This raises the question of what could be causing this reduced tissue tension. Maniotis *et al*. (1997) showed that cytoskeleton tethering to the nucleus is important to bring about shape changes in the nucleus that correlate with overall cellular tension. Moreover they showed the cytoskeleton provided a direct physical link between the nucleus and integrin cell surface receptors. This means that both the cytoskeleton and ECM could have an affect on cellular and thus tissue tension in the *hir* mutant. Indeed, the reduced FN fibrillisation seen in *hir* suggests that integrin-FN interactions may be disrupted in the mutant. However, cytoskeletal tension/arrangements are required to induce conformational changes in FN via integrin such that fibrillogenesis can occur (Mao and Schwarzbauer, 2005). Therefore cytoskeleton tension is also a candidate for being affected in *hir*.

4.5.1.2 Defective oriented cell division contributes to failed morphogenesis in the *hirame* mutant

Oriented cell division appears strongly affected in *hir* in the eyes (both lens and retina), the NT (discussed in section 4.5.2) and the ears (otic vesicles). Oriented cell division is important for morphogenesis of tissues and has been well studied in several cell types and different tissues, including the zebrafish NT (Tawk *et al*., 2007).

In the eye, the mitotic cleavage plane seems well studied in the retina, but less so in the lens. During the earlier stages of eye development, proliferation is both slower and less frequent. As morphogenesis proceeds and the optic cup starts to take shape whilst increasing in volume, the number of proliferating cells increases and the cell cycle decreases in duration (Das *et al*., 2003). In zebrafish it was shown that divisions in the retina occur parallel to the apical or basal surface (Link, 2001; Das *et al*., 2003), which is in agreement with the findings presented here in wild type medaka. Here also the neuroepithelial cell divisions in the retina occurred predominantly along the apical lumen for the developmental stages examined. These parallel divisions may serve to add cells in the antero-posterior axis to assist with basal constriction of the optic vesicle, which is required to shape the optic cup. In *hir*, retinal divisions were spread over a range of angles relative to the apical lumen with relatively equal frequency. This may explain the lack of basal constriction and consequent failure of optical cup shaping in the mutant. In the wild type lens there was a fairly equal frequency of mitoses occurring parallel or perpendicular to the placode-retina boundary (PRB), seemingly helping the lens to grow roughly proportionally and round-up to become spherical. In the mutant, there were no perpendicular divisions meaning the *hir* lens placode grossly elongated in the antero-posterior axis. It remains to be seen whether this antero-posterior lengthening contributes to the dislocation and fragmentation phenotype of the mutant lens.

The predominant parallel-to-lumen divisions in the developing wild type ear/otic vesicle, likely add cells side-by-side thus increasing the cell number around the circumference of the lumen. This means that in wild type the ear morphology elongates along the anterior-posterior axis. These predominantly luminal-parallel divisions in wild type are somewhat consistent with data from guinea pig in which epithelial cells of the cochlea divide parallel to the luminal surface of the cochlear duct (Kim and Raphael, 2007), though the cochlea is a more specialised inner ear structure and so perhaps not directly comparable. In *hir*, the even distribution between parallel and perpendicular divisions potentially means the dimensions of the ear increase equally both in the antero-posterior axis and the medio-lateral axis, perhaps contributing to the rounder shape of the mutant ear.

How could these aberrant divisions observed in the mutant eye and ear be explained in terms of tension? Reports have shown that cell division may occur according to cues provided by the cell's mechanical microenvironment, aligning daughter cells with the external force field (Fink *et al*. 2011). As FN fibrillogenesis is affected in and around both organs in *hir*, the ECM stiffness and consequently the mechanical microenvironment may be altered such that mitoses do not correctly align in the mutant. Moreover, the possibly reduced intrinsic tissue tension in the *hir* eyes and ears could be the cause. It is possible that if tissues are not under the correct tension or rigidity, cells may be less physically constrained. Spatial cues have been proposed to be important for orienting the mitotic spindle (Nakajima, *et al*. 2013). Therefore cells in the mutant may be less spatially confined such that the mitoses can occur over a greater range of angles, as is seen in the *hir* retina and NT. As actomyosin is a key regulator of cellular tension and is also involved in cell division (providing cortical contractility for rounding-up), this is a candidate for being affected in *hir*. Indeed cues rooted in the actomyosin cortex are suggested to orchestrate spindle orientation in various ways during mitotic division throughout the animal kingdom (reviewed in Sandquist *et al*., 2011). Very recent evidence from Nakajima, *et al*. (2013) shows that planar orientation of the mitotic spindle requires the interaction of the actomyosin cortex and Scrib with the mitotic apparatus, which contributes to the maintenance of epithelial architecture. Interestingly, Scrib is also important for oriented cell division in the zebrafish NT (Žigman *et al*., 2011), perhaps suggesting the mechanism orienting the spindle may be somewhat conserved between tissues/organs. It may therefore be possible that Scrib is important for oriented cell division in medaka but further work on this is required.

4.5.2 Mechanisms underlying the collapse phenotype observed in the neural tube of *hirame*

As development proceeds the wild type NT shows an increase in height and width of the organ. Conversely, the *hir* mutant exhibits a decrease in height and an increase in width, almost doubling in this dimension. In wild type, neuroepithelial (NE) cells divide mostly parallel to the ventricular zone and then stack on top of one another to facilitate a thickening of the NT. It appears widening is achieved through a combination of orthogonal division and some cell slipping. However, in *hir*, many cells stack briefly following division but then slip so that the daughter cells sit alongside one another. This leads to the formation of chains of NE cells and means the NT fails to thicken in the mutant. It may also cause the widening of the mutant NT. The cell behaviours observed in the wild type and *hir* NT are summarised in Figure 4.24. The direct cause of the cell slippage and the formation of chains of NE cells in the collapsing NT of *hir* remains to be conclusively elucidated. However, based on the results presented earlier in this chapter there are likely to be several contributors. The randomised division plane of the

mutant NE cells may mean cells cannot stack properly and directly slip after dividing at an aberrant angle relative to the ventricular zone. This could be confirmed by examining the behaviour of daughter cells in *hir* following divisions at various angles relative to the ventricle. This theory is somewhat supported by the fact that in wild type, NE cells divide mainly parallel to the ventricular zone thus meaning cell stacking may be facilitated by this orientation of division as this process directly stacks daughter cells. It is proposed that orthogonal division and a low frequency of cell slippage in wild type contributes to increase the NT width whereas cell stacking is the predominant driving force for increasing NT height. In *hir*, the increased cell slippage coupled with reduced cell stacking but a normal level of orthogonal division results predominantly in a widening and flattening of the NT (Figure 4.24).

The contribution of the randomised NE division angle in *hir* to the ultimate NT collapse could be tested by blocking cell division in the mutant NT and observing the resulting phenotype – i.e. whether the chains of NE cells still accumulate. Aphidicolin and hydroxyurea have been shown to inhibit cell division well in the NT (Tawk *et al*., 2007). However, it remains unknown whether blocking cell division may mean little to no growth occurs in the NT of *hir* and thus no collapse phenotype is observed. It may be possible to circumvent this side-affect by treating with the inhibitors only during the stages of collapse, perhaps to see if the collapse is less severe. If collapse and slippage was still observed in the absence of the aberrant cell division in *hir* then that may give rise to the possibility of a second contributing defect such as cell adhesion playing a more important role. Finally, the defective ECM surrounding the NT may be partially responsible for the collapse. The basal membrane surrounding the NT may be important for maintaining its shape where it could act like a structural scaffold. However, since blocking FN fibrillogenesis in wild type did not mimic the NT collapse seen in *hir*, it is likely that at least this ECM component is not involved in the manifestation of this aspect of the mutant phenotype.

Since crossing divisions (C-divisions) appear reduced in *hir*, and Pard3 has been shown to be an important determinant of the cleavage furrow of cells undergoing C-division (Tawk *et al*., 2007), this polarity protein may be mislocalised in *hir*. Tawk *et al*. (2007) have also shown that the division process itself is important for midline crossing as blocking cell division stopped the majority of neural plate cells undergoing C-division. However, since NE cell division does not appear that reduced in *hir*, this is a less likely cause of the lack of cell mixing or crossing divisions observed in the mutant. It remains to be seen whether there is a link between the regulation of these C-divisions and oriented cell division in the NT that contributes to the growth and shaping of this organ. A possible explanation for both the loss of oriented cell division and reduced C-divisions in the *hir* NT comes from the polarity protein Scrib. Scrib has been

shown to be required for oriented cell division and C-divisions in the zebrafish NT (Žigman *et al*., 2011). Moreover, Scrib regulates this oriented cell division, in part through a cadherin-based process (Žigman *et al*., 2011). If Scrib is affected in *hir*, this could also explain the cell slippage phenotype seen in the mutant NT, which resembles a cell-cell adhesion problem. Analysis of Scrib in the NT of *hir* may therefore prove important to narrow down the molecular mechanism underlying this interesting phenotype observed in the mutant NT.

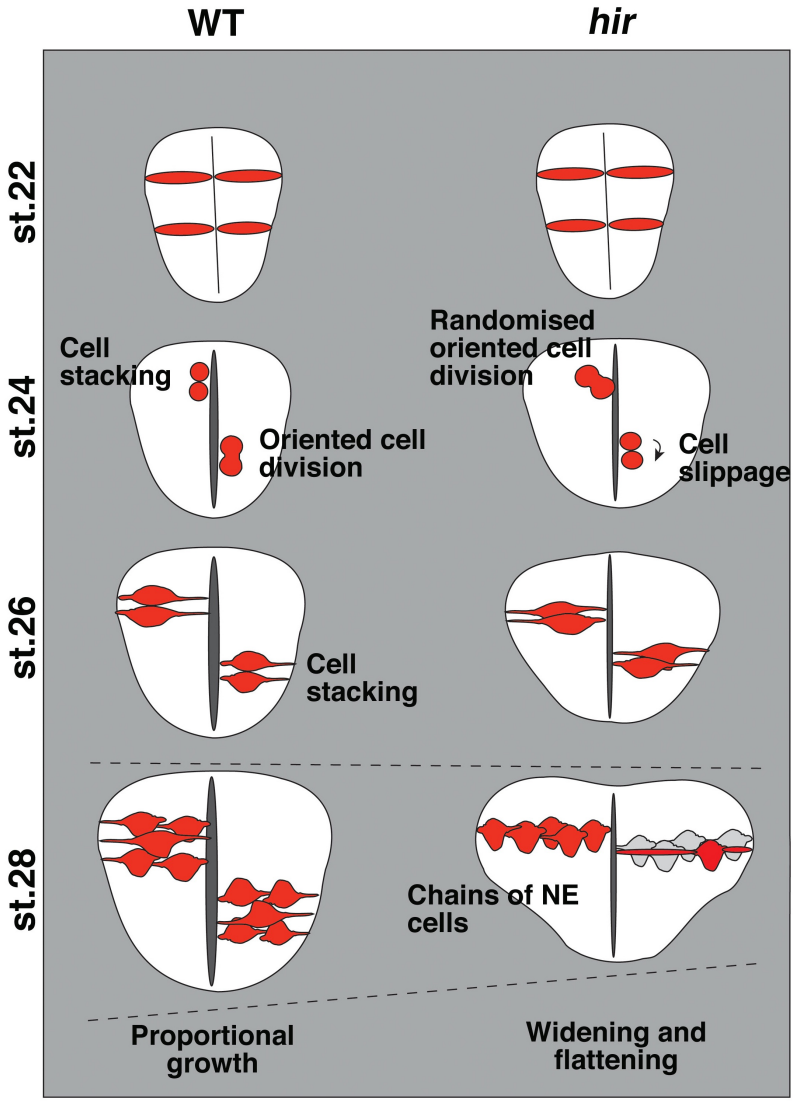

Figure 4.24. Schematic representing the cellular behaviours observed in the neural tube of wild type and *hirame*. In wild type, oriented cell division and cell stacking lead to a roughly proportional thickening and widening of the NT. In *hir,* randomised oriented cell division and cell slippage lead to a disproportionate widening and flattening of the NT. Chains of NE cells are a hallmark of the collapsed mutant NT. Despite chains of NE cells being observed in *hir*, cells still appeared attached at basal and apical ends by long processes (bottom right). NE: neuroepithelial.

4.5.3 Failure of placodes to remain apposed to adjacent tissues and undergo coordinated invagination in the eyes and ears of the *hirame* mutant

The eyes and ears also exhibit several specific phenotypes whereby the placodes of these organs are mislocated, multiple placodes/mature tissues are observed, and coordinated growth/morphogenesis does not occur. There may be several possibilities for why this happens in these organs.

4.5.3.1 Why are the sensory placodes mislocated in *hirame*?

In the case of the lens placode, it was observed that in *hir* this placode sometimes formed slightly variably in terms of position. Since the lens placode itself forms, it is unlikely that the genes responsible for its induction are not expressed, but rather in some cases they may be expressed somewhat ectopically. Interestingly, ectopic expression of *Sox3* causes ectopic expression of *Pax6* and *Eya1*, which are required for development of the lens placode (along with other sensory placodes, Köster *et al*., 2000). Ectopic *Sox3*/*Pax6*/*Eya1* expressions in medaka subsequently led to lens vesicles that were found in the lateral and ventral head ectoderm (Köster *et al*., 2000). Performing *in situ* hybridisation for the early induction gene *Sox3* revealed expression was not ectopic in *hir*, suggesting the cause of the dislocated lens placode in the mutant was attributable to something else. However, *Pax6* and *Eya1* expression has not yet been analysed in the *hir* mutant at this early stage of eye development so may warrant further investigation.

The filopodia necessary to physically tether the developing lens in the optic cup (Chauhan *et al*., 2009) were aberrant in *hir*. These filopodia are important for ensuring the presumptive lens invaginates into the developing retina in a coordinated manner, something never seen in *hir*. These dynamic F-actin rich protrusions form from E9.5-10.5 in the mouse eye and originate from the epithelial cells of the presumptive lens at E10.5, but some filopodia may also have retinal origins earlier in development at E9.5 (Chauhan *et al*., 2009). In the *hir* mutant, these filopodia were observed after the lens placode had dislocated, but on the side of the lens placode facing away from the optic cup. Few filopodia were observed to extend from the retina in *hir* in agreement with Chauhan *et al*. (2009). The results presented above suggest the cells of the *hir* lens are able to produce filopodia, but for some reason may have lost the cue or ability for where and when to produce them. There may be several explanations for why the dislocated mutant lens extends these aberrant protrusions. One may be that the dislocated lens is searching for the retina since cells frequently use filopodia as a means of probing their environment (first described in 1976 by Albrecht-Buehler). However, it might be expected to observe filopodia around the circumference of the lens in this scenario, which is not seen in *hir*. Another possibility is that the mutant lens has lost its apico-basal polarity. If this were the case the protrusions may again be

expected to form randomly around the lens. However, experimental data argues against this since filopodia in *hir* were never observed to form from the edge of the dislocated lens facing the retina – they were specifically localised to the face opposite the presumptive retina. Finally, it may be that through the dislocation process the orientation of the entire lens has somehow changed in *hir*, such that the apical and basal sides have been flipped and this is why extensions are observed on the wrong side of the lens.

There could also be several reasons at the molecular level for why these filopodia in the mutant eye are aberrant. As shown by Chauhan *et al*. (2009) the formation of filopodia between the lens and retina is dependent on Cdc42-signalling. Since Cdc42 has been proposed to regulate cell polarity (Etienne-Manneville, 2004) and general filopodia formation, both of which appear affected in *hir*, this Rho family GTPase may be disrupted in the mutant eye. It may be possible to test this using FRET for Cdc42 in the eye as recently shown by Matthews *et al*. (2008). Interestingly, mouse mutants of Cdc42 exhibited reduced numbers of filopodia (Chauhan *et al*. 2009), quantification of which needs to be performed in the *hir* mutant eye. This is important since reduced numbers of filopodia in the mouse eye resulted in the presumptive lens being further away from the retina, a feature that is seen in *hir*. It is therefore possible that the mutant has not only aberrantly located filopodia, but also reduced numbers of the protrusions. This is furthermore noteworthy as it is the opposite phenotype of that seen in the endothelial cells of the mutant CDs where increased numbers of filopodia are visualised.

In migrating Dictyostelium and fish fibroblast cells, the formation of cellular extensions are dependent on activated actomyosin signalling (Iwadate and Yumura, 2008; Nemethova *et al*., 2008). Since actomyosin is involved in regulating cellular and thus tissue tension, which appears reduced in *hir*, reduced actomyosin activity could partly explain the filopodia defect in the mutant eye, since reduction of myosin activity in the eye in mice caused a reduced number of filopodia (Chauhan *et al*., 2009). So if tissue tension in *hir* is reduced through actomyosin activity, and the number of filopodia extended from the mutant lens is indeed reduced, this might explain the reduced number of filopodia in the eye but not the CD. It is therefore possible that different mechanisms regulate filopodia production in these different tissues/organs. A final molecular consideration for why filopodia are affected is fibronectin (FN). As shown by immunohistochemistry, FN fibrillogenesis surrounding and on the eye appears defective in *hir*. A tension reduction could cause this FN assembly defect (Mao and Schwarzbauer, 2005) in turn affecting FN-integrin signalling resulting in aberrant filopodia. FN knockdown in *Xenopus* causes an excess of actin-rich cellular protrusions (Davidson *et al*., 2006). Quantification of filopodia number in the eye is therefore

necessary to ascertain whether there are differences between wild type and *hir* such that meaningful conclusions can be reached.

In zebrafish, hindbrain signals have been shown to be involved in induction of the otic placode, as well as both antero-posterior and dorso-ventral patterning of the ear (Lecaudey *et al*., 2007). However, less seems known about how the otic vesicle and hindbrain are physically attached. It remains to be seen whether filopodia exist between the otic vesicle and hindbrain, where a similar process of coordinated invagination occurs as in the eye. However, since the placode phenotype between the eye and ear is similar in certain aspects, it is tempting to speculate that these filopodia are a conserved feature of coordinated growth between organs comprised of multiple tissues throughout vertebrates. If this is the case then this filopodia regulation may also be disrupted in the ear as discussed above for the eye. There could of course be a different mechanism of adhesion that is affected, for example via E- or N-cadherin, which have been shown to be important in multiple morphogenetic events (Gumbiner, 2005).

4.5.3.2 How do multiple placodes form in the mutant, giving rise to the multiple lenses and ears seen later in development?

In the eyes and ears of *hir*, multiple placodes are seen based on MNFP time-lapse data. It is not yet clear how these multiple placodes arise in the ear. Whether multiple placodes form early in development during induction, or whether an existing placode fragments to give several portions of placode remains to be definitively elucidated. However, observations of eye formation, in particular analysis of lens placode morphology suggest fragmentation as the cause in the eye. In the case of the eye these multiple fragments/placodes sometimes re-join later in development before rounding up and loosely re-joining the retina. Further evidence for fragmentation of the original placode in the eye comes from the fact that the mutant lens often appears smaller than the wild type lens. This may be the result when multiple fragments do not coalesce. This is supported by the fact that when this occurs, multiple smaller lenses are observed in *hir*.

In the case of the original placode fragmenting, this could be caused by an adhesion problem between cells of the mutant placode. This raises several interesting questions. For example, if the placode does fragment into several pieces, why do the adhesions between cells at these breaking points fail, but not between the other cells of the placode? How could this adhesion be affected so specifically? Furthermore why do these fragments then sometimes re-join? Since an adhesion defect would likely be more general between all cells of the placode, fragmentation is difficult to explain. It may be possible that the affected placode morphology can partially explain fragmentation. Normally the lens placode forms in close apposition to the presumptive

retina. In *hir*, the placode appears elongated with large portions of the placode seemingly unattached or out of apposition with the retina. Perhaps the placode fragments at these points where the retina and placode lose contact. What could be the mechanism underlying how the fragments re-join as development proceeds? Later in development these lens fragments were observed to extend filopodia as if 'searching' for other placode fragments or the retina (Supplementary movie 8). In someways this in agreement with what was seen earlier in development when the lens placode may have extended filopodia whilst searching for the retina. However, there were cases where the fragments did not re-join leading to multiple lenses. It remains to be seen why fragments in these cases could not amalgamate.

For the emergence of the multiple ears in *hir* less is known, as this area of the project could not be fully explored due to time constraints. What appeared to be multiple ears were observed during confocal time-lapse imaging of the mutant phenotype. However, it remains unclear whether they arise from multiple placodes or fragmenting placodes and indeed whether they are of ear lineage. The collective volume/cell number of the multiple placodes/ears in *hir* could be compared to the ear in wild type to gain further insights. Again *in situ* for induction genes such as *Dlx3*, *Eya1* and *Pax2*/*5*/*8* should be performed to understand what is happening. Misexpression of *fgf3* and *fgf8* has been shown to cause ectopic otic vesicles and multiple otic vesicles respectively (Bajoghli *et al*., 2004; Phillips *et al*., 2004), but it is not known if *fgf3* and *fgf8* are affected in *hir*. Since Fgfs can regulate *Spalt4*, which if misexpressed can also cause the formation of multiple ectopic otic placodes and defects in otic vesicle formation (Barembaum and Bronner-Fraser, 2007), this could be a mechanism by which ear development is affected through FGF signalling in *hir*. As described above, the cavity or lumen formation in the mutant ear was sometimes delayed. This could be a direct result of the placode being slow to pinch off from the overlying ectoderm. This could also be a consequence of aberrance in the aforementioned induction genes. Thus this is an area of the mutant phenotype that requires further work and highlights the interesting nature of the *hir* mutant for studying tissue induction and coordinated morphogenesis.

4.5.3.3 Lack of coordinated growth in the eyes and ears of *hirame*

Whilst the multiple tissues comprising several of the mutant organs appear to form at the correct developmental time, they do not develop in a coordinated manner. In wild type, both the eyes and ears undergo coordinated morphogenesis such that the presumptive lens invaginates into the retina as it basally constricts to form the optic cup in the eye. And in the formation of the ears the otic vesicle invaginates into the hindbrain. In *hir*, these morphogenetic processes fail such that the lens placode and otic vesicle dislocate from their apposing tissue and instead develop ectopically. In the mutant eye a possible explanation for this is the failure of filopodia to form between the

retina and lens that physically tether the two tissues together. In the eye the filopodia that tether the lens to the retina predominantly emanate from the presumptive lens (Chauhan *et al*., 2009). It may be possible that these filopodia act as a cue to initiate basal constriction of the retina to form the optic cup. This is supported by the fact that in *hir* the optic cup never emerges. Interestingly, a recent report from Martinez-Morales *et al*. (2009) details a mutant called *ojoplano* (*opo*) where this basal constriction is also affected. In this mutant, tension of the retinal cells also appears reduced. *Opo* appears important for recruiting integrin-β1 and paxillin to zones of nuclear exclusion (ZNE), which are located where the retinal progenitor cells attach to the basal lamina of the retina. Perhaps signalling from the filopodia is responsible for the localisation of *opo* to the ZNE, without which basal constriction and optic cup formation does not occur. Moreover, this is an interesting possibility since integrin-β1 appears reduced in the *hir* eye. Another possibility is that the reduced tension of cells in the retina, perhaps due to affected actomyosin, means cells cannot constrict. This is plausible since actomyosin is known to be involved in the cell constriction that takes place in other processes in the body (Antunes *et al*., 2013).

An interesting feature of the mutant eye is that later in development, the dislocated lens rounds up, as is seen in wild type. Unexpectedly it was also observed that in several cases this rounded-up lens then moved back towards the retina where it appeared to form a weak association. What could be the explanation for this? These rounded *hir* lenses appeared to generate protrusions during the migration towards the retina, suggesting a probing of the environment for the correct neighbouring tissue. This phenotype is however, difficult to interpret and explain. This is because FN fibrillogenesis is defective in and around the mutant eye. This FN assembly defect in the mutant CDs may be the cause of the endothelial cell migration defect. However, some endothelial cells do still migrate to some extent, as seen in the *hir* primary stream. Since the distance the rounded lens travels does not seem that great (approximately in the order of tens of microns), perhaps the mutant neuroepithelial cells of the lens are still able to adhere to and migrate small distances on the aberrant FN substrate to drag the lens back to the retina. This may also account for how the multiple fragments of placode migrate back towards one another before re-joining.

Another possibility for the mutant lens rounding-up may be that formation of the lens capsule, a basement membrane composed of collagen, laminin and FN, as well as many other proteins that completely surrounds the lens, is slow to occur due to defective fibrillogenesis in *hir*. This lens capsule is normally formed during formation of the lens vesicle during invagination of the lens (Danysh and Duncan, 2009). If lens capsule formation is delayed in the mutant, perhaps due to FN defects which may have knock-on effects for downstream ECM component assembly, this may explain why

rounding-up of the lens is seen later in development. Interestingly, the lens capsule also plays a biomechanical role for maintaining lens shape (Danysh and Duncan, 2009), further supporting the theory that its development may be delayed in *hir* as the mutant lens appears more normally shaped later in development, despite apparent cellular tension reduction as evidenced by rounder nuclear shape. These interesting characteristics of the mutant lens appear unique and as such they warrant further investigation.

Finally, the underlying cause of the tissue mislocation in the ear remains to be elucidated, but the similarity in phenotype between the eyes and ears suggests a conserved mechanism could be responsible. The ear phenotype of *hir* requires more detailed analysis.

4.6 Summary

- Multiple tissues/organs collapse (e.g. retinas and NT) and/or are mislocated (e.g. lenses and ears) in the *hir* mutant
- Nuclei of the cells within collapsing epithelial tissues are rounder in morphology in *hir* as compared to wild type
- Oriented cell division is also affected in the eyes, NT and ears of *hir*
- These results suggest that tissue tension may be reduced in *hir* in these affected tissues/organs

Chapter 5: YAP controls tissue tension via regulating actomyosin activity

5.1 Aims

The *hir* mutant phenotype exhibits several characteristics of decreased tissue tension as outlined in previous chapters. This chapter addresses whether tissue tension is indeed reduced in YAP mutants. To this end, earlier stages in development (gastrulation) were studied to allow more definitive conclusions to be drawn about a role for YAP in tension regulation. The cell shape in the epithelial enveloping layer (EVL) of gastrulating embryos was analysed as a readout of tissue tension and direct physical measurements of tension were also executed. Since the actomyosin network is a major factor determining cellular and thus tissue tension, actomyosin activity was examined. Using laser ablation experiments the cortical tension of the actomyosin ring involved in epiboly cell movements was ascertained. Furthermore, the localisation of actin and myosin within YAP knockdown transgenic embryos was investigated using time-lapse imaging.

5.2 Introduction

Early in development a number of coordinated cell movements take place to establish the body plan of the adult organism. These regulated movements are known as gastrulation and organise the three germ layers (endoderm, mesoderm and ectoderm) and establish the body axes (Lepage and Bruce, 2010). The very early stages of development in medaka and zebrafish are controlled by maternal factors present in the egg, which include mRNA and proteins provided by the mother during oogenesis that become incorporated in the egg during its formation (Wolpert and Tickle, 2011, p.129). These maternal factors are essential for early development since most of the embryos own genes do not start being transcribed until after the mid-blastula stage/transition (approximately 8 hpf in medaka and 2.75 hpf in zebrafish) (Wolpert and Tickle, 2011, p. 129).

In the fertilised zebrafish egg, maternal factors are located along the animal-vegetal axis, with key factors for axis specification present in the vegetal zone (Wolpert and Tickle, 2010, p.130). Localisation of these maternal factors occurs in two ways. Firstly, during early oogenesis, some mRNAs are positioned in the presumptive vegetal cortex via transport involving the message transport organiser region (METRO), which is a region of the oocyte cytoplasm where mitochondria are being generated (Wolpert and Tickle, 2011, p.130). Details of mRNA transport by the METRO system are still emerging but may involve the cytoskeleton and endoplasmic reticulum (Wolpert and Tickle, 2011, p.130). Secondly, at later stages in oogenesis various mRNAs are transported vegetally by kinesin motor proteins along microtubules (Wolpert and Tickle, 2011, p.130). Therefore, maternal factors are important for specifying early embryonic structures such as the enveloping layer (EVL).

5.2.1 Gastrulation in medaka and zebrafish embryos

Whilst overall there are similarities between gastrulation in medaka and zebrafish, zebrafish development occurs much more quickly and there are also specific differences at certain stages of the process. For this reason, the two species will be briefly discussed separately here for clarity, since data pertaining to gastrulation in both teleosts is presented. In general, both gastrulation processes involve the deep cells that will give rise to the embryo, the layer directly under the deep cells – the yolk syncytial layer (YSL), and the EVL overlying the deep cells, spreading over the yolk in a process known as epiboly (Figure 5.1b). Epiboly has been found to occur in many species (Kane and Adams, 2002). Many of the components involved in epiboly have been identified, including the cytoskeleton (microtubules and microfilaments), cell adhesion proteins (e.g. Cdh1, EpCAM and CldnE), scaffold proteins (e.g. Amotl2 and Diaph2), kinases (including Yes) as well as calcium signalling and other various factors (summarised in Lepage and Bruce, 2010). However, it remains to be determined to what extent the cellular and molecular mechanisms driving this important process are evolutionarily conserved (Lepage and Bruce, 2010).

5.2.1.1 Formation of the enveloping layer and yolk syncytial layer

Whilst at early stages the developing teleost embryo resembles a mass of cells sitting on top of a yolk, there is more organisation when observed closely. Prior to epiboly onset the embryo is organised as three layers – the EVL, the deep cells and the YSL (Figure 5.1a). The EVL and deep cells together make up the blastoderm. Only a couple of hours after fertilisation of the zebrafish oocyte, distinct organisation can be seen arising in the developing embryo in the form of an outer layer of cells covering the deeper layers of cells. These outer cells are derived during the cleavage stages of the blastodisc, just before the onset of the blastula period and form an overlying layer, called the EVL, over the deep cells that contacts the yolk at the blastodisc margin (Kimmel *et al*., 1995). The EVL remains as the outermost layer during gastrulation in medaka and zebrafish embryos and is analogous to the epidermis in other vertebrates such as *Xenopus* (Sagerström *et al*., 2005). As such the EVL can be classified as a squamous epithelial monolayer that acts as a permeability barrier to allow survival in a hypotonic external environment (Fukazawa *et al*., 2010). Specification of the EVL has been shown to require close contact of cells as dissociation of the EVL diminishes *cyt1* expression, an EVL-specific marker (Sagerström *et al*., 2005). Specification also requires the maternal gene *poky* in EVL cells prior to their establishment, as *poky* mutants exhibit EVL differentiation failure (Fukazawa *et al*., 2010). Interestingly it was recently shown that the EVL persists into larval stages in zebrafish (Fukazawa *et al*., 2010) whereas previously it was thought to be a more transient structure (Kimmel *et al*., 1995).

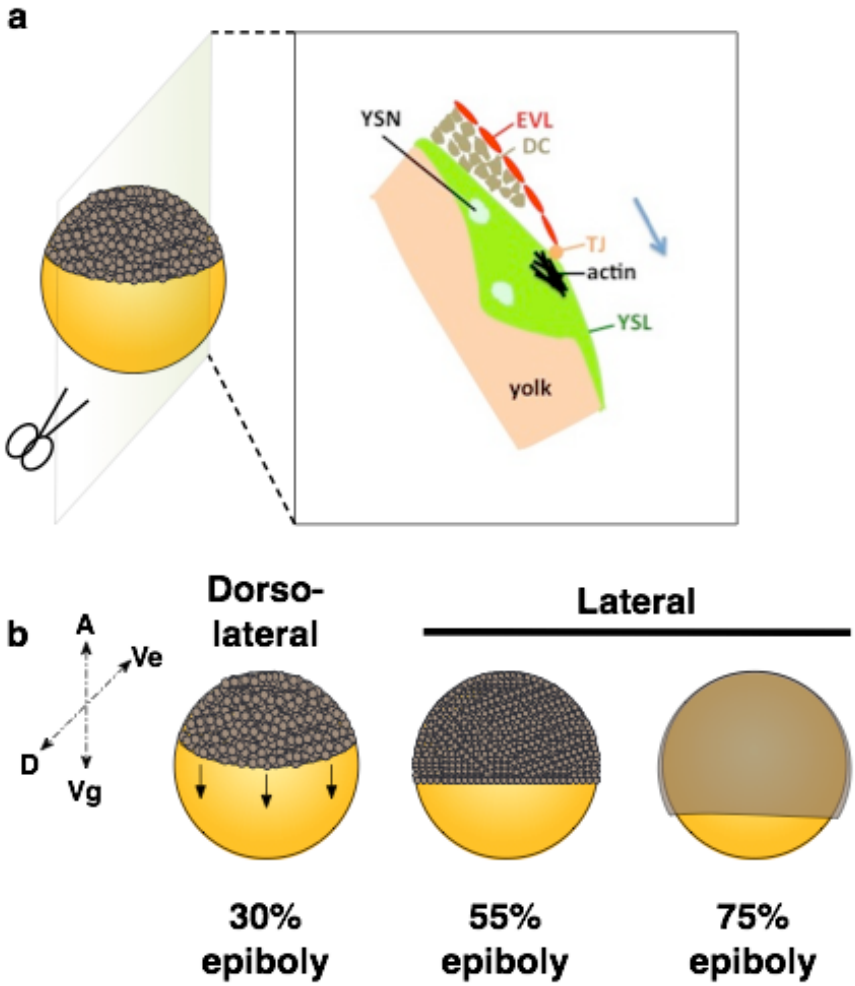

Figure 5.1. General organisation of developing zebrafish and medaka embryos during epiboly. (a) A cross-section through the developing teleost embryo showing the organisation of the blastoderm. EVL: enveloping layer; DC: deep cells; TJ: tight junction; YSN: yolk syncytial nuclei; YSL: yolk syncytial layer. Together the EVL and DC are classed as the blastoderm. Blue arrow indicates the direction of movement of the blastoderm and YSL during epiboly. **(b)** Schematic representations of various time-points during the process of epiboly during gastrulation.

After 2.75 hours of development in the zebrafish the YSL forms to give the roughly three-layered structure depicted in Figure 5.1a. The YSL is an extra-embryonic syncytium that lies at the interface between the yolk and the deep cells (Lepage and Bruce, 2010). YSL formation occurs when cells at the margin of the blastodisc collapse and lose their lower boundary fusing with the underlying yolk cell. During this collapse the nuclei of the marginal cells move into the syncytium. A similar process occurs to generate the YSL in medaka embryos though not until 6.5 hpf, when nuclei of the marginal cells migrate outwards into the periblast (Iwamatsu, 2004). These nuclei first form a wide belt around the periphery of the blastoderm margin known as the external

YSL (E-YSL) and later also locate beneath the blastoderm, giving rise to the internal YSL (I-YSL, Lepage and Bruce, 2010). The I-YSL is more involved in convergence extension movements and the E-YSL in epiboly (Carvalho and Heisenberg, 2010). Thus, when formed the YSL is a relatively thin cytoplasmic layer housing the yolk syncytial nuclei (YSN, Solnica-Krezel and Driever, 1994). Once the YSL has formed the EVL becomes tightly attached to it via tight junctions (Figure 5.1a) and this is key for EVL epiboly since this occurs independently of deep cell epiboly (Kane *et al*., 1996). Since the EVL, deep cells and YSL all undergo epiboly, it is important to define which is being referred to. Therefore, in the remainder of this chapter, when the term 'epiboly' is used this refers to the leading margin of the deep cells. To designate the extent of epiboly of the EVL, 'EVL epiboly' will be used.

At earlier stages of epiboly, around 30%, the leading edge of the EVL matches well with the margin of the underlying deep cells (Köppen *et al*., 2006). However, as epiboy proceeds, a gap opens up between the two leading edges. By 75% epiboly this EVL-deep cell gap is clear (Köppen *et al*., 2006). Thus epiboly in medaka and zebrafish can serve as a tool to study: the migration of single or small groups of cells (deep cells); how an epithelial sheet spreads (EVL); as well as the movement of a syncytium in the case of the YSL (Lepage and Bruce, 2010).

5.2.1.2 Medaka gastrulation

In the descriptions that follow, epiboly refers to the position of the margin of the deep cells. Gastrulation starts at around 10 hpf with the pre-early gastrula stage (st.12). At this point the blastoderm has flattened on the yolk and there is a thickening of cells on one side (which will give rise to the dorsal lip, akin to the shield in zebrafish, see Section 5.2.1.3) (Iwamatsu, 2004). By 13 hpf the early gastrula stage is reached (st. 13). The blastoderm begins epiboly over the yolk (coverage at this point is about 25%) and the dorsal lip is now clearly visible (Iwamatsu, 2004). At st.14 (15 hpf) in the pre-mid gastrula stage epiboly is now at about 33% and the germ ring is well defined with the embryonic shield increasing in size (Iwamatsu, 2004). 2.5 hours later at st.15 (17.5 hpf, mid gastrula stage), epiboly has reached 50% and a primitive streak becomes visible at the midline of the embryonic shield that projects into the germ ring area (Iwamatsu, 2004). By the last stage of gastrulation (st.16), the late gastrula stage (21 hpf), the blastoderm covers 75% of the yolk and the embryonic body is now clearly visible as a narrow streak. Until this stage the EVL expands uniformly over the yolk (Iwamatsu, 2004). Epiboly does not finish until st.19 (27.5 hpf) in medaka when neurulation is complete and the embryo has two somites (Iwamatsu, 2004). The rate of advancement of the margin of the blastoderm is constant at fixed temperatures and interestingly cell division occurs in the deep cells during epiboly but not in the EVL (Kageyama, 1980). This likely explains the morphology of cells in the EVL, which are

large, hexagonal and flat due to stretching over the yolk, whilst cells of the blastoderm are much smaller (Kageyama, 1980). After 75% EVL epiboly, the cells of the leading edge or margin of the EVL begin to lose their hexagonal shape, becoming elongated longitudinally in the animal-vegetal axis (Kageyama, 1980). Medaka gastrulation is summarised in Figure 5.2.

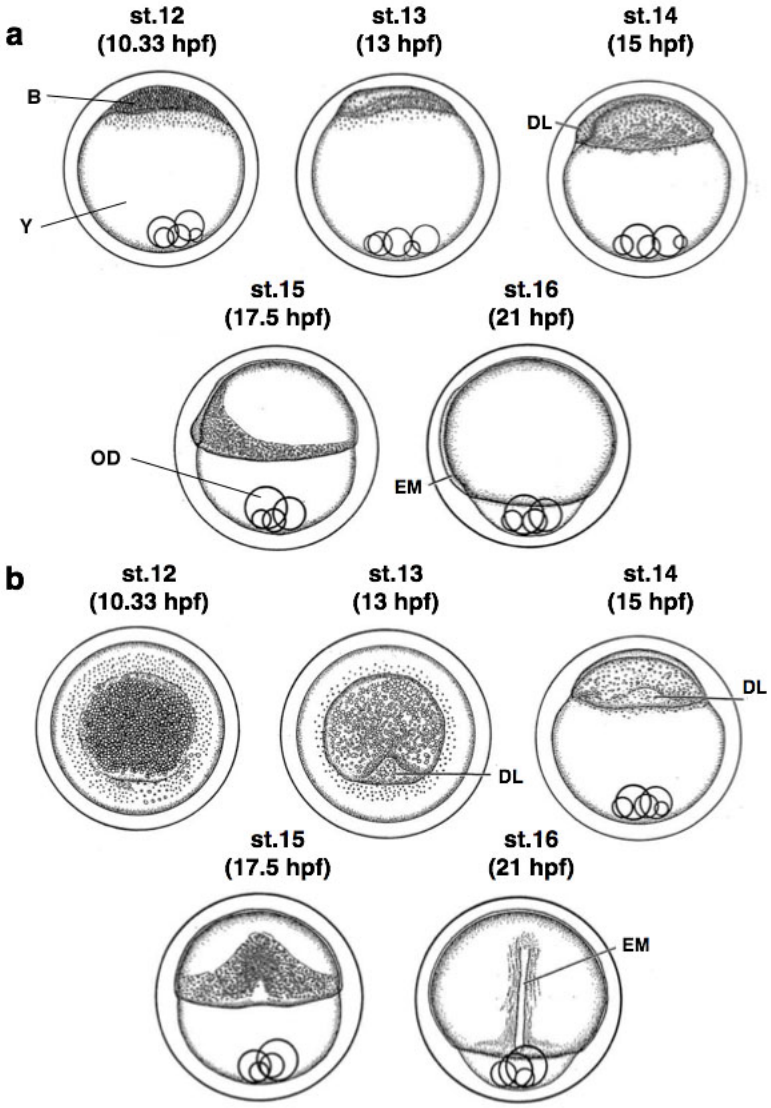

Figure 5.2. Schematic of gastrulation in medaka. (a) Lateral views of the embryo during gastrulation depicting how the blastoderm spreads over the yolk. **(b)** Animal pole views (st. 12-13) followed by dorsal views over the same time-points shown in (a). B: blastoderm; Y: yolk; DL: dorsal lip; OD: oil droplets; EM: embryo. Adapted from Iwamatsu (2004).

5.2.1.3 Zebrafish gastrulation

Again, in the descriptions that follow, epiboly refers to the position of the margin of the deep cells. In zebrafish, gastrulation has been well characterised by Kimmel *et al*. (1995). Embryos have reached 30% epiboly by the end of the blastula stage (4.66 hpf) when a blastoderm of almost uniform thickness forms. Again this blastoderm consists of deep cells (about 4 layers in depth) and an EVL. By 5.25 hpf, epiboly has reached 50% and the blastoderm is very uniform in thickness due to radial intercalation of the deep cells. The germ-ring stage is reached at 5.66 hpf during which the blastoderm margin thickens circumferentially. In this germ ring the deep cells consist of two layers, an outer epiblast layer about 3 cells thick and an inner layer called the hypoblast, which is also 2-3 cells thick. By 6 hpf embryos enter the shield stage that is demarcated by a local thickening of the epiblast and hypoblast on one side of the blastoderm (similar to the dorsal lip described above) that is easily visible from the animal pole view. Epiboly has stalled at this point through the germ ring to late shield stage whilst convergence and extension (CE) movements begin.

At 8 hpf epiboly has reached 75% and the shield is now less pronounced due to elongation in the antero-posterior axis. Furthermore the blastoderm is no longer uniformly thick. 90% epiboly is seen one hour later at 9 hpf when a prominent yolk plug can be identified (yolk cell protruding at vegetal pole). The dorsal side of the blastoderm is distinctly thicker than the ventral side and furthermore the dorsal epiblast thickens in an anterior manner to give rise to the neural plate. The bud stage is achieved by 10 hpf (contrasting with medaka, which at this time point are now about to enter gastrulation) whereby epiboly is complete. The tail bud emerges 10-15 minutes after closure as a swelling of the embryonic axis at the posterior end of the embryonic axis. The neural plate is thickened along the length of the embryonic axis from anterior to posterior. Whilst the gastrulation period in zebrafish is defined as being finished by the tailbud stage, this is not strictly the case since gastrulation movements still occur within the tailbud (Kimmel *at al*., 1995). As in medaka, it is not thought that the EVL cells divide during gastrulation. Zebrafish gastrulation is summarised in Figure 5.3.

During the genome-wide screen in zebrafish, several interesting epiboly mutants were identified. In particular, four mutations (*half baked*, *avalanche*, *lawine* and *weg*) were found that when homozygous, arrested epiboly of the deep cells but not that of the EVL or YSL (Kane *et al*., 1996). Interestingly, heterozygous mutants displayed a variety of phenotypes including slowed epiboly and detachment of cells dorsal to the neural tube when produced from heterozygous females crossed with homozygous wild type males, highlighting the importance of maternal zygotic genes in early development (Kane *et al*., 1996).

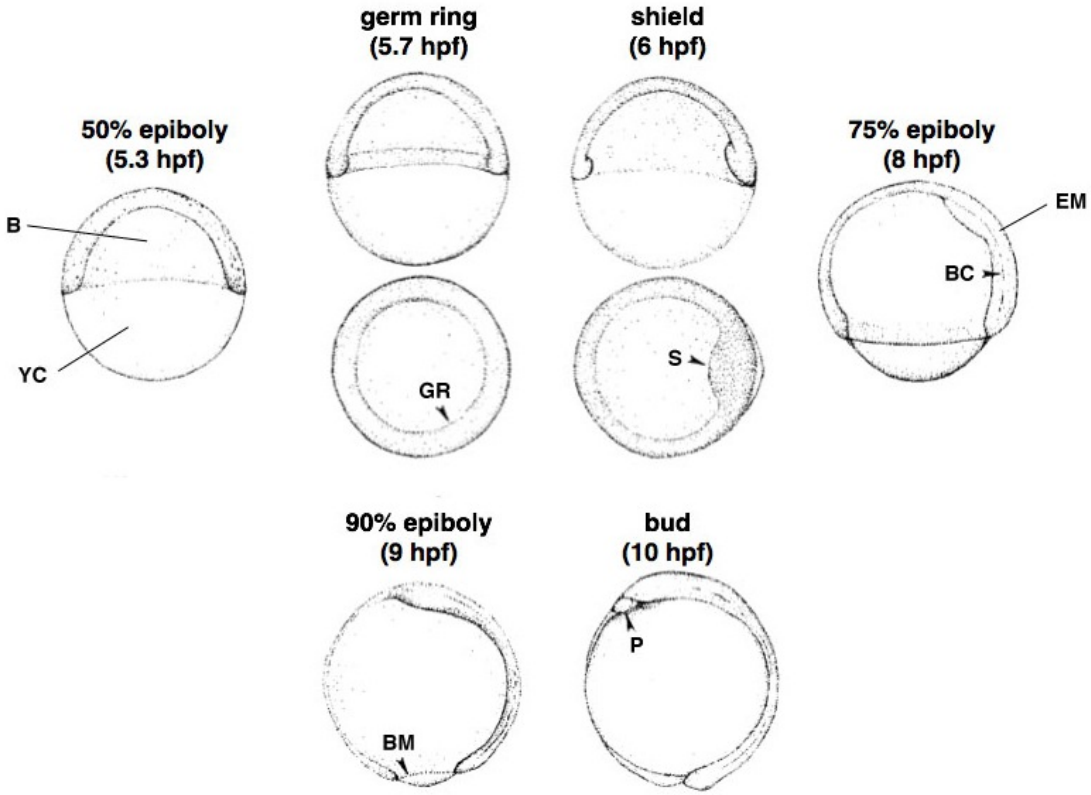

Figure 5.3. Schematic of gastrulation in zebrafish. Lateral views to show the spreading of the blastoderm over the yolk and the establishment of the embryonic axis. Germ ring and shield stage are also shown with animal pole views below the lateral views. Prominent features present during gastrulation that are used for staging embryos are included. Note how much faster gastrulation proceeds in zebrafish. B: blastoderm; YC: yolk cell; GR: germ ring; S: shield; BC: Brachet's cleft (the visible division between the epiblast and hypoblast cells); EM: embryo; BM: blastoderm margin; P: polster (hatching gland primordia). Adapted from Kimmel *et al*. (1995).

5.2.2 The importance of physical forces in sculpting the vertebrate embryo

Compared to the genetic and molecular mechanisms regulating embryonic development, less is known about the role of physical/mechanical forces (Mammoto and Ingber, 2010). However, mechanical forces have long been thought to play an important role in morphogenesis. In 1917 D'Arcy Thomson published his classical treatise *On Growth and Form* in which he suggested patterns in development could be explained by forces and motion (Mammoto and Ingber, 2010). Some of the mechanical forces acting during development include shear stress (e.g. in the circulatory system), surface tension, osmotic pressure and spring forces (Mammoto and Ingber, 2010). Within living tissues, tension changes occur when for example cells are added or removed, or when cells migrate (Heisenberg and Bellaïche, 2013). In this context cell-cell contacts and cell-ECM contacts are subject to forces and must respond

appropriately when such forces arise. Coordination of these forces via mechanotransduction and mechanosensing can lead to tissue shape changes if transmitted over long ranges (Heisenberg and Bellaïche, 2013). But how do the constituent cells of the tissue interpret these forces and convert them into meaningful responses? This is an important question and one that requires answering as it is still not well known how physical cues activate signalling and genetic responses within cells (Halder *et al*., 2012).

Mechanical forces have been shown to be important influencers of certain cellular processes such as oriented cell division (Mammoto and Ingber, 2010) and rearrangement of the actin cytoskeleton (Heisenberg and Bellaïche, 2013). The mechanical microenvironment has now also been shown to play a role for cell fate/ differentiation and migration (Mammoto and Ingber, 2010). Thus it is becoming more apparent that physical forces play a very important part during development. Consequently further study of their roles is necessary for a complete picture of embryogenesis. Recently there has been renewed interest in this field due to advancements in imaging and analysis tools that allow quantification of these forces and the dynamic changes they cause at the cellular and tissue level (Heisenberg and Bellaïche, 2013).

Recent work has proposed that YAP/TAZ have mechanotransduction properties (DuPont *et al*., 2011; Wada *et al*., 2011). These reports have shown that an ECM high in stiffness and/or cell spreading increases cortical tension and promotes stress fibre formation (composed of contractile actomyosin bundles, Tojkander *et al*., 2012). This in turn causes nuclear translocation of YAP/TAZ. It does however, remain to be seen what the mechanistic relationship is between stress fibre formation and nuclear accumulation of YAP/TAZ. Despite this, *in vivo* support for the interaction between actin-related mechanical forces and YAP/TAZ activity comes from *Drosophila* where filamentous actin (F-actin) accumulation can negatively modulate the Hippo pathway promoting cell proliferation and tissue growth via Yorkie, the *Drosophila* homologue of YAP (Sansores-Garcia *et al*., 2011; Fernández *et al*., 2011). How F-actin regulates YAP/TAZ activity via Hippo signalling requires further characterisation as this may provide important clues about whether the contractile machinery of the cell regulates YAP/TAZ-mediated cell behaviour in response to mechanical cues (Heisenberg and Bellaïche, 2013). This could provide important information regarding how mechanical inputs are converted into biological outputs such as proliferation and growth.

5.2.3 How is cellular/tissue tension regulated?

The cortical actomyosin network is a well-established key regulator of tension within the cell (Levayer and Lecuit, 2012). Using actomyosin contractility cells can deform

without any external stress applied but actomyosin also plays a role in governing the cells response to an external stress (Levayer and Lecuit, 2012). Because of these properties the actomyosin network is described as self-organising and it can exhibit different properties spatiotemporally (Levayer and Lecuit, 2012). The contractility of actomyosin comes from the structure of the network in which the interaction of many actin filaments, non-muscle myosin II (NMII) motors and crosslinkers occurs (Vicente-Manzanares *et al*., 2009). In this configuration the myosin motor proteins can walk along, cause sliding of, or apply tension on actin filaments via ATP hydrolysis at sites found in the head region of myosin (Vicente-Manzanares *et al*., 2009). NMII molecules are composed of three peptide pairs: two heavy chains, two regulatory light chains (RLCs) and two essential light chains (ELCs). The RLCs regulate NMII activity and the two ELCs stabilise the heavy chains (Vicente-Manzanares *et al*., 2009). Phosphorylation (activation) of the RLCs at Serine 19 causes unfolding of the molecule into a form that allows the assembly of bipolar NMII filaments (Scholey *et al*., 1980, Figure 5.4). Kinases implicated in this process include the Rho-associated, coiled coil-containing kinase (ROCK). The RLCs can also be diphosphorylated if also phosphorylated at Threonine 18 and this diphosphorylation significantly increases activity and stability of NMII versus monophosphorylation (Watanabe et al., 2007). Bipolar NMII filaments bind to actin through their head domains meaning they can move actin filaments in an anti-parallel manner to apply contractile forces (Vicente-Manzanares *et al*., 2009, Figure 5.4).

To permit the contractile function of the actomyosin network the assembly of actin is also important. Actin is either polymerised into dendritic networks by Arp2/3 or unbranched networks regulated by formins (Levayer and Lecuit, 2012). During migration lamellapodia are Arp2/3-dependent and filopodia are formin-dependent. Unbranched networks are more easily remodelled by NMII that alters contractility through the reorganisation of the network and subsequent recruitment of further NMII. Dendritic networks are stiffer due to crosslinks and therefore require severing or unbranching to be remodelled (Levayer and Lecuit, 2012). In order to build up high tension, formin-controlled polymerisation is necessary since this results in more stable recruitment of NMII (Levayer and Lecuit, 2012). Contractile actomyosin networks have been shown to drive many important biological processes such as dorsal closure in *Drosophila* (Martin and Wood, 2002), epithelial wound closure (Wood *et al*., 2002), cytokinesis (Barr and Gruneberg, 2007), cell shape changes during morphogenesis (Sawyer *et al*., 2010) and ventral enclosure in *Caenorhabditis elegans* (Williams-Masson *et al*., 1997). These processes involve factors such as polarisation, migration and adhesion amongst others and so actomyosin is involved in many essential functions within various organisms. The role of NMII driven processes have been

shown to be important for the three-dimensional organisation of epithelial tissues in both *Xenopus* and *Drosophila* (reviewed in Vicente-Manzanares *et al*., 2009).

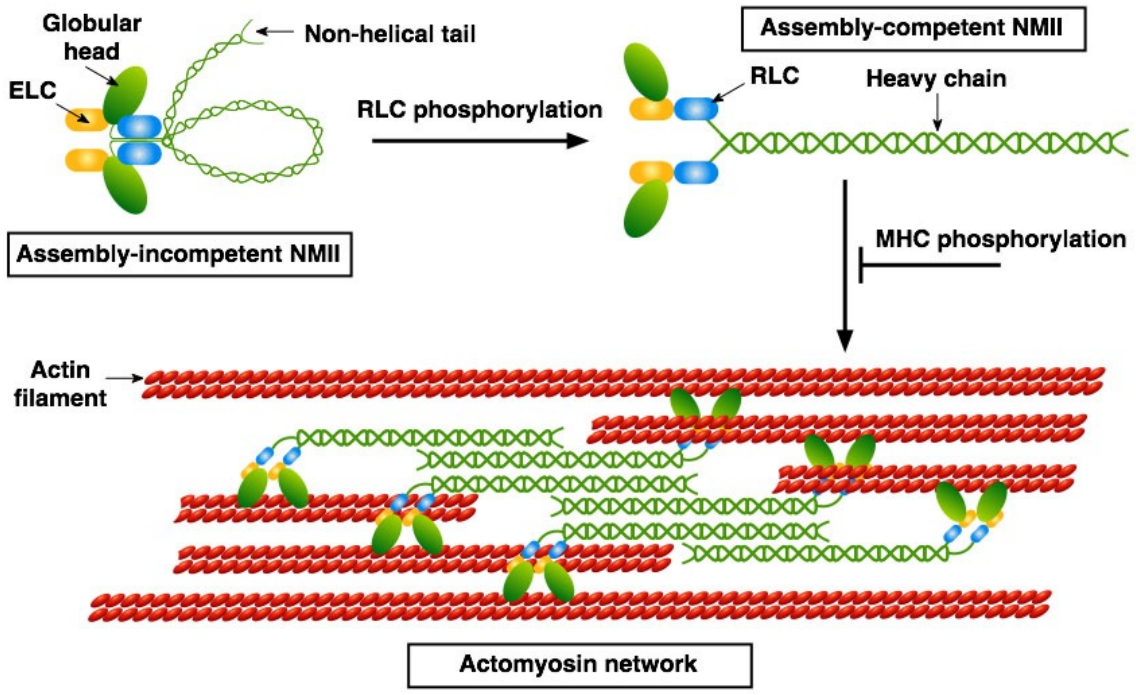

Figure 5.4. Schematic outlining the assembly of the actomyosin network. In the absence of regulatory light chain (RLC) phosphorylation, non-muscle myosin II (NMII) forms a compact and assembly-incompetent molecule. RLC phosphorylation causes unfolding of the structure and NMII molecules assemble into bipolar filaments via interactions between their rod domains (this region corresponds to the heavy chain portion of NMII minus the non-helical tail). These NMII filaments can bind to actin via their globular head domains and the ATPase activity of the head enables the confomational changes required to move actin in an anti-parallel manner. Bipolar NMII filaments can bundle actin filaments together to form a contractile actomyosin network. ELC: essential light chain. Adapted from Vicente-Manzanares *et al*. (2009).

5.2.3.1 The enveloping layer as a tissue for studying tension dynamics

It appears that physical forces may play an important role during the gastrulation process in zebrafish. During epiboly, the yolk cell has been proposed to act as an epiboly motor (Lepage and Bruce, 2010). Microtubules are located around the external and internal nuclei of the YSL as well as in the yolk cytoplasmic layer (YCL) where they emanate from organising centres located close to the most vegetal YSN and extend towards the vegetal pole (Lepage and Bruce, 2010). This YCL is a thin layer of nuclei-free cytoplasm surrounding the central yolk cell mass that is adjacent to the YSL

(Solnica-Krezel and Driever, 1994). During epiboly these microtubules shorten suggesting they may play a role in dragging the YSL and blastoderm in a vegetal direction (Solnica-Krezel and Driever, 1994).

Actin is also important for the completion of epiboly. At the high stage (3.33 hpf), F-actin starts to form at the cortex of each EVL cell (Zalik *et al*., 1999). Perhaps to provide mechanical strength against the pulling forces that will be generated by the YSL during epiboly progression. Cheng *et al*. (2004) initially reported the presence of actin in the form of a ring at the EVL-YSL margin, as well as a ring of punctate actin located in the E-YSL more vegetal to this ring. They hypothesised that this ring may be composed of contractile actomyosin in nature, serving analogous roles to actomyosin rings seen elsewhere in development as detailed above. Köppen *et al*. (2006) have since reported colocalisation of actin and myosin at the EVL-YSL margin confirming the presence of an actomyosin ring. Furthermore, they reported that at earlier stages of epiboly the marginal EVL cells are loosely aligned along the EVL-YSL interface and at later stages of epiboly, these marginal EVL cells become aligned into a taut row along the EVL-YSL boundary. This suggests this actomyosin ring is contractile in nature.

More recently, Behrndt *et al*. (2012) have demonstrated that the actomyosin ring is indeed under circumferential tension that plays a role in progressing epiboly. Moreover they also showed that both myosin and actin are present in the YSL and undergo flow movements in a vegetal to animal direction. The retrograde flow of this actomyosin has been proposed to play an important role in epiboly progression by generating frictional forces which the blastoderm opposes, thus driving its movement towards the vegetal pole (Behrndt *et al*., 2012). In line with this hypothesis, this actomyosin flow increases in velocity as epiboly proceeds and is important to drive earlier stages of epiboly before the circumferential tension of the ring can exert a pulling force on the EVL (Behrndt *et al*., 2012). Interestingly this actomyosin flow shows differential velocity to the flow of microtubules in the YCL.

Classical experiments showed that the YSL undergoes epiboly at a faster rate when the blastoderm is removed from the yolk cell in zebrafish, suggesting the YSL may pull the EVL and deep cells along with it during epiboly (Betchaku and Trinkaus, 1978). With the emergence of the more recent data above this long-standing theory now seems highly plausible since the YSL and EVL are connected by tight junctions, likely allowing the transmission of these pulling forces to the blastoderm (Lepage and Bruce 2010). Thus it is probable that the EVL is under significant tension due to these YSL-related pulling forces meaning the EVL can serve as a useful tissue for measuring tension. Indeed the longitudinal elongation of marginal EVL cells in the animal-vegetal axis later in epiboly supports this idea and provides a way to analyse the tension the

EVL is under (Köppen *et al*., 2006). Interestingly, the extent to which marginal EVL cells elongate is directly correlated with the amount of actin located in the YSL adjacent to the cell (Köppen *et al*., 2006).

5.3 Research questions

There are two main aims for this chapter as detailed below:

1. Is *in vivo* tissue tension actually decreased in *hirame* and a major cause of the mutant phenotype?

2. If so, what could be the biophysical mechanism underlying the tension decrease?

5.4 Results

5.4.1 Actomyosin activation is reduced in *hirame*

Since actomyosin is known to be a key regulator of cellular tension (Rotsch and Radmacher, 2000), which in turn dictates tissue tension, the activation status of actomyosin within the *hir* mutant was analysed. The activity of the myosin regulatory light chain (MRLC) by reversible phosphorylation at Serine 19 is essential for filament formation of non-muscle myosin II (NMII) and in turn the formation of actomyosin fibres by NMII binding to actin (Vicente-Manzanares *et al*., 2009). Therefore the phosphorylation state of MRLC (pMRLC) was compared between wild type and *hir* by western blotting. In wild type, the pMRLC level increased from st.17 (25 hpf) onwards until st.24 (44 hpf) when the amount of pMRLC reached a maximum (Figure 5.5). At all developmental stages compared, *hir* had much lower levels of pMRLC present (Figure 5.5). This suggests that dimers of NMII and consequently mature bundles of actomyosin may not correctly form in *hir*. This data lends support to a hypothesis of reduced tissue tension in *hir* and suggests YAP may play role in regulating this tension via regulating actomyosin activity.

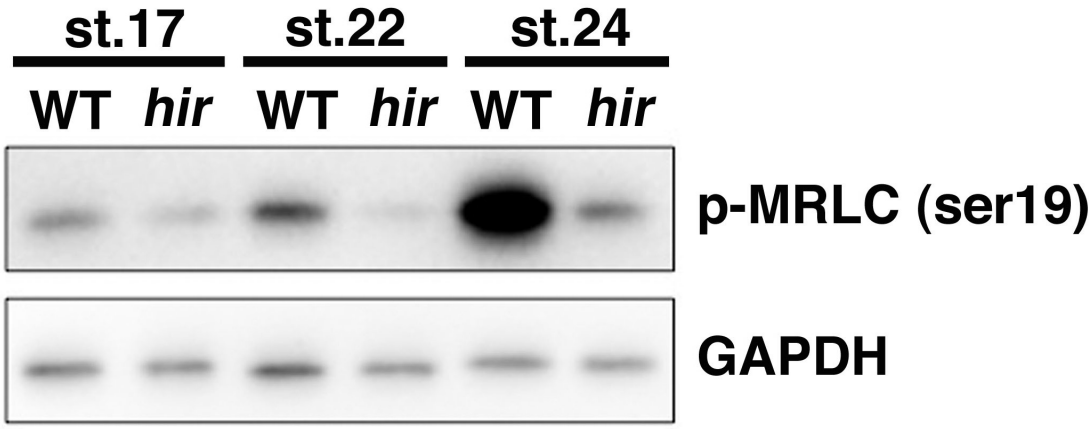

Figure 5.5. Phosphorylated MRLC levels are reduced in *hirame*. Immunoblotting of phospho-myosin regulatory light chain (pMRLC) and control (GAPDH) at the indicated stages. pMRLC levels increased from st.17 (25 hpf) onwards whereas in *hir* the levels remained very low. Data in conjunction with Shoji Hata.

5.4.2. Enveloping layer tension is reduced in *hirame* and zebrafish YAP and YAP/TAZ knockdown embryos

The EVL is a readily imaged epithelial tissue where cell shape or geometry correlates with the tension of the overall tissue (Köppen *et al*., 2006). The cells of this tissue display a characteristic change from hexagonal to elongated morphology as epiboly proceeds where the ratio of the longer to the shorter axis of the cell (length:width ratio, LWR, Figure 5.6b) is an indicator of tissue tension (measured as previously described by Köppen *et al*., 2006). To test whether reduced actomyosin activity causes reduced tissue tension, individual cell shape within the EVL was quantified at st16.5 (23 hpf) for *hir*, wild type embryos injected with a translation-blocking (TB) morpholino against YAP (YAP TBMO, 0.6ng of 200μM, optimised dose) and maternal YAP knockdown *hir* mutants (*hir* embryos injected with the 0.3ng of YAP TBMO, termed mYAPKD *hir* from herein). By this developmental stage, EVL cells have begun to elongate in wild type making differences in shape easier to detect in mutant embryos. To show the relationship between YAP, actomyosin and tissue tension, EVL analysis was also performed in MRLC AA mRNA injected (non-phosphorylatable MRLC, mimics inactive form of MRLC; Watanabe *et al*., 2007) and MYH9a/10 knockdown (myosin heavy chain 9a/10 TBMO, 0.6ng) embryos. And finally, EVL analysis was also performed for *hir* embryos injected with MRLC DD mRNA (which phosphomimics the diphosphorylated activated and very stable state of MRLC; Watanabe *et al*., 2007) to determine whether increasing tension could rescue any EVL cell shape phenotype observed in *hir* and the various knockdown conditions. Both the AA and DD mutant forms of MRLC have previously been shown to be highly effective at suppressing the endogenous levels of MRLC proteins (Watanabe *et al*., 2007).

EVL cell measurement showed cells were significantly less elongated in *hir* ($p < 0.001$, n = 70 cells, LWR = 1.61 ± 0.54) versus wild type (LWR = 2.28 ± 0.75, n = 174 cells) and this was exacerbated in mYAP KD *hir* embryos where the LWR was just 1.32 ± 0.66 (n = 81 cells, Figure 5.6a and c). Wild type embryos injected with the YAP TBMO also exhibited a significantly less elongated EVL cell morphology compared with control wild type embryos ($p < 0.001$, n = 85 cells, LWR = 1.82 ± 0.66), similar to that observed in *hir* (Figure 5.6a and c). Less elongated cells were also observed in the EVL of wild type embryos injected with either MRLC AA ($p < 0.001$, n = 135 cells, LWR = 1.82 ± 0.60) or MYH9a/10 TBMO ($p < 0.001$, n = 145 cells, LWR = 1.63 ± 0.60, Figure 5.6a and c), where both differed significantly from the wild type LWR. Interestingly, MRLC DD injection into *hir* significantly ($p < 0.05$, n = 92 cells) increased the LWR of EVL cells from 1.61 to 1.83 ± 0.61 (Figure 5.6a and c) and taken together, these results suggest that YAP is indeed regulating tissue tension, possibly through actomyosin.

Zebrafish also allow excellent EVL-related observations due to their speed of development. Consequently EVL cell LWR analysis was also performed in zebrafish to see whether there was conservation for YAP in tension regulation in zebrafish. In zebrafish YAP KD embryos, the tissue/organ collapse phenotype, and tissue mislocation phenotype seen in *hir* has not been previously reported. Since TAZ (mammalian paralogue of YAP) is also present in zebrafish, this may suggest a stronger redundancy between YAP and TAZ in zebrafish. Preliminary observations in the YAP/TAZ double mutant TALEN zebrafish line suggested some similarities to the *hir* phenotype (Makoto Furutani-Seiki, *personal communication*). Hence to more closely mimic the conditions seen in *hir*, both YAP and TAZ were targeted for morpholino knockdown in zebrafish and these double KD embryos were compared with YAP only KD embryos for certain experiments to try to decipher where the redundancy may lie between YAP and TAZ. Wild type, YAP KD (YAP TBMO, 0.25mM) and YAP/TAZ double KD (YAP/TAZ TBMO, 0.25mM) zebrafish embryos were analysed at 80% epiboly, which is the equivalent developmental stage to st.16.5 (23 hpf) in medaka (Figure 5.7).

EVL cell LWR in zebrafish was very similar to that observed in medaka with YAP KD embryos (1.5ng TBMO) having a significantly lower LWR of 1.5 ± 0.78 ($p < 0.001$, n = 174 cells) than wild type embryos (LWR = 2.36 ± 0.86, n = 136 cells, Figure 5.7a-b). As seen with MRLC DD injection into *hir*, zebrafish embryos co-injected with YAP TBMO and YAP mRNA (human variant, 100μM) displayed a partially rescued EVL cell shape with an LWR of 1.76 ± 0.69 (Figure 5.7a-b) which was significantly elongated when compared with YAP KD embryos alone ($p < 0.01$, n = 222 cells). Double KD embryos (1.5ng TBMO) also displayed a significantly reduced LWR of 1.66 ± 0.48 ($p < 0.001$, n = 131 cells, Figure 5.7a-b) versus wild type. Taken together, this data again suggests YAP may be regulating tissue tension and that this mechanism may be somewhat conserved amongst vertebrates. To ascertain whether this YAP regulation of tension is also via actomyosin in zebrafish, actomyosin activity in the KD embryos could be analysed as in Figure 5.5.

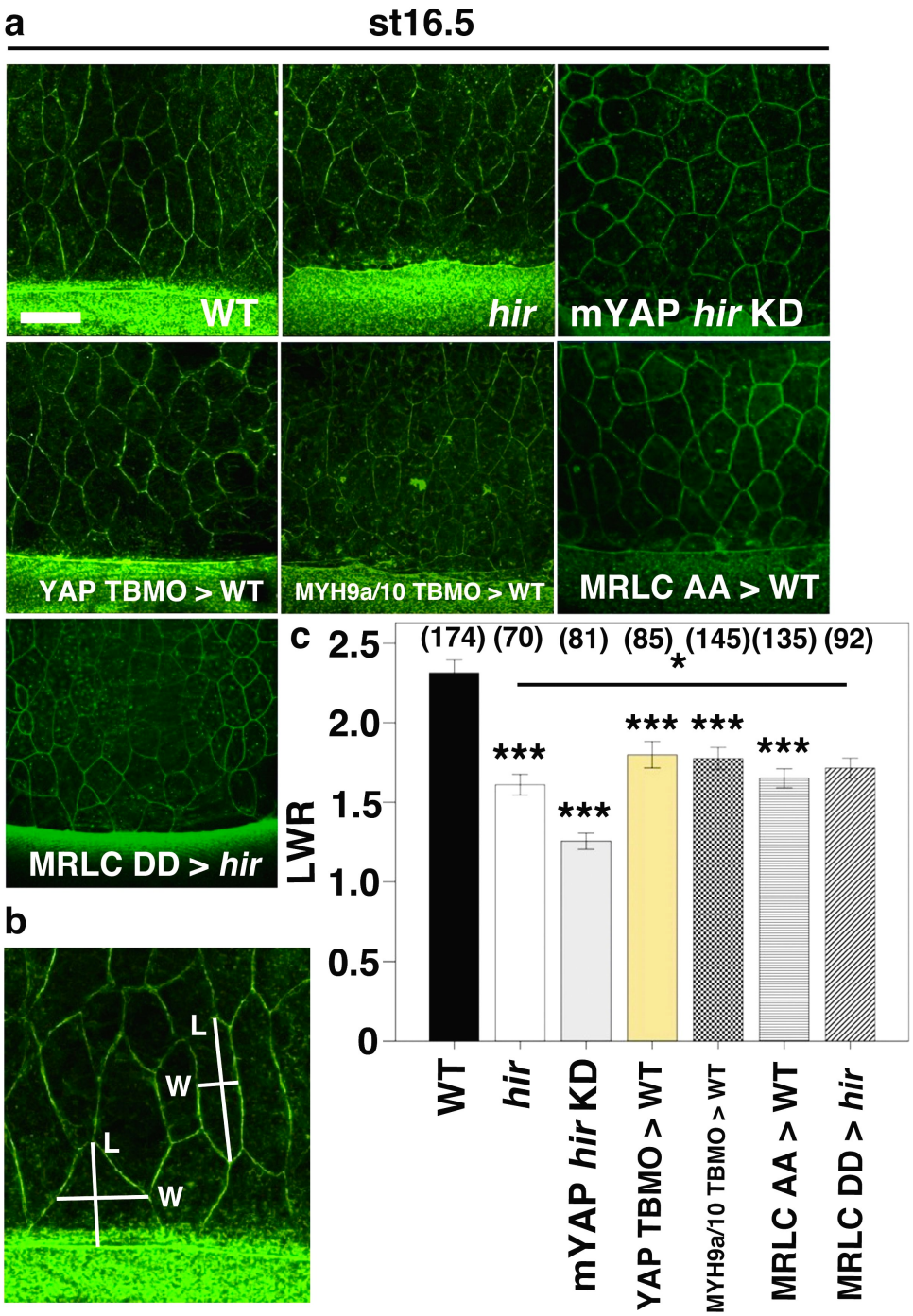

Figure 5.6. EVL tension is reduced in *hirame* mutant embryos. (a) Cells of the EVL appear less elongated in *hir*, mYAP KD *hir* embryos and wild type embryos injected with YAP TBMO. Furthermore, knockdown of components important for maintaining cellular tension (MYH9a/10 TBMO) or phosphomimicking the inactive state of MRLC (AA) in wild type embryos also results in less elongated EVL cells. Injecting phosphoactive MRLC (DD) into *hir* somewhat rescues EVL cell elongation. **(b)** Schematic depicting how EVL cell length (L) and width (W) was measured in marginal cells and those back from the margin. **(c)** Quantification of EVL LWR for embryo types shown in (a). * = p <0.05, *** = p <0.001. Scale bar: 50μm. Cell numbers are shown in parentheses above the graph. Error bars show ± S.E.M.

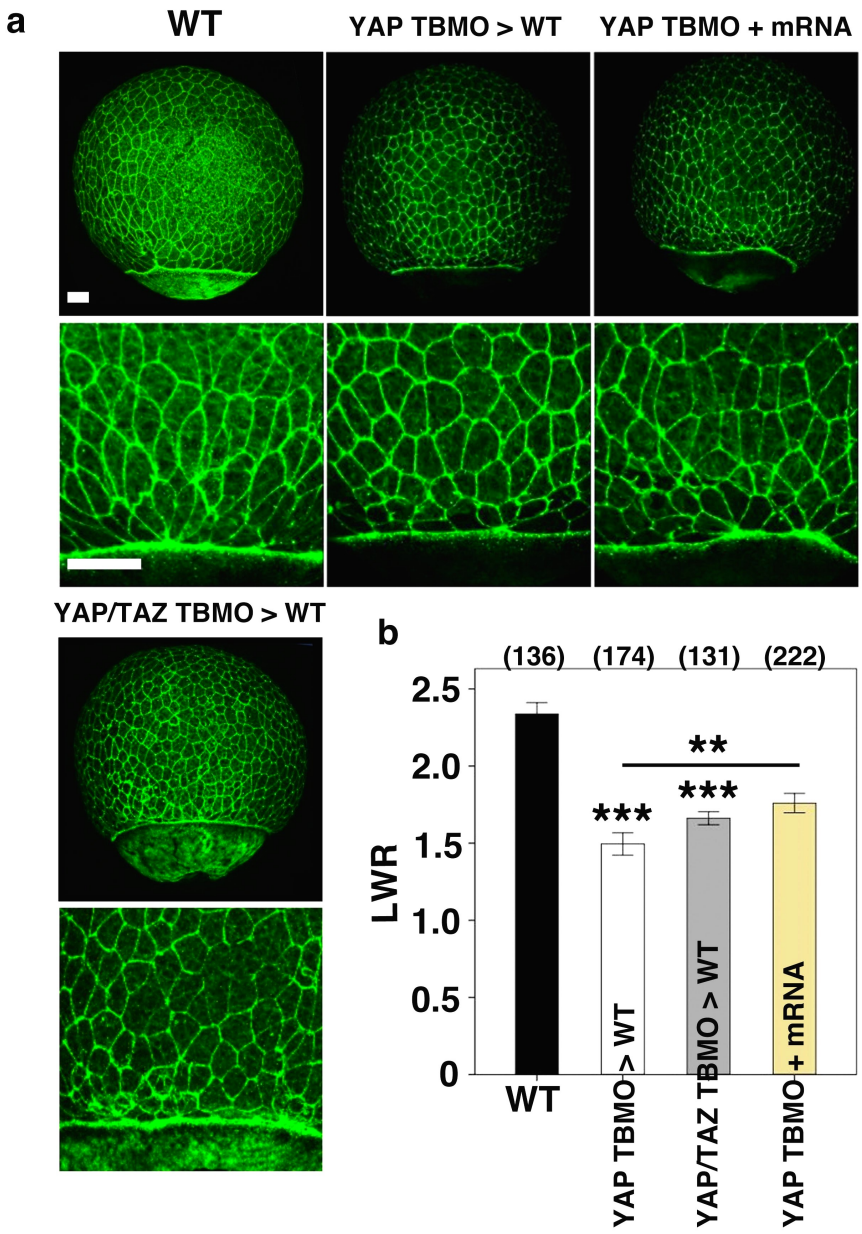

Figure 5.7. EVL tension is also reduced in YAP and YAP/TAZ knockdown zebrafish embryos. (a) YAP or YAP/TAZ knockdown in zebrafish also causes reduction of cell elongation in the EVL. Co-injection of YAP TBMO and YAP mRNA somewhat rescues EVL cell LWR. **(b)** Quantification of EVL LWR (as measured in Figure 5.6) for embryo types shown in (a). ** = p <0.01, *** = p <0.001. Scale bar: 40μm. Cell numbers are shown in parentheses above the graph. Error bars show ± S.E.M.

5.4.3 The *hirame* mutant, YAP and YAP/TAZ double knockdown zebrafish exhibit slowed epiboly, defects in YSL actin as well as aberrant myosin localisation

As EVL tension appears affected in *hir*, YAP KD and YAP/TAZ double KD zebrafish embryos, it was asked whether epiboly was affected in these embryos. In this section, 'epiboly' is used to describe the movement of the deep cell (DC) margin from the

animal to vegetal pole. When referring to epiboly of the EVL/actomyosin ring, the term 'EVL epiboly' will be used. Mutant *hir* embryos displayed a mild delay in epiboly that was most evident from st.16-18 (23-26 hpf, Figure 5.8a, arrows demarcate blastoderm margin) but nevertheless finished epiboly by around st.21 (34 hpf, Figure 5.8b). This delayed epiboly phenotype was exacerbated in mYAP KD *hir* embryos (Figure 5.8a) where epiboly did not complete (stalled at approximately 85%, Figure 5.8b, compare middle *hir* panel with right-side mYAP KD *hir* panel). Co-injection of YAP TBMO with YAP mRNA (human variant, 100μM) into *hir* rescued the delayed epiboly so that it proceeded as seen in wild type (Figure 5.8c, red and blue lines). When comparing epiboly coverage at st.17 (25 hpf), wild type and co-injected embryos (YAP TBMO + YAP mRNA) were not significantly different (92.44% ± 2.18, n = 18 embryos, and 92.45% ± 1.93, n = 20 embryos respectively, Figure 5.8d). Both *hir* (84.69% ± 5.6, n = 13 embryos) and mYAP KD *hir* (72.38% ± 5.04, n = 21 embryos) embryos had significantly less epiboly coverage as compared to wild type ($p < 0.001$, Figure 5.8d) at st.17 (25 hpf).

In zebrafish, morpholinos against YAP only (YAP TBMO 0.25mM), as well as morpholinos against YAP and TAZ in combination (YAP/TAZ TBMO, 0.25mM) were again injected. YAP KD and YAP/TAZ KD embryos also exhibited slowed epiboly that became more noticeable from the shield stage onwards (6 hpf, Figure 5.9a). Several epiboly phenotypes were observed when injecting the YAP/TAZ TBMO into zebrafish embryos, with a weak phenotype generated by 1ng, an intermediate phenotype seen with a 1.5ng dose, and a severe phenotype observed from 2ng (Figure 5.9a). In YAP/TAZ TBMO embryos, epiboly seemed delayed but EVL epiboly appeared unaffected (Figure 5.9a). Severe morphants became gradually unhealthy in appearance as epiboly proceeded with large voids appearing in the DCs, suggesting the high dose of morpholino was toxic (Figure 5.9b). Therefore, these dose-dependent phenotypes allowed optimisation of the dose of morpholino required to induce a phenotype via sufficient knockdown, whilst at the same time not causing toxicity and the misinterpretation of phenotypes.

Consequently intermediate doses (1.5ng) of the YAP/TAZ TBMO were utilised for comparisons with control embryos. Convincingly, injection of 2ng of YAP/TAZ splicing-blocking morpholino (SBMO, 0.25mM) replicated the epiboly phenotype seen in TBMO-injected embryos. The SBMO phenotype was milder than the corresponding phenotype in 2ng TBMO-injected embryos, and more in line with the YAP/TAZ TBMO intermediate (1.5ng) phenotype. This is likely because the SBMO probably only knocks down zygotic protein expression. Injection of the TBMO may also affect maternal protein expression (which is important in early development), giving a stronger phenotype. Further details regarding the specificity of morpholino KD can be found in Section 2.4.

This multi-morpholino approach is useful for determining the relative contribution of maternal and zygotic transcripts to the KD phenotypes observed. Furthermore, this approach highlights the importance of optimising the morpholino dose before characterising the associated phenotype in detail.

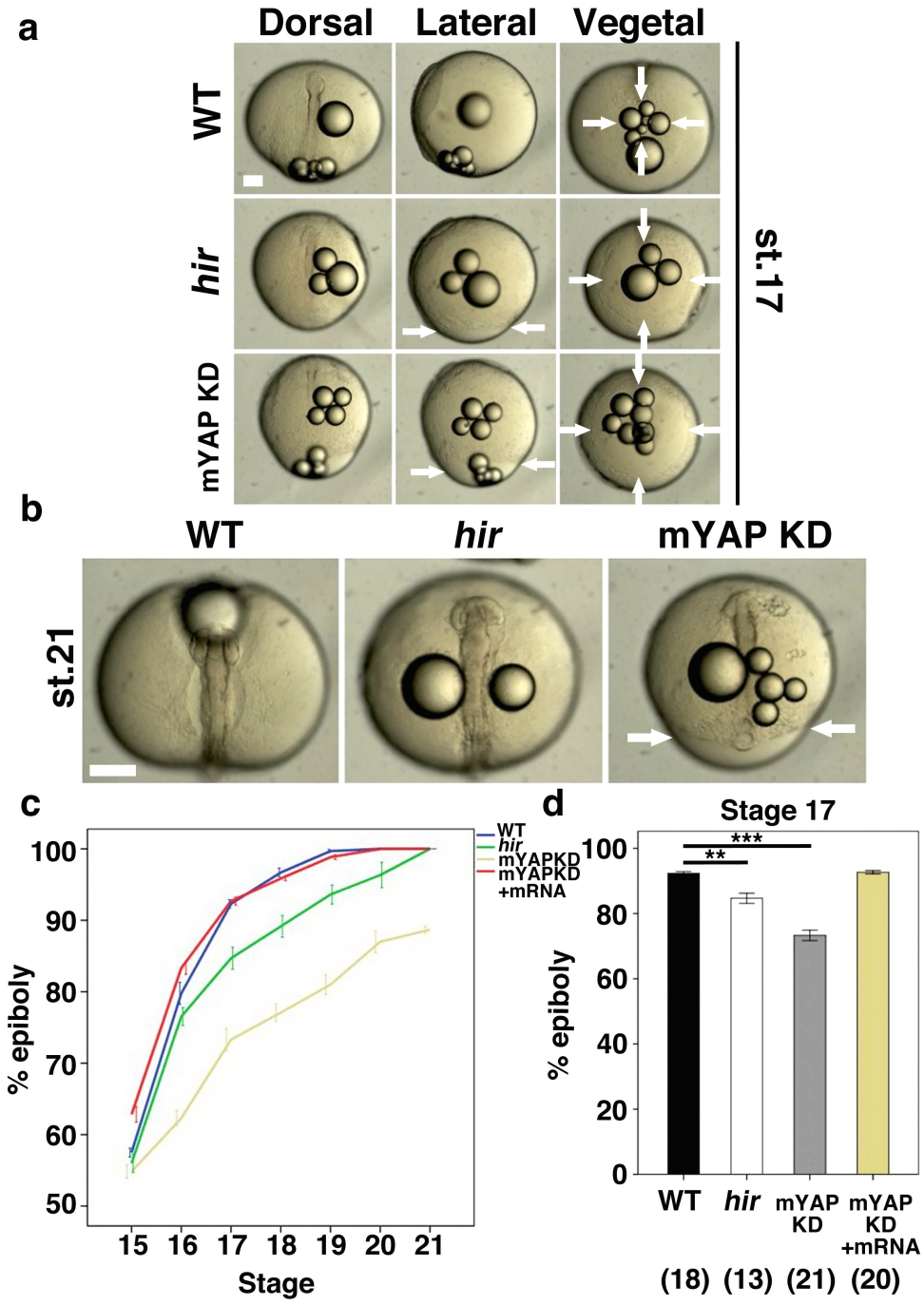

Figure 5.8. *hirame* and mYAP KD *hirame* embryos exhibit slow epiboly. (a) *hir* and mYAP KD *hir* embryos exhibit delayed blastopore closure (vegetal views). Arrows demarcate blastoderm margin. **(b)** *hir* epiboly eventually completes but mYAP KD *hir* epiboly never does. **(c)** Quantification of epiboly over development shows *hir* (green line) eventually completes by st.21 (34 hpf) whereas mYAP KD *hir* embryos (gold line) do not finish. Co-injection of YAP

TBMO + YAP mRNA (red line) results in epiboly proceeding as in wild type (blue line). **(d)** Comparison of epiboly between embryos at st.17 (25 hpf) shows both *hir* and mYAP KD *hir* are significantly delayed. ** = p <0.01, *** = p <0.001. Scale bars: (a) = 100μm; (b) = 150μm. Error bars show ± S.E.M.

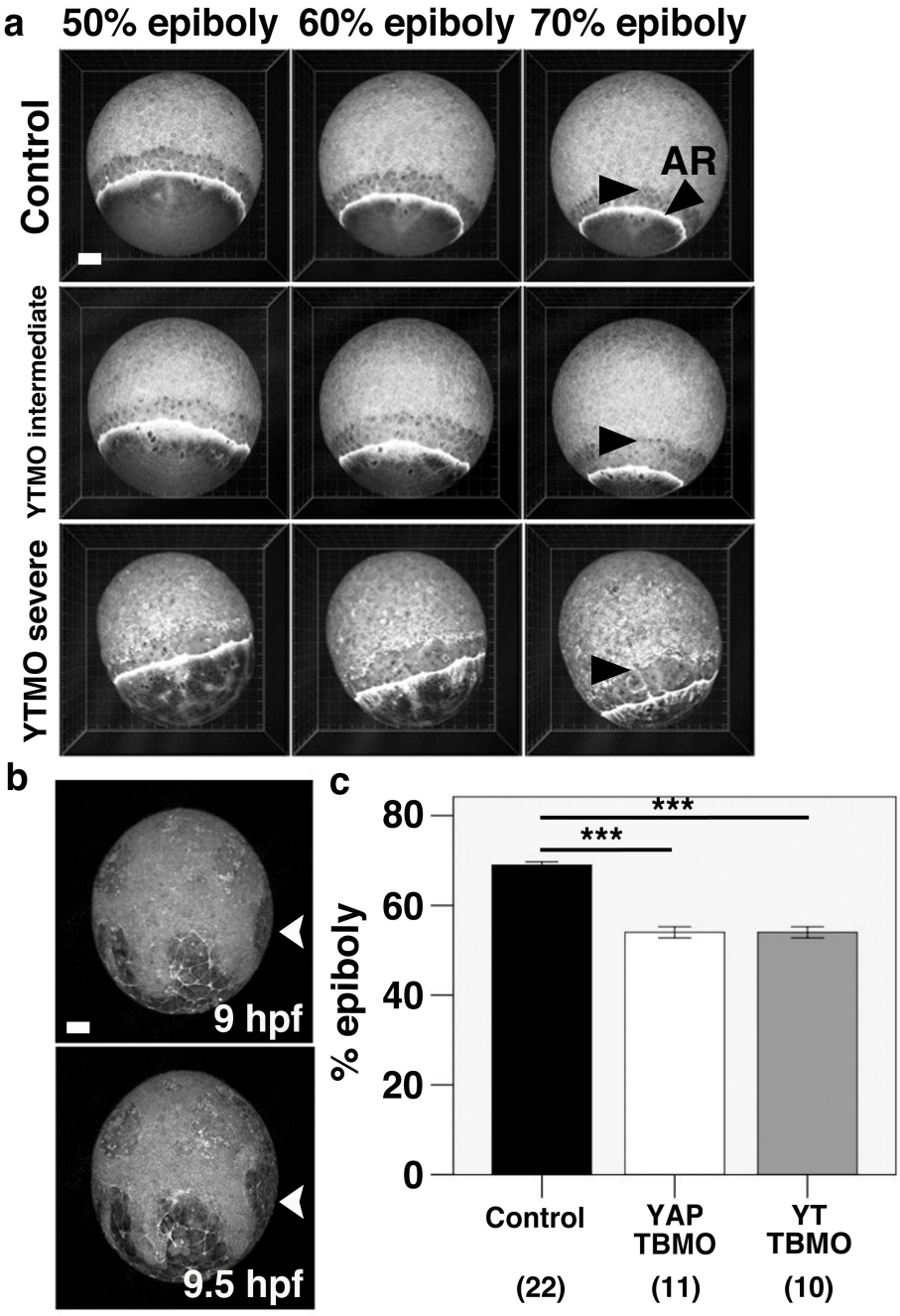

Figure 5.9. YAP and YAP/TAZ knockdown zebrafish embryos also exhibit slower epiboly. **(a)** Deep cell epiboly (arrowheads) appears delayed in YAP/TAZ (YT) KD embryos and is dose-dependent. EVL epiboly appears unaffected **(b)** High doses of YAP/TAZ are toxic highlighting the importance of morpholino dose optimisation. Arrowheads show examples of voids appearing in the deep cell layers. **(c)** Quantification of epiboly in YAP and YAP/TAZ (YT) knockdown embryos versus control embryos. *** = p <0.001. AR: actomyosin ring. Scale bars: (a) = 80μm; (b) = 60μm. Error bars show ± S.E.M.

When zebrafish control embryos were at 70% ± 2.18 epiboly (n = 22 embryos), both YAP KD only (n = 11 embryos) and double (YAP/TAZ) morphants (both 2ng of SBMO or 1.5ng of TBMO, n = 10 embryos) had significantly less DC coverage of the yolk, approximately at the 55% ± 3.94 epiboly stage ($p < 0.001$, Figure 5.9c). Unlike in mYAP KD *hir* embryos, intermediate double KD zebrafish embryos (1.5ng TBMO) finished epiboly. In terms of EVL epiboly, YAP TBMO KD (n = 3) embryos exhibited a higher degree of delay than seen in the EVL of the YAP/TAZ SBMO KD embryos (n = 3), which appeared more comparable to control embryos (Figure 5.10a). Further investigation is required here but the other data shown suggests some importance of maternal YAP in early development of the EVL is similar between medaka and zebrafish.

In light of the DC and EVL epiboly delay observed, the distance between the EVL margin and the DC margin was examined in more detail (Figure 5.10b-c). Measuring the EVL-DC distance can give clues as to whether there is a general developmental defect or a true defect in epiboly (of either the EVL or DC). In this context an increase or decrease in the EVL-to-DC distance may indicate a specific defect in EVL or DC epiboly. This is because changes in EVL-DC distance are likely to mean the EVL and DCs are moving at different speeds. If the distance remains relatively constant but epiboly is slower then it is possible that there is a more general delay in development as both margins are moving more slowly. With this in mind, time-lapse imaging of YAP TBMO- and YAP/TAZ TBMO/SBMO-injected zebrafish embryos was performed to gain further insights into the delayed epiboly observed. Analysis of the zebrafish YAP/TAZ TBMO KD embryos of varying phenotypes showed that epiboly was likely to be delayed by a decrease in migration rate of the DC margin since EVL epiboly appeared comparable to wild type (Figure 5.9a). This was confirmed by measuring the distance between the margin of the DCs and EVL margin at 3 points during different stages of epiboly (Figure 5.10d) as previously described (Slanchev *et al*., 2009). In the double YAP/TAZ TBMO morphants, the EVL-DC distance increased as epiboly proceeded, whereas the EVL-DC distance decreased in control embryos (Figure 5.10d). YAP TBMO (75.35μm ± 7.42, n = 3 embryos) and YAP/TAZ SBMO KD (87.73μm ± 9.99, n = 3 embryos) embryos also exhibited a greater EVL-DC distance as compared to control embryos (63.47μm ± 1.90, n = 3 embryos) at approximately 7.5 hpf, with the YAP/TAZ SBMO embryos having a significantly greater EVL-DC distance ($p < 0.05$, Figure 5.10e).

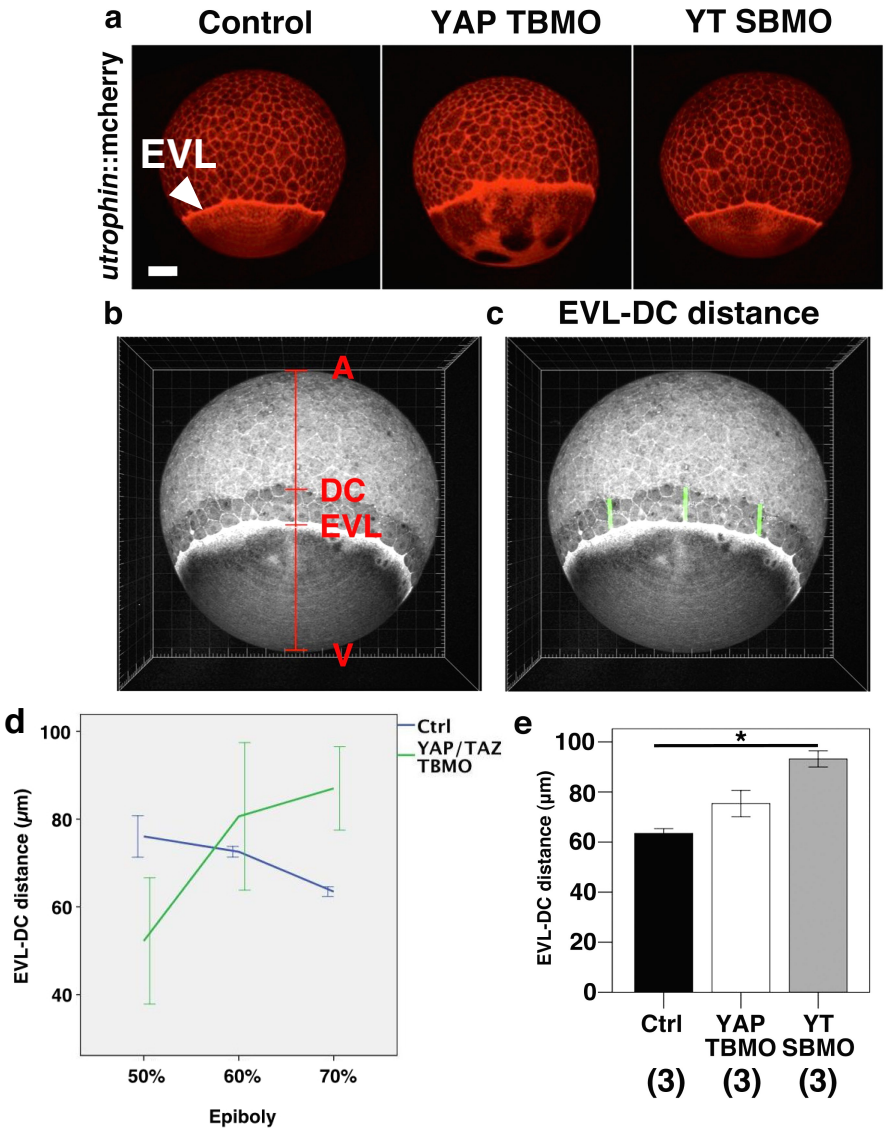

Figure 5.10. EVL-DC distance measurements in YAP and YAP/TAZ knockdown zebrafish embryos. **(a)** EVL epiboly is more affected in YAP TBMO than YAP/TAZ SBMO KD embryos. **(b and c)** Schematics depicting the measurement of EVL-DC distance. **(d)** EVL-DC distance over time in embryos with phenotypes equivalent to those shown in Figure 5.9. **(e)** Comparison of EVL-DC distance at 7.5 hpf shows significant differences between control embryos and YAP/TAZ SBMO embryos. Scale bar: 120µm. * = p <0.05. Error bars show ± S.E.M.

In summary, both YAP TBMO and YAP/TAZ TBMO/SBMO embryos exhibit similar delays in DC epiboly (Figure 5.9c). However, YAP TBMO embryos exhibit slower EVL epiboly compared to YAP/TAZ SBMO embryos (Figure 5.10a). This result is in contrast with the EVL epiboly for YAP/TAZ TBMO embryos which does not seem affected and therefore requires confirmation by further investigation since few embryos were analysed. Slowed EVL epiboly leads to a shorter DC-EVL distance in YAP TBMO

embryos and normal EVL epiboly results in a greater DC-EVL distance in YAP/TAZ SBMO embryos (Figure 5.10e).

Time-lapse analysis also suggested that both actin and myosin localisations were affected as development proceeded. In the cortex of EVL cells, F-actin (visualised using *utrophin*::mcherry) did not appear affected in the double morphant embryos (YAP/TAZ TBMO) in terms of location and intensity distribution as assessed at three points across the span of the EVL at 60% epiboly (Figure 5.11a-c), suggesting F-actin was normally distributed and present at comparable levels to the control embryos. However, in all YAP/TAZ double KD embryos (21/21 embryos), the punctate actin in the cortex of the yolk appeared to show condensed localised regions within the E-YSL (Figure 5.11b and d, arrowheads show examples), instead of being equally widespread as seen in the E-YSL of control embryos (Figure 5.11b and d). This hints at a possible disruption in the actomyosin retrograde flows in the YSL that are important for the progression of epiboly (Behrndt *et al*. 2012).

Together these data suggest that in the absence of YAP/TAZ, there may be some sort of uncoupling of the actomyosin network dynamics required to maintain tissue tension, but which is also important at earlier stages of development for epiboly progression. To test this possibility further, the physical properties of the actomyosin network comprising the actomyosin ring were examined.

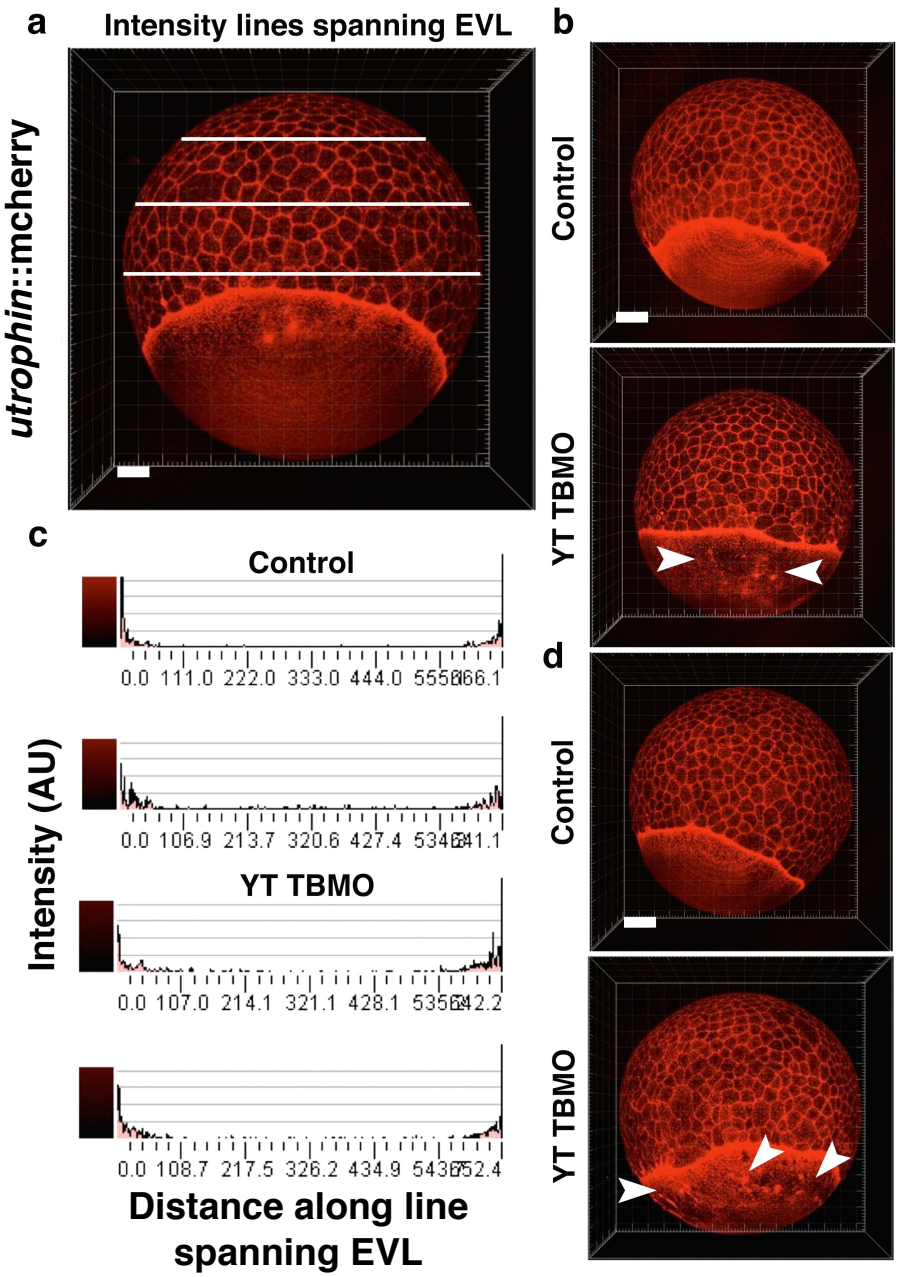

Figure 5.11. Actin appears unaffected in the enveloping layer but is disrupted in the yolk syncytial layer of YAP/TAZ knockdown zebrafish embryos. (a) Schematic depicting actin intensity measurement. **(b)** Comparison of actin localisation in the EVL between control embryos and YAP/TAZ (YT) KD embryos. **(c)** Quantification of actin intensity in the EVL at 60% epiboly. Representative plots are shown, measurements were performed a minimum of 3 times. **(d)** Actin localisation in the YSL of YAP/TAZ KD embryos is affected forming dense foci (arrowheads in b and d). Scale bars: (a) = 25µm; (b and d) = 60µm.

5.4.4 Direct physical measurements of tension in YAP knockdown embryos shows tension is indeed reduced when YAP levels are reduced

To directly measure whether tension is reduced in the absence of YAP in the *hir* mutant, biophysical laser ablation experiments to test the cortical tension of the actomyosin ring present during epiboly were performed. This was carried out in zebrafish embryos since this laser ablation method was established in zebrafish (Behrndt *et al*., 2012). Morpholino knockdown of YAP and TAZ (YAP/TAZ TBMO) was implemented as above. It has been observed that the actomyosin ring experiences more tension in a circumferential manner around the embryo/yolk cell than in the animal-vegetal pole axis thus making tension differences likely to be more distinguishable in the circumferential plane (Behrndt *et al*., 2012). Therefore, to test circumferential/cortical tension, the ring should be cut perpendicular to the circumferential plane (Figure 5.12a).

The actomyosin ring of the YSL was cut perpendicular to the EVL margin (Figure 5.12a) with the cut starting 20μm from the EVL margin and the cut itself being 20μm in length. Time-lapse imaging was performed during the cut to record the response of the actomyosin network comprising the ring. Particle image velocimetry (PIV) analysis was then performed on the images of the cut to determine both displacement and velocity of the displacement of the edges either side of the cut. In PIV, whole velocity fields are measured by taking images in quick succession and calculating the distance individual particles have travelled within this time. In this case the position of actomyosin particles either side of the laser cut was tracked for velocity measurement before and directly after the cut to give an indication of how quickly the cut opened (initial cortical recoil velocity). These recoil velocities give an indication of the tension the actomyosin ring is under as faster recoil velocities imply higher tension. Since the morphant embryos displayed slow epiboly as described above, it was decided to compare recoil velocity at both the same epiboly stage and the same developmental time stage since the tension the actomyosin ring is under increases during epiboly (Behrndt *et al*., 2012).

PIV analysis following the laser cuts showed that the YAP/TAZ double KD embryos (1.5ng) had less displacement of actomyosin away from the centre of the laser cut as evidenced by smaller yellow displacement vectors (Figure 5.13a). Typically, cuts in the control appeared to open wider than in the double KD mutants, and appeared to open more quickly at both stages of comparison (Figure 5.12b, compare top, middle and bottom time series of cuts). Furthermore, initial cortical recoil velocity was significantly reduced in the YAP/TAZ KD embryos (14.63μm/min ± 4.49, n = 32 embryos) versus the control embryos at both comparison time points (control at 50-60% epiboly was 18.68μm/min ± 6.22, n = 21 embryos, $p < 0.05$; control at 70-80% epiboly was 20.8μm/min ± 4.58, n = 13 embryos, $p < 0.001$, Figure 5.14). These figures are in relatively

close agreement with published numbers (Behrndt *et al*., 2012) but further cuts are required to improve accuracy. Longer analysis of recoil velocity, for up to 8 seconds after the cut was made, showed that in all embryos the speed of cut opening decreased with time, consistent with anisotropic relaxation of the actomyosin ring (Figure 5.13b, Behrndt *et al*., 2012). However, the control cut at both 50-60% and 70-80% epiboly opened at a greater velocity than the morphant (Figure 5.13b). Collectively, these physical experiments suggest YAP is required for maintaining tension through an actomyosin network-dependent mechanism.

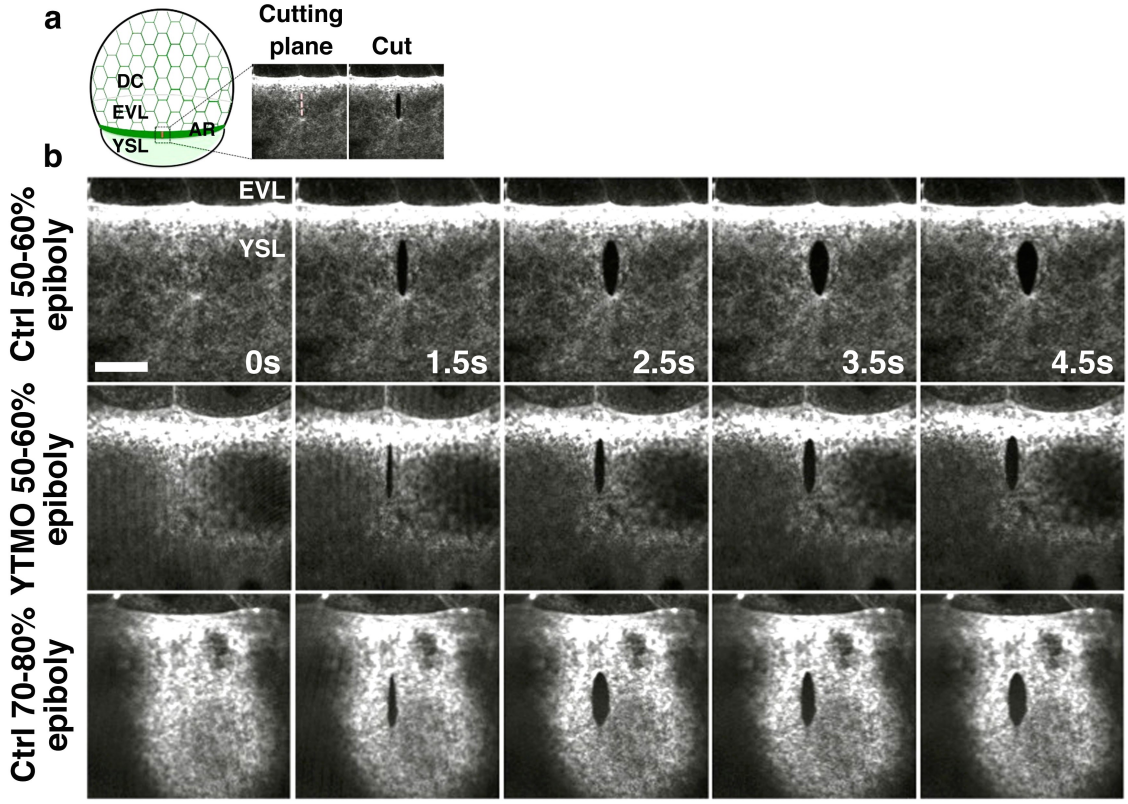

Figure 5.12. Laser ablation of the actomyosin ring *in vivo*. (a) Schematic depicting location and orientation of UV laser cut. **(b)** Images from time-lapse capture of laser cutting show the actomyosin network opens wider and faster in control embryos versus YAP/TAZ (YT) KD zebrafish embryos both at the same epiboly and developmental stage. DC: deep cells (margin shown by feint grey line in (a)); EVL: enveloping layer; YSL: yolk syncytial layer (light green in (a)); AR: actomyosin ring (dark green in (a)). Scale bar: 20μm.

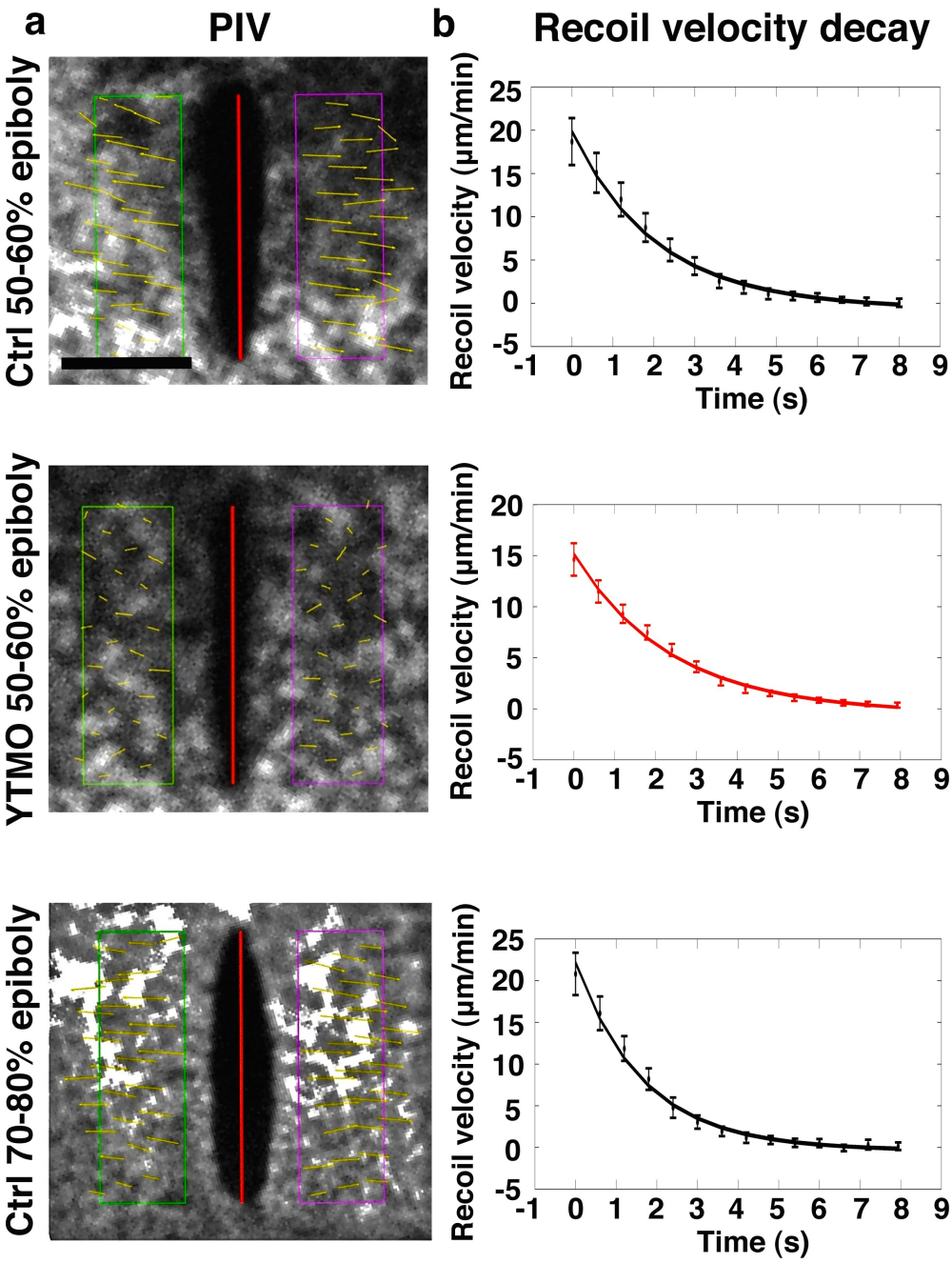

Figure 5.13. PIV analysis of laser ablation cuts of the actomyosin ring. (a) Calculation of the rate of movement of actomyosin particles away from the cut site (yellow vectors) on either side of the cut (purple and green boxes). Red line indicates position of laser cut. **(b)** The recoil velocity of actomyosin particles away from the cut is greater in control embryos (black lines) versus YAP/TAZ (YT) KD (red line) zebrafish embryos both at the same epiboly and developmental stage. Scale bar: 10µm. Error bars show ± S.E.M.

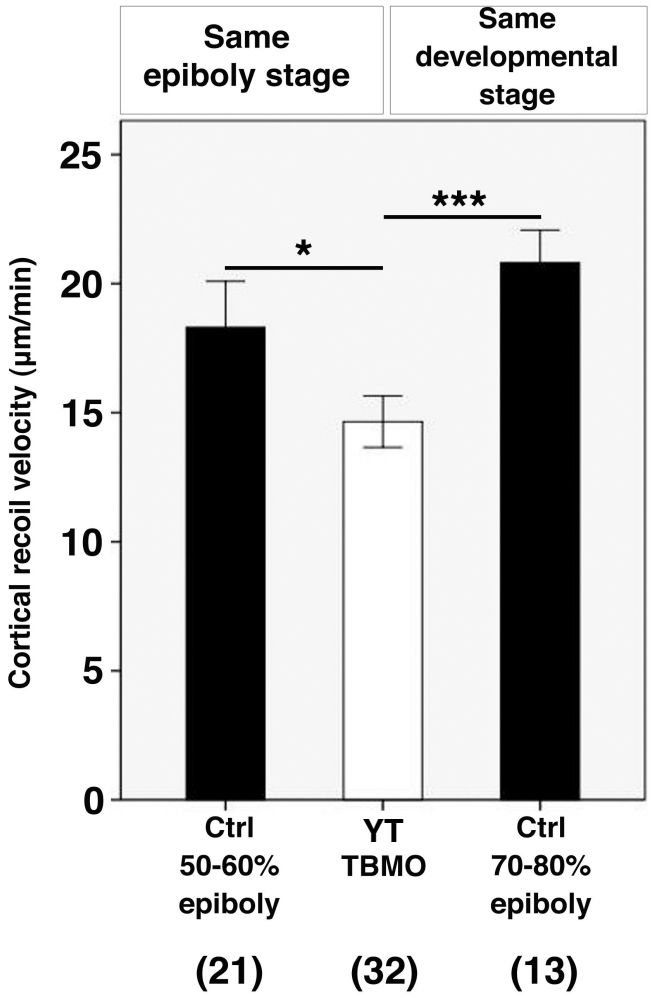

Figure 5.14. Initial recoil velocity analysis of laser ablation cuts of the actomyosin ring. Mean initial recoil velocity of actomyosin particles is significantly greater in the control embryos versus YAP/TAZ (YT) KD zebrafish embryos at both the same epiboly and developmental stage. Number of embryos cut is shown in parentheses. * = $p < 0.05$, *** = $p < 0.001$. Error bars show ± S.E.M.

5.5 Discussion

5.5.1 Actomyosin activity is reduced in *hirame*

Western blotting for activated actomyosin (as assessed by blotting for non-muscle myosin II (NMII) phosphorylated at Serine 19) showed that there were significantly reduced levels of activated NMII in *hir*. This likely means that less NMII in the mutant is able to dimerise and subsequently bind to actin to provide the contractile anti-parallel pulling forces required to remodel the actin network. Without this properly functioning actomyosin network, the ability of *hir* cells to maintain their shape, tension and polarity is likely severely compromised. The phosphorylated NMII levels could also be examined in mYAP KD *hir* mutants and wild type embryos injected with the YAP TBMO to corroborate the finding of reduced active NMII in *hir* and in KD zebrafish.

5.5.2 Tissue tension is significantly reduced in the absence of YAP/TAZ

EVL cell shape was significantly less elongated in the *hir* mutant and in zebrafish embryos in the absence of YAP/TAZ as well as when various components of the actomyosin network were knocked down or effectively inactivated in the case of myosin heavy chain 9a/10 (MYH9a/10) and myosin regulatory chain (MRLC AA) respectively. This loss of tissue tension could be somewhat restored in the *hir* mutant by injection of MRLC DD (activated form of MRLC) to artificially increase tension, resulting in more elongated EVL cells. These data suggest a relationship between tissue tension and YAP, with YAP possibly regulating actomyosin activity. How YAP does this remains unknown for now, despite recent reports that act to strengthen the existence of a relationship between the cytoskeleton and YAP (Aragona *et al*., 2013, discussed further in Chapter 7).

5.5.3 Epiboly is slower in *hirame* and YAP/TAZ knockdown zebrafish mutants

Both *hir* embryos and YAP/TAZ KD zebrafish embryos exhibited delayed epiboly. This was analysed by comparing the extent of DC epiboly in mutants and morphants with controls, as well as by measuring the distance between the DC and EVL margins in zebrafish embryos. For DC epiboly both the *hir* mutant and morphants displayed slower epiboly. For the DC-EVL distance measurements this value increased in the morphants (YAP and YAP/TAZ TBMO) over time. It may be interesting to perform the same measurements in TAZ only TBMO KD embryos to see if there is any variation. This would allow conclusions to be drawn about whether YAP and TAZ differentially affect EVL or DC epiboly.

Since YAP/TAZ mutant zebrafish were not available at the time of this study, morpholino KD was utilised to affect YAP/TAZ expression. The resulting slow epiboly was confirmed in zebrafish through the use of three different morpholinos (5' untranslated region; translation-blocking, TB; and splicing-blocking, SB), suggesting

that even though YAP mRNA co-injection with the translation-blocking morpholino could not efficiently rescue the phenotype, this phenotype was not due to off-target effects or a lack of specificity of the morpholino. Moreover, preliminary analysis of a recently received YAP/TAZ mutant fish line has confirmed this slow epiboly phenotype. Furthermore, this slowed epiboly phenotype has also been reported in *Xenopus* (Gee *et al*., 2011) by morpholino KD of YAP. The same report also could not observe rescue of this epiboly phenotype in *Xenopus* by co-injection of *xyap* (*Xenopus yap*), *myap* (*mouse yap*) or *hyap* (*human yap*) mRNA with the xYAP morpholino (Gee *et al*., 2011). Including the gastrulation defects seen in mice (Morin-Kensicki *et al*., 2006), there are now four vertebrate model organisms that display early developmental defects when *yap* expression is reduced, suggesting a conserved and genuine requirement of YAP in early development/gastrulation. Finally, in mYAP KD *hir* mutants the phenotype was exacerbated as epiboly arrested, again suggesting a role for YAP in epiboly.

What could be the cause of the slowed epiboly observed in embryos with YAP/TAZ KD? There are several possible candidates. First and foremost is the actomyosin ring. Since the tension of the actomyosin ring in the YAP/TAZ KD embryos is reduced, this likely means the constriction that occurs at the later stages of epiboly to eventually close the blastopore is affected. As shown by Behrndt *et al*. (2012) the tension of the actomyosin ring is important for driving epiboly from 50% epiboly onwards, once the ring has passed the equator and widest region of the yolk. This corresponds well with the experimental data gathered on epiboly rates since the delay in epiboly becomes more apparent from 50% epiboly onwards in both *hir* and YAP/TAZ KD zebrafish mutants. The role of actin has previously been shown to be important for epiboly since depolymerising actin with cytochalasin causes slowed epiboly and a failure of the blastopore to close (Cheng *et al*., 2004). Therefore the work presented in this thesis is in agreement with this report from Cheng *et al*. (2004) and work from Behrndt *et al*. (2012) and strongly suggests a role for YAP in the regulation of this actomyosin ring.

Other candidates that may cause the slowed epiboly include proteins that have been shown to be associated with, or affect the distribution of YAP, including Angiomotin (Angiomotin-like 2, Amotl2), Yes and Diaphanous (Diaphanous homologue 2, Diaph2). All of these proteins have been implicated in epiboly as their knockdown with morpholinos causes defects such as delayed epiboly (Amotl2) or epiboly arrest in the case of Yes and Diaph2 (reviewed in Lepage and Bruce 2010). Furthermore, Amotl2 KD causes cell migration defects (Huang *et al*., 2007) and Diaph2 KD results in the EVL-YSL marginal actin ring being reduced (Lai *et al*., 2008). The scaffold proteins Amotl2 and Diaph2 may be important for transmitting tension changes between the dynamically changing actomyosin cortex and YAP and vice-versa. In the absence of YAP these changes may not be detected/sensed by the cell and therefore not

responded to appropriately. Since Diaph2 interacts directly with RhoA and Cdc42 (Lai *et al*., 2008) this may also explain some of the other phenotypes seen in *hir*, particularly the cell migration/polarisation defects. Diaph2 also interacts with Profilin, which is a protein that associates with actin monomers contributing to actin polymerisation (Goode and Eck, 2007). Since actin polymerisation affects Hippo signalling this provides another potential clue for the link between YAP and the cytoskeleton. A final consideration for the cause of delayed epiboly is the reduced FN fibrillisation seen in the *hir* mutant (reported in Chapters 3 and 4). In *Xenopus*, FN KD retards gastrulation causing delayed blastopore closure (Davidson *et al*., 2006), a similar phenotype to that of the mutant/KD embryos described above. Whilst FN staining was not carried out in the YAP/TAZ KD zebrafish it is possible that FN assembly is also affected here and this therefore warrants further investigation.

5.5.4 Actin and myosin are affected in YAP/TAZ knockdown zebrafish embryos

Actin does not appear affected in the EVL so this raises the important question of why the EVL cells lose their shape. As discussed above myosin is required to cause contraction of the actin network within the cell. Even if actin is correctly polymerised in the cells of the EVL, if myosin is not properly activated, which appears the case in *hir*, and may also be the case in YAP/TAZ KD embryos, then the cells may be unable to maintain their shape against external forces. In some regards this is counterintuitive as if this is the case it might be expected that the pulling force of the YSL on the EVL would overly elongate the EVL cells. However, cells that are elongated in the animal-vegetal axis and narrower in the medio-lateral axis are not observed earlier in epiboly, even in the mutants/morphants. This may be explained by the fact that actomyosin flows seem affected in the YSL meaning the YSL may not be able to exert its normal pulling forces on the EVL.

Punctate actin in the cortex of the yolk cell of double zebrafish morphants appeared to be unevenly distributed, forming dense foci at several regions. This E-YSL actin, together with myosin, is important in establishing a retrograde flow along the vegetal-to-animal axis. This flow provides friction against which the blastoderm resists in order to propel itself vegetally (Behrndt *et al*. 2012). These flows are important early in epiboly (< 50%) when the actomyosin ring cannot exert its effect so strongly. It is therefore conceivable that these dense regions of actin correlate with disrupted actomyosin flows. However, since epiboly delay becomes more apparent from the 50% stage onwards when the actomyosin ring is more important for epiboly, it may mean these potentially disrupted flows play less of a part in the slow epiboly observed in YAP/TAZ KD embryos. If the flows were the major cause of slow epiboly we might expect to see a delay earlier in epiboly, perhaps from the 30-50% stage. It is currently unclear whether these flows contribute to the later stages of epiboly.

Myosin appeared mislocated in the DCs of double morphants and this became more prominent as epiboly proceeded (from 60% onwards). Concurrently DC epiboly became slower over this period. DC epiboly primarily relies on radial intercalations to cause thinning and spreading of the DCs over the yolk since this occurs independently from the overlying EVL (Warga and Kimmel, 1990). Radial intercalations have been shown to require actomyosin contractility (reviewed in Solnica-Krezel and Sepich, 2012). Since myosin appears affected in morphants this may be an underlying cause of the DC epiboly defect. pMRLC activity should therefore be examined in the morphant zebrafish to clarify this.

5.5.5 *In vivo* physical tension of actomyosin is reduced when YAP/TAZ levels are reduced

Direct physical measurements of actomyosin tension by UV laser cutting experiments showed that actomyosin tension is significantly reduced in the absence of YAP/TAZ, suggesting the contractility of actomyosin is indeed affected. Since myosin motors provide the contractility property of actomyosin networks, this in agreement with the findings that lower levels of myosin are phosphorylated and therefore active in the mutant. This is likely to be the major cause of the tension decrease observed in the various tissues of *hir*. It remains to be seen whether myosin recruitment during actin polymerisation is affected in the mutant. Since epiboly does finish in *hir* but not in mYAP KD *hir* this suggests that the actomyosin ring is further affected in maternal KD embryos. This could be confirmed by pMRLC western blotting and would further strengthen the argument for YAP regulating actomyosin activity.

The recoil velocity values obtained in wild type when cutting the actomyosin ring are in approximate agreement with previously published data from Behrndt *et al*. (2012). Additionally, it was observed that in approximately 13% of control cuts and 15% of morphant cuts there was a wound response. This was recognisable by a strong accumulation of actomyosin in a circumferential manner around the cut suggesting damage to the YSL. Where this was observed, the cut was rejected for analysis such that cytoplasm leakage through damaged membrane did not factor. Embryos were also quality controlled prior to cutting as the process of dechorionation itself could put mechanical stress on the embryo, including the EVL and actomyosin ring. In the morphants less elongated EVL cell shapes and a less straight/taut EVL margin along with slowed epiboly were used to confirm embryos with correct knockdown.

It has been shown that neighbouring cell changes trigger tissue shape alteration in 2D tissues, and this is controlled by anisotropic actomyosin mediated tension (Mayer *et al*., 2010). Furthermore, YAP has been shown to be activated by mechanosensory signals by the *in vitro* analysis of single cells in soft and hard environments (Dupont *et al*.,

2011). Therefore YAP may be the bridge between extrinsic mechanical cues and cellular responses to these signals. Further evidence for this role comes from *Drosophila* where it has been shown that F-actin polymerisation regulates Hippo signalling which in turn serves to feedback and regulate F-actin polymerisation (Sansores-Garcia *et al*., 2011; Fernández *et al*., 2011). Therefore the data presented in this chapter suggesting YAP regulates actomyosin is somewhat in agreement with these published reports linking the cytoskeleton with YAP. Interestingly, cortical actomyosin contractility has been shown to be important for rounding-up of cells, which does not seem affected in *hir* since cell proliferation is relatively normal. There may be another mechanism more important for rounding-up since general actomyosin activity is assumed to be reduced in *hir* due to reduced levels of pMRLC, therefore all processes involving actomyosin might be expected to be affected. Perhaps YAP may regulate the actomyosin network for certain processes but not all. This remains to be seen with further work on this interesting relationship.

5.6 Summary

- pMRLC activity is reduced in *hir* and potentially in YAP/TAZ knockdown embryos
- Actomyosin tension and localisation is perturbed in YAP/TAZ knockdown embryos
- These data suggest that YAP regulates actomyosin activity to provide tissue tension

Chapter 6: The *hirame* mutation of YAP acts in a non-cell autonomous manner

6.1 Aims

The Cuvierian ducts (CDs) and the eyes in *hir* present interesting and distinct phenotypes. Since YAP is suspected to be regulating certain components of the extracellular environment as detailed in Chapters 3 and 4, it was investigated whether YAP is acting in a cell- or non-cell autonomous manner for the formation of the CDs and eyes. It was also analysed what YAP may be doing to govern the extracellular environment in this context, and whether this role truly involves tissue tension regulation, as suggested by the previous results in Chapters 4 and 5.

6.2 Introduction

Determination of whether a protein is acting within the cell (autonomously) or outside the cell (non-cell autonomously) is important to truly understand its function. The technique of cell transplantation is often used to address this question. The theory behind these experimental techniques is best explained with an example (summarised in Figure 6.1). In this example it is hypothesised that there is a different type of host and donor. It is necessary to have wild type organisms and mutant organisms where the only difference is a mutation in one gene. To make firm conclusions about the autonomy of the mutation it is necessary to perform two sets of experiments. Firstly, transplanting cells from a wild type donor into a mutant host. Secondly, transplanting mutant cells (donor) into a wild type host. If wild type cells are transplanted into a mutant host/environment and rescue the phenotype of the mutant cells/tissues then it is interpreted that the mutation acts non-cell autonomously since the normal gene product (present in the wild type cells) can affect the behaviour of the surrounding mutant cells. It is likely that is something it can only do if exerting its function outside the cell. If no rescue occurs then the gene is thought to act cell-autonomously.

Conversely, when placing mutant cells into a wild type host, if the mutant cells are able to behave normally and integrate into wild type tissues then again the gene is presumed to act non-cell autonomously, since the wild type environment can rescue the function of the mutant cells. Oppositely, if the mutant cells are not rescued in the wild type host then again the gene product is likely acting cell-autonomously.

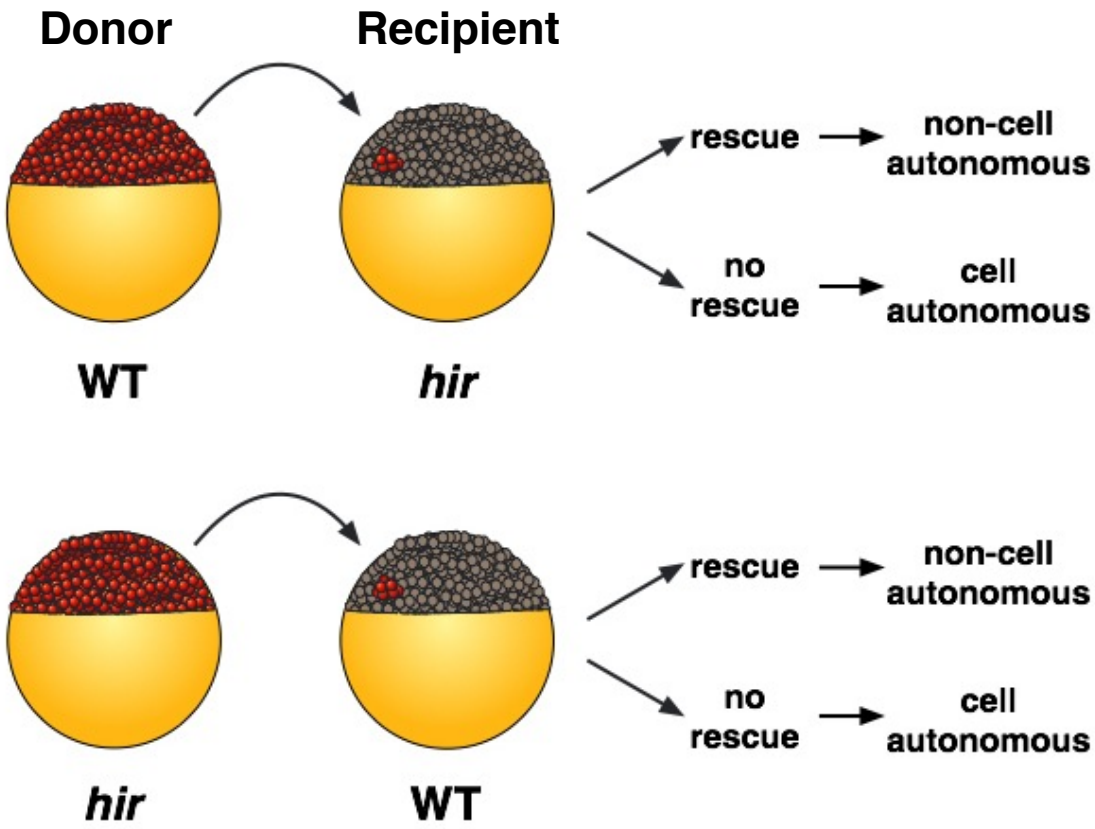

Figure 6.1. Transplantation experiments allow the determination of a gene or proteins autonomy. Schematic detailing how to interpret the results of heterogenetic cell transplantation experiments. In the top example, rescue refers to the *hir* phenotype in the targeted tissue. In the bottom example, rescue refers to whether the *hir* cells can functionally integrate into the wild type target tissue. Donor/transplanted cells are shown in red in the recipient.

6.2.1 The use of transplantation experiments to study developmental biology and gene/protein function

Many types of transplantation experiments have been carried out in the history of developmental biology, greatly deepening our understanding of how various mechanisms of vertebrate development occur. One of the most important findings as a result of transplantation experiments was that one group of cells could affect the development of a group of neighbouring cells. This phenomenon, known as induction was discovered in 1924 by Hans Spemann (Wolpert and Tickle, 2011, p.8). In these classical experiments, Spemann grafted tissue from the dorsal lip of the blastopore of one newt (*Triton cristatus*) to a different region of another newt at the same developmental stage. This grafted tissue induced a new body axis that contained a neural tube and somites (Wolpert and Tickle, 2011, p.8). This dorsal lip region became known as the Spemann organiser because of its ability to control the organisation of

the complete embryonic body and resulted in Spemann receiving the first ever Nobel Prize for embryology in 1935 (Wolpert and Tickle, 2011, p.8).

The tissue transplantation described above and the cell transplantation detailed in this chapter can have somewhat different aims. Cell transplantation experiments have been performed in vertebrates and invertebrates to answer several different and important developmental questions. For example, heterotopic cell transplantation allows the analysis of how the transplanted cells interact with the surrounding tissue, as well as lineage determination of cells within specific regions using tracers (Technau, 1987). Heterochronic transplantations can be used to assess whether the determination of transplanted cells is reversible or allow analysis of the time window in which certain cellular communication processes are functioning (Müller and Best, 1989). Interspecific cell transplantations have also been used to address the compatibility of functional mechanisms involving intercellular communication (Le Douarin *et al*., 1975; Becker and Technau, 1990). Finally, as described above in Section 6.2, heterogenetic cell transplantations allow the testing of the autonomy of phenotypes (e.g. Rosenberg *et al*., 1988).

Many of the currently used model organisms have emerged as useful exponents for transplantation experiments, including medaka, zebrafish, *Xenopus*, mouse and chick, with each offering different advantages. For example, the transparent nature of medaka and zebrafish embryos mean the labelled transplanted cells are easily traceable following the procedure, whereas the *Xenopus* is highly resistant to infection post-transplantation (Wolpert and Tickle, 2011, p.116). Grafting experiments in chick have shown that similar to *Xenopus*, the avian organiser (called Hensen's node) can induce an additional axis when transplanted at early stages (Wolpert and Tickle, 2011, p.177). In fact, the recently derived technique of somatic cell nuclear transfer (SCNT) could be considered a type of transplantation technique.

6.2.2 The medaka fate map of neurulation

Fate maps, that detail which cells of the early embryo will give rise to which tissues of the adult have been produced for medaka (Hirose *et al*., 2004), zebrafish (e.g. Woo and Fraser, 1995), *Xenopus*, mouse and chick (Wolpert and Tickle, 2011, pp.147-148). Because of the way cells mix during the blastula-to-gastrulation transition these fate maps can only be produced for the gastrula stages onwards and not during the cleavage stages of development (Wolpert and Tickle, 2011, p.147). Nevertheless, these fate maps are invaluable tools during transplantation experiments to ensure donor cells are transplanted to the correct location in the host/recipient such that the tissue of interest is properly targeted.

In medaka, the cells that give rise to the eyes originate in the deep cells of the neurogenic sector, an area of the blastoderm that can be distinguished by st.13 (13 hpf) as the area ±70° latitude relative to the dorsal midline/embryonic shield (Figure 6.2, Hirose *et al*., 2004). This sector of the blastoderm mainly gives rise to the neural and placodal tissues as demonstrated by Hirose *et al*. (2004). Specifically, the cells that will contribute to the retina are located in a roughly horseshoe shape near the centre of the neural sector at st.13 (13 hpf, Figure 6.2, green cells). This horseshoe arrangement of cells then starts to shorten in the animal-to-vegetal axis as well as narrowing in the medio-lateral axis as development proceeds from st.13-16 (13-21 hpf). By st.17 (25 hpf) the retinal precursors have coalesced at the embryonic midline in the eye field region. By st.19 (27.5 hpf) this single retinal compartment has been completely separated to give two distinct lateral groups that give rise to the bilateral retinas (Figure 6.2). This separation of the eye field is correlated with expression of *Pax6* in the cells that have moved laterally (Hirose *et al*., 2004).

Cells of the lens arise from a different region of the neurogenic sector to those of the retina (Hirose *et al*., 2004). The cells that will form the lens placode arise lateral to the more medially located retinal cells. These placodal cells form an oppositely orientated crescent shape relative to the retinal population (Figure 6.2, yellow cells). However, the placodal cells are also more clearly divided into several populations of cells along the axis between the animal pole and embryonic/dorsal shield (Figure 6.2). These different populations will give rise to the placodes of the eye and ear, as well as the peripheral nervous system. Like the retinal cells, the placodal cells converge towards the embryonic midline from st.13-17 (13-25 hpf) but remain as distinct populations along the forming antero-posterior axis. By st.19 (27.5 hpf) the cells that will give rise to the lens placode can be seen closely apposing the presumptive retina (Figure 6.2).

The endothelial progenitor cells that form the CDs arise from the lateral mesoderm as previously described in Chapter 3. In medaka it has not been previously shown how these cells migrate to lie close to the embryonic body or how they contribute to CD formation as the medaka fate mate focuses on cells with a neural fate (Hirose *et al*., 2004). In order to determine a suitable host location for the transplantation of cells to incorporate into the CDs, a zebrafish fate map detailing the origins of cells that give rise to an endothelial lineage was used (Warga and Nüsslein-Volhard, 1999). As there are some similarities between the fate maps of medaka and zebrafish, particularly regarding the presumptive retinal, telencephalon and diencephalon cells, Warga and Nüsslein-Volhard's zebrafish findings were used to direct the location of cells transplanted to hit the CDs in medaka.

6.3 Research questions

The aims of this chapter can be summarised by the following questions:

1. Does YAP act cell- or non-cell autonomously for the development of the Cuvierian ducts and eyes?

2. What could be the molecular or biophysical mechanism by which YAP acts autonomously or non-autonomously for the development of these tissues?

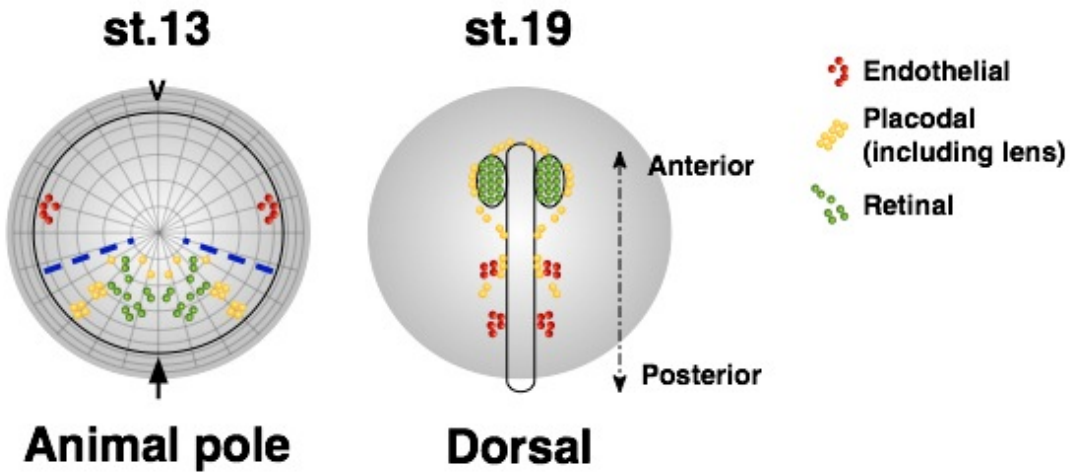

Figure 6.2. The medaka fate map of neurulation. Schematic showing the locations of cells at st.13 (13 hpf) that give rise to the retina and lens, as well as those of the endothelial lineage at st.19 (27.5 hpf). Red cells at st.13 show where endothelial cells arise from in zebrafish according to Warga and Nüsslein-Volhard (1999). Perspective is indicated under each illustration. Arrow indicates the location of the dorsal lip at st.13. Blue dashed line indicates the neurogenic sector. The yolk is represented by the grey sphere. Animal pole shows view looking down onto blastoderm. V: ventral. Based on Hirose *et al*. (2004).

6.4 Results

6.4.1 Wild type cells transplanted into *hirame* can rescue the phenotype of mutant tissues/organs, namely the Cuvierian ducts and eyes

To further understand the cellular mechanisms underlying the *hir* phenotype and given that *hir* displays defects in the ECM, it was investigated whether the *hir* mutation acts cell- or non-cell autonomously using cell transplantation. Cells from the blastoderm of st.12 (10 hpf) wild type embryos were transplanted into the blastoderm of st.12 (10 hpf) *hir* embryos and vice-versa to examine whether wild type cells could rescue the *hir* phenotype, and whether *hir* cells could function normally in a wild type environment (Figure 6.3a). Stage 12 embryos were used since by this point the presumptive dorsal lip can be identified allowing more accurate transplantation of cells. Different areas of the recipient blastoderm were targeted such that donor cells would integrate into either the CDs or the eyes (Figure 6.3b). These structures were targeted as both have very distinct phenotypes of low variability in *hir* and phenotypic rescue would therefore be easier to assess. Both tissues are also readily accessible for cell behaviour study.

When transplanting approximately 15 cells from wild type to target the *hir* CD, the presence of wild type cells in the area surrounding the *hir* CD could partially rescue the structure such that it was extended more anteriorly than normally seen in *hir* (42% of transplants, 5/12 embryos, Figure 6.4a, compare *hir* control in top left panel with *hir* showing rescue in top right panel). Interestingly, it was also found in several *hir* embryos transplanted with wild type cells that the mutant CD appeared to extend directionally in an anterior way towards the wild type cells over the course of several hours (25% of transplants, 3/12 embryos, Figure 6.4a bottom panels). When transplanting similar numbers of cells in the opposite direction, from *hir* to wild type, *hir* cells were able to fully integrate into the wild type CD to form part of the fully functioning structure (39% of transplants, 46/119 embryos, Figure 6.4b). In particular it was observed that the transplanted *hir* cells appeared able to integrate into the wall of the vessel comprising the CD (Figure 6.5 asterisks), as well as contributing to the circulating blood cell population found within the lumen of the CD (Figure 6.5 arrowheads). Transplanted *hir* cells also appeared to display the ability to act as pericyte cells as assessed by morphology (Figure 6.5 arrow). Pericytes communicate with endothelial cells of the blood vessels through direct physical contact as well as paracrine signalling (Bergers and Song, 2005). However, the identity of these peripheral cells was not confirmed so it is speculative to suggest they are pericyte cells. These results suggest the ability of wild type cells transplanted into *hir* to rescue the mutant CD, and that the wild type environment can rescue the behaviour of *hir* cells when acting as a host. This is a somewhat surprising finding as YAP is an intracellular protein.

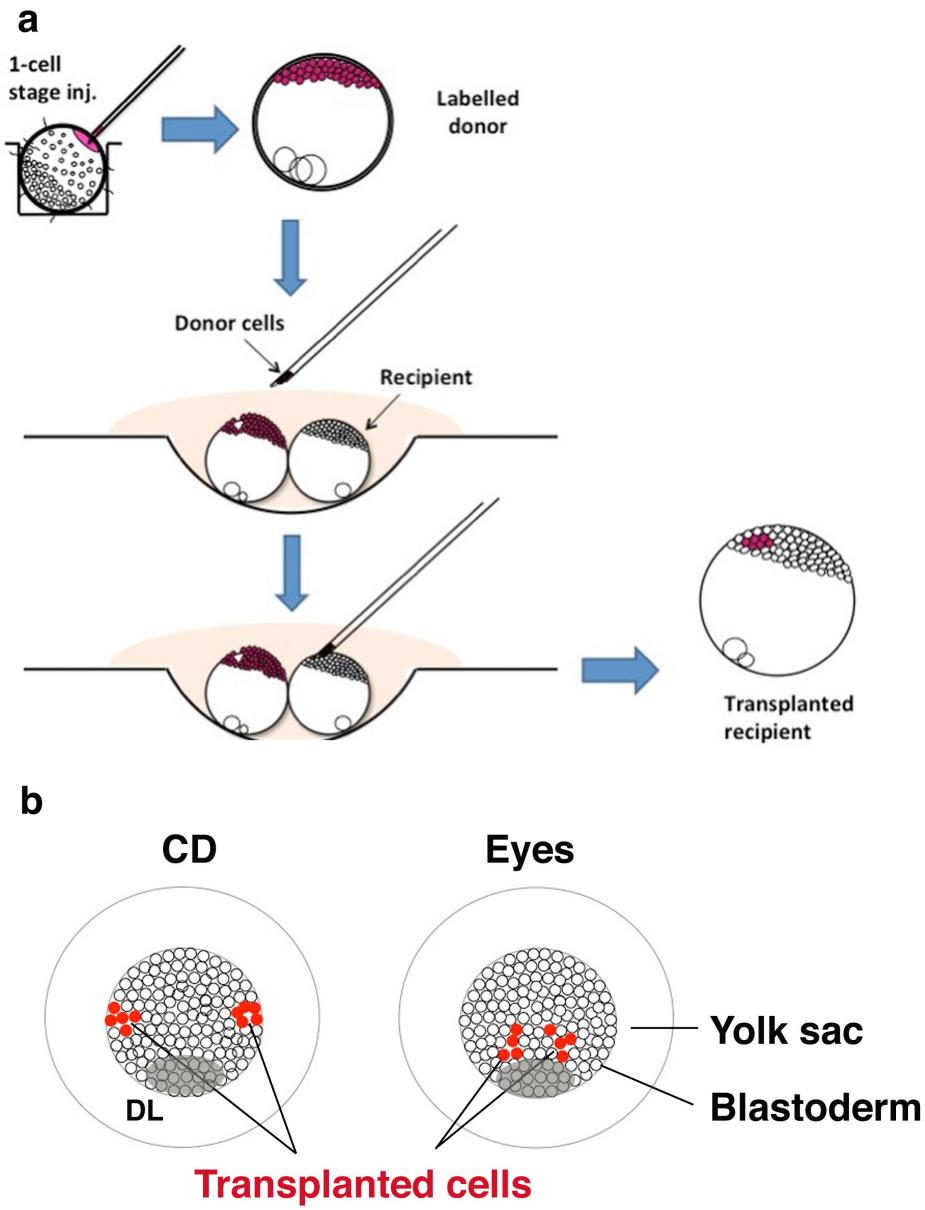

Figure 6.3. Schematic outlining the transplantation approach used. (a) Steps involved in cell transplantation. First, donor cells should be suitably labelled with a tracer, e.g. fluorescent rhodamine-dextran. Alternatively, transgenic GFP cells can be used as donors. Donor and recipient embryos should be developed to a suitable stage (e.g. st.12, 10 hpf). An appropriate number of cells should then be taken from the donor blastoderm using a fine glass pipette and transferred to the recipient blastoderm such that the tissue of interest is targeted. Recipient embryos should then be developed until the target tissue becomes visible to allow assessment of phenotypic rescue. **(b)** Animal pole views of st.12-13 embryos (10-13 hpf) showing the placement of donor cells within the recipient blastoderm in order to target the CDs or eyes. Shaded area represents the dorsal lip (DL).

Transplanted wild type cells (approximately 5) could also rescue *hir* eye formation, though several variations of rescue based on the location of transplanted wild type clones within the mutant eye were observed. The presence of just a single clone in the mutant lens (Figure 6.6, asterisk), along with just a few clones in the retina (Figure 6.6, arrows), was sufficient to rescue the *hir* eye to the extent that the lens completely invaginated into the retina and did not dislocate (as shown in Figure 6.6 left panel, arrow). Moreover, the shape of the rescued *hir* retina in these embryos much more closely resembled that of the wild type, as basal constriction of the retina seemed to occur properly to form the optic cup in which the lens was positioned (compare middle panel of Figure 6.6 with left panel of *hir* control). The size of both the lens and retina were comparable between rescued mutant eyes and wild type eyes (Figure 6.6 middle and right panels). When transplanted wild type cells were present in both the lens and retina almost complete rescue was recorded at a frequency of 100% (5/5 embryos, Figure 6.7b). However, when transplanted wild type clones were present only in the retina of *hir* recipients, partial rescue of mutant eye development was observed in only 22% of *hir* recipients (5/23 embryos, Figure 6.7b and Figure 6.8a'-b'). In this incomplete rescue, the lens partially invaginated into the retina but there appeared to be a lack of basal constriction of the retina to form the cup shape seen in wild type (Figure 6.8a'-b'). Again the size of the lens and retina in this partial *hir* rescue was comparable to that of wild type. This reduced level of rescue was particularly evident in embryos that had transplanted clones in the lens and retina of one eye but only in the retina of the other eye allowing direct comparison of the phenotypic rescue (Figure 6.8a'-c').

Unfortunately it was extremely difficult to target transplanted wild type cells to the *hir* lens alone, possibly due to the manner in which the mutant placode arises as described previously in Chapter 4. This meant it was not possible to assess whether there was any phenotypic rescue effect of wild type clones only in the *hir* lens. Such data may have provided interesting and important clues about the role of YAP in eye formation through signalling between the lens and retina, which has been well documented by Chauhan *et al*. (2009) as described in Chapter 4. Taken together with the CD transplantation data, these results for the eye demonstrate the requirement of YAP for the proper formation of the CDs and the eyes, and imply a non-cell autonomous function for YAP in normal development of the CDs and eyes. These data also suggest that YAP may be acting in a long-range manner for the rescue of the CD since the mutant CD migrated towards the transplanted cells which were located relatively anteriorly. To some extent YAP may also have longer-range effects in the rescue of the eye. This is due to the correlation between both clone number and location and the level of rescue, meaning even relatively few transplanted cells or cells located more distally within the tissue could still permit rescue.

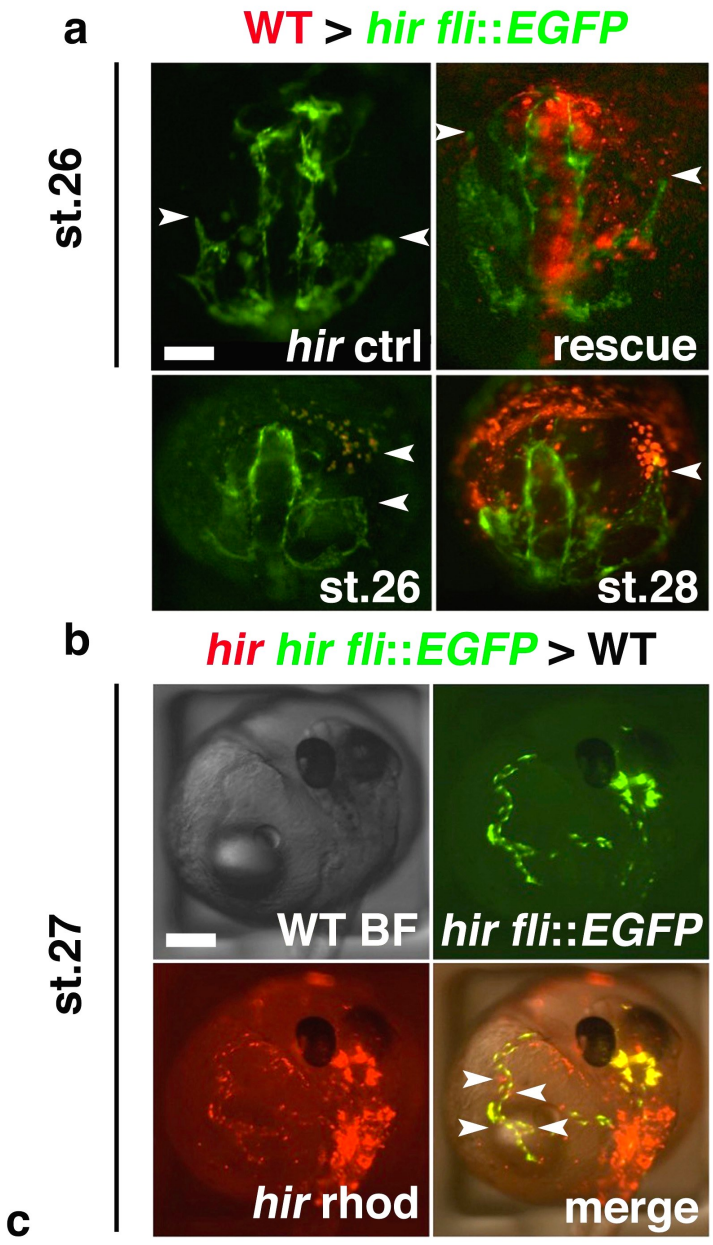

c

Type of transplantation	WT > *hir*	*hir* > WT
Recipients with transplanted cells in the CD (n)	12	119
% of recipients rescued/WT with integrated *hir*	42	39

Figure 6.4. Wild type cells partially rescue the truncated CDs in *hirame* and *hirame* cells can integrate into the wild type CDs. (a) Wild type cells in the tissue surrounding the mutant CDs cause them to extend anteriorly. In some cases (lower panels) the ducts in *hir* appear to extend towards the wild type transplanted cells. Views are dorsal and arrowheads indicate most anterior tip of duct. **(b)** Mutant cells are able to incorporate into the wild type CDs. View is dorsolateral. Arrowheads demarcate the left CD. **(c)** Table showing the numbers of successful

transplants and the rescue/integration frequency. Scale bars: 100μm. Anterior is up and posterior is down in all images.

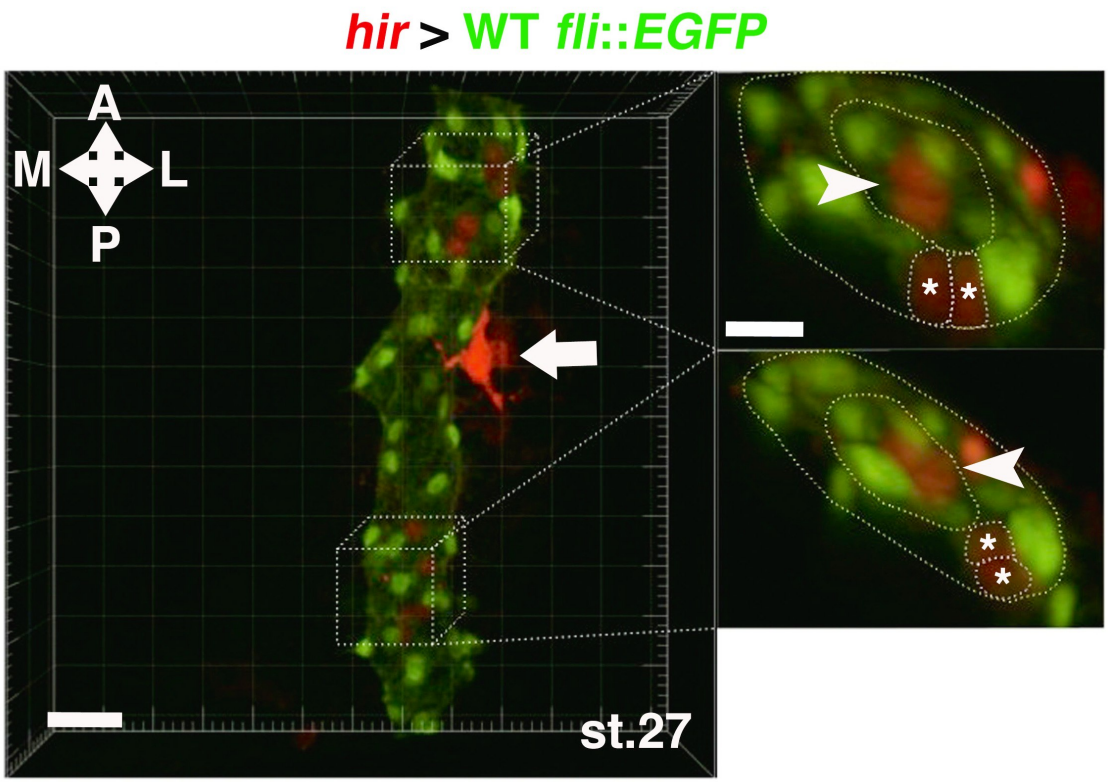

Figure 6.5. Transplanted *hirame* cells are able to incorporate into the wild type Cuvierian ducts. Confocal image showing transplanted *hir* cells integrate into the wild type CDs. Cross sections through the duct (right panels) reveal the *hir* cells are incorporated into the vessel wall but may also contribute to the circulating population of endothelial cells. A: anterior; P: posterior; M: medial; L: lateral. Scale bars: (main panel) = 40μm; (cross sections) = 10μm. View is dorsal. Arrow indicates a potential pericyte formed from a *hir* donor cell.

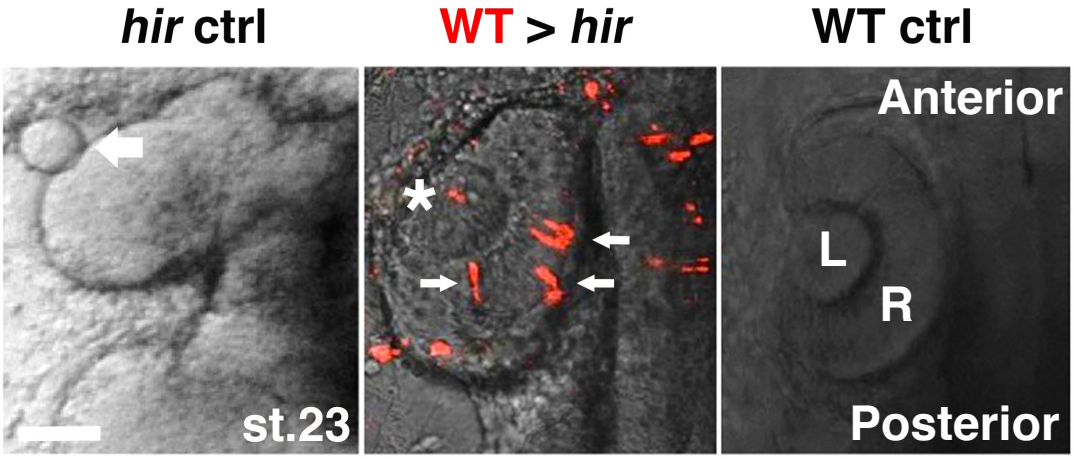

Figure 6.6. Transplanted wild type cells can rescue the *hirame* eye. Wild type clones (red) in the lens (L, asterisk) and retina (R, arrows) of *hir* (middle panel) almost fully rescue the mutant eye. Arrow in left panel indicates dislocated lens. Scale bar: 20μm. Views are dorsal.

6.4.2 Tissue tension reductions in *hirame* may be rescued by the presence of transplanted wild type cells

The data reported in Chapters 4 and 5 strongly suggests that epithelial tissue tension in *hir* mutants is decreased. It was decided to ascertain whether the mode of *hir* phenotype rescue by transplantation is tension-dependent. As such this was investigated in more detail using further transplantation experiments. Transplantation of wild type cells with reduced levels of components important for regulating tension, into *hir* was performed to observe whether phenotypic rescue still occurred. This was carried out in the eye, as the phenotypic rescue here was more dramatic than seen in the CDs and thus easier to assess.

6.4.2.1 Tension-reduced wild type cells cannot rescue the *hirame* eye phenotype

Since the myosin regulatory light chain (MRLC) and myosin heavy chain (MYH) are essential components of actomyosin, which is a major determinant of cellular and thus tissue tension, these components were disrupted in wild type cells prior to their transplantation into *hir*. This was done by injecting wild type embryos with a translation-blocking morpholino against MYH9a and MYH10 (MYH9a/10 TBMO), and also by injecting an RNA variant of MRLC (known as MRLC AA) which phosphomimics the unphosphorylated and inactive form of MRLC as in Chapter 5. Knockdown was confirmed by developing and checking the phenotype of donors post-transplantation. MYH9a/10 knockdown (KD) and MRLC AA wild type donors exhibited slow epiboly as seen in *hir* where actomyosin activity is reduced.

Transplantation of either wild type MYH9a/10 KD or MRLC AA cells could not rescue the *hir* eye phenotype as assessed at st.22 (38 hpf). This non-rescue was observed in all mutant host embryos where MYH9a/10 KD (4/4 embryos) and MRLC AA (5/5 embryos) clones were present in the mutant eye (Figure 6.7a and b). As FN fibrillogenesis is directly linked to cellular/tissue tension and feeds back through integrin, it was tested whether cells incapable of FN fibrillisation could rescue the *hir* eye phenotype. This transplantation also served as a means of strengthening the above results that may suggest that FN fibrillogenesis is somewhat partially restored in *hir* mutants hosting wild type cells. To achieve FN KD, the FN 70kD fragments utilised in previous chapters was injected into wild type embryos. As for the tension-deficient cells, it was found that FN KD cells could not rescue the *hir* eye phenotype (3/3 embryos, Figure 6.7a and b). This failure of KD wild type cells to rescue the mutant phenotype was not due to a failure of wild type cells integrating into the recipient mutant tissue. Furthermore, all types of KD wild type clone appeared to exhibit a lesser degree of elongation when compared with normal wild type clones in *hir.* This suggests that these transplanted KD wild type cells did indeed have reduced tension (compare morphology of transplanted cells in panels of Figure 6.7a). However, quantification of

transplanted cell elongation by LWR measurements needs to be performed to confirm this.

Taken together these results suggest a non-cell autonomous role for YAP and that the *hir* eye phenotype is at least in part, due to reduced tissue tension.

a

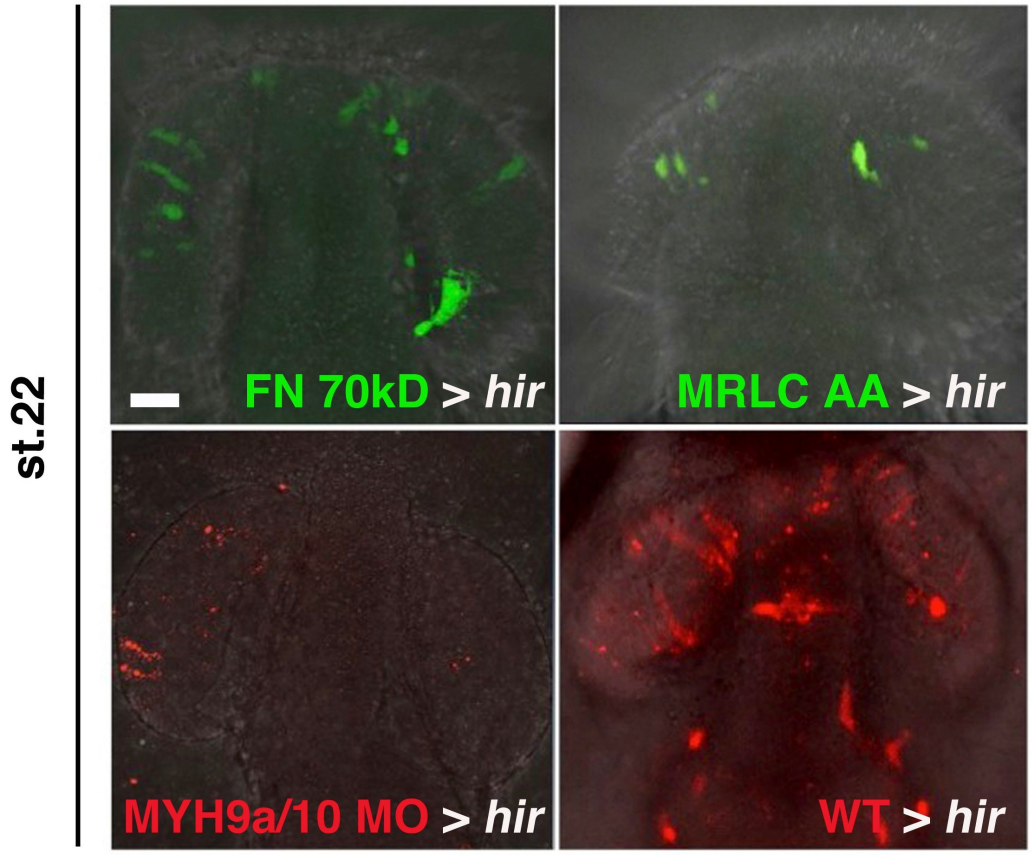

b

Type of transplantation	FN 70kD > *hir*	MRLC AA > *hir*	MYH9a/10 MO > *hir*	WT > *hir* (lens & retina)	WT > *hir* (retina only)
Recipients with transplanted cells in eye (n)	3	5	4	5	23
% of recipients rescued	0	0	0	100	22

Figure 6.7. Tension-deficient cells are unable to rescue the *hirame* eye phenotype. (a) Wild type cells deficient in tension (MYH9a/10 MO and MRLC AA) are unable to rescue the *hir* eye phenotype. Furthermore, cells with compromised ability to assemble FN also do not rescue the mutant eye (FN 70kD). This suggests a role for tension-mediated FN fibrillogenesis in rescuing the eye of *hir*. All views are dorsal with anterior up and posterior down. Scale bar: 10μm. **(b)** The number of transplants and the rescue frequency is shown in the table.

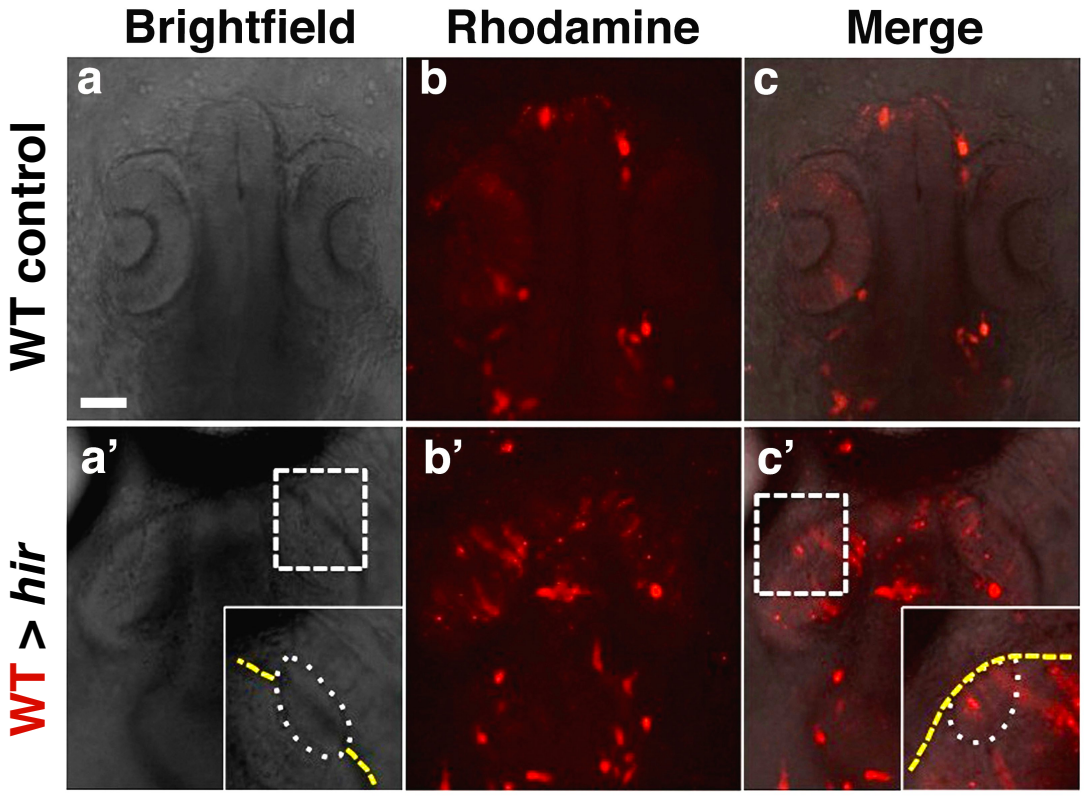

Figure 6.8. Transplanted wild type cells are required in the lens and retina for nearly complete rescue of the mutant eye. (a-c) Wild type transplanted control embryos showing the procedure of transplantation itself does not affect normal morphology. **(a'-c')** Varying degrees of rescue depending on the location of wild type cells in the mutant eye. Rescue of the left eye is more complete (c') where wild type clones are present in the lens and retina as indicated by more complete invagination of the lens (demarcated by white dotted line) into the retina (yellow dotted line). In the right mutant eye where clones are only apparent in the retina the lens remains only partially invaginated (a'). Views are st.23 dorsal with anterior up. Scale bar: 30μm.

6.4.3 Mosaic expression of YAP in *hirame* mimics the rescue seen by cell transplantation

Since cell transplantation produces mosaic wild type clones in *hir*, it was reasoned that expressing YAP mosaically in the mutant should have a similar effect. To do this, two approaches were utilised. Firstly, mRNA encoding GFP-tagged wild type YAP (YAP-EGFP, 100μg/μl) was injected at the 8-cell stage to randomly give rise to YAP expressing clones throughout the embryo at a lower frequency, comparable to that observed during transplantation. Secondly, DNA encoding a hyperactive form of YAP, called YAP5SA, tagged with GFP and under the control of the *Sox3* promoter was injected at the 8-cell stage (*Sox3*::*YAP5SA-EGFP*). This constitutively active form of YAP cannot be phosphorylated by the Hippo pathway as all five serine residues where phosphorylation normally occurs have been mutated to alanine (Dong *et al*., 2007;

Zhao *et al*., 2007), and thus YAP5SA cannot be sequestered in the cytoplasm. The *Sox3* promoter allows for a more tissue-targeted and efficient approach as it was decided to again use the eye as a measure for phenotypic rescue and *Sox3* is expressed in the placodes of several developing tissues early in medaka development (Koster *et al*., 2000), including the lens placode.

Both 8-cell YAP-EGFP and *Sox3*::*YAP5SA-EGFP* injection rescued the *hir* eye phenotype to a similar level as observed during the cell transplantation experiments (Figure 6.9a and b). For rescue by YAP-EGFP, it appeared several clones were required in the lens and retina (2/12 *hir* embryos rescued, Figure 6.9b), similar to what was seen for the transplantation experiments. Furthermore, FN staining was performed on these rescued embryos and more convincingly showed that FN fibrillisation appeared somewhat restored (Figure 6.9b). This is demonstrated in Figure 6.9b where the green FN staining can be compared between the rescued *hir* on the right and the wild type control on the left. In the rescued *hir* the fibrils have a much smoother and finer appearance similar to that in the wild type and in stark contrast to the coarse and spiked fibrils normally seen on the *hir* eye (e.g. Figure 3.7). Interestingly and unlike in the transplantation experiments, a difference in the level of rescue was less evident using the mosaic *Sox3*::*YAP5SA-EGFP* injection. Single YAP5SA clones in the lens (5/20 *hir* embryos rescued) or retina alone (also 5/20 *hir* embryos rescued) appeared to produce a similar level of rescue, perhaps indicating a potency of the hyperactive YAP5SA (Figure 6.9a). YAP5SA rescue was not however complete. This may be explained by the low concentration (30µg/µl) of DNA that was injected due to the somewhat toxic nature of the construct. This data remains preliminary and requires further investigation using other YAP variants (e.g. S87A) to confirm phenotypic rescue and restoration of FN fibrillogenesis.

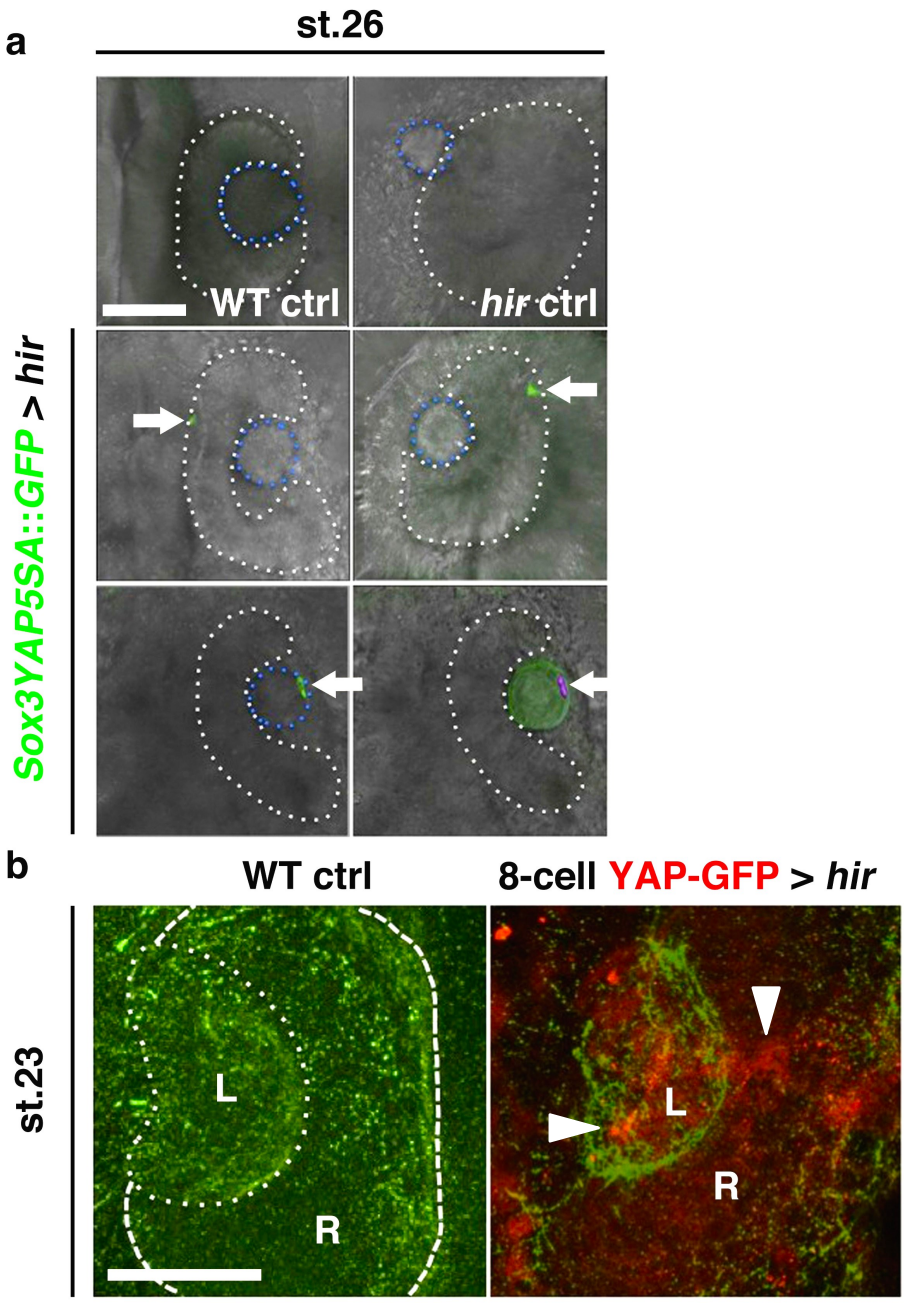

Figure 6.9. Mosaic expression of YAP variants in *hirame* can also rescue the mutant eye phenotype. (a) Top panels show wild type and *hir* control eyes for comparison purposes. The presence of YAP5SA in the retina alone could cause a relatively high degree of rescue (middle panels) though the lens was not as encompassed by the retina as in wild type. Similarly, when YAP5SA clones were present only in the lens (bottom panels), basal constriction of the mutant retina and lens invagination occurred. In the bottom right panel the lens and a YAP5SA-expressing clone are 3D-rendered in green and purple respectively. Arrows indicate GFP expressing clones. The lens is demarcated by a blue dotted line and the retina by a white dotted line. **(b)** Wild type YAP injection into *hir* showing rescue of retinal constriction and lens invagination. Examples of clones (red) present in the lens and retina are indicated by arrowheads. FN antibody staining is shown in green and appears finer and more even than normally seen in *hir*. L: lens; R: retina. All views are dorsal with anterior upwards. Scale bars: (a) = 40μm; (b) = 30μm.

6.5 Discussion

6.5.1 YAP has a non-cell autonomous function

Since the data in Chapter 3 suggested YAP is regulating FN fibrillogenesis, it was analysed whether YAP can indeed act non-cell autonomously as might be expected from these prior FN results. To this end, cell transplantation experiments were performed using wild type cells as donors and *hir* as recipients, as well as vice-versa. Cell transplantation experiments show *hir* cells appear to function normally in a wild type environment, integrating into wild type tissues such as the CDs and the neuroepithelium to form part of a fully functioning tissue/organ. More work is needed to ascertain whether *hir* cells can also integrate into other wild type structures (e.g. the eyes and otic vesicles), which are normally affected in *hir*. It is however, anticipated that this will likely be the case. Wild type cells transplanted into *hir* could rescue several aspects of the mutant phenotype, namely the invagination of the lens into the retina and basal constriction of the retina, as well as to a lesser extent, anterior movement of the CDs. These findings imply a non-cell autonomous role for YAP.

This conclusion is reached in the following ways. Firstly, when *hir* cells are transplanted into wild type embryos the wild type cellular environment is able to restore *hir* cell function. This means something surrounding the mutant cells is directing them to behave correctly. Furthermore it also suggests that *hir* cells can respond to extracellular cues which is somewhat contradictory to data published by Dupont *et al*. (2011) which inferred that YAP acts to sense mechanical cues in the cell's environment. Another possibility is that the cue the *hir* cells are responding to within the wild type environment does not act through YAP or may not be mechanical in nature. However, this seems less likely as the data in this chapter and Chapter 4 present several lines of data strongly suggesting YAP is regulating tissue tension. Furthermore tension-compromised wild type cells cannot rescue the mutant eye phenotype. Thus it seems plausible that the mode of rescue may be tension related, i.e. through wild type cells transmitting tension upon *hir* cells. This does however remain to be seen as the direct cause of the rescue.

It may also be possible that rescue of the mutant involves fibronectin (FN) fibrillogenesis, which appears partially restored in the *hir* tissues containing cells expressing wild type YAP, but requires further investigation in mutant embryos rescued by transplantation. Wild type cells may be restoring lost tension in the mutant host tissue, possibly causing downstream assembly of FN. It is also possible however, that the extracellular component resulting in rescue of the mutant phenotype may be a non-cell autonomous secreted factor regulated by YAP, such as amphiregulin (AREG). AREG has previously been shown to be a transcriptional target of YAP, and YAP-expressing immortalised mammary epithelial cells induce AREG-mediated proliferation

and migration in neighbouring cells (Zhang *et al*., 2009). It remains to be seen whether AREG is affected in *hir* and if AREG is indeed involved in the rescue of the mutant phenotype by transplanted wild type cells, then the mechanism of this rescue requires determination. Such a non-cell autonomous function of YAP has so far only been conclusively shown *in vitro*. However, a positive correlation between TAZ and AREG has been shown *in vivo* in breast cancer samples (Yang *et al*., 2012).

Secondly, when wild type cells are transplanted into *hir* the mutant cells are again able to respond to cues provided by the wild type cells. In the case of the eye, the rescue of the mutant phenotype by this transplantation is quite striking from a gross morphological perspective. Whilst the rescue of the mutant CDs by wild type cells was not as complete as the eye, it still demonstrates an ability of the *hir* cells to respond to potentially long distance signals, since the mutant CDs migrated towards the transplanted cells, which were located relatively anteriorly. Perhaps in this instance the rescue was less complete as the cue provided by wild type cells is not transmitted as well over such a large distance. Whereas in the mutant eye where the wild type cells are directly incorporated into the organ themselves, the cue is more easily transferred resulting in a more complete rescue.

The mosaic expression of wild type YAP and YAP5SA acted as an important control for confirming the observations of the transplantation experiments. This is because using this system expresses YAP mosaically, as in the transplants, but rules out the possibility of the transplantation procedure itself having any affect on the mutant phenotype. It is interesting to contemplate whether the addition of extra cells plays any role in increasing the tension of the host tissue due to spatial constraints. In this case this may not be relevant due to the low number of cells being transplanted. Finally, what could be the reason for why wild type cells successfully incorporated into the desired mutant target tissue did not rescue the mutant phenotype in all cases? This was evident in both the CD and the eye when only the retina was hit where overall rescue frequencies for wild type to mutant transplants were 67% and 22% respectively.

A previous report from Cecilia Moen's group showed both a cell and non-cell autonomous function during transplantation, dependent on the number of cells transplanted (Žigman *et al*., 2009). They described that when transplanting *cdh2*$^{-/-}$ or *mzscrib* mutant cells into a wild type environment, the *cdh2*$^{-/-}$ and *mzscrib* cells could behave normally if four or fewer cells were transplanted. When higher numbers were transplanted the mutant cells were not rescued. Therefore it is possible that a similar community effect may be occurring in the transplantation experiments described in this chapter. For example, in the non-rescue cases, maybe an insufficient number of wild type cells were located in the mutant host tissue and were therefore unable to exert a

significant enough effect on the surrounding mutant cells. Though this is somewhat contrary to the results in the eye where just a few wild type cells could strongly rescue the mutant phenotype. However, tissue size and location may be important here. Chauhan *et al*. (2009) previously showed the filopodia between the lens and retina mostly originate from the lens. Perhaps wild type clones are required in the lens to cause sufficient tension for FN-integrin signalling and the production of filopodia. These filopodia then allow communication between the lens and retina leading to coordinated morphogenesis and rescue of the mutant eye. Furthermore, since the lens is smaller than the retina it may require less wild type cells to be present to significantly raise the tension of the tissue. This may also explain why cells in the retina alone do not result in a higher level of rescue. Another reason may be that fewer of the filopodia between the lens and retina originate from the retina. Therefore even if the tension is somewhat raised by wild type cells in the mutant retina and filopodia form from this tissue, this cannot be as effectively transmitted via the fewer filopodia to the lens resulting in a weaker rescue. Perhaps there is a different threshold for the number of cells required to rescue the eye versus the CDs.

Finally, the mosaic expression of wild type YAP and YAP5SA also yielded somewhat lower rescue frequencies. In the case of the injected wild type YAP it is possible that phosphorylation occurred since the status of the more upstream components of the Hippo pathway remains unknown in *hir* but is presumed to be functioning. The YAP5SA DNA was found to be toxic during optimisation meaning only a low concentration (30µg/µl) could be used. Perhaps this reduced the efficacy of rescue. Further investigation using other potentially less toxic but hyperactive medaka YAP variants (e.g. S87A) to confirm phenotypic rescue and restoration of FN fibrillogenesis is required.

These transplantation results support a role for YAP as a key regulator of organ size as in order to fulfil this role YAP would need to be able to regulate the surrounding extracellular environment of cells, tissues and organs – a non-cell autonomous function. This in turn would permit changes in size and shape to occur as development proceeds. This non-cell autonomous finding is interesting however, as it is somewhat contrary to what has largely been thought to be a cell-autonomous role for the Hippo pathway and YAP (Zhao *et al*., 2010a). Thus this finding may add to what is a growing and extensive repertoire of functions proposed for YAP.

6.6 Summary

- YAP acts in a non-cell autonomous manner for the development of the eyes and Cuvierian ducts
- Transplantation of wild type cells into *hir* can rescue the phenotype of the mutant eye and Cuvierian ducts
- YAP appears to cause this rescue by regulating tension via actomyosin activation, which may in turn lead to the regulation of proper fibronectin fibrillogenesis

Chapter 7: General discussion

7.1 The *hirame* phenotype and its underlying causes

The *hir* mutant is unique in phenotype and allows dissection of the role of YAP in organogenesis since mutants survive until 6 days post-fertilisation (when most organs are present) unlike YAP knockout mice which die at E8.5 (Morin-Kensicki *et al*., 2006). The mutant displays several prominent traits as part of its complex phenotype. The main traits being epithelial tissue and organ collapse, tissue mislocalisation and cell migration defects. Organ and tissue collapse is seen most clearly in the neural tube (NT), somites and eyes. Tissue mislocation is most evident with the lenses dislocating from the retinas and the ears failing to invaginate into the hindbrain. Cell migration defects are plainly observed in the formation of the Cuvierian ducts (CDs) and the heart. The major features of the *hir* phenotype and their possible causes are summarised in Table 7.1. This thesis has examined the NT, eyes, ears (to some extent) and the CDs but due to time constraints could not yet address the defects underlying the somites and heart. Therefore the causes of the phenotypes in these tissues/organs are speculative but based on their apparent similarity to the phenotypes observed in other tissues, the underlying mechanisms may be similar.

7.2 Can a reduction in actomyosin-dependent tension explain all aspects of the *hirame* phenotype?

As outlined in Table 7.1, several of the features of the *hir* phenotype indicated reduced tissue tension in the mutant, including epithelial tissue/organ collapse, rounder epithelial nuclei and loss of oriented cell division. Indeed, the activation status of the myosin regulatory light chain (MRLC), key for regulating non-muscle myosin II function, in particular its role in providing contractility for the actin cytoskeleton, is drastically reduced in the *hir* mutant. This, together with *in vivo* experiments assessing the tension of the actomyosin network following YAP knockdown, suggest that tissue tension via actomyosin is in fact reduced in *hir*. Most aspects of the *hir* phenotype appear to be the consequence of this reduction in tension. As such, the features of the mutant will now be briefly discussed in light of tension/actomyosin and a general model to link the possible cascade of events causing the *hir* phenotype will be proposed (Figure 7.1a).

Trait of *hirame* phenotype	**Possible causal defect**
Tissue and organ collapse:	
1. Neural tube	Actomyosin activity reduction (leading to aberrant division plane, failure of cell stacking, cell slippage and overall reduced tissue tension indicated by rounder nuclei).
2. Eyes	Actomyosin activity reduction (leading to aberrant division plane and overall reduced tissue tension indicated by rounder nuclei).
3. Somites	Actomyosin activity reduction (leading to aberrant division plane, cell slippage and overall reduced tissue tension since somites display a similar collapse phenotype to the NT exhibiting flattening and widening)?
Tissue mislocalisation:	
1. Lens	FN fibrillogenesis defect (leading to disrupted filopodia formation and dislocation of tissue).
2. Ears	FN fibrillogenesis defect?
Cell migration defects:	
1. Cuvierian ducts	FN fibrillogenesis defect (leading to disrupted polarity and lack of migration).
2. Heart	FN fibrillogenesis defect?

Table 7.1 Summary of the *hirame* phenotype and the potential underlying causes. The *hir* mutant displays three major traits: tissue/organ collapse, tissue mislocation and cell migration defects. Reduced actomyosin activity is likely to lead to reduced tissue tension and collapse of the neural tube (NT) – i.e. widening and flattening, as well as flattening of the eyes and somites. Lens and ear dislocation are suspected to be a consequence of fibronectin (FN) fibrillogenesis defects which mean filopodia between tissues and cell-ECM adhesions do not form due to affected fibronectin-integrin signalling. Subsequently tissues are not spatially organised to undergo coordinated morphogenesis. Finally, cell migration defects may be caused by FN fibrillogenesis defects resulting in a loss of polarity and an aberrant migration substrate.

Reduced overall tissue tension is the most probable cause of the epithelial tissue and organ collapse observed in *hir*. If tissues and organs do not have the proper mechanical strength/rigidity then they may simply lose their 3D shape. In line with this, gravitational forces influenced NT collapse in *hir* causing flattening aligned with the external force. Actomyosin is a key regulator of cellular and thus tissue tension (Salbreux *et al*., 2012) and the lack of contractility of actomyosin in *hir* may mean that maintenance of organ/tissue shape cannot occur, as rigidity is low. Furthermore the morphogenesis required for coordinated growth is also affected in *hir*. Again actomyosin is important in this process for changing cell shape and sculpting tissue morphology (Wolpert and Tickle, 2010, p.291). Reduced actomyosin tension within individual cells is also a likely cause of the rounder nuclei observed in the mutant neuroepithelial cells, as well as the less elongated cells of the enveloping layer of *hir*.

Non-muscle myosin II phosphorylation is required for filopodia formation (Ridley *et al*., 2003) but is reduced in *hir*. This finding is in agreement with data from the eye where it appears that filopodia number may be decreased, but is not consistent with the CD observations where there are increased numbers of filopodia. It may be possible that different mechanisms are more important for filopodia formation in the CDs. For example, perhaps the ECM has a greater role in filopodia formation in these migratory endothelial cells and the aberrancy of fibronectin (FN) polymerisation in the mutant has a more important effect on the production of extensions by the endothelial cells. Such a possibility is somewhat supported by the fact that in *Xenopus*, FN knockdown causes an increase in actin-rich cellular extensions (Davidson *et al*., 2006). Whilst this is a slightly different scenario to *hir* where FN levels are not reduced but instead fibrillisation seems affected, the net result may be similar as both cases may result in reduced functional FN in the ECM for orchestrating cell behaviour.

Tension is also required for polarised collective migration (Weber *et al*., 2012) and actomyosin build up has been observed close to where migrating cells are tethered suggesting tension build up and transmission in such systems (Michael Smutny, *personal communication*). The tension reduction in *hir* may partly contribute to the CD migration defect if this system involves collective migration for its development. Moreover, since actomyosin activity is required for suppressing lateral membrane protrusion formation in migrating cells (Ridley *et al*., 2003) and is reduced in *hir*, this could be the cause of the ectopic and abundant extensions formed in the *hir* endothelial cells. Further support for this comes from Kubow *et al*. (2013) who very recently reported that myosin activity is important for cells to form mature adhesions on 3D substrates. They found that in the human osteosarcoma U2OS cell line, activation of MRLC (using the DD variant) resulted in cells with significantly less protrusions. However, Kubow *et al*. (2013) also noted that matrix fibre architecture, in particular

orientation, was important for mediating adhesion maturation. Again this suggests that the high protrusive activity seen in the mutant CD cells could be a combinatorial effect of reduced NMII activity and defective FN fibrillisation.

In *Xenopus*, when actin polymerisation is blocked by cytochalasin D, thicker and longer aberrant cables of FN are observed (Davidson *et al*., 2008), similar to those seen in *hir* around the CD and eyes. This suggests an actomyosin defect could be to blame for the apparent lack of FN fibrillisation in the mutant since blocking actin polymerisation may also affect the function of the actomyosin network. Finally, Fink *et al*. (2011) have proposed that cells divide according to cues provided by their mechanical microenvironment, aligning daughter cells with the external force field. It is possible that in *hir* the cellular microenvironment is not providing sufficient mechanical cues due to defective FN fibrillisation. Furthermore since actomyosin activity is affected, the cells of the mutant may be unable to respond to such extracellular mechanical cues and regulate spindle orientation. Spatial confinement of cells within tissues has also been suggested to be important for regulating spindle orientation in dividing cells (Nakajima, *et al*. 2013). Since spatial constraints may be affected in *hir* due to lower overall tissue tension and incorrect tissue morphology, this regulation may not be occurring. Therefore a combination of these factors may explain the loss of oriented cell division in *hir*.

7.2.1 A role for YAP in regulating the global 3D body shape of vertebrates

Based on the features of the *hir* phenotype described above, the following model for YAP-orchestration of the complex processes of 3D body shape formation, that extends from the molecular level to global body shape is proposed (Figure 7.1b): (1) YAP regulates actomyosin activity; (2) this is required for collective cell behaviour, e.g. epiboly, migration and cell stacking which generates 3D tissues with proper tissue tension; (3) tension exerted by 3D tissues mediates assembly of FN on the basal surface of the tissue. This activates integrin-mediated cell-matrix adhesion that maintains spatial relationships of tissues/organs and thus (4) generates and maintains global 3D body shape. The FN assembly blocking experiments presented in this work demonstrate that steps 3 and 4 are FN assembly dependent, while steps 1 and 2 are not and instead are upstream, leading to proper FN assembly. In the absence of YAP, actomyosin activity is attenuated in the *hir* mutants (step 1). Attenuation of actomyosin activity causes a reduction in tissue tension leading to slow epiboly and aberrant FN assembly as seen in *hir* during gastrulation (step 2). Furthermore this causes prominent cell migration defects at later stages of development (step 2).

How does actomyosin regulate cell stacking (step 2)? Both oriented cell division that likely contributes to generating stacked cells and the maintenance of stacked cells

were affected in *hir*. Therefore actomyosin activity might be required for both of these cell behaviours. It has been shown that neighbouring cell changes trigger tissue shape alteration in 2D tissues, and this is controlled by anisotropic actomyosin-mediated tension (Mayer *et al*., 2010). Therefore, one interesting possibility is that anisotropic actomyosin mediated tension may be associated with cell stacking to generate 3D tissues.

3D tissue formation is coordinated with alignment of adjacent tissues/organs via tension-mediated assembly of FN fibrils (step 3). Tension-mediated FN assembly could be the mechanism that integrates mechanical signals, i.e. tension generated by actomyosin activity regulated by YAP (steps 1 and 2), with biochemical signals, i.e. integrin signalling that mediates cell-matrix adhesion for alignment of adjacent tissues/ organs to build up body shape (steps 3 and 4). This mechanism seems plausible and is likely to be efficient since FN is the most upstream component in ECM assembly and initiates ECM organisation (Daley *et al*., 2008). It is worth noting that YAP knockout mice show a phenotype similar to FN knockout mice (Nishioka *et al*., 2009).

This multistep model is somewhat supported by the transplantation experiments described in Chapter 6. Here, the transplantation of wild type cells into *hir* leads to the rescue of mutant tissues hosting the wild type transplanted cells, i.e. the eyes and CDs. In the rescued mutants, the process of FN fibrillogenesis may be somewhat improved though further work is needed to confirm this. Moreover, the transplantation data is complemented by the mosaic expression of YAP and YAP5SA in *hir*. Both types of mosaic injection had a similar effect to transplanted wild type cells and rescued the mutant phenotype and appeared to some extent to restore FN fibrillogenesis. Since tension-deficient wild type cells could not rescue aspects of the mutant phenotype, this suggests YAP regulates tension upstream of FN fibrillogenesis.

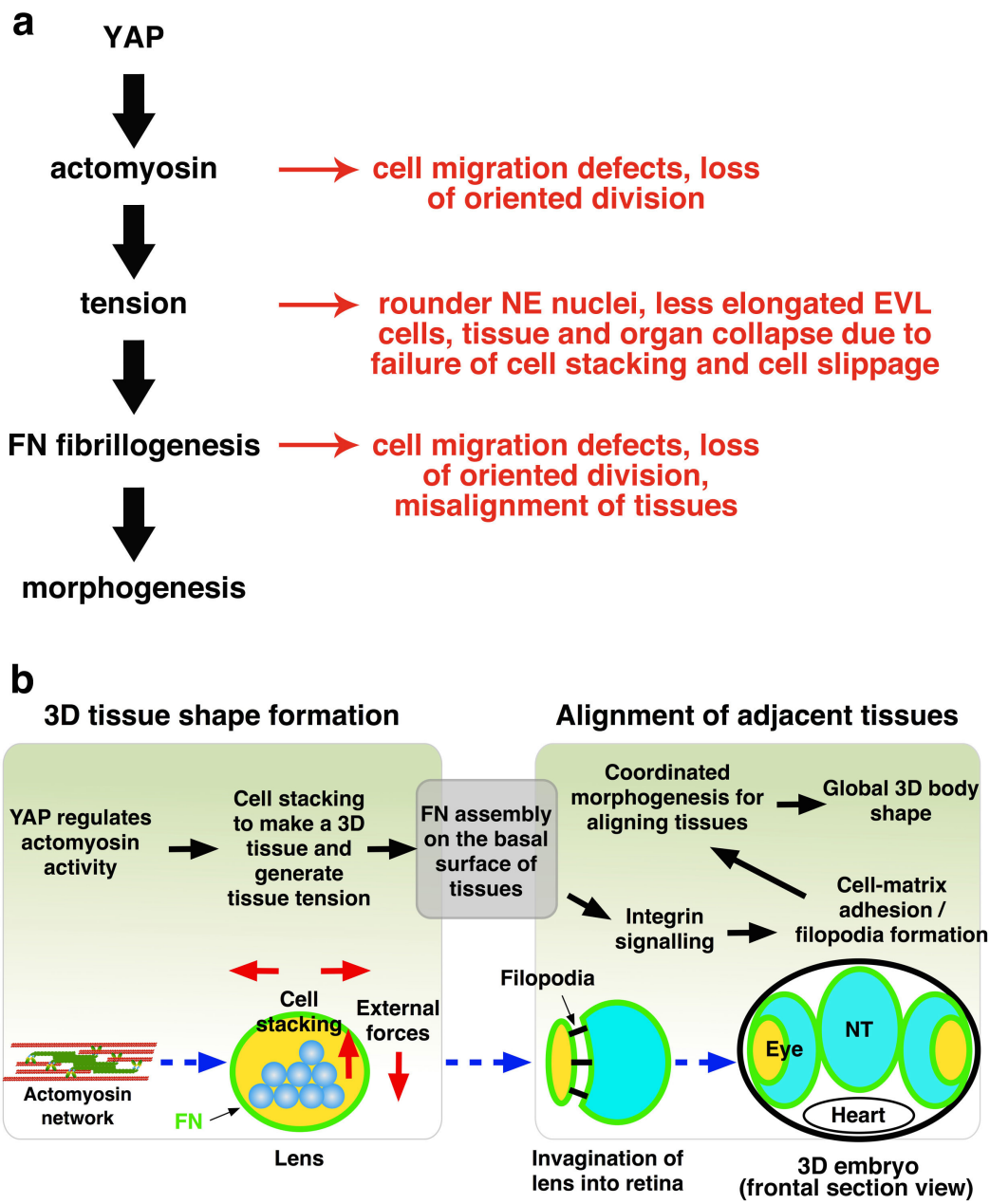

Figure 7.1. Model and illustrative example for YAP-regulation of actomyosin leading to morphogenesis. (a) General model for YAP-regulation of actomyosin and the downstream processes required for morphogenesis. Some of the affected steps in *hir* and their phenotypic consequences are shown in red. **(b)** Illustrative example for how YAP regulates the formation of 3D tissues and their coordinated morphogenesis to build up the global vertebrate body shape. YAP regulation of actomyosin coordinates cell behaviours to build 3D tissues (e.g. the eye) with the correct tension. This causes assembly of FN on the surface of these tissues, in turn activating integrin signalling. This results in the formation of cell-matrix adhesions and the filopodia between tissues ensuring tissues are properly aligned. Consequently tissues can undergo coordinated morphogenesis leading to the global 3D body shape. Horizontal red arrows indicate increasing tissue tension. NE: neuroepithelial; NT: neural tube; EVL: enveloping layer; FN: fibronectin.

7.3 How does YAP regulate actomyosin activity?

Evidence for a relationship between YAP and mechanical cues/forces has been growing recently. For example, YAP/TAZ have been proposed as mechanotransducers and have been shown to be localised in the cytoplasm when cells are under low tension or plated on soft ECMs, and localised in the nucleus when cells are spread under high tension or ECM stiffness is high (Dupont *et al*., 2011). Cells respond to external mechanical cues via tension and conformational changes in their cytoskeleton (Berrier and Yamada, 2007). Interestingly, actin polymerisation/stress fibre formation, which is associated with changes in cell shape (Wada *et al*., 2011, Aragona *et al*., 2013) has been shown to inhibit the Hippo pathway resulting in the nuclear accumulation of YAP/TAZ (Wada *et al*., 2011). Thus it is interesting to consider whether a relationship where YAP could regulate actomyosin may be plausible, given the involvement of the cytoskeleton in the transduction of mechanical forces. Indeed, as detailed in Chapter 5, phosphorylated MRLC (on Serine 19) levels in *hir* are significantly reduced suggesting non-muscle myosin II may not be dimerising and binding actin properly in the mutant, resulting in a reduction of contractility/tension of the actin cytoskeleton. As this reduced actomyosin activity is likely to be the most upstream cause of the *hir* phenotype as outlined above, a major question that remains from this work is how YAP could regulate the phosphorylation of MRLC.

MRCK (myotonic dystrophy kinase-related Cdc42-binding kinase) and ROCK (Rho-associated, coiled-coil-containing protein kinase) are major kinases phosphorylating the MRLCs and are activated by Cdc42 and RhoA respectively (Levayer and Lecuit, 2012). However, expressing constitutively active forms of RhoA and Cdc42 in *hir* did not rescue the phenotype (Huijia Wang, *personal communication*). This suggests YAP may be regulating phosphorylation of MRLC independently of these small family GTPases. Halder *et al*. (2012) suggest that extracellular forces are transmitted through integrin to the actomyosin network, which regulates YAP/TAZ activity (summarised in Figure 7.2). This raises the question of why pMRLC levels are reduced in *hir*. It may be possible that in this model, activated YAP/TAZ positively feedback to maintain the activity of the actomyosin network whilst the extracellular cues are present (dashed arrow in Figure 7.2). If this is the case, without this positive feedback in *hir* due to the absence of YAP, then actomyosin activity becomes reduced.

Halder *et al*. (2012) and Aragona *et al*. (2013) also suggest that the mechanical cues regulating YAP/TAZ may be acting in an independent and parallel pathway to that of Hippo signalling. This is based on two lines of evidence. Firstly, on soft ECMs, YAP/TAZ have been shown to be inactive (cytoplasmic, Dupont *et al*., 2011). Knockdown of the Hippo pathway components LATS1 and LATS2, which negatively regulate YAP/TAZ by phosphorylation causing their cytoplasmic sequestering, did not restore the activity

of YAP/TAZ on these soft ECMs, suggesting a Hippo-independent mechanism. Secondly, actin polymerisation has been shown to reduce Hippo signalling and increase YAP/TAZ activity. In the presence of Latrunculin A, an actin polymerisation inhibitor, the reverse is observed and YAP/TAZ activity is reduced. Knockdown of LATS1 and LATS2 in this case again did not restore YAP/TAZ activity (Dupont *et al*., 2011) again suggesting a Hippo-independent mechanism regulates the activity of YAP/TAZ in relation to mechanical cues.

Based on these data, Halder *et al*. (2012) propose several mechanisms by which YAP/TAZ activity may be regulated somewhat independently of LATS1/2. Firstly, since cell-cell junctions are important for transmitting mechanical cues in epithelial sheets and join to the actin cytoskeleton of cells, this may provide a level of regulation downstream of junctional complexes. This idea is supported by the fact that several regulators of YAP/TAZ activity associate with junctions including Scribble, Crumbs, Kibra, Merlin, Angiomotin, α-catenin and ZO-2 (Halder and Johnson, 2011; Halder *et al*., 2012). Indeed, many of these proteins can also bind to and activate actin and therefore respond to changes in the actin cytoskeleton (Halder *et al*., 2012). Secondly, Halder *et al*. (2012) speculate that conformational changes in the actin cytoskeleton dependent on external mechanical cues could sequester and release factors that can affect YAP/TAZ activity depending on the extracellular environment. Further to this they hypothesise that actomyosin contractility could expose cryptic sites in YAP/TAZ regulators physically associated with the actomyosin network such that under the right conditions they can interact with YAP/TAZ. However, it is possible that mechanical cues regulate YAP/TAZ activity through both LATS1/2-dependent and -independent pathways and that the two parallel pathways may act to rebalance each other (Halder *et al*., 2012) depending on the cells context.

Another model based on the study of cancer-associated fibroblasts (CAFs) has shown that YAP may be involved in a feedback mechanism with the extracellular environment (Calvo *et al*., 2013). This model proposes that mechanotransduction and YAP-dependent matrix remodelling is required for the generation and maintenance of CAFs. Calvo *et al*. (2013) suggest that soluble factors secreted by cancer cells increase the activity of YAP/TAZ in normal neighbouring fibroblasts (NFs). These NFs then remodel the matrix such that it increases in stiffness. Matrix stiffening is hypothesised to cause isometric tension within the fibroblasts leading to stress fibre formation and Src-kinase activity at focal adhesions. This results in further YAP activity (as actin polymerisation inhibits Hippo signalling) and the transcription of *Anln* and *Diaph3*, which stabilise actomyosin resulting in further matrix stiffening by sustained YAP activity. Enhanced levels of YAP in NFs may eventually transform them to CAFs. This model is therefore a positive feedback loop in which YAP is crucial for the establishment and maintenance

of CAFs (Calvo *et al*., 2013). However, it remains to be seen whether this positive feedback loop exists in non-cancerous cells.

It was very recently proposed that YAP activity is regulated by a mechanical checkpoint that dominates over Hippo pathway regulation of YAP (Aragona *et al*., 2013). This checkpoint/cytoskeletal regulation of YAP was shown to involve the actin-processing factors Cofilin, Capzb and Gelsolin. These F-actin capping and severing proteins act as inhibitors of YAP by causing the turnover of F-actin. Furthermore, YAP activity appears confined to regions where cells are under mechanical stresses due to stretching or the curvature of epithelial sheets, or a surrounding stiff ECM (Aragona *et al*., 2013). It is proposed that mechanical forces are the overarching regulators of YAP in multicellular contexts and that these mechanical cues set responsiveness to Hippo, Wnt and GPCR signalling (Aragona *et al*., 2013). This data has interesting implications for the work contained in this thesis. What is particularly noteworthy is that YAP activity is located in the cells in regions where morphogenesis or tissue deformation occurs. Since the results presented here demonstrate a role for YAP in regulating actomyosin activity, this seems to fit well given actomyosin is known to contribute to the shaping of multicellular tissues. It could therefore be envisaged that smaller-scale mechanical stresses in a few cells are transmitted to the actin cytoskeleton of neighbouring cells, perhaps through cell-cell contacts. This could then lead to the activity of YAP in these neighbouring cells resulting in increased actomyosin activity. If this force is then propagated over a longer-range it could lead to a more global tissue shape change such as bending or folding etc. as is seen in morphogenesis throughout development.

Finally, a role for YAP in regulating the activity of MRLC is supported by the fact that YAP has been shown to control the protein levels of Myosin regulatory light chain 9 (MYL9, also known as Phospho-Myosin Light Chain 2, MLC2). Interestingly, YAP was not shown to affect the transcription of *MYL9*. Instead YAP was shown to regulate the protein level of MYL9 and the amount of active MYL9 (phosphorylated at Serine 19) as depletion of YAP reduced the levels of both of these components (Calvo *et al*., 2013). However, the mechanism of this regulation was not addressed/described. Therefore the exact molecular manner in which YAP regulates actomyosin or vice versa remains elusive for now but is an essential question to answer in order to truly understand the role of YAP as a key regulator of organ size and the morphogenesis associated with shaping tissues and building organs.

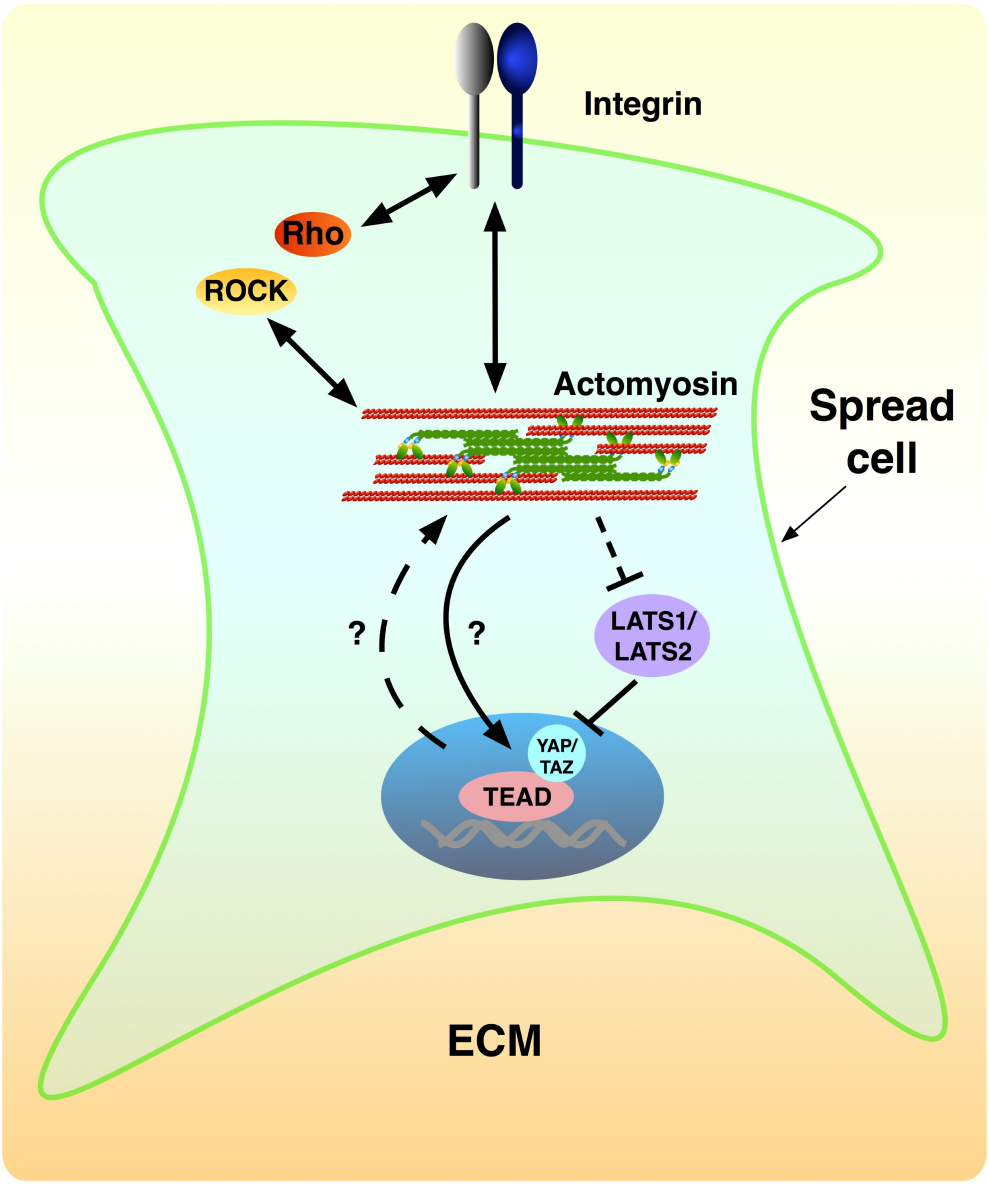

Figure 7.2. Model for actomyosin network regulation of YAP. Spread cells or cells grown on a stiff ECM form adhesions via integrin, activating the actomyosin network. This is mediated by bidirectional signalling between Rho, ROCK (Rho-associated kinase), integrin and myosin activity. The actomyosin network results in YAP/TAZ nuclear activity through as yet unknown Hippo-independent mechanisms (arrow with question mark) and through inhibition of LATS1/2 (dashed line). The mechanism of YAP-regulation of the actomyosin network proposed in this thesis remains unknown (dashed arrow with question mark). Adapted from Halder *et al*. (2012).

7.4 Cells extrude from the retina and epithelia of the ear in *hirame* mutants

During analysis of time-lapse movies of eye development it was observed that cells at the periphery of the retina in *hir* occasionally extruded from the tissue following cell division. This extrusion was also seen in the epithelial cells of the ear. In contrast, cell extrusion in wild type embryos appeared less evident. Quantification of the number of cells extruding in *hir* and wild type tissues could be performed to address whether this is an additional phenotype of the *hir* mutant. Cell extrusion has been shown to be a means by which epithelial tissues maintain cell numbers so that overcrowding does not occur (Eisenhoffer *et al*., 2012). Since cell proliferation is largely normal in *hir*, tissue overcrowding is unlikely to be the cause. Very recently it has been shown that cells dividing with defective mitotic spindle alignment, delaminate and undergo apoptosis in order to maintain the architecture of the epithelial tissue (Nakajima *et al*., 2013). Since oriented cell division is affected in *hir*, this may be an explanation if the extrusion rate was found to be higher in the mutant.

7.5 Are there also cell-cell adhesion defects in *hirame*?

Several characteristics of the *hir* phenotype are indicative of cell adhesion defects such as the cell slippage observed in the NT. It is not yet definitive whether there is a cell-cell adhesion defect in the mutant but immunohistochemistry on both whole-mount and sectioned embryos showed pan-cadherin, atypical PKC (aPKC) and ZO-1 were unaltered in *hir* (Huijia Wang, *personal communication*). It may be that the machinery/ components to build cell-cell junctions are present in the mutant but perhaps junctions do not assemble properly. It may be necessary to examine these structures at the electron microscopy level to resolve this. If cell-cell contacts are disrupted, in the case of the NT for example, this may be due to a lack of tension in the tissue periphery/ boundary, which may not impose sufficient spatial constraints. Thus the close contact between cells required to form sufficient cell-cell adhesions could be absent, leading to cell slippage. Moreover, if CD endothelial migration is collective then adhesion defects may also contribute to the phenotype observed here, as collective migration requires cell-cell contact. Finally, since adherens junction components such as cadherin are linked to the actin cytoskeleton and this appears affected in *hir*, perhaps this has an affect on the formation of cell adhesions. This could again lead to the cell slippage phenotype seen in the mutant NT or perhaps the potentially higher rate of cell extrusion from various tissues.

7.6 Potential therapeutic implications of this research

The results presented in this thesis show that modulation of YAP activity could have an impact for regenerative medicine, which aims to facilitate 3D tissue formation and/or to integrate transplanted tissues in the proper 3D alignment to allow their full functionality. So far, the production of functioning 3D organs *in vitro* has been limited but a few exceptions such as the pituitary and liver are now starting to show promise (Suga *et al*., 2011, Takebe *et al*., 2013). It may be possible that regulating YAP activity in such cases can improve the 3D morphogenesis of *in vitro* tissues and organs. In line with this, it was very recently shown that activation of YAP/TAZ (nuclear localisation) in 3D cultures of mammary epithelial cells (MECs) via the use of a stiff ECM resulted in the production of actively growing tubules and organoid-like structures (Aragona *et al*., 2013).

It was also very recently reported that YAP is involved in neonatal cardiac regeneration in mice by activating cardiomyocytes to undergo proliferation. Furthermore forced expression of YAP in adult mice hearts improved the regenerative response after myocardial infarction (Xin *et al*., 2013). This is not a surprising role for YAP since regeneration involves the attempted restoration of an organ to its former architecture pre-injury. Moreover, since the work in this thesis has shown a role for YAP in regulating actomyosin activity which is important in wound healing, this further strengthens a role for YAP in regeneration. Ascertaining which functions of YAP can be attributed to which functional domain of the protein will be very important for therapies aimed at targeting YAP activity.

7.7 Final thoughts

YAP has been identified as the nuclear executor of the Hippo signalling pathway that regulates epithelial tissue/organ size. An important question in this field has been how cells sense the size of the organ to which they belong in order to stop growing/ proliferating, i.e. how the Hippo signalling pathway is activated. In light of this, the role of YAP in regulating single-cell behaviour during development was investigated. YAP was recently proposed as a mechanotransducer by *in vitro* work (Dupont *et al*., 2011). However, due to several hurdles progress *in vivo* has been somewhat difficult. Firstly, previous loss-of-function analysis for YAP or Yorkie (*Drosophila* YAP orthologue) in the whole-body has been hampered by early lethality. In contrast, in the medaka *hir* mutants, the presence of maternal YAP mRNA prevents early onset of gastrulation defects. Such defects would otherwise conceal later neural morphogenesis defects as shown by maternal YAP mRNA knockdown in *hir* mutants, which died during gastrulation (approximately 15 hpf). Secondly, due to compromised cell proliferation of YAP-deficient cells (Genevet *et al*., 2009; Hamaratoglu *et al*., 2009; Zhao *et al*., 2008). The use of medaka has allowed decoupling of cell proliferation defects from other

phenotypes of YAP mutants, since cell proliferation occurred nearly normally in *hir* mutants. In the mouse, YAP knockout embryos are early lethal (Ota and Sasaki, 2008) whereas TAZ knockouts are viable (Makita *et al*., 2008). In medaka, TAZ knockdown embryos had strong cell proliferation defects and became early embryonic lethal. These differences could arise due to diversification of the functional subdivision between YAP and its paralogue TAZ, between mice and medaka.

YAP-mediated tissue tension and FN assembly may be conserved in humans (Tetsuo Miyamoto, *personal communication* and *unpublished results*). However, even the tissue/organ specific knockout of YAP that was recently reported in the mammalian kidney did not exhibit flattening nor dislocation (Reginensi *et al*., 2013). Perhaps this is due to the non-cell autonomous function of YAP from the cells surrounding the kidney, since YAP mutant cells could function normally in a wild-type environment as demonstrated by the cell-transplantation experiments in Chapter 6.

To this author's best knowledge, the flattened body phenotype reported here is unique and has not been observed in vertebrates highlighting a previously unknown role for YAP in regulating the global 3D body shape of vertebrates. Thus the medaka mutant described and characterised in this work has allowed the determination of a potential mechanism by which YAP allows cells of an organ to sense size. Since the actin cytoskeleton acts as a receiver and responder to external cues, the proposed YAP-regulation of the cytoskeleton allows control of a broad range of biological activities and behaviours (including cell proliferation, migration and morphogenesis) such that cellular functions are controlled in order to produce functional and structurally organised organs.

7.8 Impact of this work

The novel findings contained within this work are summarised as follows:

1. YAP is required for the polarised endothelial progenitor cell migration necessary to form the primary vasculature
2. YAP regulates the actomyosin network to maintain cellular and tissue tension leading to the formation of 3D tissues via cell behaviours including cell stacking and oriented cell division.
3. YAP regulates the coordinated morphogenesis of these tissues via fibronectin-integrin signalling to develop the global 3D vertebrate body shape.
4. YAP has a non-cell autonomous role *in vivo* for some of the processes involved in morphogenesis.

Chapter 8: References

Papers

Albrecht-Buehler, G. 1976. Filopodia of spreading 3T3 cells. Do they have a substrate-exploring function? The Journal of Cell Biology, 69(2), pp.275–286.

Albuschies, J., Vogel, V. 2013. The role of filopodia in the recognition of nanotopographies. Scientific Reports, 3, 1658.

Antunes, M., Pereira, T., Cordeiro, J.V., Almeida, L., Jacinto, A. 2013. Coordinated waves of actomyosin flow and apical cell constriction immediately after wounding. The Journal of Cell Biology, 202(2), pp.365–379.

Aragona, M., Panciera, T., Manfrin, A., Giulitti, S., Michielin, F., Elvassore, N., Dupont, S., Piccolo, S. 2013. A Mechanical Checkpoint Controls Multicellular Growth through YAP/TAZ Regulation by Actin-Processing Factors. Cell, 154(5), pp.1047–1059.

Argiro, V., Bunge, M.B., Johnson, M.I. 1985. A quantitative study of growth cone filopodial extension. Journal of Neuroscience Research, 13(1-2), pp.149–162.

Argraves, W.S., Larue, A.C., Fleming, P.A., Drake, C.J. 2002. VEGF signaling is required for the assembly but not the maintenance of embryonic blood vessels. Developmental Dynamics, 225(3), pp.298–304.

Armstrong, L.-J., Heath, V.L., Sanderson, S., Kaur, S., Beesley, J.F., Herbert, J.M., Legg, J.A., Poulsom, R., Bicknell, R. 2008. ECSM2, an endothelial specific filamin a binding protein that mediates chemotaxis. Arteriosclerosis, Thrombosis, and Vascular Biology, 28(9), pp.1640–1646.

Asahara, T., Kawamoto, A., Masuda, H. 2011. Concise review: Circulating endothelial progenitor cells for vascular medicine. Stem Cells, 29(11), pp.1650–1655.

Astrof, S., Hynes, R.O. 2009. Fibronectins in vascular morphogenesis. Angiogenesis, 12(2), pp. 165–175.

Bajoghli, B., Aghaallaei, N., Heimbucher, T., Czerny, T. 2004. An artificial promoter construct for heat-inducible misexpression during fish embryogenesis. Developmental Biology, 271(2), pp. 416–430.

Becker, T., Technau, G.M. 1990. Single cell transplantation reveals interspecific cell communication in Drosophila chimeras. Development, 109(4), pp.821–832.

Berrier, A.L., Yamada, K.M. 2007. Cell-matrix adhesion. Journal of Cellular Physiology, 213(3), pp.565–573.

Bonsignorio, D., Perego, L., Del Giacco, L., Cotelli, F. 1996. Structure and macromolecular composition of the zebrafish egg chorion. Zygote, 4(2), pp.101–108.

Bao, Y., Hata, Y., Ikeda, M., Withanage, K. 2011. Mammalian Hippo pathway: from development to cancer and beyond. J. Biochem., 149, pp.361–379.

Barembaum, M., Bronner-Fraser, M. 2007. Spalt4 mediates invagination and otic placode gene expression in cranial ectoderm. Development, 134(21), pp.3805–3814.

Barr, F.A., Gruneberg, U. 2007. Cytokinesis: placing and making the final cut. Cell, 131(5), pp. 847–860.

Bateman, J.F., Boot-Handford, R.P., Lamandé, S.R. 2009. Genetic diseases of connective tissues: cellular and extracellular effects of ECM mutations. Nature Reviews Genetics, 10(3), pp.173–183.

Bayless, K. J., Davis, G. E. 2002. The Cdc42 and Rac1 GTPases are required for capillary lumen formation in three-dimensional extracellular matrices. J Cell Sci. 115(Pt 6), pp.1123-1136.

Behrndt, M., Salbreux, G., Campinho, P., Hauschild, R., Oswald, F., Roensch, J., Grill, S.W., Heisenberg, C.-P. 2012. Forces Driving Epithelial Spreading in Zebrafish Gastrulation. Science, 338(6104), pp.257–260.

Beitel, G.J., Krasnow, M.A. 2000. Genetic control of epithelial tube size in the Drosophila tracheal system. Development, 127(15), pp.3271–3282.

Bergers, G., Song, S. 2005. The role of pericytes in blood-vessel formation and maintenance. Neuro-Oncology, 7(4), pp.452–464.

Bernascone, I., Martín-Belmonte, F. 2013. Crossroads of Wnt and Hippo in epithelial tissues. Trends in Cell Biology, 23(8), pp.380–389.

Betchaku, T., Trinkaus, J.P. 1978. Contact relations, surface activity, and cortical microfilaments of marginal cells of the enveloping layer and of the yolk syncytial and yolk cytoplasmic layers of fundulus before and during epiboly. Journal of Experimental Zoology Part A: Comparative Experimental Biology, 206(3), pp.381–426.

Bianco, A., Poukkula, M., Cliffe, A., Mathieu, J., Luque, C.M., Fulga, T.A., Rørth, P. 2007. Two distinct modes of guidance signalling during collective migration of border cells. Nature, 448(7151), pp.362–365.

Buck, C.A., Horwitz, A.F. 1987. Cell surface receptors for extracellular matrix molecules. Annual Review of Cell Biology, 3, pp.179–205.

Calvo, F., Ege, N., Grande-Garcia, A., Hooper, S., Jenkins, R.P., Chaudhry, S.I., Harrington, K., Williamson, P., Moeendarbary, E., Charras, G., Sahai, E. 2013. Mechanotransduction and YAP-dependent matrix remodelling is required for the generation and maintenance of cancer-associated fibroblasts. Nature Cell Biology, 15(6), pp.637–646.

Camargo, F.D., Gokhale, S., Johnnidis, J.B., Fu, D., Bell, G.W., Jaenisch, R., Brummelkamp, T.R. 2007. YAP1 increases organ size and expands undifferentiated progenitor cells. Current Biology, 17(23), pp.2054–2060.

Cao, X., Pfaff, S.L., Gage, F.H. 2008. YAP regulates neural progenitor cell number via the TEA domain transcription factor. Genes & Development, 22(23), pp.3320–3334.

Carvalho, L., Heisenberg, C.-P. 2010. The yolk syncytial layer in early zebrafish development. Trends in Cell Biology, 20(10), pp.586–592.

Castanon, I., González-Gaitán, M. 2011. Oriented cell division in vertebrate embryogenesis. Current Opinion in Cell Biology, 23(6), pp.697–704.

Chauhan, B.K., Disanza, A., Choi, S.Y., Faber, S.C., Lou, M., Beggs, H.E., Scita, G., Zheng, Y., Lang, R.A. 2009. Cdc42- and IRSp53-dependent contractile filopodia tether presumptive lens and retina to coordinate epithelial invagination. Development, 136(21), pp.3657–3667.

Cheng, J.C., Miller, A.L., Webb, S.E. 2004. Organization and function of microfilaments during late epiboly in zebrafish embryos. Developmental Dynamics, 231(2), pp.313–323.

Cherrett, C., Furutani-Seiki, M., Bagby, S. 2012. The Hippo pathway: key interaction and catalytic domains in organ growth control, stem cell self-renewal and tissue regeneration. Essays in Biochemistry, 53(1), pp.111–127.

Choquet, D., Felsenfeld, D.P., Sheetz, M.P. 1997. Extracellular matrix rigidity causes strengthening of integrin-cytoskeleton linkages. Cell, 88(1), pp.39–48.

Clarke, J. 2009. Role of polarized cell divisions in zebrafish neural tube formation. Current Opinion in Neurobiology, 19(2), pp.134–138.

Colas, J.F., Schoenwolf, G.C. 2001. Towards a cellular and molecular understanding of neurulation. Developmental Dynamics, 221(2), pp.117–145.

Cox, E.A., Sastry, S.K., Huttenlocher, A. 2001. Integrin-mediated adhesion regulates cell polarity and membrane protrusion through the Rho family of GTPases. Molecular Biology of the Cell, 12(2), pp.265–277.

Daley, W.P., Peters, S.B. & Larsen, M., 2008. Extracellular matrix dynamics in development and regenerative medicine. Journal of Cell Science, 121(3), pp.255–264.

Danysh, B.P., Duncan, M.K. 2009. The lens capsule. Experimental Eye Research, 88(2), pp. 151–164.

Das, T., Payer, B., Cayouette, M., Harris, W.A. 2003. In vivo time-lapse imaging of cell divisions during neurogenesis in the developing zebrafish retina. Neuron, 37(4), pp.597–609.

Davidson, L.A., Dzamba, B.D., Keller, R., Desimone, D.W. 2008. Live imaging of cell protrusive activity, and extracellular matrix assembly and remodeling during morphogenesis in the frog, Xenopus laevis. Developmental Dynamics, 237(10), pp.2684–2692.

Davidson, L.A., Marsden, M., Keller, R., Desimone, D.W. 2006. Integrin alpha5beta1 and fibronectin regulate polarized cell protrusions required for Xenopus convergence and extension. Current Biology, 16(9), pp.833–844.

De Bellard, M.E., Rao, Y., Bronner-Fraser, M. 2003. Dual function of Slit2 in repulsion and enhanced migration of trunk, but not vagal, neural crest cells. J. Cell Biol., 162, pp.269–279.

Dong, J., Feldmann, G., Huang, J., Wu, S., Zhang, N., Comerford, S., Gayyed, M., Anders, R., Maitra, A., Pan, D. 2007. Elucidation of a Universal Size-Control Mechanism in Drosophila and Mammals. Cell, 130(6), pp.1120–1133.

Dupont, S., Morsut, L., Aragona, M., Enzo, E., Giulitti, S., Cordenonsi, M., Zanconato, F., Le Digabel, J., Forcato, M., Bicciato, S., Elvassore, N., Piccolo, S. 2011. Role of YAP/TAZ in mechanotransduction. Nature, 474(7350), pp.179–183.

Eickholt, B.J., Mackenzie, S.L., Graham, A., Walsh, F.S., Doherty, P. 1999. Evidence for collapsin-1 functioning in the control of neural crest migration in both trunk and hindbrain regions. Development, 126, pp.2181–2189.

Eisenhoffer, G.T., Loftus, P.D., Yoshigi, M., Otsuna, H., Chien, C.B., Morcos, P.A., Rosenblatt, J. 2012. Crowding induces live cell extrusion to maintain homeostatic cell numbers in epithelia. Nature, pp.1–6.

Elzen, den, N., Buttery, C.V., Maddugoda, M.P., Ren, G., Yap, A.S. 2009. Cadherin adhesion receptors orient the mitotic spindle during symmetric cell division in mammalian epithelia. Molecular Biology of the Cell, 20(16), pp.3740–3750.

Endo, H., Ogawa, K., Kurohmaru, M., Hayashi, Y. 1996. Development of cardiac musculature in the cranial vena cava of rat embryos. Anatomy and Embryology, 193(5), pp.501–504.

Era, T., Izumi, N., Hayashi, M., Tada, S., Nishikawa, S., Nishikawa, S. 2008. Multiple mesoderm subsets give rise to endothelial cells, whereas hematopoietic cells are differentiated only from a restricted subset in embryonic stem cell differentiation culture. Stem Cells, 26(2), pp.401–411.

Espanel, X. Sudol, M. 2001. Yes-associated protein and p53-binding protein-2 interact through their WW and SH3 domains. The Journal of Biological Chemistry, 276(17), pp.14514–14523.

Etienne-Manneville, S. 2004. Cdc42--the centre of polarity. Journal of Cell Science, 117(Pt 8), pp.1291–1300.

Etienne-Manneville, S., Hall, A. 2002. Rho GTPases in cell biology. Nature, 420(6916), pp.629–635.

Etienne-Manneville, S., Hall, A. 2003. Cell polarity: Par6, aPKC and cytoskeletal crosstalk. Current Opinion in Cell Biology, 15(1), pp.67–72.

Fankhauser, G. 1945. Maintenance of normal structure in heteroploid salamander larvae, through compensation of changes in cell size by adjustment of cell number and cell shape. Journal of Experimental Zoology Part A: Comparative Experimental Biology, 100, pp.445–455.

Fernandez, A., Northcott, P.A., Dalton, J., Fraga, C., Ellison, D., Angers, S., Taylor, M.D., Kenney, A.M. 2009. YAP1 is amplified and up-regulated in hedgehog-associated medulloblastomas and mediates Sonic hedgehog-driven neural precursor proliferation. Genes Dev., 23, pp.2729–2741.

Fernandez, B.G., Gaspar, P., Brás-Pereira, C., Jezowska, B., Rebelo, S.R., Janody, F. 2011. Actin-Capping Protein and the Hippo pathway regulate F-actin and tissue growth in Drosophila. Development, 138(11), pp.2337–2346.

Fernandez-Sauze, S., Grall, D., Cseh, B., Van Obberghen-Schilling, E. 2009. Regulation of fibronectin matrix assembly and capillary morphogenesis in endothelial cells by Rho family GTPases. Experimental Cell Research, 315(12), pp.2092–2104.

Fingleton, B. 2006. Matrix metalloproteinases: roles in cancer and metastasis. Front. Biosci., 11, pp.479–491.

Fink, J., Carpi, N., Betz, T., Bétard, A., Chebah, M., Azioune, A., Bornens, M., Sykes, C., Fetler, L., Cuvelier, D., Piel, M. 2011. External forces control mitotic spindle positioning. Nature Cell Biology, 13(7), pp.771–778.

Fischer, E., Legue, E., Doyen, A., Nato, F., Nicolas, J.F., Torres, V., Yaniv, M., Pontoglio, M. 2006. Defective planar cell polarity in polycystic kidney disease. Nature Genetics, 38(1), pp.21–23.

Fogerty, F.J., Akiyama, S.K., Yamada, K.M., Mosher, D.F. 1990. Inhibition of binding of fibronectin to matrix assembly sites by anti-integrin (alpha 5 beta 1) antibodies. The Journal of Cell Biology, 111(2), pp.699–708.

Force, A., Lynch, M., Pickett, F.B., Amores, A., Yan, Y.L., Postlethwait, J. 1999. Preservation of duplicate genes by complementary, degenerative mutations. Genetics, 151, pp.1531–1545.

Francis, S.E., Goh, K.L., Hodivala-Dilke, K., Bader, B.L., Stark, M., Davidson, D., Hynes, R.O. 2002. Central Roles of alpha5beta1 Integrin and Fibronectin in Vascular Development in Mouse Embryos and Embryoid Bodies. Arteriosclerosis, Thrombosis, and Vascular Biology, 22(6), pp. 927–933.

Friedl, P., Gilmour, D. 2009. Collective cell migration in morphogenesis, regeneration and cancer. Nature Reviews Molecular Cell Biology, 10(7), pp.445–457.

Friedl, P., Weigelin, B. 2008. Interstitial leukocyte migration and immune function. Nature Immunology, 9(9), pp.960–969.

Fujita, M., Isogai, S., Kudo, A. 2006. Vascular anatomy of the developing medaka,Oryzias latipes: A complementary fish model for cardiovascular research on vertebrates. Developmental Dynamics, 235(3), pp.734–746.

Fukazawa, C., Santiago, C., Park, K.M., Deery, W.J., Gomez de la Torre Canny, S., Holterhoff, C.K., Wagner, D.S. 2010. poky/chuk/ikk1 is required for differentiation of the zebrafish embryonic epidermis. Developmental Biology, 346(2), pp.272–283.

Furutani-Seiki, M., Jiang, Y.J., Brand, M., Heisenberg, C.-P., Houart, C., Beuchle, D., van Eeden, F.J., Granato, M., Haffter, P., Hammerschmidt, M., Kane, D.A., Kelsh, R.N., Mullins, M.C., Odenthal, J., Nüsslein-Volhard, C. 1996. Neural degeneration mutants in the zebrafish, Danio rerio. Development, 123, pp.229–239.

Furutani-Seiki, M., Sasado, T., Morinaga, C., Suwa, H., Niwa, K., Yoda, H., Deguchi, T., Hirose, Y., Yasuoka, A., Henrich, T., Watanabe, T., Iwanami, N., Kitagawa, D., Saito, K., Asaka, S., Osakada, M., Kunimatsu, S., Momoi, A., Elmasri, H., Winkler, C., Ramialison, M., Loosli, F., Quiring, R., Carl, M., Grabher, C., Winkler, S., Del Bene, F., Shinomiya, A., Kota, Y., Yamanaka, T., Okamoto, Y., Takahashi, K., Todo, T., Abe, K., Takahama, Y., Tanaka, M., Mitani, H., Katada, T., Nishina, H., Nakajima, N., Wittbrodt, J., Kondoh, H. 2004. A systematic genome-wide screen

for mutations affecting organogenesis in Medaka, Oryzias latipes. Mechanisms of Development, 121(7-8), pp.647–658.

Furutani-Seiki, M., Wittbrodt, J. 2004. Medaka and zebrafish, an evolutionary twin study. Mechanisms of Development, 121(7-8), pp.629–637.

Füller, T., Korff, T., Kilian, A., Dandekar, G., Augustin, H.G. 2003. Forward EphB4 signaling in endothelial cells controls cellular repulsion and segregation from ephrinB2 positive cells. Journal of Cell Science, 116(Pt 12), pp.2461–2470.

Gavrieli, Y., Sherman, Y., Ben-Sasson, S.A. 1992. Identification of programmed cell death in situ via specific labeling of nuclear DNA fragmentation. The Journal of Cell Biology, 119(3), pp.493–501.

Gee, S.T., Milgram, S.L., Kramer, K.L., Conlon, F.L., Moody, S.A. 2011. Yes-Associated Protein 65 (YAP) Expands Neural Progenitors and Regulates Pax3 Expression in the Neural Plate Border Zone. PLoS ONE, 6(6), p.e20309.

Geissmann, F., Manz, M.G., Jung, S., Sieweke, M.H., Meras, M., Ley, K. 2010. Development of monocytes, macrophages, and dendritic cells. Science, 327(5966), pp. 656-61.

Genevet, A., Polesello, C., Blight, K., Robertson, F., Collinson, L.M., Pichaud, F., Tapon, N. 2009. The Hippo pathway regulates apical-domain size independently of its growth-control function. Journal of Cell Science, 122(14), pp.2360–2370.

George, E.L., Baldwin, H.S., Hynes, R.O. 1997. Fibronectins are essential for heart and blood vessel morphogenesis but are dispensable for initial specification of precursor cells. Blood, 90(8), pp.3073–3081.

George, E.L., Georges-Labouesse, E.N., Patel-King, R.S., Rayburn, H., Hynes, R.O. 1993. Defects in mesoderm, neural tube and vascular development in mouse embryos lacking fibronectin. Development, 119(4), pp.1079–1091.

Gomes, E.R., Jani, S., Gundersen, G.G. 2005. Nuclear movement regulated by Cdc42, MRCK, myosin, and actin flow establishes MTOC polarization in migrating cells. Cell, 121(3), pp.451–463.

Goode, B.L., Eck, M.J. 2007. Mechanism and function of formins in the control of actin assembly. Annual Review of Biochemistry, 76, pp.593–627.

Gray, D.S., Tien, J., Chen, C.S. 2003. Repositioning of cells by mechanotaxis on surfaces with micropatterned Young's modulus. Journal of biomedical materials research. Part A, 66(3), pp. 605–614.

Gumbiner, B.M. 2005. Regulation of cadherin-mediated adhesion in morphogenesis. Nat Rev Mol Cell Biol., 6(8), pp.622–634.

Haas, P., Gilmour, D. 2006. Chemokine Signaling Mediates Self-Organizing Tissue Migration in the Zebrafish Lateral Line. Developmental Cell, 10(5), pp.673–680.

Haffter, P., Granato, M., Brand, M., Mullins, M.C., Hammerschmidt, M., Kane, D.A., Odenthal, J., van Eeden, F.J., Jiang, Y.J., Heisenberg, C.P., Kelsh, R.N., Furutani-Seiki, M., Vogelsang, E., Beuchle, D., Schach, U., Fabian, C., Nüsslein-Volhard, C. 1996. The identification of genes with unique and essential functions in the development of the zebrafish, Danio rerio. Development, 123, pp.1–36.

Halder, G., Dupont, S., Piccolo, S. 2012. Nature Reviews Molecular Cell Biology, 13(9), pp.591–600.

Halder, G., Johnson, R.L. 2011. Hippo signaling: growth control and beyond. Development, 138(1), pp.9–22.

Hall, A. 2005. Rho GTPases and the control of cell behaviour. Biochemical Society transactions, 33(Pt 5), pp.891–895.

Hamaratoglu, F., Gajewski, K., Sansores-Garcia, L., Morrison, C., Tao, C., Halder, G. 2009. The Hippo tumor-suppressor pathway regulates apical-domain size in parallel to tissue growth. Journal of Cell Science, 122(14), pp.2351–2359.

Harrington, L., Klintworth, G.K., Secor, T.E., Breitman, M.L. 1991. Developmental analysis of ocular morphogenesis in alpha A-crystallin/diphtheria toxin transgenic mice undergoing ablation of the lens. Developmental Biology, 148(2), pp.508–516.

Heallen, T., Zhang, M., Wang, J., Bonilla-Claudio, M., Klysik, E., Johnson, R.L., Martin, J.F. 2011. Hippo pathway inhibits Wnt signaling to restrain cardiomyocyte proliferation and heart size. Science, 332, pp.458–461.

Heisenberg, C.-P., Bellaïche, Y. 2013. Forces in Tissue Morphogenesis and Patterning. Cell, 153(5), pp.948–962.

Hill, V.K., Dunwell, T.L., Catchpoole, D., Krex, D., Brini, A.T., Griffiths, M., Craddock, C., Maher, E.R., Latif, F. 2011. Frequent epigenetic inactivation of KIBRA, an upstream member of the Salvador/Warts/Hippo (SWH) tumor suppressor network, is associated with specific genetic event in B-cell acute lymphocytic leukemia. Epigenetics, 6(3), pp.326–332.

Hirose, Y., Varga, Z.M., Kondoh, H., Furutani-Seiki, M. 2004. Single cell lineage and regionalization of cell populations during Medaka neurulation. Development, 131(11), pp.2553–2563.

Hochmann, S., Aghaallaei, N., Bajoghli, B., Soroldoni, D., Carl, M., Czerny, T. 2007. Expression of marker genes during early ear development in medaka. Gene Expression Patterns, 7(3), pp. 355–362.

Hong, J.-H., Yaffe, M.B. 2006. TAZ: a beta-catenin-like molecule that regulates mesenchymal stem cell differentiation. Cell Cycle, 5(2), pp.176–179.

Hrabe de Angelis, M.H., Flaswinkel, H., Fuchs, H., Rathkolb, B., Soewarto, D., Marschall, S., Heffner, S., Pargent, W., Wuensch, K., Jung, M., Reis, A., Richter, T., Alessandrini, F., Jakob, T., Fuchs, E., Kolb, H., Kremmer, E., Schaeble, K., Rollinski, B., Roscher, A., Peters, C., Meitinger, T., Strom, T., Steckler, T., Holsboer, F., Klopstock, T., Gekeler, F., Schindewolf, C., Jung, T., Avraham, K., Behrendt, H., Ring, J., Zimmer, A., Schughart, K., Pfeffer, K., Wolf, E., Balling, R. 2000. Genome- wide, large-scale production of mutant mice by ENU mutagenesis. Nat. Genet., 25, pp.444–447.

Hu, J., Sun, S., Jiang, Q., Sun, S., Wang, W., Gui, Y., Song, H. 2013. Yes-Associated Protein (Yap) Is Required for Early Embryonic Development in Zebrafish (Danio Rerio). International Journal of Biological Sciences, 9(3), pp.267–278.

Huang, H., Lu, F.I., Jia, S., Meng, S., Cao, Y., Wang, Y., Ma, W., Yin, K., Wen, Z., Peng, J., Thisse, C., Thisse, B., Meng, A. 2007. Amotl2 is essential for cell movements in zebrafish embryo and regulates c-Src translocation. Development, 134(5), pp.979–988.

Huang, J., Wu, S., Barrera, J., Matthews, K., Pan, D. 2005. The Hippo signaling pathway coordinately regulates cell proliferation and apoptosis by inactivating Yorkie, the Drosophila Homolog of YAP. Cell, 122(3), pp.421–434.

Itoh, R.E., Kurokawa, K., Ohba, Y., Yoshizaki, H., Mochizuki, N., Matsuda, M. 2002. Activation of rac and cdc42 video imaged by fluorescent resonance energy transfer-based single-molecule probes in the membrane of living cells. Mol. Cell Biol., 22(18), pp.6582-6591.

Iwadate, Y., Yumura, S. 2008. Actin-based propulsive forces and myosin-II-based contractile forces in migrating Dictyostelium cells. Journal of Cell Science, 121(Pt 8), pp.1314–1324.

Iwamatsu, T. 2004. Stages of normal development in the medaka Oryzias latipes. Mechanisms of Development, 121(7-8), pp.605–618.

Jessen, J.R., Topczewski, J., Bingham, S., Sepich, D.S., Marlow, F., Chandrasekhar, A., Solnica-Krezel, L. 2002. Zebrafish trilobite identifies new roles for Strabismus in gastrulation and neuronal movements. Nat. Cell Biol., 4, pp.610–615.

Jones, C.A., Li, D.Y. 2007. Common cues regulate neural and vascular patterning. Current Opinion in Genetics & Development, 17(4), pp.332–336.

Joshi, S.D., Davidson, L.A. 2012. Epithelial machines of morphogenesis and their potential application in organ assembly and tissue engineering. Biomechanics and Modeling in Mechanobiology, 11(8), pp.1109–1121.

Kageyama, T. 1980. Cellular basis of epiboly of the enveloping layer in the embryo of medaka, Oryzias latipes. I. Cell architecture revealed by silver staining method. Development, Growth & Differentiation, 22(4), pp.659–668.

Kane, D., Adams, R. 2002. Life at the edge: epiboly and involution in the zebrafish. Results and Problems in Cell Differentiation, 40, pp.117–135.

Kane, D.A., Hammerschmidt, M., Mullins, M.C., Maischein, H.M., Brand, M., van Eeden, F.J., Furutani-Seiki, M., Granato, M., Haffter, P., Heisenberg, C.-P., Jiang, Y.J., Kelsh, R.N., Odenthal, J., Warga, R.M., Nüsslein-Volhard, C. 1996. The zebrafish epiboly mutants. Development, 123, pp.47–55.

Kango-Singh, M., Singh, A. 2009. Regulation of organ size: insights from the Drosophila Hippo signaling pathway. Dev. Dyn., 238, pp.1627–1637.

Karnik, S.K., Brooke, B.S., Bayes-Genis, A., Sorensen, L., Wythe, J.D., Schwartz, R.S., Keating, M.T., Li, D.Y. 2003. A critical role for elastin signaling in vascular morphogenesis and disease. Development, 130(2), pp.411–423.

Karpowicz, P., Perez, J., Perrimon, N. 2010. The Hippo tumor suppressor pathway regulates intestinal stem cell regeneration. Development, 137, pp.4135–4145.

Kasahara, M., Naruse, K., Sasaki, S., Nakatani, Y., Qu, W., Ahsan, B., Yamada, T., Nagayasu, Y., Doi, K., Kasai, Y., Jindo, T., Kobayashi, D., Shimada, A., Toyoda, A., Kuroki, Y., Fujiyama, A., Sasaki, T., Shimizu, A., Asakawa, S., Shimizu, N., Hashimoto, S., Yang, J., Lee, Y., Matsushima, K., Sugano, S., Sakaizumi, M., Narita, T., Ohishi, K., Haga, S., Ohta, F., Nomoto, H., Nogata, K., Morishita, T., Endo, T., Shin-I, T., Takeda, H., Morishita, S., and Kohara, Y. 2007. The medaka draft genome and insights into vertebrate genome evolution. Nature, 447, pp.714-9.

Katogi, R., Nakatani, Y., Shin-I, T., Kohara, Y., Inohaya, K., and Kudo, A. 2004. Large-scale analysis of the genes involved in fin regeneration and blastema formation in the medaka, Oryzias latipes. Mech. Dev., 121, pp.861-72.

Kiecker, C., Niehrs, C. 2001. A morphogen gradient of Wnt/beta-catenin signalling regulates anteroposterior neural patterning in Xenopus. Development, 128(21), pp.4189–4201.

Kim, N.-G., Koh, E., Chen, X., Gumbiner, B.M. 2011. E-cadherin mediates contact inhibition of proliferation through Hippo signaling-pathway components. Proc. Natl. Acad. Sci. U.S.A., 108(29), pp.11930–11935.

Kim, Y.H., Raphael, Y. 2007. Cell division and maintenance of epithelial integrity in the deafened auditory epithelium. Cell Cycle, 6(5), pp.612–619.

Kimmel, C.B., Ballard, W.W., Kimmel, S.R., Ullmann, B., Schilling, T.F. 1995. Stages of embryonic development of the zebrafish. Developmental Dynamics, 203(3), pp.253–310.

Klinghoffer, R.A., Sachsenmaier, C., Cooper, J.A., Soriano, P. 1999. Src family kinases are required for integrin but not PDGFR signal transduction. EMBO J., 18(9), pp.2459-71.

Kollmar, R., Nakamura, S.K., Kappler, J.A., Hudspeth, A.J. 2001. Expression and phylogeny of claudins in vertebrate primordia. Proc. Natl. Acad. Sci. U.S.A., 98(18), pp.10196–10201.

Köppen, M., Fernández, B.G., Carvalho, L., Jacinto, A., Heisenberg, C.-P. 2006. Coordinated cell-shape changes control epithelial movement in zebrafish and Drosophila. Development, 133(14), pp.2671–2681.

Köster, R.W., Kühnlein, R.P., Wittbrodt, J. 2000. Ectopic Sox3 activity elicits sensory placode formation. Mechanisms of Development, 95(1-2), pp.175–187.

Kubow, K.E., Conrad, S.K., Horwitz, A.R. 2013. Matrix Microarchitecture and Myosin II Determine Adhesion in 3D Matrices. Current Biology, 23(17), pp.1607–1619.

Kuriyama, S., Mayor, R. 2008. Molecular analysis of neural crest migration. Philosophical Transactions of the Royal Society B: Biological Sciences, 363(1495), pp.1349–1362.

Ladwein, M., Rottner, K. 2008. On the Rho'd: the regulation of membrane protrusions by Rho-GTPases. FEBS letters, 582(14), pp.2066–2074.

Lai, S.-L., Chan, T.H., Lin, M.J., Huang, W.P., Lou, S.W., Lee, S.J. 2008. Diaphanous-related formin 2 and profilin I are required for gastrulation cell movements. PLoS ONE, 3(10), p.e3439.

Lamar, J.M., Stern, P., Liu, H., Schindler, J.W., Jiang, Z.G., Hynes, R.O. 2012. The Hippo pathway target, YAP, promotes metastasis through its TEAD-interaction domain. Proceedings of the National Academy of Sciences, 109(37), pp.E2441–50.

Lang, R.A. 2004. Pathways regulating lens induction in the mouse. The International Journal of Developmental Biology, 48(8-9), pp.783–791.

Latimer, A., Jessen, J.R. 2010. Extracellular matrix assembly and organization during zebrafish gastrulation. Matrix biology : journal of the International Society for Matrix Biology, 29(2), pp.89–96.

Law, J.M. 2001. Mechanistic considerations in small fish carcinogenicity testing. ILAR J., 42, pp. 274–284.

Le Clainche, C., Carlier, M.-F. 2008. Regulation of actin assembly associated with protrusion and adhesion in cell migration. Physiological Reviews, 88(2), pp.489–513.

Le Douarin, N.M. et al., 1975. Cholinergic differentiation of presumptive adrenergic neuroblasts in interspecific chimeras after heterotopic transplantations. Proc. Nat. Acad. Sci U.S.A., 72(2), pp.728–732.

Le Dréau, G., Martí, E. 2012. Dorsal-ventral patterning of the neural tube: a tale of three signals. Developmental Neurobiology, 72(12), pp.1471–1481.

Lecaudey, V. Cakan-Akdogan, G., Norton, W.H., Gilmour, D. 2008. Dynamic Fgf signaling couples morphogenesis and migration in the zebrafish lateral line primordium. Development, 135(16), pp.2695–2705.

Lecaudey, V., Ulloa, E., Anselme, I., Stedman, A., Schneider-Maunoury, S., Pujades, C. 2007. Role of the hindbrain in patterning the otic vesicle: a study of the zebrafish vhnf1 mutant. Dev. Biol., 303(1), pp.134-43.

Lee, J.M., Dedhar, S., Kalluri, R., Thompson, E.W. 2006. The epithelial-mesenchymal transition: new insights in signaling, development, and disease. J Cell Biol. 172(7), pp.973-891.

Lee, K.P., Lee, J.H., Kim, T.S., Kim, T.H., Park, H.D., Byun, J.S., Kim, M.C., Jeong, W.I., Calvisi, D.F., Kim, J.M., Lim, D.S. 2010. The Hippo-Salvador pathway restrains hepatic oval cell proliferation, liver size, and liver tumorigenesis. Proc. Natl. Acad. Sci. U.S.A., 107, pp.8248–8253.

Leiss, M., Beckmann, K., Girós, A., Costell, M., Fässler, R. 2008. The role of integrin binding sites in fibronectin matrix assembly in vivo. Current Opinion in Cell Biology, 20(5), pp.502–507.

Lepage, S.E., Bruce, A.E.E. 2010. Zebrafish epiboly: mechanics and mechanisms. The International Journal of Developmental Biology, 54(8-9), pp.1213–1228.

Levayer, R., Lecuit, T. 2012. Biomechanical regulation of contractility: spatial control and dynamics. Trends in Cell Biology, 22(2), pp.61–81.

Levine, A.J., Munoz-Sanjuan, I., Bell, E., North, A.J., Brivanlou, A.H. 2003. Fluorescent labeling of endothelial cells allows in vivo, continuous characterization of the vascular development of Xenopus laevis. Developmental Biology, 254(1), pp.50–67.

Li, S., Huang, N.F., Hsu, S. 2005. Mechanotransduction in endothelial cell migration. Journal of Cellular Biochemistry, 96(6), pp.1110–1126.

Linask, K.K., Lash, J.W. 1986. Precardiac cell migration: fibronectin localization at mesoderm-endoderm interface during directional movement. Developmental Biology, 114(1), pp.87–101.

Link, B.A. 2001. Evidence for directed mitotic cleavage plane reorientations during retinal development within the zebrafish. The Biological Bulletin, 201(2), pp.254–255.

Loosli, F., Staub, W., Finger-Baier, K.C., Ober, E.A., Verkade, H., Wittbrodt, J., Baier, H. 2003. Loss of eyes in zebrafish caused by mutation of chokh/rx3. EMBO Rep., 4, pp.894–899.

Lowery, L.A., Sive, H. 2004. Strategies of vertebrate neurulation and a re-evaluation of teleost neural tube formation. Mechanisms of Development, 121(10), pp.1189–1197.

Lu, L., Li, Y., Kim, S.M., Bossuyt, W., Liu, P., Qiu, Q., Wang, Y., Halder, G., Finegold, M.J., Lee, J.S., Johnson, R.L. 2010. Hippo signaling is a potent in vivo growth and tumor suppressor pathway in the mammalian liver. Proc. Natl. Acad. Sci. U.S.A., 107, pp.1437–1442.

Lucas, E.P., Khanal, I., Gaspar, P., Fletcher, G.C., Polesello, C., Tapon, N., Thompson, B.J. 2013. The Hippo pathway polarizes the actin cytoskeleton during collective migration of Drosophila border cells. The Journal of Cell Biology, 201(6), pp.875–885.

Maddala, R., Deng, P.F., Costello, J.M., Wawrousek, E.F., Zigler, J.S., Rao, V.P. 2004. Impaired cytoskeletal organization and membrane integrity in lens fibers of a Rho GTPase functional knockout transgenic mouse. Laboratory Investigation, 84(6), pp.679–692.

Makita, R., Uchijima, Y., Nishiyama, K., Amano, T., Chen, Q., Takeuchi, T., Mitani, A., Nagase, T., Yatomi, Y., Aburatani, H., Nakagawa, O., Small, E.V., Cobo-Stark, P., Igarashi, P., Murakami, M., Tominaga, J., Sato, T., Asano, T., Kurihara, Y., Kurihara, H. 2008. Multiple renal cysts, urinary concentration defects, and pulmonary emphysematous changes in mice lacking TAZ. American journal of physiology Renal physiology, 294(3), pp.F542–53.

Mammoto, T., Ingber, D.E. 2010. Mechanical control of tissue and organ development. Development, 137(9), pp.1407–1420.

Maniotis, A.J., Chen, C.S., Ingber, D.E. 1997. Demonstration of mechanical connections between integrins, cytoskeletal filaments, and nucleoplasm that stabilize nuclear structure. Proc. Natl. Acad. Sci. U.S.A., 94(3), pp.849–854.

Mao, Y., Schwarzbauer, J.E. 2005. Fibronectin fibrillogenesis, a cell-mediated matrix assembly process. Matrix Biology, 24(6), pp.389–399.

Marcelo, K.L., Goldie, L.C., Hirschi, K.K. 2013. Regulation of endothelial cell differentiation and specification. Circulation Research, 112(9), pp.1272–1287.

Martin, P., Wood, W. 2002. Epithelial fusions in the embryo. Current Opinion in Cell Biology, 14(5), pp.569–574.

Martinez-Morales, J.R., Rembold, M., Greger, K., Simpson, J.C., Brown, K.E., Quiring, R., Pepperkok, R., Martin-Bermudo, M.D., Himmelbauer, H., Wittbrodt, J. 2009. ojoplano-mediated basal constriction is essential for optic cup morphogenesis. Development, 136(13), pp.2165–2175.

Matsuda, M., Nagahama, Y., Shinomiya, A., Sato, T., Matsuda, C., Kobayashi, T., Morrey, C.E., Shibata, N., Asakawa, S., Shimizu, N., Hori, H., Hamaguchi, S., Sakaizumi, M. 2002. DMY is a Y-specific DM-domain gene required for male development in the medaka fish. Nature, 417, pp. 559-563.

Matthews, H.K., Marchant, L., Carmona-Fontaine, C., Kuriyama, S., Larraín, J., Holt, M.R., Parsons, M., Mayor, R. 2008. Directional migration of neural crest cells in vivo is regulated by Syndecan-4/Rac1 and non-canonical Wnt signaling/RhoA. Development, 135(10), pp.1771–1780.

Mayer, M., Depken, M., Bois, J.S., Jülicher, F., Grill, S.W. 2010. Anisotropies in cortical tension reveal the physical basis of polarizing cortical flows. Nature, 467(7315), pp.617–621.

Mayor, R., Carmona-Fontaine, C. 2010. Keeping in touch with contact inhibition of locomotion. Trends in Cell Biology, 20(6), pp.319–328.

Mayor, R., Morgan, R., Sargent, M.G. 1995. Induction of the prospective neural crest of Xenopus. Development, 121, pp.767–777.

McDonald, J.A., Quade, B.J., Broekelmann, T.J., LaChance, R., Forsman, K., Hasegawa, E., Akiyama, S. 1987. Fibronectin's cell-adhesive domain and an amino-terminal matrix assembly domain participate in its assembly into fibroblast pericellular matrix. The Journal of Biological Chemistry, 262(7), pp.2957–2967.

McFadden, D.G., Olson, E.N. 2002. Heart development: learning from mistakes. Current Opinion in Genetics & Development, 12(3), pp.328–335.

Merrill, A.E., Bochukova, E.G., Brugger, S.M., Ishii, M., Pilz, D.T., Wall, S.A., Lyons, K.M., Wilkie, A.O., Maxson Jr, R.E. 2006. Cell mixing at a neural crest–mesoderm boundary and deficient ephrin-Eph signaling in the pathogenesis of craniosynostosis. Hum. Mol. Genet., 15, pp.1319–1328.

Metcalfe, C.D., Metcalfe, T.L., Kiparissis, Y., Koenig, B.G., Khan, C., Hughes, R.J., Croley, T.R., March, R.E., Potter, T. 2001. Estrogenic potency of chemicals detected in sewage treatment plant effluents as determined by in vivo assays with Japanese medaka (Oryzias latipes). Environ. Toxicol. Chem., 20, pp.297–308.

Mic, F.A., Molotkov, A., Molotkova, N., Duester, G. 2004. Raldh2 expression in optic vesicle generates a retinoic acid signal needed for invagination of retina during optic cup formation. Developmental Dynamics, 231(2), pp.270–277.

Michaelis, U.R., Chavakis, E., Kruse, C., Jungblut, B., Kaluza, D., Wandzioch, K., Manavski, Y., Heide, H., Santoni, M.J., Potente, M., Eble, J.A., Borg, J.P., Brandes, R.P. 2013. The polarity protein Scrib is essential for directed endothelial cell migration. Circulation Research, 112(6), pp.924–934.

Miyazono, K., Kamiya, Y., Morikawa, M. 2010. Bone morphogenetic protein receptors and signal transduction. J. Biochem, 147(1), pp.35–51.

Mochizuki, E., Fukuta, K., Tada, T., Harada, T., Watanabe, N., Matsuo, S., Hashimoto, H., Ozato, K., Wakamatsu, Y. 2005. Fish mesonephric model of polycystic kidney disease in medaka (Oryzias latipes) pc mutant. Kidney Int., 68(1), pp.23-34.

Morin-Kensicki, E.M., Boone, B.N., Howell, M., Stonebraker, J.R., Teed, J., Alb, J.G., Magnuson, T.R., O'Neal, W., Milgram, S.L. 2006. Defects in yolk sac vasculogenesis, chorioallantoic fusion, and embryonic axis elongation in mice with targeted disruption of Yap65. Molecular and Cellular Biology, 26(1), pp.77–87.

Müller, C.M., Best, J. 1989. Ocular dominance plasticity in adult cat visual cortex after transplantation of cultured astrocytes. Nature, 342(6248), pp.427–430.

Nakajima, Y.-I., Meyer, E.J., Kroesen, A., McKinney, S.A., Gibson, M.C. 2013. Epithelial junctions maintain tissue architecture by directing planar spindle orientation. Nature, pp.1–5.

Nemethova, M., Auinger, S., Small, J.V. 2008. Building the actin cytoskeleton: filopodia contribute to the construction of contractile bundles in the lamella. The Journal of Cell Biology, 180(6), pp.1233–1244.

Nolan, P.M., Peters, J., Strivens, M., Rogers, D., Hagan, J., Spurr, N., Gray, I.C., Vizor, L., Brooker, D., Whitehill, E., Washbourne, R., Hough, T., Greenaway, S., Hewitt, M., Liu, X., McCormack, S., Pickford, K., Selley, R., Wells, C., Tymowska-Lalanne, Z., Roby, P., Glenister, P., Thornton, C., Thaung, C., Stevenson, J.A., Arkell, R., Mburu, P., Hardisty, R., Kiernan, A., Erven, A., Steel, K.P., Voegeling, S., Guenet, J.L., Nickols, C., Sadri, R., Nasse, M., Isaacs, A., Davies, K., Browne, M., Fisher, E.M., Martin, J., Rastan, S., Brown, S.D., Hunter, J. 2000b. A

systematic, genome-wide, phenotype-driven mutagenesis programme for gene function studies in the mouse. Nat. Genet., 25, pp.440–443.

Nolan, P.M., Peters, J., Vizor, L., Strivens, M., Washbourne, R., Hough, T., Wells, C., Glenister, P., Thornton, C., Martin, J., Fisher, E., Rogers, D., Hagan, J., Reavill, C., Gray, I., Wood, J., Spurr, N., Browne, M., Rastan, S., Hunter, J., Brown, S.D. 2000a. Implementation of a large-scale ENU mutagenesis program: towards increasing the mouse mutant resource. Mamm. Genome, 11, pp.500–506.

Norton, P.A., Hynes, R.O., 1990. In vitro splicing of fibronectin pre-mRNAs. Nucleic Acids Research, 18(14), pp.4089–4097.

O'Connell, C.B., Wang, Y.L. 2000. Mammalian spindle orientation and position respond to changes in cell shape in a dynein-dependent fashion. Molecular Biology of the Cell, 11(5), pp. 1765–1774.

Odenthal, J., Rossnagel, K., Haffter, P., Kelsh, R.N., Vogelsang, E., Brand, M., van Eeden, F.J., Furutani-Seiki, M., Granato, M., Hammerschmidt, M., Heisenberg, C.-P., Jiang, Y.J., Kane, D.A., Mullins, M.C., Nüsslein-Volhard, C. 1996. Mutations affecting xanthophore pigmentation in the zebrafish, Danio rerio. Development, 123, pp.391-8.

Ohno, S. 2001. Intercellular junctions and cellular polarity: the PAR-aPKC complex, a conserved core cassette playing fundamental roles in cell polarity. Current Opinion in Cell Biology, 13(5), pp.641–648.

Ota, M., Sasaki, H. 2008. Mammalian Tead proteins regulate cell proliferation and contact inhibition as transcriptional mediators of Hippo signaling. Development, 135(24), pp.4059–4069.

Overholtzer, M., Zhang, J., Smolen, G.A., Muir, B., Li, W., Sgroi, D.C., Deng, C.X., Brugge, J.S., Haber, D.A. 2006. Transforming properties of YAP, a candidate oncogene on the chromosome 11q22 amplicon. Proc. Natl. Acad. Sci. U.S.A., 103(33), pp.12405–12410.

Pan, D. 2010. The hippo signaling pathway in development and cancer. Developmental Cell, 19(4), pp.491–505.

Pankov, R., Cukierman, E., Katz, B.Z., Matsumoto, K., Lin, D.C., Lin, S., Hahn, C., Yamada, K.M. 2000. Integrin dynamics and matrix assembly: tensin-dependent translocation of alpha(5)beta(1) integrins promotes early fibronectin fibrillogenesis. The Journal of Cell Biology, 148(5), pp.1075–1090.

Parsons, L.M., Grzeschik, N.A., Allott, M.L., Richardson, H.E. 2010. Lgl/aPKC and Crb regulate the Salvador/Warts/Hippo pathway. Fly, 4(4), pp.288–293.

Paul, J.I., Schwarzbauer, J.E., Tamkun, J.W., Hynes, R.O. 1986. Cell-type-specific fibronectin subunits generated by alternative splicing. The Journal of Biological Chemistry, 261(26), pp. 12258–12265.

Pei, W., Feldman, B. 2009. Identification of common and unique modifiers of zebrafish midline bifurcation and cyclopia. Developmental Biology, 326(1), pp.201–211.

Peters, J.H., Chen, G.E., Hynes, R.O. 1996. Fibronectin isoform distribution in the mouse. II. Differential distribution of the alternatively spliced EIIIB, EIIIA, and V segments in the adult mouse. Cell Adhesion and Communication, 4(2), pp.127–148.

Phillips, B.T., Storch, E.M., Lekven, A.C., Riley, B.B. 2004. A direct role for Fgf but not Wnt in otic placode induction. Development, 131(4), pp.923–931.

Poole, T.J., Finkelstein, E.B., Cox, C.M. 2001. The role of FGF and VEGF in angioblast induction and migration during vascular development. Developmental Dynamics, 220(1), pp.1–17.

Porazinski, S.R., Wang, H., Furutani-Seiki, M. 2011. Essential techniques for introducing medaka to a zebrafish laboratory--towards the combined use of medaka and zebrafish for further genetic dissection of the function of the vertebrate genome. Methods in Molecular Biology (Clifton, NJ), 770, pp.211–241.

Poujade, M., Grasland-Mongrain, E., Hertzog, A., Jouanneau, J., Chavrier, P., Ladoux, B., Buguin, A., Silberzan, P. 2007. Collective migration of an epithelial monolayer in response to a model wound. Proc. Natl. Acad. Sci. U.S.A, 104(41), pp.15988–15993.

Pézeron, G., Lambert, G., Dickmeis, T., Strähle, U., Rosa, F.M., Mourrain, P. 2008. Rasl11b knock down in zebrafish suppresses one-eyed-pinhead mutant phenotype. PLoS ONE, 3(1), p.e1434.

Quyn, A.J., Appleton, P.L., Carey, F.A., Steele, R.J., Barker, N., Clevers, H., Ridgway, R.A., Sansom, O.J., Näthke, I.S. 2010. Spindle orientation bias in gut epithelial stem cell compartments is lost in precancerous tissue. Cell Stem Cell, 6(2), pp.175–181.

Rebagliati, M.R., Toyama, R., Haffter, P., Dawid, I.B. 1998. cyclops encodes a nodal-related factor involved in midline signaling. Proceedings of the National Academy of Sciences of the United States of America, 95(17), pp.9932–9937.

Reddy, B.V.V.G., Rauskolb, C., Irvine, K.D. 2010. Influence of Fat-Hippo and Notch signaling on the proliferation and differentiation of Drosophila optic neuroepithelia. Development, 137, pp. 2397–2408.

Reginensi, A., Scott, R.P., Gregorieff, A., Bagherie-Lachidan, M., Chung, C., Lim, D.S., Pawson, T., Wrana, J., McNeill, H. 2013. Yap- and Cdc42-dependent nephrogenesis and morphogenesis during mouse kidney development. PLoS Genetics, 9(3), p.e1003380.

Ridley, A.J., Schwartz, M.A., Burridge, K., Firtel, R.A., Ginsberg, M.H., Borisy, G., Parsons, J.T., Horwitz, A.R. 2003. Cell Migration: Integrating Signals from Front to Back. Science, 302(5651), pp.1704–1709.

Rosenberg, M.B., Friedmann, T., Robertson, R.C., Tuszynski, M., Wolff, J.A., Breakefield, X.O., Gage, F.H. 1988. Grafting genetically modified cells to the damaged brain: restorative effects of NGF expression. Science, 242(4885), pp.1575–1578.

Rotsch, C., Radmacher, M., 2000. Drug-induced changes of cytoskeletal structure and mechanics in fibroblasts: an atomic force microscopy study. Biophysical Journal, 78(1), pp.520–535.

Ruoslahti, E. 1988. Fibronectin and its receptors. Annual Review of Biochemistry, 57, pp.375–413.

Ruoslahti, E., Obrink, B. 1996. Common principles in cell adhesion. Experimental Cell Research, 227(1), pp.1–11.

Ruoslahti, E., Pierschbacher, M.D. 1987. New perspectives in cell adhesion: RGD and integrins. Science, 238(4826), pp.491–497.

Russell, L.B., Montgomery, C.S. 1982. Supermutagenicity of ethylnitrosourea in the mouse spot test: comparisons with methylnitrosourea and ethylnitrosourethane. Mutat Res., 92(1-2), pp. 193-204.

Rørth, P. 2009. Collective Cell Migration. Annual review of Cell and Developmental Biology, 25(1), pp.407–429.

Sagerström, C.G. Gammill, L.S., Veale, R., Sive, H. 2005. Specification of the enveloping layer and lack of autoneuralization in zebrafish embryonic explants. Developmental dynamics, 232(1), pp.85–97.

Salbreux, G., Charras, G., Paluch, E. 2012. Actin cortex mechanics and cellular morphogenesis. Trends in Cell Biology, 22(10), pp.536–545.

Sanders, E.J., Hu, N. & Prasad, S., 1994. Guidance of filopodial extension by fibronectin-rich extracellular matrix fibrils during avian gastrulation. A study using confocal microscopy. The International Journal of Developmental Biology, 38(4), pp.701–707.

Sandquist, J.C., Kita, A.M., Bement, W.M. 2011. And the dead shall rise: actin and myosin return to the spindle. Developmental Cell, 21(3), pp.410–419.

Sansores-Garcia, L., Bossuyt, W., Wada, K., Yonemura, S., Tao, C., Sasaki, H., Halder, G. 2011. Modulating F-actin organization induces organ growth by affecting the Hippo pathway. The EMBO Journal, 30(12), pp.2325–2335.

Saucedo, L.J., Edgar, B.A. 2007. Filling out the Hippo pathway. Nature Reviews: Molecular Cell Biology, 8(8), pp.613–621.

Sawyer, J.M., Harrell, J.R., Shemer, G., Sullivan-Brown, J., Roh-Johnson, M., Goldstein, B. 2010. Apical constriction: a cell shape change that can drive morphogenesis. Developmental Biology, 341(1), pp.5–19.

Schartl, M. 2004. A comparative view on sex determination in medaka. Mech. Dev., 121, pp. 639–645.

Scholey, J.M., Taylor, K.A., Kendrick-Jones, J. 1980. Regulation of non-muscle myosin assembly by calmodulin-dependent light chain kinase. Nature, 287(5779), pp.233–235.

Segalen, M., Johnston, C.A., Martin, C.A., Dumortier, J.G., Prehoda, K.E., David, N.B., Doe, C.Q., Bellaïche, Y. 2010. The Fz-Dsh planar cell polarity pathway induces oriented cell division via Mud/NuMA in Drosophila and zebrafish. Developmental Cell, 19(5), pp.740–752.

Schlegelmilch, K., Mohseni, M., Kirak, O., Pruszak, J., Rodriguez, J.R., Zhou, D., Kreger, B.T., Vasioukhin, V., Avruch, J., Brummelkamp, T.R., Camargo, F.D. 2011. Yap1 acts downstream of α-catenin to control epidermal proliferation. Cell, 144(5), pp.782–795.

Sheldon, H., Andre, M., Legg, J.A., Heal, P., Herbert, J.M., Sainson, R., Sharma, A.S., Kitajewski, J.K., Heath, V.L., Bicknell, R. 2009. Active involvement of Robo1 and Robo4 in filopodia formation and endothelial cell motility mediated via WASP and other actin nucleation-promoting factors. The FASEB Journal, 23(2), pp.513–522.

Shimada, N., Aya-Murata, T., Reza, H.M., Yasuda, K. 2003. Cooperative action between L-Maf and Sox2 on delta-crystallin gene expression during chick lens development. Mechanisms of Development, 120(4), pp.455–465.

Singh, P., Carraher, C. & Schwarzbauer, J.E. 2010. Assembly of Fibronectin Extracellular Matrix. Annual Review of Cell and Developmental Biology, 26(1), pp.397–419.

Slanchev, K., Carney, T.J., Stemmler, M.P., Koschorz, B., Amsterdam, A., Schwarz, H., Hammerschmidt, M. 2009. The epithelial cell adhesion molecule EpCAM is required for epithelial morphogenesis and integrity during zebrafish epiboly and skin development. PLoS Genetics, 5(7), p.e1000563.

Solnica-Krezel, L., Driever, W. 1994. Microtubule arrays of the zebrafish yolk cell: organization and function during epiboly. Development, 120(9), pp.2443–2455.

Solnica-Krezel, L., Sepich, D.S. 2012. Gastrulation: making and shaping germ layers. Annual Review of Cell and Developmental Biology, 28, pp.687–717.

Song, H., Mak, K.K., Topol, L., Yun, K., Hu, J., Garrett, L., Chen, Y., Park, O., Chang, J., Simpson, R.M., Wang, C.Y., Gao, B., Jiang, J., Yang, Y. 2010. Mammalian Mst1 and Mst2 kinases play essential roles in organ size control and tumor suppression. Proc. Natl. Acad. Sci. U.S.A., 107, pp.1431–1436.

Sperry, R.B., Bishop, N.H., Bramwell, J.J., Brodeur, M.N., Carter, M.J., Fowler, B.T., Lewis, Z.B., Maxfield, S.D., Staley, D.M., Vellinga, R.M., Hansen, MD. 2009. Zyxin controls migration in epithelial-mesenchymal transition by mediating actin-membrane linkages at cell-cell junctions. Journal of Cellular Physiology, 222(3), pp.612-24.

Srinivasan, S., Wang, F., Glavas, S., Ott, A., Hofmann, F., Aktories, K., Kalman, D., Bourne, H.R. 2003. Rac and Cdc42 play distinct roles in regulating PI(3,4,5)P3 and polarity during neutrophil chemotaxis. The Journal of Cell Biology, 160(3), pp.375–385.

Stainier, D.Y. 2001. Zebrafish genetics and vertebrate heart formation. Nature, 2(1), pp.39–48.

Stainier, D.Y., Fouquet, B., Chen, J.N., Warren, K.S., Weinstein, B.M., Meiler, S.E., Mohideen, M.A., Neuhauss, S.C., Solnica-Krezel, L., Schier, A.F., Zwartkruis, F., Stemple, D.L., Malicki, J., Driever, W., Fishman, M.C. 1996. Mutations affecting the formation and function of the cardiovascular system in the zebrafish embryo. Development, 123, pp.285–292.

Strano, S., Monti, O., Pediconi, N., Baccarini, A., Fontemaggi, G., Lapi, E., Mantovani, F., Damalas, A., Citro, G., Sacchi, A., Del Sal, G., Levrero, M., Blandino, G. 2005. The transcriptional coactivator Yes-associated protein drives p73 gene-target specificity in response to DNA Damage. Molecular Cell, 18(4), pp.447–459.

Sudol, M. 1994. Yes-associated protein (YAP65) is a proline-rich phosphoprotein that binds to the SH3 domain of the Yes proto-oncogene product. Oncogene, 9(8), pp.2145–2152.

Sudol, M., Bork, P., Einbond, A., Kastury, K., Druck, T., Negrini, M., Huebner, K., Lehman, D. 1995b. Characterization of the mammalian YAP (Yes-associated protein) gene and its role in defining a novel protein module, the WW domain. J. Biol. Chem. 270, pp.14733-41.

Sudol, M., Chen, H.I., Bougeret, C., Einbond, A., Bork, P. 1995a. Characterization of a novel protein-binding module--the WW domain. FEBS Lett. 369, pp.67-71.

Sudol, M., Shields, D.C., Farooq, A. 2012. Structures of YAP protein domains reveal promising targets for development of new cancer drugs. Seminars in Cell & Developmental Biology, 23(7), pp.827-33.

Suga, H., Kadoshima, T., Minaguchi, M., Ohgushi, M., Soen, M., Nakano, T., Takata, N., Wataya, T., Muguruma, K., Miyoshi, H., Yonemura, S., Oiso, Y., Sasai, Y. 2011. Self-formation of functional adenohypophysis in three-dimensional culture. Nature, 480(7375), pp.57–62.

Takahashi, S., Leiss, M., Moser, M., Ohashi, T., Kitao, T., Heckmann, D., Pfeifer, A., Kessler, H., Takagi, J., Erickson, H.P., Fässler, R. 2007. The RGD motif in fibronectin is essential for development but dispensable for fibril assembly. The Journal of Cell Biology, 178(1), pp.167–178.

Takebe, T., Sekine, K., Enomura, M., Koike, H., Kimura, M., Ogaeri, T., Zhang, R.R., Ueno, Y., Zheng, Y.W., Koike, N., Aoyama, S., Adachi, Y., Taniguchi, H. Vascularized and functional human liver from an iPSC-derived organ bud transplant. 2013. Nature, 499(7459), pp.481-5.

Takuwa, Y., Du, W., Qi, X., Okamoto, Y., Takuwa, N., Yoshioka, K. 2010. Roles of sphingosine-1-phosphate signaling in angiogenesis. World J. Biol. Chem., 1(10), pp.298-306.

Tang, N., Marshall, W.F., McMahon, M., Metzger, R.J., Martin, G.R. 2011. Control of mitotic spindle angle by the RAS-regulated ERK1/2 pathway determines lung tube shape. Science, 333(6040), pp.342–345.

Tawk, M., Araya, C., Lyons, D.A., Reugels, A.M., Girdler, G.C., Bayley, P.R., Hyde, D.R., Tada, M., Clarke, J.D. 2007. A mirror-symmetric cell division that orchestrates neuroepithelial morphogenesis. Nature, 446(7137), pp.797–800.

Technau, G.M. 1987. A single cell approach to problems of cell lineage and commitment during embryogenesis of Drosophila melanogaster. Development, 100(1), pp.1–12.

Teti, A. 1992. Regulation of cellular functions by extracellular matrix. Journal of the American Society of Nephrology, JASN, 2(10 Suppl), pp.S83–7.

Thiery, J.P. 2002. Epithelial-mesenchymal transitions in tumour progression. Nature Reviews Cancer, 2(6), pp.442–454.

Thiery, J.P., Sleeman, J.P. 2006. Complex networks orchestrate epithelial–mesenchymal transitions. Nature Reviews Molecular Cell Biology, 7(2), pp.131–142.

Tibber, M.S., Kralj-Hans, I., Savage, J., Mobbs, P.G., Jeffery, G. 2004. The orientation and dynamics of cell division within the plane of the developing vertebrate retina. The European Journal of Neuroscience, 19(3), pp.497–504.

Tojkander, S., Gateva, G., Lappalainen, P. 2012. Actin stress fibers--assembly, dynamics and biological roles. Journal of Cell Science, 125(Pt 8), pp.1855–1864.

Toyoshima, F., Nishida, E. 2007. Integrin-mediated adhesion orients the spindle parallel to the substratum in an EB1- and myosin X-dependent manner. The EMBO Journal, 26(6), pp.1487–1498.

Trinh, L.A., Stainier, D.Y.R. 2004. Fibronectin regulates epithelial organization during myocardial migration in zebrafish. Developmental Cell, 6(3), pp.371–382.

Udan, R.S., Kango-Singh, M., Nolo, R., Tao, C., Halder, G. 2003. Hippo promotes proliferation arrest and apoptosis in the Salvador/Warts pathway. Nat Cell Biol, 5(10), pp.914–920.

Van Haastert, P.J.M., Devreotes, P.N. 2004. Chemotaxis: signalling the way forward. Nat. Rev. Mol. Cell. Biol., 5(8), pp.626–634.

Varelas, X., Miller, B.W., Sopko, R., Song, S.Y., Gregorieff, A., Fellouse, F.A., Sakuma, R., Pawson, T., Hunziker, W., McNeill, H., Wrana, J.L., Attisano, L. 2010a. The Hippo pathway regulates Wnt/β-Catenin signaling. Dev. Cell, 18, pp.579–591.

Varelas, X., Samavarchi-Tehrani, P., Narimatsu, M., Weiss, A., Cockburn, K., Larsen, B.G., Rossant, J., Wrana, J.L. 2010b. The Crumbs complex couples cell density sensing to Hippo-dependent control of the TGF-β-SMAD pathway. Dev. Cell, 19, pp.831–844.

Varelas, X., Wrana, J.L. 2012. Coordinating developmental signaling: novel roles for the Hippo pathway. Trends in Cell Biology, 22(2), pp.88–96.

Vassilev, A., Kaneko, K.J., Shu, H., Zhao, Y., DePamphilis, M.L. 2001. TEAD/TEF transcription factors utilize the activation domain of YAP65, a Src/Yes-associated protein localized in the cytoplasm. Genes Dev, 15(10), pp.1229–1241.

Verma, A., Bhattacharya, R., Remadevi, I., Li, K., Pramanik, K., Samant, G.V., Horswill, M., Chun, C.Z., Zhao, B., Wang, E., Miao, R.Q., Mukhopadhyay, D., Ramchandran, R., Wilkinson, G.A. 2010. Endothelial cell-specific chemotaxis receptor (ecscr) promotes angioblast migration during vasculogenesis and enhances VEGF receptor sensitivity. Blood, 115(22), pp.4614–4622.

Vicente-Manzanares, M., Ma, X., Adelstein, R.S., and Horwitz, A.R. 2009. Non-muscle myosin II takes centre stage in cell adhesion and migration. Nat. Rev. Mol. Cell. Biol., 10(11), pp. 778-790.

Wada, K.-I., Itoga, K., Okano, T., Yonemura, S., Sasaki, H. 2011. Hippo pathway regulation by cell morphology and stress fibers. Development, 138(18), pp.3907–3914.

Wakamatsu, Y., Pristyazhnyuk, S., Kinoshita, M., Tanaka, M., Ozato, K. 2001. The see-through medaka: a fish model that is transparent throughout life. Proc. Natl. Acad. Sci. USA, 98, pp. 10046-50.

Wang, K., Degerny, C., Xu, M., Yang, X.J. 2009. YAP, TAZ, and Yorkie: a conserved family of signal-responsive transcriptional coregulators in animal development and human disease. Biochemistry and Cell Biology, 87(1), pp.77–91.

Wang, H.-R., Zhang, Y., Ozdamar, B., Ogunjimi, A.A., Alexandrova, E., Thomsen, G.H., Wrana, J.L. 2003. Regulation of cell polarity and protrusion formation by targeting RhoA for degradation. Science, 302(5651), pp.1775–1779.

Warga, R.M., Kimmel, C.B. 1990. Cell movements during epiboly and gastrulation in zebrafish. Development, 108(4), pp.569–580.

Warga, R.M., Nusslein-Volhard, C. 1999. Origin and development of the zebrafish endoderm. Development, 126(4), pp.827–838.

Watanabe, T., Hosoya, H. & Yonemura, S. 2007. Regulation of myosin II dynamics by phosphorylation and dephosphorylation of its light chain in epithelial cells. Molecular Biology of the Cell, 18(2), pp.605–616.

Weber, G.F., Bjerke, M.A., DeSimone, D.W. 2012. A Mechanoresponsive Cadherin-Keratin Complex Directs Polarized Protrusive Behavior and Collective Cell Migration. Developmental Cell, 22(1), pp.104–115.

Whitfield, T.T., Riley, B.B., Chiang, M.Y., Phillips, B. 2002. Development of the zebrafish inner ear. Developmental Dynamics, 223(4), pp.427–458.

Wierzbicka-Patynowski, I., Schwarzbauer, J.E. 2002. Regulatory role for SRC and phosphatidylinositol 3-kinase in initiation of fibronectin matrix assembly. The Journal of Biological Chemistry, 277(22), pp.19703–19708.

Wierzbicka-Patynowski, I., Schwarzbauer, J.E. 2003. The ins and outs of fibronectin matrix assembly. Journal of Cell Science, 116(Pt 16), pp.3269–3276.

Williams-Masson, E.M., Malik, A.N., Hardin, J. 1997. An actin-mediated two-step mechanism is required for ventral enclosure of the C. elegans hypodermis. Development, 124(15), pp.2889–2901.

Wittbrodt, J., Shima, A., Schartl, M. 2002. MEDAKA — A MODEL ORGANISM FROM THE FAR EAST. Nature Reviews Genetics, 3(1), pp.53–64.

Woo, K., Fraser, S.E. 1995. Order and coherence in the fate map of the zebrafish nervous system. Development, 121(8), pp.2595–2609.

Wood, W., Jacinto, A., Grose, R., Woolner, S., Gale, J., Wilson, C., Martin, P. 2002. Wound healing recapitulates morphogenesis in Drosophila embryos. Nature Cell Biology, 4(11), pp. 907–912.

Xin, M., Kim, Y., Sutherland, L.B., Murakami, M., Qi, X., McAnally, J., Porrello, E.R., Mahmoud, A.I., Tan, W., Shelton, J.M., Richardson, J.A., Sadek, H.A., Bassel-Duby, R., Olson, E.N. 2013. Hippo pathway effector Yap promotes cardiac regeneration. Proc. Natl. Acad. Sci. U.S.A., 110(34), pp.13839–13844.

Xu, K., Cleaver, O. 2011. Tubulogenesis during blood vessel formation. Seminars in Cell & Developmental Biology, 22(9), pp.993–1004.

Yamada, K.M. & Cukierman, E. 2007. Modeling Tissue Morphogenesis and Cancer in 3D. Cell, 130(4), pp.601–610.

Yang, C., Svitkina, T. 2011. Filopodia initiation: Focus on the Arp2/3 complex and formins. Cell Adhesion & Migration, 5(5), pp.402–408.

Yang, N., Morrison, C.D., Liu, P., Miecznikowski, J., Bshara, W., Han, S., Zhu, Q., Omilian, A.R., Li, X., Zhang, J. 2012. TAZ induces growth factor-independent proliferation through activation of EGFR ligand amphiregulin. Cell Cycle, 11(15), pp.2922–2930.

Yelon, D., Ticho, B., Halpern, M.E., Ruvinsky, I., Ho, R.K., Silver, L.M., Stainier, D.Y. 2000. The bHLH transcription factor hand2 plays parallel roles in zebrafish heart and pectoral fin development. Development, 127(12), pp.2573–2582.

Yoder, M.C. 2012. Human endothelial progenitor cells. Cold Spring Harbor Perspectives in Medicine, 2(7), p.a006692.

Yu, C.H., Law, J.B., Suryana, M., Low, H.Y., Sheetz, M.P. 2011. Early integrin binding to Arg-Gly-Asp peptide activates actin polymerization and contractile movement that stimulates outward translocation. Proc. Natl. Acad. Sci. U.S.A., 108(51), pp.20585–90.

Yu, F.-X., Guan, K.-L. 2013. The Hippo pathway: regulators and regulations. Genes & Development, 27(4), pp.355–371.

Yuan, Z., Kim, D., Shu, S., Wu, J., Guo, J., Xiao, L., Kaneko, S., Coppola, D., Cheng, J.Q. 2010. Phosphoinositide 3-kinase/Akt inhibits MST1-mediated pro-apoptotic signaling through phosphorylation of threonine 120. J. Biol. Chem., 285, pp.3815–3824.

Yun, S., Saijoh, Y., Hirokawa, K.E., Kopinke, D., Murtaugh, L.C., Monuki, E.S., Levine, EM. 2009. Lhx2 links the intrinsic and extrinsic factors that control optic cup formation. Development, 136(23), pp.3895–3906.

Zalik, S.E., Lewandowski, E., Kam, Z., Geiger, B. 1999. Cell adhesion and the actin cytoskeleton of the enveloping layer in the zebrafish embryo during epiboly. Biochemistry and Cell Biology, 77(6), pp.527–542.

Zeng, G., Taylor, S.M., McColm, J.R., Kappas, N.C., Kearney, J.B., Williams, L.H., Hartnett, M.E., Bautch, V.L. 2007. Orientation of endothelial cell division is regulated by VEGF signaling during blood vessel formation. Blood, 109(4), pp.1345–1352.

Zhang, X., Grusche, F.A., Harvey, K.F. 2012. Control of tissue growth and cell transformation by the Salvador/Warts/Hippo pathway. PLoS ONE 7(2): e31994.

Zhang, J., Ji, J.Y., Yu, M., Overholtzer, M., Smolen, G.A., Wang, R., Brugge, J.S., Dyson, N.J., Haber, D.A. 2009. YAP-dependent induction of amphiregulin identifies a non-cell-autonomous component of the Hippo pathway. Nature cell biology, 11(12), pp.1444–1450.

Zhang, J., Talbot, W.S., Schier, A.F., 1998. Positional cloning identifies zebrafish one-eyed pinhead as a permissive EGF-related ligand required during gastrulation. Cell, 92(2), pp.241–251.

Zhao, B., Kim, J., Ye, X., Lai, Z.C., Guan, K.L. 2009. Both TEAD-binding and WW domains are required for the growth stimulation and oncogenic transformation activity of yes-associated protein. Cancer Research, 69(3), pp.1089–1098.

Zhao, B. Li, L., Lei, Q., Guan, K.L. 2010a. The Hippo-YAP pathway in organ size control and tumorigenesis: an updated version. Genes & Development, 24(9), pp.862–874.

Zhao, B., Li, L., Tumaneng, K., Wang, C.Y., Guan, K.L. 2010b. A coordinated phosphorylation by Lats and CK1 regulates YAP stability through SCF(beta-TRCP). Genes & Development, 24(1), pp.72–85.

Zhao, B., Wei, X., Li, W., Udan, R.S., Yang, Q., Kim, J., Xie, J., Ikenoue, T., Yu, J., Li, L., Zheng, P., Ye, K., Chinnaiyan, A., Halder, G., Lai, Z.C., Guan, K.L. 2007. Inactivation of YAP oncoprotein by the Hippo pathway is involved in cell contact inhibition and tissue growth control. Genes & Development, 21(21), pp.2747–2761.

Zhao, B., Ye, X., Yu, J., Li, L., Li, W., Li, S., Yu, J., Lin, J.D., Wang, C.Y., Chinnaiyan, A.M., Lai, Z.C., Guan, K.L. 2008. TEAD mediates YAP-dependent gene induction and growth control. Genes & Development, 22(14), pp.1962–1971.

Zhong, T.P., Childs, S., Leu, J.P., Fishman, M.C. 2001. Gridlock signalling pathway fashions the first embryonic artery. Nature, 414(6860), pp.216–220.

Zhou, D., Conrad, C., Xia, F., Park, J.S., Payer, B., Yin, Y., Lauwers, G.Y., Thasler, W., Lee, J.T., Avruch, J., Bardeesy, N. 2009. Mst1 and Mst2 maintain hepatocyte quiescence and suppress hepatocellular carcinoma development through inactivation of the Yap1 oncogene. Cancer Cell, 16, pp.425–438.

Zhou, X., Rowe, R.G., Hiraoka, N., George, J.P., Wirtz, D., Mosher, D.F., Virtanen, I., Chernousov, M.A., Weiss, S.J. 2008. Fibronectin fibrillogenesis regulates three-dimensional neovessel formation. Genes & Development, 22(9), pp.1231–1243.

Zhuang, X., Cross, D., Heath, V.L., Bicknell, R. 2011. Shear stress, tip cells and regulators of endothelial migration. Biochemical Society Transactions, 39(6), pp.1571–1575.

Žigman, M., Trinh le, A., Fraser, S.E., Moens, C.B. 2011. Zebrafish Neural Tube Morphogenesis Requires Scribble-Dependent Oriented Cell Divisions. Current Biology, 21(1), pp.79–86.

Textbooks

Chen, S.-A., Haïssaguerre, M., Zipes, D. 2004. Thoracic Vein Arrhythmias, Wiley-Blackwell Publishing. 1st edition. Iowa, USA.

Graw, J. 2010. Eye Development. In: P. Koopman, ed. Organogenesis in development. San Diego: Elsevier, pp.344-378.

Kinoshita, M., Murata, K., Naruse, K., Tanaka, M. 2009. Medaka: Biology, Management, and Experimental Protocols. Wiley-Blackwell Publishing. Iowa, USA.

Ohno, S. 1970. Evolution by Gene Duplication. Springer, Heidelberg, Germany.

Wolpert, L., Tickle, C. 2011. Principles of Development. Oxford University Press. 4th Edition. Oxford, UK.

Chapter 9: Appendix

9.1 Legends for Supplementary movies

Supplementary movie 1

This representative movie shows the formation of the Cuvierian ducts (CDs) in wild type embryos. The CDs are the large ring structure that forms and consists of the transverse blood vessels formed by the merging of the anterior and posterior cardinal veins. This vasculature carries blood from the heart to the rest of the body and back again. The duct is formed initially by the migration of a primary stream of cells from a more posterior position near the otic vesicle (yellow arrow). A more anterior secondary stream of cells (white arrow) then migrates laterally to add to the tip of this primary stream and extend the duct cohesively in an anterior direction. Endothelial cells in this movie and movie 2 are labelled with EGFP using the *fli* promoter. Anterior is to the right and the movie starts at st.19 (27.5 hpf) of development finishing at st.25 (50 hpf). View shown is dorsal.

Supplementary movie 2

In this movie failure of the CDs formation in *hir* is documented. It can be seen that the primary stream extends to a limited extent in *hir* embryos, but does not form the rod-like structure as seen in wild type. Furthermore, cells of the secondary stream fail to significantly migrate outwards laterally to meet the tip of the primary stream and extend the duct anteriorly (yellow arrow). Again anterior is to the right and the movie starts at st.20 (31.5 hpf) of development also ending at stage 25 (50 hpf). View shown is dorsal.

Supplementary movie 3

Bright-field movie detailing the formation of the eye by coordinated invagination of the lens and retina in wild type. Dorsal view, anterior up. Movie is from st.19-23 (27.5-41 hpf). In wild type, the nascent lenses and retinas undergo coordinated morphogenesis to locate the lens properly in the eye cup.

Supplementary movie 4

This movie shows the dislocation of the lens in *hir*. Dorsal bright-field view, anterior up. Movie is from st.20-24 (31.5-44 hpf). The mutant lens placodes dislocate, round up and migrate anteriorly where they appear to loosely reattach to the retina.

Supplementary movie 5

Confocal time-lapse microscopy of wild type eye morphogenesis. Fluorescence images overlaid on DIC images. Embryos were injected with EGFP-CAAX+H2B-RFP (MNFP) at the 1-cell stage to label cell membranes green and nuclei red. Dorsal view of the left eye, anterior up, from st.20-24 (31.5-44 hpf). This shows cell divisions and rearrangements that underlie lens and retina invagination.

Supplementary movie 6

Confocal time-lapse microscopy of *hir* eye morphogenesis. Cells were labelled in a mosaic manner by MNFP mRNA injection at the 8-cell stage. Dorsal view of the left eye, anterior up, from st.25-26 (50-54 hpf). Movie details how two lens fragments migrate towards each other and appear to rejoin.

Supplementary movie 7

Confocal time-lapse microscopy of *hir* eye morphogenesis. Cells were labelled by MNFP mRNA injection. Dorsal view of the left eye, anterior up, at st.22 (38 hpf). In the nascent lens placode cells have aberrant filopodia that extend from the surface opposite the retina.

Supplementary movie 8

Confocal time-lapse microscopy of *hir* eye morphogenesis. Cells were labeled in a mosaic manner by MNFP mRNA injection at the 8-cell stage. Dorsal view of the left eye, anterior up, at st.23 (41 hpf). Earlier in the movie the detached lens can be seen extending filopodia as if ‘searching’ for the retina. Later in the movie filopodia can be seen extending from the retina.